Development of patient-specific knee joint prostheses for unicompartmental knee replacement (UKR)

by
David Jacobus van den Heever

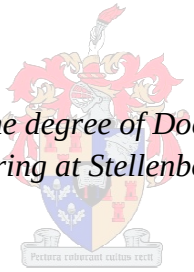

Dissertation presented for the degree of Doctor of Philosophy in the Faculty of Engineering at Stellenbosch University

Promotor: Prof. Cornie Scheffer
Faculty of Engineering
Department of Mechanical and Mechatronic Engineering

December 2011

Declaration

By Submitting this dissertation electronically, I declare that the entirety of the work contained therein is my own, original work, that I am the sole author thereof (save to the extent explicitly otherwise stated), that reproduction and publication thereof by Stellenbosch University will not infringe any third party rights and that I have not previously in its entirety or in part submitted it for obtaining any qualification.

Signature: Date:

ABSTRACT

The knee is the largest, most complicated and incongruent joint in the human body. It sustains very high forces and is susceptible to injury and disease. Osteoarthritis is a common disease prevalent among the elderly and causes softening or degradation of the cartilage and subcondral bone in the joint, which leads to a loss of function and pain. This problem can be alleviated through a surgical intervention commonly termed a “knee replacement”. The aim of a knee replacement procedure is to relieve pain and restore normal function. Ideally, the knee replacement prosthesis should have an articulating geometry similar to that of the patient’s healthy knee, and must allow for normal motion. Unfortunately, this is often problematic since knee prostheses are supplied in standard sizes from a variety of manufacturers and each one has a slightly different design. Furthermore, commercial prostheses are not always able to restore the complex geometry of an individual patient’s original articulating surfaces. This dissertation shows that there is a significant variation between knee geometries, regardless of gender and race. This research aims to resolve the problem in two parts: Firstly by presenting a method for preoperatively selecting the optimal knee prosthesis type and size for a specific patient, and secondly by presenting a design procedure for designing and manufacturing patient-specific unicompartmental knee replacements. The design procedure uses mathematical modelling and an artificial neural network to estimate the original and healthy articulating surfaces of a patient’s knee. The models are combined with medical images from the patient to create a knee prosthesis that is patient-specific. These patient-specific implants are then compared to conventional implants with respect to contact stresses and kinematics. The dissertation concludes that patient-specific implants can have characteristics that are comparable to or better than conventional prostheses. The unique design methodology presented in this dissertation introduces a significant advancement in knee replacement technology, with the potential to dramatically improve clinical outcomes of knee replacement surgery.

OPSOMMING

Die knie is die grootste, mees komplekse en mees ongelyksoortige gewrig in die liggaam. Osteoarthritis is ’n siekte wat algemeen by bejaardes voorkom en die versagting of agteruitgang van die kraakbeen en subchondrale bene in die gewrig tot gevolg het, wat tot ’n verlies van funksionering en pyn lei. Hierdie probleem kan verlig word deur ’n chirurgiese ingryping wat algemeen as ’n “knievervanging” bekend staan. Die doel van ’n knievervangingsprosedure is om pyn te verlig en normale funksionering te herstel. Ideaal gesproke behoort die knievervangingsprostese ’n gewrigsgeometrie te hê wat soortgelyk aan die pasiënt se gesonde knie is, en normale beweging moontlik maak. Ongelukkig is dit dikwels problematies aangesien knieprosteses in standaardgroottes en deur ’n verskeidenheid vervaardigers verskaf word, wat elkeen se ontwerp effens anders maak. Verder kan kommersiële prosteses nie altyd die komplekse geometrie van ’n individuele pasiënt se oorspronklike gewrigsoppervlakke vervang nie. Hierdie proefskrif wys dat daar ’n betekenisvolle variasie tussen knieafmetings is, afgesien van geslag en ras. Hierdie navorsing is daarop gemik om die problem op tweërlei wyse te benader: Eerstens deur ’n metode aan te bied om die optimal knieprostesetipe en -grootte vir ’n spesifieke pasiënt voor die operasie uit te soek, en tweedens om ’n ontwerpprosedure aan te bied vir die ontwerp en vervaardiging van pasiëntspesifieke unikompartementele knievervangings. Die ontwerpprosedure gebruik wiskundige modellering en ’n kunsmatige neurale netwerk om die oorspronklike en gesonde gewrigsoppervlakke van ’n pasiënt se knie te bepaal. Die modelle word met mediese beelde van die pasiënt gekombineer om ’n knieprostese te skep wat pasiëntspesifiek is. Hierdie pasiëntspesifieke inplantings word dan met konvensionele inplantings vergelyk wat kontakstres en kinematika betref. Daar word tot die slotsom gekom dat die pasiëntspesifieke inplantings oor eienskappe kan beskik wat vergelykbaar is met of selfs beter is as dié van konvensionele prosteses. Die unieke ontwerpmetodologie wat in hierdie proefskrif aangebied word, stel beduidende vordering in knievervangingstegnologie bekend, met die potensiaal om die kliniese uitkomste van knievervangingsoperasies dramaties te verbeter.

Dedicated to my parents.

ACKNOWLEDGEMENTS

First and foremost I want to thank my promotor Prof. Cornie Scheffer. I thank him for his patience, insights and suggestions which were invaluable in completing my dissertation.

I am grateful to Dr. Spike Erasmus and Dr. Edwin Dillon for their guidance and valuable input, which made the research possible. I also thank Cobus Muller and Garth Cloete, who advised me and helped me in various aspects of my research. I am also grateful to all staff, students and friends, who gave me support in my research and life during the course of the project.

Last but not least, I thank my parents and Cherisse for their support and for always believing in me. Without your support this would never have been possible.

TABLE OF CONTENTS

LIST OF FIGURES

LIST OF TABLES

1. INTRODUCTION

The knee, located between the body's two longest lever-arms, sustains high forces and is the biggest, most complicated and incongruent joint in the body (Biščević et al., 2005). Due to the high forces, the knee is susceptible to injury and chronic diseases of which osteoarthritis (OA) is the most common (Sherwood et al., 2002), (Krevolin, 2003), (Saxler et al., 2004). Osteoarthritis is the softening and degradation of the cartilage and the subchondral bone of joints. In the case of OA in the knee, the major bones making up the knee joint rub against one another, causing pain and stiffness. This can lead to the loss of function of the knee which can severely impact the quality of life of the patient.

The most common treatments for OA include high tibial osteotomy (HTO), unicompartmental knee replacement (UKR) and total knee replacement (TKR) (Sugita et al., 2000). HTO is a surgical procedure whereby the tibia is cut to re-establish correct alignment with the femur. UKR and TKR are surgical procedures in which the articulating surfaces of the joint are replaced by prostheses. In some cases only one side of the joint is affected and it is better to only replace the affected compartment. Such a knee replacement is known as an unicompartmental knee replacement. Figure 1-1 shows a UKR where only the affected compartment is replaced and a TKR where all three compartments are replaced.

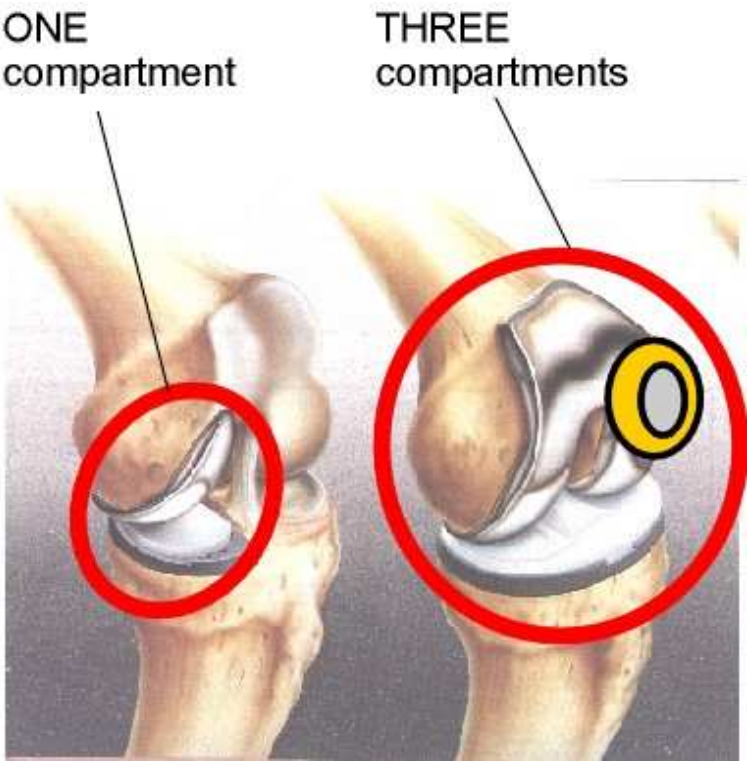

Figure 1-1: Unicompartmental knee replacement and total knee replacement (Total joints, 2011)

The main aim of the procedures is to relieve pain and restore normal function to the joint (Krevolin, 2003). Over 350 000 TKRs are performed annually in the United States alone, and the number is increasing (Eisenhuth et al., 2006), (Harrysson et al., 2007).

An ideal knee replacement prosthesis would have an articulating geometry similar to that of the patient's healthy knee and allow for normal activities and motion. This would imply restoring the degenerated articulating portions of the femoral condyles to the original geometry and level. TKR has shown good success rates over a long period of time (Font-Rodriguez et al., 1997), (Ma et al., 2005), (Gioe et al., 2007). However, in recent years, UKR has shown an improvement in success rate that compares to that of TKR (Grelsamer, 1995), (Cartier et al., 1996), (Svärd & Price, 2001). In appropriate cases, UKR has an advantage over TKR that can include a better range of motion, preservation of the bone, a shorter recovery time, maintenance of normal cruciate ligament function and more normal kinematics (Pinczewski, 2003), (Meek et al., 2004), (Keene & Forster, 2005).

It is suggested that UKR restores normal knee kinematics better than TKR because the cruciate ligaments are retained; however, it is still very different than natural knee kinematics. This is due to the fact that most UKR and TKR prosthesis designs are available in standard sizes only and the surface geometry in the sagittal and transverse planes is of a specific single- or multi-radius design that is predetermined by the manufacturer (Figure 1-2). The geometry of the prosthesis severely affects the kinematics of the knee joint after knee replacement surgery (Walker & Sathasivam, 2000), and it is argued that the long-term performance of a knee replacement is dependent on the kinematics of the knee joint (Shi, 2007). It is therefore important to select the appropriate prosthesis for any individual patient to ensure restoration of the normal geometry. This research focused on restoring an individual patient's knee joint to its original geometry by using a patient-specific UKR.

A brief overview of the dissertation is given below:

Background to the knee joint and knee replacements is discussed in Chapter 2. Chapter 3 investigates an improved method for selecting the ideal femoral component in TKR from commercially available prostheses. However, this option is not always ideal, as the normal knee has a much more complex geometry than provided by standard knee replacements. Consequently, Chapter 4 investigates the complex profiles of the femoral condyles and proposes a mathematical model to reconstruct the articulating profiles. In Chapter 5, anatomical differences between genders and races are investigated to address the need for separate knee

replacements. Chapter 6 presents a novel method of designing and manufacturing a patient-specific UKR that has a complex anatomical geometry.

Chapter 7 compares the contact stresses in a patient-specific UKR to conventional UKRs, while Chapter 8 investigates the knee kinematics using patient-specific UKRs. Finally, Chapter 9 discusses the findings of this research and presents conclusions and recommendations.

Figure 1-2: Standard shapes and sizes of conventional knee replacement designs (BioMet, 2011)

Contribution of this research

This study first looks at a method of selecting the ideal prosthesis type and size in total knee replacement for a specific patient. This option, however, is not always viable and the main aim of the study is thus to introduce a novel method for designing a custom (patient-specific) knee replacement. The original contributions of this study to the field of knowledge are:

- Using a χ^2 goodness-of-fit method for selecting the ideal implant from a wide range of different implant types and sizes (Chapter 3).
- Making use of self-organising maps (SOM) and mathematical models to predict the original articulating surfaces of affected knee joints. This forms

the basis for designing patient-specific knee replacements (Chapter 4 to Chapter 6).

- Comparing the contact stresses of patient-specific implants with conventional implants (Chapter 7).
- Comparing the kinematics of patient-specific implants to the natural knee and conventional knee implants (Chapter 8).

All these points collectively contribute to the field of knowledge of knee replacements.

2. LITERATURE

Biomechanics is the application of mechanical principles, and often engineering sciences, to biological systems. A definition of biomechanics is given by Hatze (1974): “Biomechanics is the study of the structure and function of biological systems by means of the methods of mechanics.” In this sense, the knee can be seen as a biomechanical system consisting of complex structures interacting with each other in a dynamic way. Before the anatomy and physiology of the knee are introduced, it is first necessary to define the anatomical planes of the human body. These are shown in Figure 2-1.

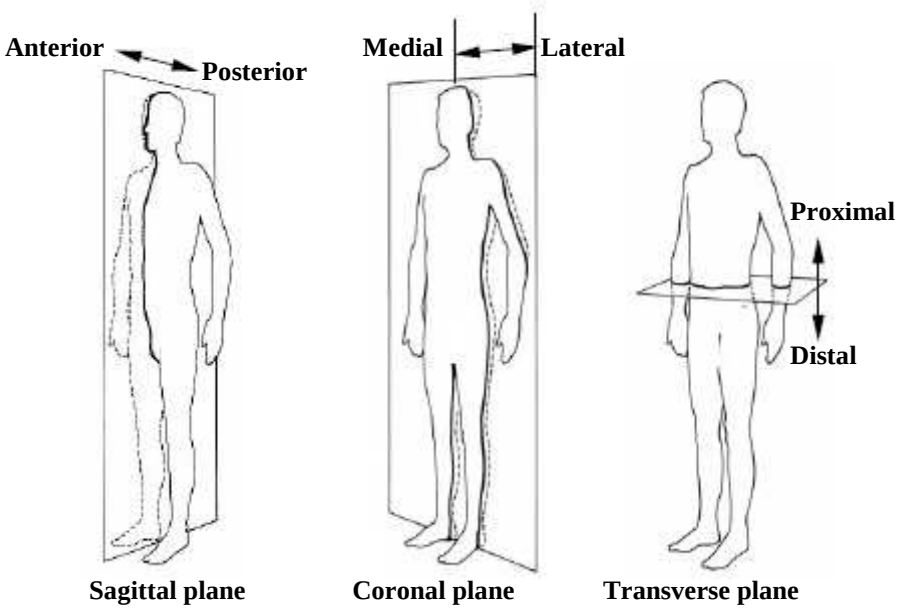

Figure 2-1: Anatomical planes of the human body

The sagittal plane divides the body into right and left portions, with the anterior direction towards the front and posterior towards the back. The coronal plane divides the body into front and back portions, with the lateral direction to the outside and the medial direction inside, towards the middle. The transverse plane divides the body into upper and lower portions, with the proximal direction to the top and the distal direction towards the bottom. These are the main planes and directions that will be used throughout the dissertation.

2.1 Anatomy of the normal knee joint

The knee is the largest and most complicated joint in the human body (Biščević et al., 2005), (Shi, 2007). The knee is a joint connecting the femur (thigh bone), patella (knee cap) and the tibia (shin bone). The fibula, connected to the tibia, also forms part of the knee joint. Figure 2-2 shows the main components of the knee joint. In humans, the knees support almost the entire weight of the body and are therefore very vulnerable to injury and to the development of osteoarthritis. Osteoarthritis is the abnormal wearing of the cartilage that covers the joints, as well as the decrease of synovial fluid, which acts as lubricant for the joints. This results in low-grade inflammation of the joints, which leads to pain and can greatly affect the quality of life of a person. For instance, simple tasks like walking or climbing stairs can become difficult. Movement of the knee can be separated into the two major articulations within the knee, the tibio-femoral articulation and the patello-femoral articulation.

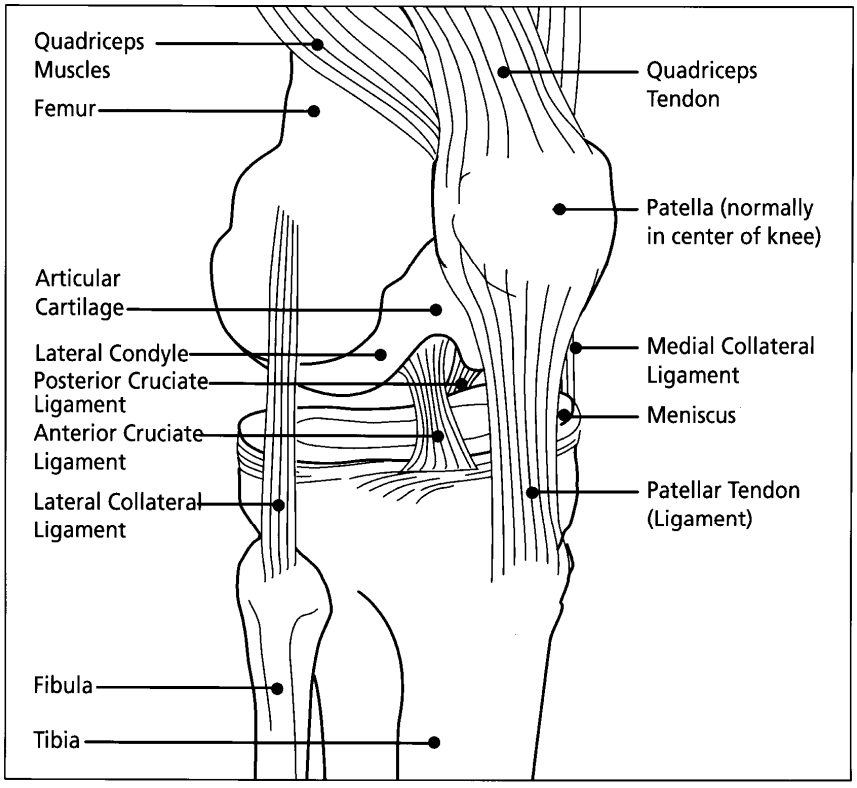

Figure 2-2: Main components of the knee joint (MDchoice, 2009)

2.1.1 The tibio-femoral joint

Contact is made between the tibial plateau and the two condyles on the distal end of the femur. The femoral condyles are known as the medial and lateral condyles, referring to their position. These condyles are covered with a thin layer of cartilage. Two fibro-cartilaginous discs, known as the menisci, lie between the tibia and femoral condyles. The meniscus compensates for the incongruence of the two articulating bones. The femoral condyles articulate with the tibial plateau, forming the tibio-femoral joint. The knee moves with excitation of the quadriceps and hamstring muscles, which flex and extend the knee. The geometry of the articulating surfaces and the knee ligaments govern knee movement. When the knee moves, it does not just flex and extend, but it also has a slight medial and lateral rotation (Knee Joint, 2008).

2.1.2 The patello-femoral joint

The patella glides up and down the anterior surface of the femur as the knee moves, and forms the patello-femoral joint. The primary role of the patella is to transfer forces in the quadriceps tendon to the patellar tendon (Figure 2-2) (Huberti & Hayes, 1984). From a biomechanics viewpoint, the patello-femoral joint was originally thought of as a frictionless pulley (Reilly & Martens, 1972), (Hungerford & Barry, 1979). However, it was found that the quadriceps force does not equal the patellar tendon force, contradicting this viewpoint (Huberti & Hayes, 1984), (Nissel & Ericson, 1992), (Krevolin, 2003). The patella transfers the quadriceps force as a bearing surface for the quadriceps tendon, and as a biomechanical lever (Krevolin, 2003). The effective capacity of the quadriceps during extension is increased by this lever action (Krevolin, 2003).

2.1.3 Ligaments

The femur and tibia are held together by ligaments. There are four main ligaments in the knee joint, the lateral and medial collateral ligaments (LCL and MCL), as well as the posterior and anterior cruciate ligaments (PCL and ACL). These are displayed in Figure 2-2. The ligaments work together to stabilise the knee joint and play a crucial role in its kinematics. The LCL and MCL are attached on the sides of the joint and are responsible for the side-to-side stability of the joint. The ACL lies to the front, in the centre of the knee joint, and restricts anterior movement of the tibia relative to the femur. The PCL restricts posterior movement of the tibia relative to the femur and lies to the back of the knee joint.

2.2 Knee kinematics

The knee joint has six degrees of freedom, as is shown in Figure 2-3. It is important to note that the knee joint is not a pure hinge joint, but moves with a complex set of translations and rotations in all six degrees of freedom (Shi, 2007). During normal flexion of the knee, tibio-femoral motion is a combination of sliding and rolling motion between the contacting tibia and femoral condyles. The motion is constrained by the geometry of the bones, as well as the menisci and the muscular attachments via ligaments and tendons. The knee can only reach full extension with a small amount of external tibial rotation on the femur. This is due to the fact that the medial condyle is typically in the order of 12 mm longer than the lateral condyle. This tibial rotation is known as the 'screw home' mechanism and it allows the knee to be held in full extension without undue fatigue of the surrounding muscles (Shi, 2007). The shapes of the articulating surfaces in the knee are the most important factor when dealing with knee movement.

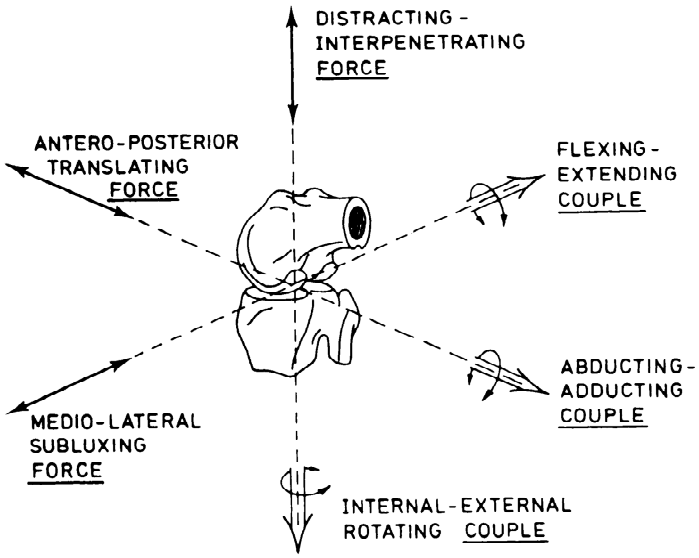

Figure 2-3: Reference directions for knee movement

(Goodfellow & O'Connor, 1978)

2.2.1 Tibio-femoral motion

The geometry of the posterior condyles was first reported to be circular and roughly of the same size in 1836 by Weber and Weber (Freeman & Pinskernova, 2005). This hypothesis has been used in numerous kinematics-related studies

(Elias et al., 1990), (Hollister et al., 1993), (Freeman, 2001), (Williams & Logan, 2004) and is still very popular today.

Freeman (2001) proposes that the flexion arc can be divided into three segments. The mode of articulation differs for each portion as the shape of the condyle changes. The active functional arc is the portion ranging from about 20º to 120º. This part is known as the Flexion Facet (FFC). The 'screw-home' arc stretches from 20º to full extension and is also known as the Extension Facet (EFC). The third portion is known as the passive arc and stretches from about 120 º to full flexion. The three portions are shown in Figure 2-4.

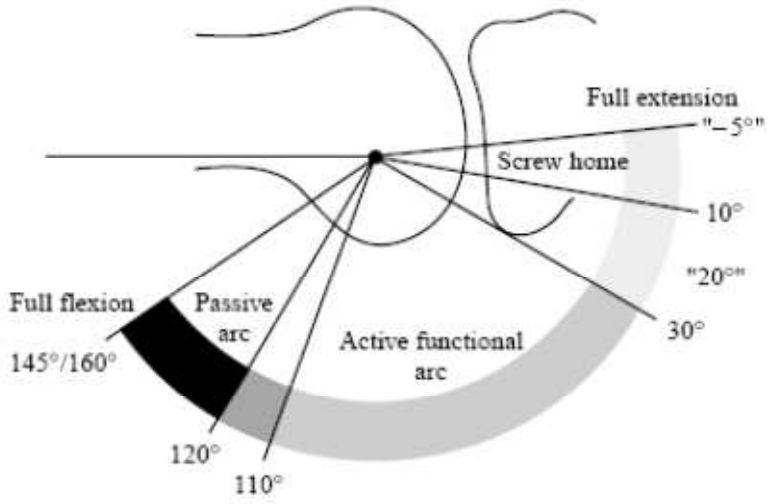

Figure 2-4: The three arcs of flexion (Freeman, 2001)

Freeman and Pinskernova (2005) suggest that the active functional arc, or FFC, is circular with a radius in the order of 22 mm. This applies to both the medial and lateral condyles. The 'screw-home' arc, or EFC, has a larger radius compared to the FFC. Freeman and Pinskernova suggest a radius of 32 mm on the medial side with a span of 50º. In the case of the lateral condyle, the EFC radius is so large that it becomes almost flat, and it also has a shorter span than the medial condyle. The extreme posterior portion, the passive arc, has a smaller radius than the FFC only on the medial side, but is not exactly defined. This part of the condyles only comes into contact with the posterior horn of the meniscus (Figure 2-5) and is known as the posterior horn facet (PHF).

According to Kosel et al. (2010), there exists a problem of modelling the distal femoral condyle surface with distinct portions of different radii, as described above. This problem arises at the junction where the radii have to change abruptly from the one portion to the other. Kosel et al. (2010) investigated the curvature of 16 cadaver distal femurs and found continuous varying radii for both the medial and lateral condyles. The anatomy of the distal femur affects the location of the flexion-extension axis, and continuous varying radii of the condyles results in a flexion-extension axis that continuously changes its position during flexion-extension. This is known as the *instantaneous centre of rotation* and has been described by numerous studies (Frankel et al., 1972), (Walker et al., 1972), (Blacharski et al., 1975), (Soudan et al., 1979), (Shiavi et al., 1987).

Freeman and Pinskernova (2005) also investigated the shape of the medial and lateral parts of the tibia. The medial tibial surface is believed to be posteriorly flat and horizontal for about 25 mm. To the anterior there is an upward slope of 11º (Figure 2-5). The lateral tibial surface is usually thought of as being convex. Freeman and Pinskernova (2005), however, argue that where the femur makes contact, the surface is flat. Anteriorly and posteriorly there are downward curves, to receive the horns of the meniscus, which gives the impression of convexity.

a) b)

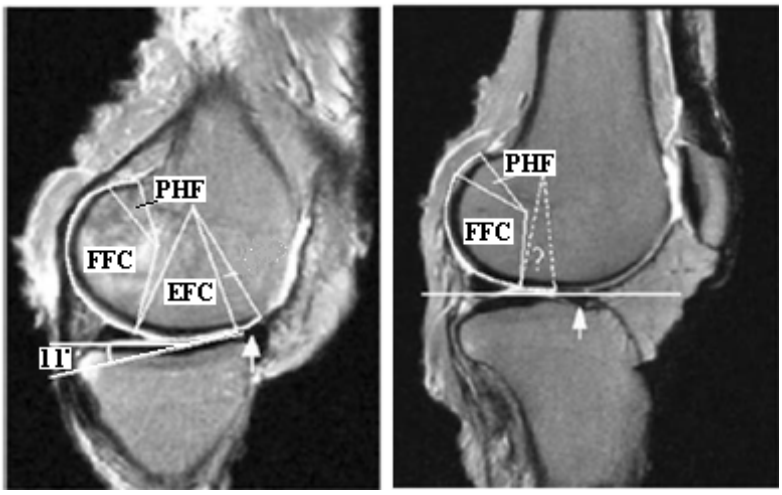

Figure 2-5: Sagittal view of a) Medial femoral condyle and tibia, b) Lateral femoral condyle and tibia (Freeman & Pinskernova, 2005)

Note:	
FFC	Flexion Facet
EFC	Extension Facet
PHF	Posterior Horn Facet

With a general understanding of the shape of the femur and tibia, attention can be turned to the movement of the tibio-femoral joint. In order to define the relative motion between the femur and tibia, numerous techniques have been used including a very fast computed tomography (CT) scanner called a cine-CT (Shapeero et al., 1988), CT combined with computerised image matching (Asano et al., 2001), CT combined with fluoroscopy, X-rays combined with fluoroscopy (Kanisawa et al., 2003), (Komistek et al., 2003), radiographs with CT (McPherson et al., 2005), conventional MRI (Niitsu et al., 1990), (Ando et al., 1994) or 'interventional' MRI (Williams & Logan, 2004). MRI has been validated against dissection, 3D digitisation and radiograph/CT (Freeman & Pinskernova, 2005).

Using such techniques, the relative motion of the articulating surfaces of the knee has been well documented (Shapeero et al., 1988), (Niitsu et al., 1990), (Ando et al., 1994), (Asano et al., 2001), (Freeman, 2001), (Kanisawa et al., 2003), (Komistek et al., 2003), (Williams & Logan, 2004), (Freeman & Pinskernova, 2005), (McPherson et al., 2005). In the medial compartment there is little anterior-posterior movement of the femur on the tibia from full extension to about 120º flexion. After that there is a sharp posterior displacement (± 10 mm) as the knee moves into passive flexion and the femur makes contact with the posterior horn of the meniscus. This range of movement is shown in Figure 2-6.

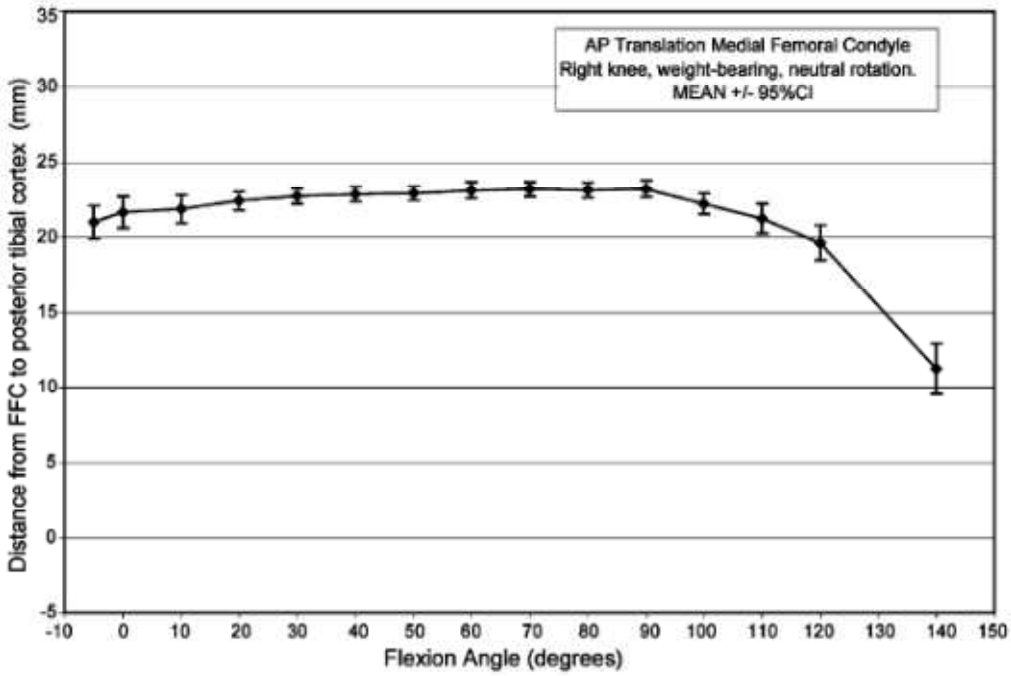

Figure 2-6: Anterior-posterior (AP) movement of the medial compartment of the knee joint (Williams & Logan, 2004)

Laterally, the femur moves posterior throughout the movement from extension to 120º flexion, with an approximate displacement of 20 mm. Going into passive flexion the femur again shows a sharp posterior movement of ± 10 mm. This is shown in Figure 2-7.

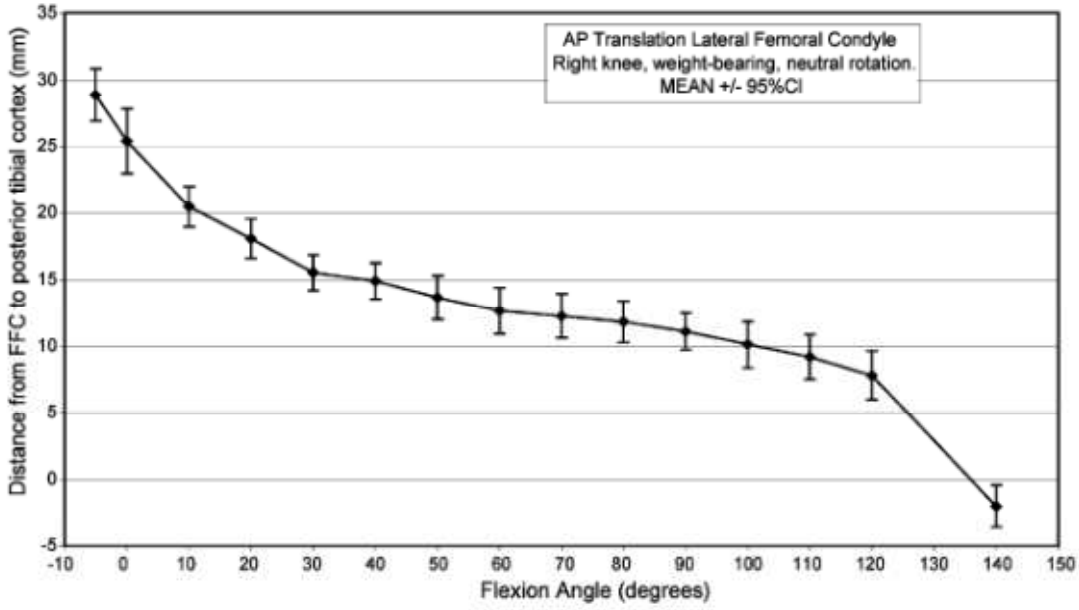

Figure 2-7: Anterior-posterior (AP) movement of the lateral compartment of the knee joint (Williams & Logan, 2004)

The surfaces in the coronal plane are also important, as they influence the movements of longitudinal rotation (Freeman & Pinskernova, 2005). The cross-sections of the femoral condyles are circular in the posterior part. As a result, the medial condyle can be seen as spherical in that region because the radius is similar to that of the posterior medial condyle in sagittal view (Kurosawa et al., 1985). The tibial surface on the medial side is also circular, making the medial compartment almost a ball-in-socket joint in flexion (Figure 2-8). The lateral femoral condyle has a flattened portion on the medial side. This is more prominent distally and has a slope of 21º to the horizon (Martelli & Pinskernova, 2002).

Figure 2-8: Frontal section of the knee

(Martelli & Pinskernova, 2002)

The ball-in-socket characteristic of the medial compartment suggests that abduction/adduction rotation (Figure 2-3) might occur around the medial femoral condyle, causing an inward angulation of the tibia. Such a rotation is known as a varus rotation. This may cause lift-off on the lateral side. Valgus rotation causes an outward angulation of the tibia. Internal-external rotation also occurs around the same centre.

2.2.2 Patello-femoral motion

Patello-femoral kinematics mainly involves patellar tracking, i.e., the path followed by the patella during flexion-extension. Numerous in vitro and in vivo patellar tracking studies have been conducted (Heegaard et al., 1994), (Ahmed & Tanzer, 1999), (Katchburian et al., 2003), (Shih et al., 2004), (Amis et al., 2006). The general pattern is one where there is a slight medial translation of the patella from full extension until it engages the trochlear groove. The trochlear groove is the anterior portion of the femur where the two condyles form a distinct groove.

Once engaged in the trochlear groove, the patella is guided by the geometry of the trochlear groove and translates laterally up to 90º knee flexion. Throughout flexion, the patella also experiences a slight lateral tilt. Patellar maltracking refers to the condition when the patella is not following a normal path of movement within the trochlear groove during knee flexion.

2.3 Mechanical properties of bone

Bones are anisotropic (properties are directionally dependent), heterogeneous (consist of multiple parts with large structural variations) and viscoelastic (exhibit time-dependent strain) organs that form part of the endoskeleton of vertebrates. At the macroscopic level, bone tissue can be divided into two major forms, cortical and cancellous. The structure of bone is shown in Figure 2-9.

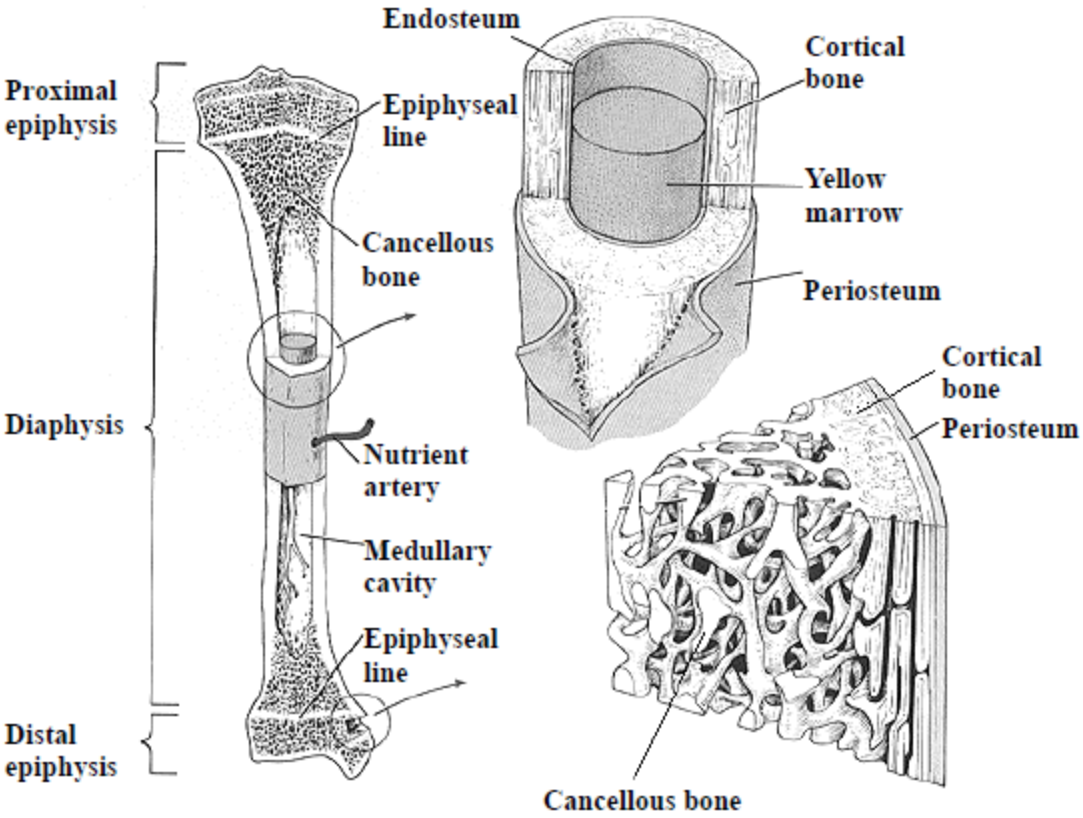

Figure 2-9: Structure of bone (Spence, 1990)

As the name implies, cortical bone forms the cortex, or outer shell, of most bones and it has a compact and stiff structure with a maximal density of about 1.8 g/cm^3. Cancellous bone (also called trabecular bone) on the other hand, has a porous structure and is less dense and stiff with a density that varies from 0.05 to 0.7

g/cm^3 (Terrier, 1999). It typically occupies the inner region of the bone and the pores are filled with marrow.

The anisotropy of cortical bone is mainly caused by the alignment of the osteons along the longitudinal axis of long bones like the femur and tibia. Osteons are cylindrical structures, typically several millimetres long and around 0.2 mm in diameter, that are present in the cortical bones of mammals. Because of this, the longitudinal elastic modulus is about 50% greater than the transverse elastic modulus. The shear modulus and Poisson ratio are also different in the longitudinal and transverse directions (Shi, 2007). The mechanical properties of cortical bone as described by Reilly and Burstein (1975) are shown in Table 2-1. Reilly and Burstein carried out the experiments on femoral diaphyseal cortical bone. The mechanical properties of cancellous bone are dependent on where they are measured and they also show variability between different studies (Linde et al., 1992), (Kopperdahl & Keaventy, 1998), (Fyhrie & Vashishth, 2000), (Morgan & Keaveny, 2001). The Young Modulus varied between 344 Pa in the human vertebra to 3230 Pa in the femoral neck (Morgan & Keaveny, 2001). This is due to the structural nature of cancellous bone, which will be different at different positions and will also differ between different subjects.

Table 2-1: Mechanical properties of cortical bone (Reilly & Burstein, 1975)

Mechanical property	Longitudinal	Transverse
Young's modulus (MPa)	17 000	11 500
Ultimate tensile strength (MPa)	133	51
Ultimate compressive strength (MPa)	193	133
Ultimate strain	3.1%	0.7%

Bone also has the peculiar characteristic of remodelling. Bone remodelling is the continuous process of resorption and densification of the bone in response to changed mechanical loading. Wolff (1986) studied the relationship between mechanical environment and bone structure and suggested the important hypothesis that bone grows wherever it is needed and resorbs where it is not needed. In artificial joint replacement, like knee replacement, the orthopaedic implant is in direct contact with the bones, and alters the stress distribution within the bones. This induces a functional adaptation of the bone tissue (Shi, 2007). In

knee replacement, this bone reaction can last for several years and can lead to failure of the implant or even permanent bone loss for revision.

Soininvaara et al. (2002) argue that the undesired bone loss around implants occurs mainly because of a stress-shielding phenomenon. Bone surrounding the implant adjusts its bone mineral density (BMD) and structure to meet the new mechanical demands introduced by the implant. Hazelwood et al. (2001) developed a model for bone remodelling that simulated bone structure and material property changes due to disuse and damage. This model was used by Nyman et al. (2004) to simulate the bone remodelling in long-stemmed TKR procedures. The relationship between changes in BMD in the proximal tibia and fixation of the tibial component was investigated in a study by Li and Nilsson (2001). They found that changes in the BMD assessed below the interface were not the main cause for migration, but rather local activities at the interface.

The effect of bone remodelling suggests that an uneven stress distribution produced by knee replacement implants can greatly affect bone density and structure. Removing little or no bone from the femur, and therefore not altering the femur shape significantly, will produce more uniform stress distributions. This will lead to little or no bone remodelling. At the tibia it is necessary to ensure that the cortical rim sustains most of the pressure from the tibial component. A more anatomically correct, or a custom tibial component, would therefore be ideal to ensure complete cortical rim coverage.

2.4 Knee replacement

Common causes of knee pain and loss of normal knee function include osteoarthritis (OA), rheumatoid arthritis and post-traumatic arthritis. OA usually occurs in the elderly population and is the degradation of the cartilage that cushions the bones of the knee joint. The bones are then exposed and rub against one another, causing pain and discomfort (Shi, 2007). The prevalence of OA in younger patients is increasing and is presumably the result of a change in lifestyle, with more physically demanding leisure-time activities and sports. These lead to more injuries to the ACL, the menisci and the articular surfaces (Laskin, 2002), (Henricson, 2008).

The most common treatments for osteoarthritis include high tibial osteotomy (HTO), unicompartmental knee replacement (UKR) and total knee replacement (TKR) (Sugita et al., 2000). Osteotomy is a surgical operation whereby bone is cut away and, in the case of HTO, a wedge is removed from the tibia underneath the healthy side of the knee. This forces the tibia and femur to shy away from the

damaged side of the knee. UKR is a procedure in which only the damaged compartment of the knee joint is replaced with a prosthesis. In contrast, TKR is a procedure in which the entire knee joint is replaced with a prosthesis.

The first attempt to replace the human knee joint with an artificial implant was made by Gluck in 1890, using ivory components to replace the articulating surfaces (Daněk et al., 2007), (Henricson, 2008). The modern era of knee replacement began in 1971, when Frank Gunston introduced an implant using a metal component articulating against a polyethylene component to replace the articulating surfaces (Gunston, 1971), (Henricson, 2008). The popularity of the procedure has since increased and more than 350 000 knee replacement surgeries are performed in the US alone each year (Eisenhuth et al., 2006). The surgical procedure was at first focussed on total knee arthroplasty, during which two or three compartments of the joint were replaced with prostheses. The three compartments refer to the medial and lateral tibial-femoral compartments and the patella-femoral compartment. However, it was found that, in some patients, the joint disease was restricted to only one compartment of the knee. Accordingly, unicompartmental knee replacements were developed. UKR was developed in the 1970's and has also gained popularity in recent years (Vardi & Strover, 2004). The main aim of both the procedures is to relieve pain and restore normal function to the joint. The success of achieving this depends on how closely the procedure replicates the normal biomechanics of the knee (Krevolin, 2003). A unicompartmental and total knee replacement are shown in Figure 1-1.

2.4.1 TKR

There are more than 150 TKR designs on the market today, from several different manufacturers (American Academy of Orthopedic Surgeons, 2008). The design used by a surgeon is influenced by numerous factors, including the patient's age, weight, activity level and health; the doctor's familiarity and experience with a specific design; and the performance record of the design (Sharkey et al., 1999). Different TKR systems can vary in shape, materials, fixation and surgical technique, but they usually consist of: an anatomically shaped femoral component, a tibial component and an optional patellar component. The femoral component is normally made of a hard metal, such as a cobalt-based alloy, and articulates against the tibial component, which is normally made of ultra-high molecular weight polyethylene (UHMWPE). The tibial component can have an optional metal backing.

Typically, TKRs require the ACL to be removed, but retaining or sacrificing the PCL lies at the surgeon's discretion, depending on the state of the PCL. Retaining

the PCL increases knee stability and improves knee kinematics. However, the PCL load is increased with a TKR because anterior movement of the tibia is limited to the posterior upward slope of the conforming tibial components (Walker & Garg, 1991), (Krevolin, 2003). The amount of passive flexion and the functional range of motion during weight-bearing activities may reduce due to excessive load in the PCL (Walker & Garg, 1991), (Andriacchi, 1993). Due to these reasons, many surgeons insist on sacrificing the PCL. This requires a special TKR design that provides the stability associated with the PCL in the normal knee. This is usually achieved by a cam and post mechanism added to the prosthesis components (Conditt et al., 2004), (Bauer et al., 2010).

TKR has shown good success rates over a long period of time (Font-Rodriguez et al., 1997), (Pagnano et al., 1999), (Worland et al., 2002), (Illgen et al., 2004), (Ma et al., 2005), (Gioe et al., 2007). Ma et al. (2005) report success rates of 91.9% with a 20-year follow-up period. These rates were divided between 96.4 % survival for the all-polyethylene tibial component and 88.4% survival for the metal-backed tibial component. Survival refers to an implant that showed no complications. After biomechanical studies, a metal-backed tibial component was developed to improve the tibial fixation and loading and this component is also used for mobile-bearings (Lewis et al., 1982), (Bartel et al., 1986). Finite element analysis (FEA) suggests that using a metal backing would distribute the load more evenly to the tibial bone, thus assisting the prevention of loosening. However, the results of Ma et al. (2005) suggest that metal-backed tibial components showed a lower survivorship than the all-polyethylene components. This can be due to micromotion between the insert and metal backing, which causes undersurface backside wear that may contribute to tibial osteolysis (Wasielewski et al., 1997). Udomkiat et al. (2001) failed to find any statistically significant differences between all polyethylene and metal-backed tibial components.

2.4.2 UKR

Unicompartmental knee replacement (UKR) has enjoyed a resurgence in popularity of late that can be contributed to better success rates and the mini-incision technique (Repicci, 2003), (Bert, 2005). The success rate of UKRs has improved in recent years and is comparable to that of TKRs. The UKR success rate improved from between 37% and 92% in the early 1970's and 1980's to between 87% and 98% with six to 14-year follow-ups, as reported for the period 1993 to 2003 (Marmor, 1977), (Laskin, 1978), (Insall & Aglietti, 1980), (Cameron et al., 1981), (Bae et al., 1983), (Grelsamer, 1995), (Cartier et al., 1996), (Svärd & Price, 2001), (Gioe et al., 2003), (Bert, 2005). UKR has been shown to have clear advantages over TKR and HTO. These advantages include

speed of recovery (due to minimal invasive surgery), less bone loss, improved range of motion, reduced blood loss, functional outcome and complication rates in properly selected patients (Newman & Weale, 1994), (Laurencin et al., 1991), (Rougraff et al., 1991), (Newman et al., 1998), (Emerton & Burton, 2001), (Bert, 2005), (Keene & Forster, 2005). Also, in 1998, Lewold noted that conversion from UKR to TKR is easier and more successful than conversion from HTO to TKR (Lewold, 1998). In a study conducted by Bert (2005), 75% of patients who had UKR in one knee and TKR in the other noted that the UKR implant "feels closer to a normal knee" (Figure 2-10).

Figure 2-10: TKR and UKR in same patient (Bert, 2005)

The disadvantages of UKR include poor fixation as well as poor instrumentation and design (Bert, 1991), (Bert, 2005). However, the most important factor for the success of UKR is appropriate patient selection (Bert, 2005). There are certain accepted requirements for UKR, the most obvious being that the arthritis be isolated to one compartment only. Other requirements include (Emerton & Burton, 2001), (Bert, 2005):

- An intact anterior cruciate ligament (ACL).
- Less than 10º of fixed flexion deformity.
- Less than 10º of varus deformity.
- Flexion of more than 90º.
- Diagnosis should be degenerative arthritis.

- Patient should not be obese.

It is suggested that UKR restores normal knee kinematics better than TKR because of retaining the cruciate ligaments; it is however still very different than natural knee kinematics. This can be attributed to the complex, asymmetrical geometry of the condyles and articulating tibial surfaces of the normal knee.

In commercially available prostheses, the surface geometry of the femoral component in sagittal view is either of a specific single- or multi-radius design that is predetermined by the manufacturer. This geometry does not necessarily present the true radius of a specific knee. Most manufacturers also develop only one UKR, to be used on either the lateral or the medial side, even though there is a difference in geometry and movement between the two (Ashraf et al., 2002), (Näger et al., 2008). The same applies to the medial-lateral radius of both the medial and lateral condyles when viewed in the coronal plane. It has been shown that the lateral condyle has a flattened shape medially when viewed in the coronal plane (Kurosawa et al., 1985), (Martelli & Pinskernova, 2002).

The curvatures of the individual condyles, as viewed in the transverse plane, are also ignored and, in most designs, there is no difference between the design for the medial and lateral condyles. In practice, the curvature on the medial side is much more pronounced than on the lateral side. These anatomical differences between medial and lateral condyles, together with the other structures of the knee joint, produce the complex movement of the natural knee joint. A successful knee replacement should restore normal knee kinematics. In order to improve the kinematics of a knee replacement system, to reduce polyethylene wear and to lower the risk of tibial component loosening, a mobile-bearing knee replacement design was developed (Goodfellow & O'Connor, 1986), (Henricson, 2008).

2.4.3 Mobile and fixed-bearing designs

As mentioned in the preceding paragraph, there are two main types of prostheses, namely fixed-bearing and mobile-bearing prostheses. Fixed-bearing prostheses are the most commonly used replacement, consisting of a polished metal shell on the femur, a high-density polyethylene piece on top of a metal tray attached to the tibia (or an all-polyethylene tibial component), and a high-density polyethylene piece replacing the kneecap (Medline Plus, 2008). In Figure 2-11, a fixed-bearing TKR is shown. It can be seen that the polyethylene insert clicks into place in the tibial tray, thus fixing the insert to the tray. Excessive activity and extra weight may increase the wear rate in fixed-bearing prostheses.

Mobile-bearing prostheses use a polyethylene insert across which the femur and tibia move. This creates a dual-surface articulation. Mobile-bearing knee prostheses are designed to allow greater rotation of the knee, but they are less forgiving of imbalances in the soft tissue and they cost more. Different ranges of mobility of the mobile-bearing prostheses are offered by different designs, some only permitting rotation, others rotation and some anterior-posterior translation, and some permitting totally unconstrained mobility. In Figure 2-11 a rotating platform mobile-bearing TKR is shown that permits rotation around a securing pin.

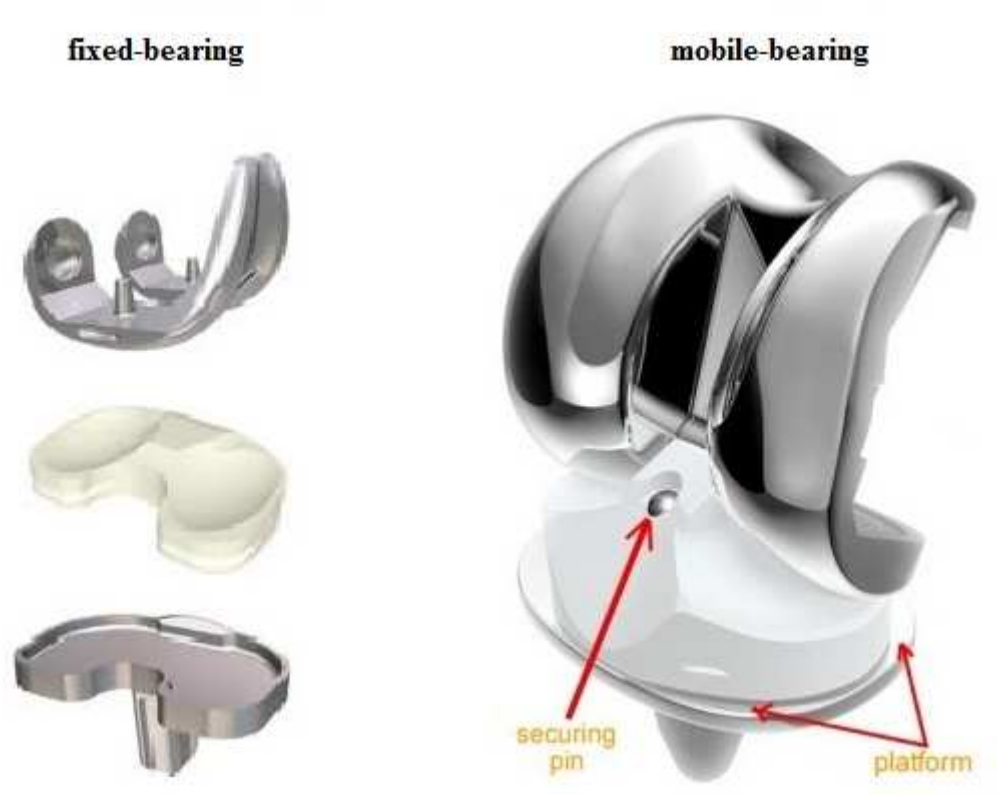

Figure 2-11: Mobile-bearing and fixed-bearing total knee replacements (Josephine, 2010)

Mobile-bearing designs have enjoyed much popularity in recent times due to their theoretical advantages over fixed-bearing designs (Lädermann et al., 2008). These theoretical advantages include more normal tibio-femoral kinematics, reduced loosening forces at the bone-implant interface, improved stress distribution between the articulating components, the minimising of polyethylene wear, and decreased problems with stability (Goodfellow & O'Connor, 1978), (Buechel &

Pappas, 1989), (Buechel & Pappas, 1990), (O'Connor & Goodfellow, 1996), (D'Lima et al., 2000). Studies indicate, however, that there is no advantage of using a mobile TKR design over a fixed TKR design with a follow-up of over five years (Kim et al., 2001), (Kim et al., 2007), (Lädermann et al., 2008). This was demonstrated with respect to the American Knee Society score (AKSS), pain score, range of motion and complication rates. However, the contact stress of a mobile-bearing implant is reported to be substantially lower than in a fixed-bearing implant (Tsakonas & Polyzoides, 1997), (Matsuda et al., 1998), (Stukenborg-Colsman et al., 2002), (Sharma et al., 2007).

The literature contains several studies comparing mobile-bearing to fixed-bearing UKRs; however, the results are contradictory. Emerson et al. (2002) reports better component survivorship for mobile-bearing UKRs, and Li et al. (2006) found that the use of mobile-bearing UKRs produces better knee kinematics and further report that the mobile-bearing knees had a lower incidence of radiolucency at the bone implant interface (8% vs. 37%). No differences were found regarding pain relief. Gleeson et al. (2004), however, report better results in terms of knee function and pain relief for patients that received a fixed-bearing UKR. Confalonieri et al. (2004) found no statistically significant difference in outcomes between the two groups. Figure 2-12 shows a picture of a typical mobile-bearing UKR, the Oxford mobile-bearing UKR.

Mobile-bearing UKRs do have the advantage of allowing for unconstrained movement, which can improve knee kinematics. This is especially important for the lateral compartment of the knee joint, as it was shown to have greater anterior-posterior displacement than the medial side. Internal and external rotation should also be considered. Mobile UKRs are suitable for younger, active patients as a result of this improved knee movement. Another advantage of mobile-bearing UKRs is that they compensate for slight misalignment on the surgeon’s part, as the polyethylene insert can self-align into the correct position.

The major disadvantage of mobile-bearing UKRs is the ease with which the polyethylene insert can move out of the intended area and get stuck in that position. This causes pain and discomfort. This is the case when the selected insert is too small, thus allowing too much movement.

Figure 2-12: Oxford mobile-bearing UKR

(Weiss Joint University, 2009)

2.4.4 Cemented vs. cementless fixation

Another consideration in TKRs and UKRs is the fixation method used to hold the prostheses in place. The two types of fixation are cemented and cementless. Cemented fixation relies on fast-curing bone cement and a solid mechanical bond to hold the prostheses in place. Cementless fixation relies on bone growing into the special surface topography to hold the prostheses in place. Again, results found in literature are contradictory. Chockalingam et al. (2000) investigated the survivorship difference between cemented and cementless fixation of the femoral component at a six year follow-up period. The incidence of loosening of the component was found to be 9.8% with cementless fixation and 0.6% with cement.

This suggests that cemented fixation has a slight advantage over cementless fixation. However, Gao et al. (2009) found that uncemented components behave as well as cemented components, and Schrøder et al. (2001) also found very good results with uncemented femoral components. However, cemented tibial components tend to perform better than their uncemented counterparts and Lachiewics (2001) stated that they were the gold standard (Duffy et al., 1998), (Lachiewics, 2001), (Cloke et al., 2008). It can be argued that a better designed prosthesis (i.e. a better bone-implant interface as is the case with custom prostheses) will produce better results for a cementless component.

2.4.5 Knee replacement failures

Loosening of the components is not the only type of failure in knee replacement. The femoral component in a knee replacement implant is typically made of a cobalt-chrome alloy (CoCr). This is a very hard and durable material and has the good ability to wear a highly polished surface that is durable. Softer materials, such as titanium alloy, scuff easily and cannot hold a polished surface for very long. The tibial tray is typically made of titanium alloy or CoCr, and either material is acceptable because of lesser relative movement between components. The tibial bearing component (the bearing component between the femoral component and tibial tray) is made of a plastic called ultra-high molecular weight polyethylene (UHMWPE).

More than 35 000 TKR revisions are performed worldwide each year and more than 50% of them are performed within two years of primary surgery (Sharkey et al., 2002). The main reason for revision is wear of the polyethylene bearing and aseptic loosening. Other reasons for failure include tibial femoral instability, patellar instability, fatigue failure of the tibial tray and infection (Windsor et al., 1989), (Sharkey et al., 2002), (Villa et al., 2004). Selecting the correct size of implant plays an important role in successful knee arthroplasty (Howcroft et al., 2006).

The early wear of UHMWPE is mainly affected by the conformity of the articulating surfaces, the thickness of the UHMWPE component, the elastic modulus of the component, contact loads and surface kinematics (Petty et al., 1999), (Fregely et al., 2003), (Bei et al., 2004), (McEwen et al., 2005). Retrieval studies have shown that the wear of TKR is highly variable and this is due to the diverse kinematics and stress conditions that occur in vivo (Shi, 2007). Figure 2-13 shows a failed polyethylene insert eight years after total knee replacement surgery.

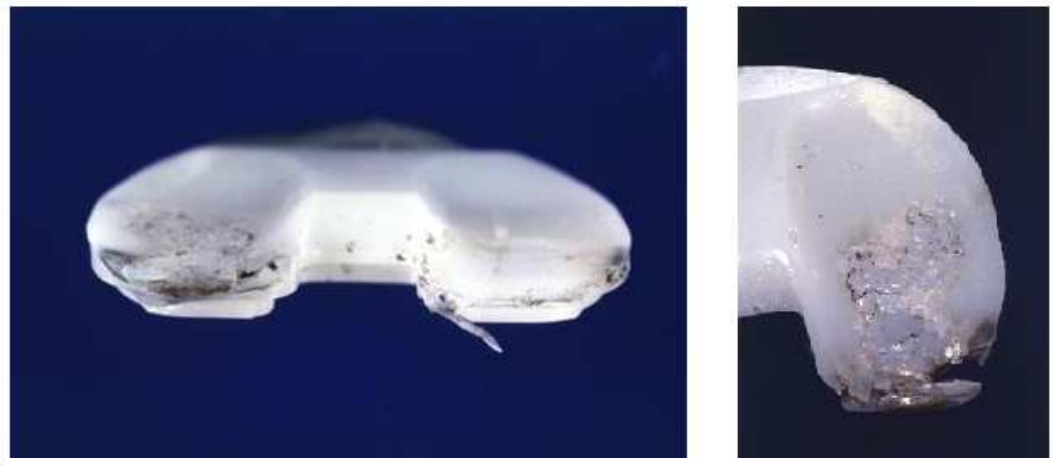

Figure 2-13: Failed polyethylene eight years after total knee replacement (Petty et al., 1999)

Implant alignment and the shape of the articulating surface of the tibial component greatly influence the local magnitude and the eccentricity of the tibial bone-implant interface pressure. This has large effects on the pressure distribution and amount of relative micro motion at the tibial component (Shi, 2007). A mobile-bearing implant can theoretically increase conformity and improve the stress distribution to the bone-implant interface. It thus appears that wear can be reduced in mobile-bearing designs compared to fixed-bearing designs because of the increase in conformity and thus increase in contact areas. Implant malalignment usually results in loosening of the component (Vince, 2003). Cheng (2003) found that mobile-bearing designs can reduce maximum contact pressures more significantly than their fixed-bearing counterparts when malalignment conditions occur. Bartel (1986) found that higher contact pressures on the tibial bearing component were associated with more severe damage to TKR tibial components.

Aseptic loosening is when relative motion between the bone and the implanted component causes the component to loosen from the bone. This can cause pain, instability and loss of function (Shi, 2007). Windsor et al. (1989) reported that aseptic loosening of the tibial component remained a major cause of failure after TKR. Vince et al. (2003) argued that varus malalignment can result in loosening of the cemented tibial components as well as failed ingrowth of the cementless components. Another important consideration is long-term remodelling of bone tissue. Levitz et al. (1995) reported a decrease of bone density by a rate of up to 5% per year just beneath the tibial component. Figure 2-14 and Figure 2-15 show bone loss in the tibia and the failure of ingrowth of the femoral component, respectively.

a) b)

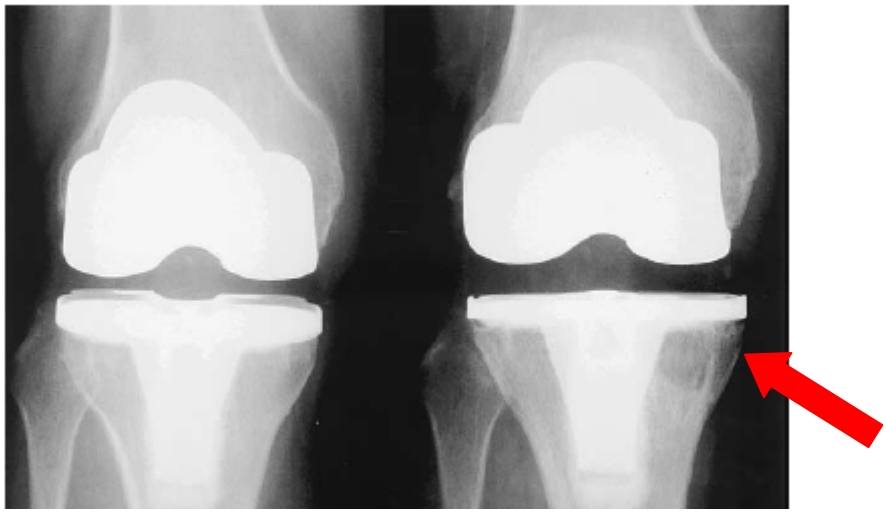

Figure 2-14: Radiographs immediately after TKR (a) and four years after surgery (b). Note the bone loss in the medial tibial plateau (Callaghan et al., 2004)

Figure 2-15: Lateral radiograph two years after surgery with failure of ingrowth of the cementless femoral implant (Callaghan et al., 2004)

2.5 Conclusion

The knee is the largest and most complicated joint in the human body. The knee joint can be separated into three compartments, the medial and lateral tibio-femoral compartments and the patello-femoral compartment. The combined articulations of the three compartments produce the complex movement of the knee joint. Osteoarthritis is the degradation of the articular cartilage in one or all of the compartments. Patients suffering from OA will experience pain and loss of motion in the knee joint. Common treatments for OA include total knee replacement and unicompartmental knee replacement.

TKR is the resurfacing of all the compartments in the knee joint with artificial implants. However, sometimes OA is only present in one of the compartments, and in such cases UKR may offer better treatment. The advantages of UKR include the preservation of bone stock, a shorter recovery time, reduced blood loss and more normal kinematics. UKR can provide more normal kinematics because

only one third of the knee joint is replaced; hence the biomechanics of a UKR are closer to those of a normal knee than are those of TKR (Hodge & Chandler, 1992). Preserving the ACL also contributes to more normal kinematics.

There are numerous modes of failure concerned with knee replacements. The main reason for failure and revision surgery is wear of the polyethylene bearing and aseptic loosening. As stated, selecting the correct size of an implant plays an important role in successful knee arthroplasty (Howcroft et al., 2006).

3. METHOD FOR SELECTION OF THE FEMORAL COMPONENT

3.1 Introduction

As previously stated, the purpose of knee replacement is to reconstruct the original, healthy knee surfaces in order to relieve pain and restore normal knee kinematics. However, when the patient presents to the surgeon, the original surfaces are often in a severe state of degradation and hence it is not possible to determine the location and morphology of the original surfaces. Commercial prostheses are available in a wide range of types and sizes in order to replicate the human knee anatomy for a host of individuals. Selecting the correct size of an implant plays an important role in successful knee arthroplasty (Howcroft et al., 2006).

Estimating the appropriate size of implant preoperatively has become an integral part of the procedure and, as a result, most knee replacement companies advocate the use of templates to enable the surgeon to make this selection. The templates are placed over an X-ray of the patient's femur and give an indication of which size implant to use. These templates are designed with a specific magnification which usually ranges between 15 and 20%. However, this magnification factor can vary considerably between different radiology departments as well as between different patients. This can lead to inaccurate planning, and research has suggested that preoperative templating not only gives inaccurate results, but is rarely reproducible (Howcroft et al., 2006).

Howcroft et al. (2006) assessed the accuracy and reproducibility of the preoperative templating of three commonly used total knee implants. They found widespread variation in the levels of agreement, both for intra- and inter-observer, with accuracies that ranged from 38% to 55%. Other studies have assessed preoperative templating of the femoral component in TKR and have shown accuracies that varied from 38% to 62% (Heal & Blewitt, 2002), (Arora et al., 2005), (Howcroft et al., 2006). Howcroft et al. (2006) suggested that the use of templating in total knee arthroplasty be interpreted with caution and further urged the development of more accurate sizing techniques.

Van der Linden et al. (2008) investigated the use of a CAOS (Computer Assisted Orthopaedic Surgery) system for evaluating component size. They also found unreliable results and concluded a risk of oversizing the femoral component when using the system. Fawzy et al. (2008) proposed using height and tibial component

size as predictors of femoral component size in unicompartmental knee replacement, with fair results. However, the final decision on the best size of prosthesis for a particular patient is still generally made during surgery by direct measurement, whereby the anterior-posterior (AP) and the medial-lateral (ML) dimensions of the knee are evaluated (Figure 3-1). In some instances, a compromise has to be made when the patient's anterior-posterior/medial-lateral ratio is different from the average.

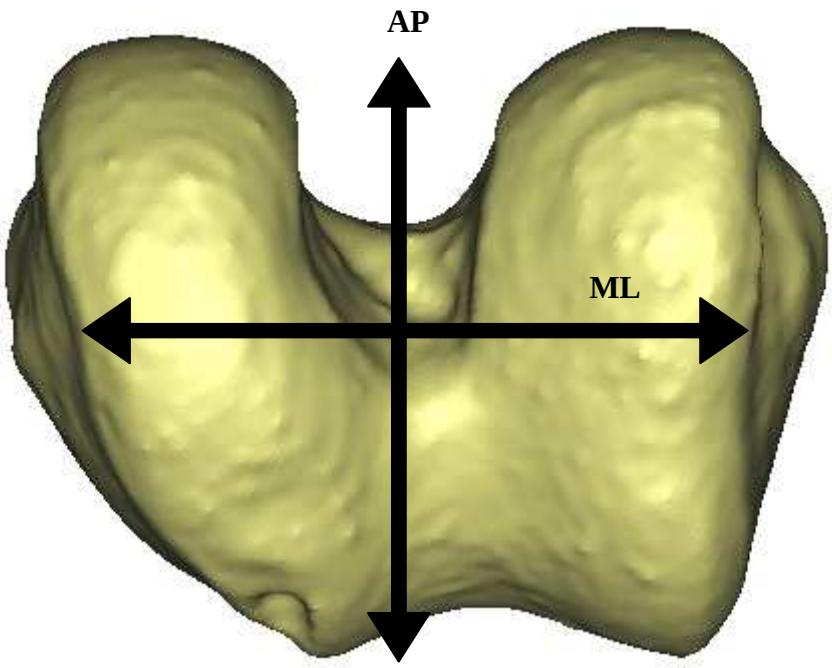

Figure 3-1: Anterior-posterior and medial-lateral dimensions of the knee

Different types of prostheses have inter type differences in their AP and ML size ratios and also differences in other parameters, like the radii of the medial and lateral condyles, the sulcus length etc. There is also a large variation in the size and morphology of the knees of different people (İşcan & Shihai, 1995), (Steyn & İşcan, 1997), (Asala et al., 2004), (Purkait & Chandra, 2004). This variety in the shape and size of knees in the population and available prostheses has led to the potential for a specific type and size to be a more optimal implant for a specific patient. When performing a TKR it would be of great value to the surgeon and the patient if the best-fitting prosthesis could be selected from the array of different

types and sizes available to the surgeon, likely producing a better functional outcome.

The geometry of some commercial prostheses is still based on observations made as early as 1836 by Weber and Weber (Freeman & Pinskernova, 2005), who reported the posterior condyles of the knees to be circular and of the same size medially and laterally. Numerous other studies have adopted a similar, simplified view of the geometry of the condyles. Elias et al. (1990) examined 16 cadaver knees and identified two circular surfaces to represent the articulating distal femur. These were located distally (active for articulation between 0º to 10º flexion) and posteriorly (active for articulation between 10º to 150º flexion). This would typically result in two axes of rotation being present, at the centres of the two circular surfaces. Hollister et al. (1993) found a fixed flexion-extension (FE) axis perpendicular to the sagittal plane based on in vitro experiments. Six knee specimens were cycled manually through their passive range of motion and a mechanical device was used to locate the FE axis in a trial and error manner. They found the FE axis to be constant and directed from antero-superior on the medial side to posterior-inferior on the lateral side. Churchill et al. (1998) also suggested that knee flexion and extension occur about an optimal FE axis located in the femur. It is further suggested that there is a relationship between the FE axis and the surgical epicondylar axis. Other studies have also found similar results (Agaki et al., 2001), (Asano et al., 2001), (Matsuda et al., 2004).

There is another theory, however, namely that of *instantaneous centres of rotation*. This implies that the condyles do not have a single radius describing them, but rather a continuously varying radius throughout the range of movement (Frankel et al., 1972), (Blacharski et al., 1975), (Soudan et al., 1979), (Shiavi et al., 1987). It can be argued, however, that either of the two theories, fixed or instantaneous axis, can be true for a specific individual. Certain individuals' knees show a more constant radius compared to others, and therefore it could be advantageous for such an individual to receive a commercial knee implant with a similar geometry. These commercial prostheses are available in a set of prearranged sizes, with only the articulating radii (posterior and distal) and other morphological parameters altered. However, these measurements are different for different prosthesis designs. Furthermore, most prostheses are developed in the Western world and are based on morphological studies of Caucasian people. They are thus race-specific, and Kwak et al. (2007) have reported numerous sizing problems when they are used in the Asian population.

A study by Sharkey et al. (1999) found that 52.7% of knee surgeons use two or more different types of knee implants. Different varieties of implants typically

have different geometries, which are important when considering total knee arthroplasty. Anterior-posterior mismatch can result in abnormalities such as notching of the anterior femur, patellofemoral overstuffing or a mismatch between flexion and extension gaps (Chin et al., 2002). The sulcus length plays a role in patellar tracking. Medial-lateral mismatch can cause either painful impingement of the soft tissue or inadequate bone support, which can lead to fixation problems (Barnes & Scott, 1995), (Poilvache et al., 1996). The radii of the condyles, both distally and posteriorly, greatly influence the kinematics of the knee by altering the tension in the ligaments, while the RPC influences the posterior condylar offset, impacting on impingement of the soft tissue.

Factors such as insufficient posterior femoral translation are reported to influence flexion with TKR (Kitagawa et al., 2009). Komistek et al. (2008) argued that implant design seems to be the leading factor for normal knee kinematic patterns and suggested that an asymmetrical design produces more normal posterior femoral rollback on the lateral side. Even though certain trends exist in normal knee kinematic patterns relating to posterior femoral rollback and axial rotation (Komistek et al., 2008), each individual knee joint produces distinct kinematics related to its individual knee geometry.

The benefit of selecting the optimal prosthesis type and size for a specific patient is evident. The objective of this chapter is to establish a method for the preoperative determination of the optimal prosthesis type and size for a particular patient undergoing TKR.

Before the method for selecting the ideal prosthesis type and size can be discussed, it is important to discuss self-organising maps (SOM). The SOM technique plays an integral part in the method for selecting a femoral component presented here, as well as in the development of a custom femoral component presented in Chapter 6. It is therefore necessary to give an introduction to SOMs at this time.

3.2 Self-organising map

The self-organising map was developed by Finnish professor Tuevo Kohonen and is therefore also sometimes called a Kohonen map (Kohonen, 1998). The SOM has been implemented successfully in numerous applications, including fields such as process analysis, machine perception, medical diagnosis, speech recognition and many more. The SOM is a type of neural network that is trained using unsupervised learning. It implements the orderly mapping of high-dimensional input data onto a low-dimensional grid, called a map. It is

distinguished from supervised learning in that target outcomes are not specified. In supervised learning, the training data consist of pairs of examples, each with an input object and an accompanying desired output value. In other words, the outputs for each of the training examples need to be known beforehand. When used to classify data, the classification of each of the training examples needs to be known, and the different classifications required must also be known.

Like most neural networks, the SOM has two modes of operation, training and mapping. In the training mode, the map is built using numerous input samples and the mapping mode automatically classifies a new input vector. Basically, the SOM learns to classify data without supervision, i.e. without a target vector. Unsupervised learning is more efficient with pattern association, with the obvious disadvantage that the user must interpret the results (Matthews, 2004). Other commonly used unsupervised learning algorithms are factor analysis and k-means clustering. The goal of factor analysis is to isolate underlying factors that explain the input data. The factors potentially have a lower number of variables than the input data. The observed variables in the input data are modelled as linear combinations of the potential factors. Disadvantages of factor analysis are that the number of factors must be chosen before training and also that it is very difficult to interpret the results.

K-means clustering partitions the training data into a chosen number of clusters. Each input vector belongs to the cluster with the nearest mean. Disadvantages are that the number of clusters must be chosen before training, and that all the clusters will have a similar size. Kiang and Kumar (2001) evaluated the feasibility of using SOM networks for data mining as an alternative to factor analysis and k-means clustering. The three methods were compared using simulated data sets with known underlying factor and cluster structures, and it was indicated that the SOM networks provide solutions superior to unrotated factor solutions in general. For skewed input data, the SOM networks also provided more accurate recovery of underlying cluster structures. Mangiameli et al. (1996) demonstrated that an SOM network is superior to hierarchical clustering methods by testing the SOM network and seven hierarchical clustering methods on 252 data sets with various levels of imperfections. They concluded that the effectiveness of research based on the clustering of noisy data can be improved with the superior accuracy and robustness of the SOM network.

The SOM is easy to understand, simple to use, and has the appealing property of doing clustering and visualisation simultaneously by producing a one- or two-dimensional output space (Flexer, 2001). The SOM starts out with a 2D lattice of neurons or nodes. Each node has a specific topological position (x and y

coordinate) and contains a vector of weights of the same dimension as the input vectors (sample inputs in vector format). That is to say, if the training data consist of numerous vectors of dimension *n*, V_n, each node will contain a corresponding weight vector of dimension *n*, W_n. Prior to training, each node's weights are initialised. The weights of the neurons are initialised either to small standardised random values or sampled evenly from the subspace spanned by the largest principal component eigenvectors.

During training, a training example (one of the sample input vectors) is fed to the network or lattice and the best matching unit (BMU) is calculated. The BMU is the single neuron with a weight vector most similar to the sample input vector. One method to calculate the BMU is to iterate through all the nodes and calculate the Euclidean distance between the sample input vector and each node's weight vector using the following equation:

$$Distance = \sqrt{\sum_{i=0}^{i=n} (V - W_i)^2} \tag{1}$$

where V is the current sample input vector and W is the node's weight vector. The weights of the BMU and the neighbour neurons (neurons close to the BMU in the lattice) are then adjusted toward the input vector using the following equation:

$$W_i(t+1) = W_i(t) + \theta_i(t)\alpha(t)[V(t) - W_i(t)] \tag{2}$$

where $\alpha(t)$ is a decreasing learning coefficient and $\theta_i(t)$ is the neighbourhood function. The learning coefficient, $\alpha(t)$, is a small variable that decreases over time and that is close to zero during the last few iterations. The neighbourhood function, $\theta_i(t)$, represents the amount of influence a neuron's distance from the BMU has on its weight adjustment. As the distance between a neuron and the BMU increases, the neighbourhood function decreases, usually according to a Gaussian function. The neighbourhood function also shrinks with time, and at the start of training the self-organising takes place on a global scale. With just a few iterations left, the neighbourhood has shrunk to just a couple of neurons and the weights are converging to local estimates.

This process is repeated for each of the sample input vectors for a specified number of cycles, λ. The result is a network (sometimes referred to as a lattice)

associating neurons with groups or patterns in the sample input data. Similar data will thus tend to cluster together in certain positions on the map. During the mapping phase, a single input vector will be the input data, and the output will be the single neuron whose weight vector lies closest to the input vector. The output neuron is easily determined by calculating the Euclidian distance between the input vector and each neuron's weight vector. The output is therefore an indication of where on the map the input will find itself, i.e. its classification.

3.3 Methods

A computer algorithm based on SOMs was developed to aid surgeons in selecting the optimal prosthesis type and size for a particular patient. Preoperative CT data of patients that underwent TKR were reviewed retrospectively. A variety of commercial prostheses were used in the computer algorithm to select the optimal type and size of prosthesis for each of the individual patients. The selected prosthesis was then compared to the actual implanted prosthesis type and size.

3.3.1 Prostheses

In this study, three different types of commercial prostheses were used. Implants A and B have symmetrical condyle designs and both are available in six sizes. Implant C has an asymmetrical design and is available in seven sizes. All three implants had a multi-radius design, with different measurements for posterior and distal radii. Certain morphological measurements were used in determining the optimal fit (Figure 3-2). These measurements are important when considering TKR.

A 3D laser scanner from NextEngine (NextEngine, Santa Monica, USA) was used to determine measurements for each type and size of implant (Figure 3-3). By means of this scanner, a 3D computer model was constructed of each prosthesis, after which the models were imported into the Mimics v. 12.1 (Materialise, Leuven, Belgium) software environment, where the measurements were performed (Figure 3-4).

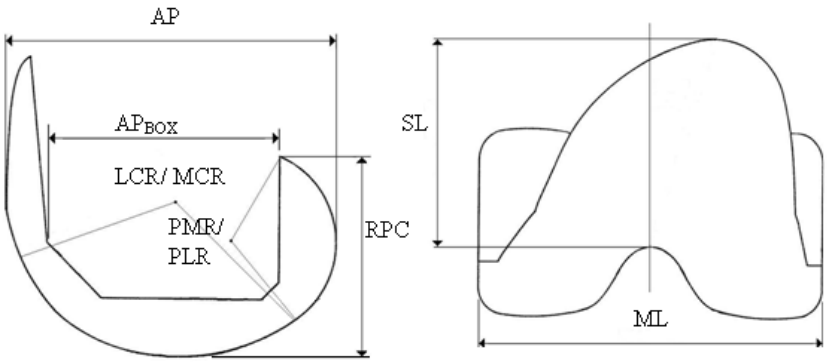

Figure 3-2: Morphological measurements

Note:	
AP	Anterior-posterior
ML	Medial-lateral
AP_{BOX}	Anterior-posterior box
LCR	Lateral condyle radius
MCR	Medial condyle radius
PMR	Posterior medial radius
PLR	Posterior lateral radius
SL	Sulcus length
RPC	Resected posterior condyle

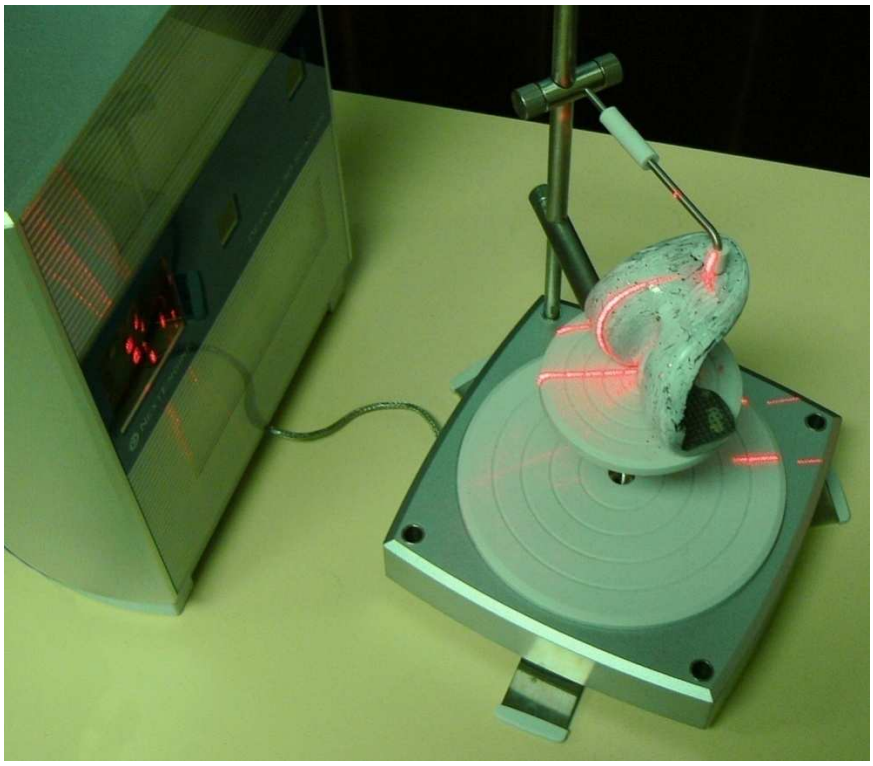

Figure 3-3: 3D laser scanning of a femoral component

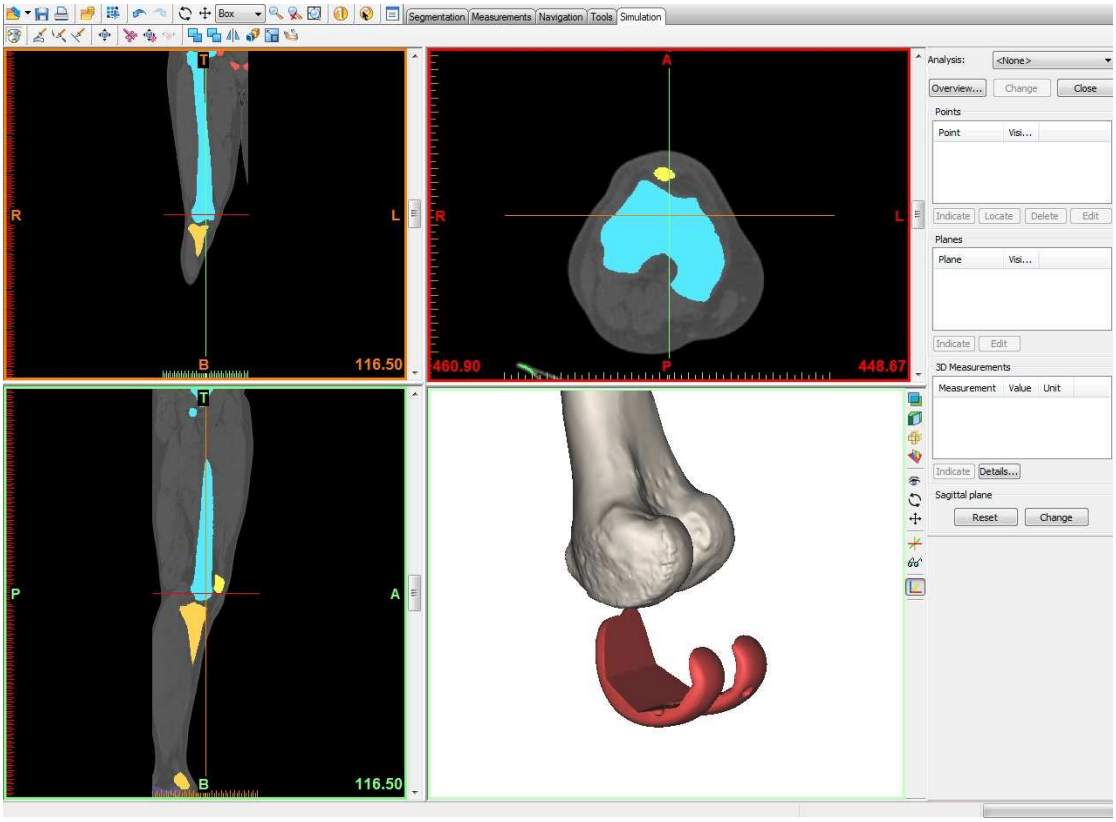

Figure 3-4: Mimics environment

3.3.2 Patients

Similar measurements were made using preoperative CT data of 34 patients with a mean age of 65 years (range 44 to 80 years, 17 male and 17 female) who had undergone TKR. A comparison of the three different implant designs was made in terms of how well they fit the patient's femur according to a computer algorithm (Section 3.3.3). In order to obtain certain measurements, simulated cuts had to be performed on the 3D models equivalent to the surgical procedure. A size-matched resection technique was used, with a 9 mm posterior cut parallel to the surgical transepicondylar axis. The surgical transepicondylar axis was approximated by a 3º external rotation of the posterior condylar axis. The posterior condylar axis is an axis connecting the most posterior points on the condyles (Figure 3-5). This approximation is valid and the angle has been shown to typically be between 3º and 6º (Churchill et al., 1998), (Maestro et al., 2000), (Asano et al., 2001). Brooks (2008) also suggests using a 3º angle to perform the posterior cut.

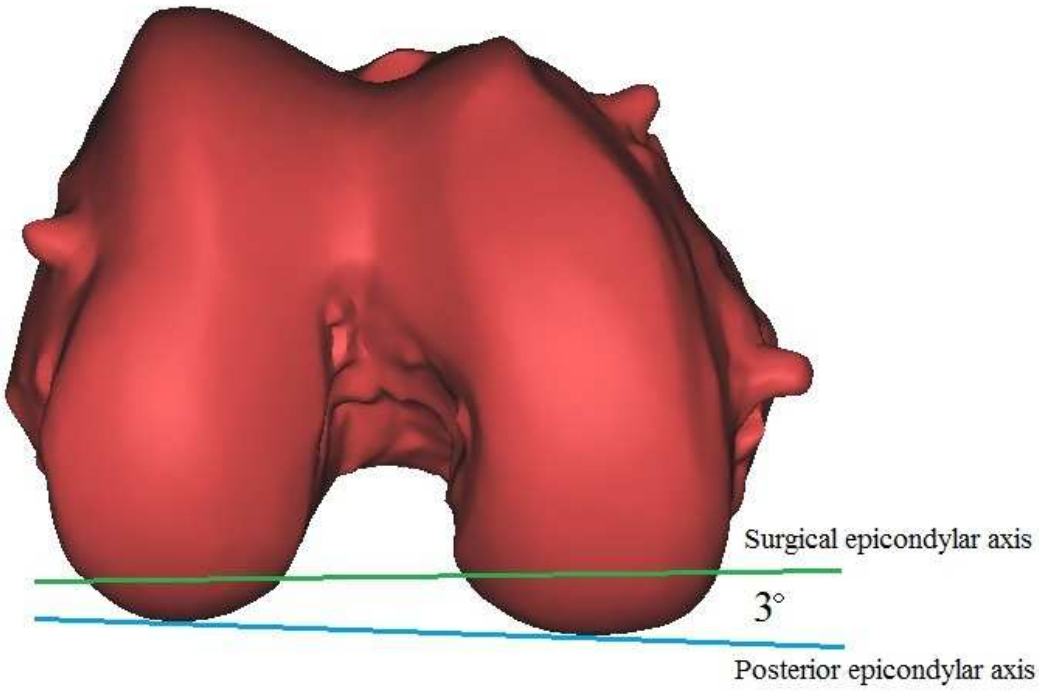

Figure 3-5: Surgical epicondylar axis

The anterior cut was then made parallel to the posterior, with an angle ranging from 3º to 6º to the posterior plane depending on the prosthesis used. Lastly, the distal cut was made perpendicular to the mechanical axis, 9 mm proximal to the most distal aspect of the condyles (Figure 3-6).

Following the simulated cuts, the RPC, SL, AP and ML measurements were made. The condyle radii were measured before the simulated cuts with a three-point technique requiring three points to be placed on the arc of the measured radius. All measurements were validated by measuring objects with known dimensions in the Mimics environment. The objects were created using CAD software and the dimensions were specified. The CT and 3D scan accuracy were also evaluated and both were found to be accurate to within 1% (Van Schalkwyk, 2010). The computer algorithm performed three steps before determining which prosthesis type and size was the optimal for a specific patient.

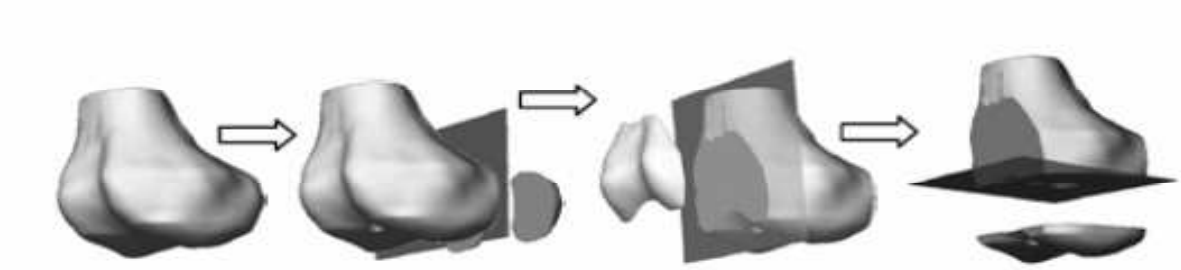

Figure 3-6: Simulation of bone cuts made to femur prior to implantation of prosthesis (Villa et al., 2003)

3.3.3 Computer algorithm

The computer algorithm consisted of three steps (discussed below) in order to select the optimal prosthesis type and size for an individual patient requiring TKR.

3.3.3.1 Step 1: Estimation of healthy knee parameters

The first step in the computer algorithm was to estimate what the morphological measurements described would have been for a TKR patient prior to the degradation of the knee joint. This was accomplished by using an SOM and a database of healthy knee measurements as the training data. The SOM is the ideal tool to use for this application because the types of classifications are not known beforehand nor is the number of output clusters or factors. The aim is to train the network to cluster similar knees in order to perform estimations. An SOM toolbox that was developed for the Matlab environment at the Helsinki University of technology was used (Kohonen, 2005).

The SOM was trained with data representing healthy knee measurements (training data). These measurements are the same as for the prostheses, enabling the healthy measurements to be compared to the prosthesis measurements. The SOM training was initialised by a 35x9 matrix using the *som_make* function in the toolbox, containing the nine measurements described for 35 healthy knee joints. The measurements were normalised with the ML measurement, which would therefore be set to 1 in each of the 35 columns of the matrix.

After training, when the SOM was presented with data representing certain measurements of an unhealthy knee, the SOM made an estimation of what the healthy knee measurements of that knee would have been. This was accomplished by determining the best matching unit for the input data using the *som_bmus* function of the toolbox. The map created during the training phase was entered as the first argument, and a patient-defined vector as the second argument. The patient-defined vector was a 1 x 9 vector and contained the unhealthy knee measurements that were not severely affected by degradation, and blanks or *Not-a-Number* (NaN) were entered for the rest.

The measurements not severely affected by degradation were taken as the AP, ML, AP_{BOX} and SL (Erasmus & Dillon, 2008). All measurements were also normalised with the ML measurement. The input data were matched to the best matching unit (BMU) and delivered an estimation of the original RPC, MCR, LCR, PMR and PLR measurements of the unhealthy knee, entered as NaNs.

Healthy knee measurements were obtained by means of two methods, namely CT scans obtained from 17 healthy volunteers with a mean age of 42 years (range 23 to 79 years, 16 males and one female) and direct scanning of 18 cadaveric specimens with a mean age of 51.7 years (range 30 to 85 years, all males) using the 3D laser scanner. The data were imported into the Mimics environment and the necessary measurements, the same nine measurements as for the prostheses, were taken. The Mimics models of the CT data obtained from the volunteers did not contain the cartilage surface, but only showed the bony structures. The cadaveric specimens were therefore used to determine an average cartilage thickness to be added to the CT measurements. This was important, as the measurements that are of concern are taken at the articulating surfaces, which contain the cartilage.

Three reference markers (nails covered with an iodine/glue mixture) were inserted into each cadaveric specimen in order to overlay a CT scan of the dissected knee with a 3D laser scan of the same knee for comparative purposes (Figure 3-7). The average cartilage was then determined in Mimics by performing measurements at numerous points. The distance between the CT surface and the 3D cadaver surface gave an indication of the cartilage thickness at that point.

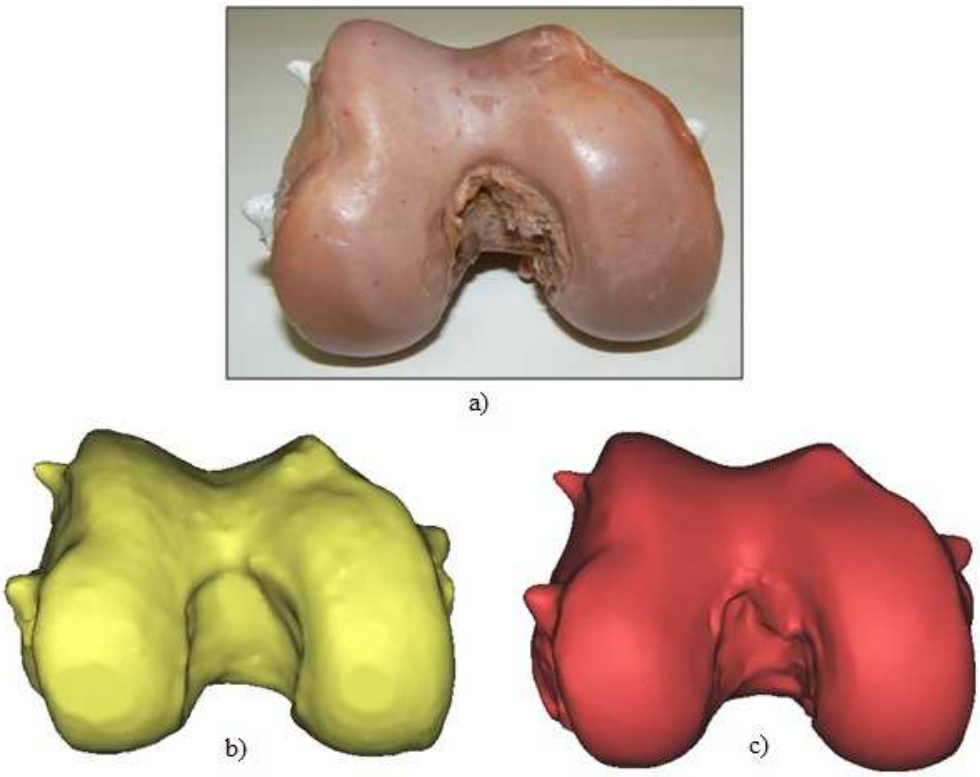

Figure 3-7: a) Cadaver femur, b) 3D model of CT, c) 3D model of laser scan including cartilage

The measurements of the 35 healthy knees were used in the SOM to estimate the original measurements of the unhealthy patient. In order to validate the SOM estimations, ten cadaver knees were used as test cases. Each cadaver's measurements were removed from the database so as not to influence the outcome. The reference measurements were then taken and used with the SOM algorithm to estimate the original knee measurements. These were then compared with the actual measurements of each cadaver knee by calculating a percentage error for each measurement. The error was calculated as:

$$e = \frac{|SOMestimate - Actual|}{Actual} \times 100 \quad (3)$$

3.3.3.2 Step 2: Selection of viable sizes

The next step in the computer algorithm was to select viable sizes from among the different prostheses according to the AP_{BOX} measurement. This was an important

step, as a surgeon would prefer to use a prosthesis with an AP_{BOX} measurement that is not too small compared to that of the patient, even though all the other measurements are optimal. If the AP_{BOX} is too small, the prosthesis will intersect with the anterior cortex of the patient's femur, possibly leading to a fracture of the femur above the prosthesis. On the other hand, if bone is resected from the posterior cortex, this will result in a too large flexion gap requiring more distal resection with subsequent elevation of the joint line.

Step 2 therefore required the algorithm to compare the AP_{BOX} measurement of each prosthesis to that of the patient's AP_{BOX} measurement. Only the prostheses with an AP_{BOX} measurement equal to or greater than that of the patient were selected as viable options.

3.3.3.3 Step 3: Goodness-of-fit analysis

The last step was to determine which of the remaining prostheses would restore the patient's knee geometry best as described by the SOM estimated measurements. The χ^2 test is a common method of determining the appropriate fit of a model to experimental data. The test was used to determine the difference between the morphological measurements of the distal femur of the patient and the femoral prostheses. Not all the measurements are equally important when choosing the optimal prosthesis for a specific patient. Weighting factors were used to add higher importance to certain parameters. A questionnaire was sent to 20 orthopaedic surgeons experienced in TKR, requesting them to rank the parameters from most to least important. Only five surgeons responded and all listed AP_{BOX}, ML and AP as most important in that order. The resultant weighting factors derived from the questionnaire rankings for the measurements are shown in Table 3-1. The weights were calculated using a two pair forced decisions method (Coetzer, 2004). Due to the fact that the AP_{BOX} measurement was already used in Step 2 to select viable prostheses, it was omitted in the calculations here.

Table 3-1: Parameters and their associated weight

Parameter	ML	AP	LCR	MCR	PMR	PLR	PRC	SL
Weight	1.8	1.6	0.8	0.8	0.7	0.7	0.6	0.5

The χ^2 value was determined using the following equation:

$$\chi^2 = \sum_{i=1}^{k} w_i \frac{\left(\overline{Z}_i - \overline{E}_i\right)^2}{\overline{E}_i} \qquad (4)$$

$$\overline{E} = \left|E_1 \quad E_2 \quad .... \quad E_k\right|$$
$$\overline{Z} = \left|Z_1 \quad Z_2 \quad .... \quad Z_k\right|$$

The value *k* is the number of parameters used in the equation (the eight remaining morphological measurements). The vector $\overline{E}$ contains the selected morphological dimensions of the patient's femur (measured in Mimics from CT data). The vector $\overline{Z}$ contains the dimensions of the prosthesis for a specific size (CAD models using the 3D scanner). A $\overline{Z}$ vector was generated for each size in the prosthesis range and an $\overline{E}$ vector was generated for each patient. The weighting factors are represented by w_i.

After executing Step 3, a value for each of the viable prostheses was obtained, indicating its goodness of fit. The value was given out of 100, and a prosthesis with a higher value will indicate a better fit for the specific patient. The optimal prosthesis type and size from the three implants considered were determined for each of the 34 patients.

3.4 Results

The average cartilage values added for each segment of the knee are shown in Table 3-2. The cartilage thickness added at the AP measurement consists of cartilage on both the anterior and posterior aspects of the distal femur.

Table 3-2: Average cartilage thickness

Parameter	AP	LCR/ MCR	PMR/ PLR
Mean added value (mm)	3.75	1.96	2.33
Standard deviation (mm)	1.43	0.93	1.49

The measurements of the 35 healthy knees were used in the SOM to estimate the original measurements of the unhealthy patient. Table 3-3 shows an example of the outcome of step 1 for a patient. The SOM estimated measurements indicate what the healthy articulating surfaces of a similarly sized knee would have been

by considering the database of healthy knees. The unaffected measurements could thus also change slightly, as they were also estimated by the SOM.

Table 3-3: Estimate of healthy measurements (mm)

	AP	ML	Box	RPC	LCR	MCR	PLR	PMR	SL
Actual	62.51	65.36	45.57	37.83	55.53	38.16	18.73	18.54	31.21
SOM estimated	64.11	65.36	45.7	40.67	57.09	44.45	21.19	21.25	31.62

The accuracy of the SOM, calculated as the mean errors for each of the estimated parameters and the standard deviations, is shown in Table 3-4. The greatest mean error of 4.78% (standard deviation 6.4%) was found for the MCR measurement.

Table 3-4: Accuracy of the SOM algorithm

	RPC	LCR	MCR	PLR	PMR
Mean error	3.58	4.19	4.78	3.24	4.48
Std dev	4.93	5.72	6.44	5.64	4.83

Using the computer algorithm to select the optimal prosthesis type and size for the 34 cases yielded the following results: in 59% of the cases (20 out of 34), Implant C was the suggested implant; Implant A was the suggested implant in 38% of the cases (13 out of 34) and Implant B was the suggested implant in only 3% of the cases (1 out of 34).

Table 3-5 shows the average goodness-of-fit score for each of the three types of prosthesis.

Table 3-5: Goodness-of-fit results for implants

	Implant A n=34	**Implant B** n=34	**Implant C** n=34
Average GoF score	93.88	90.63	94.65
Standard deviation	2.10	2.49	1.75

Comparing the GoF suggested implant size to the actual implanted size could only be considered for Implant A and B, as Implant C had not yet been used for the procedures in the study's patient population. Implant A was used in 19 cases and the GoF suggested implant size was the same as the actual implanted size in 42% of the cases (eight out of 19). The GoF method was one size off in 53% of the cases (10 out of 19), and only once was it out by two sizes. Implant B was used in 15 of the cases, and the GoF suggested implant size was the same as the actual implanted size in 93% of the cases (14 out of 15). The GoF method was one size off in only one case.

Figure 3-8 shows the MCR measurement plotted against the LCR measurement for all the healthy knees as well as the three implants. A least-squares line was fitted through the healthy volunteer data. The fitted line clearly shows that the LCR measurements are greater than the corresponding MCR measurements. This is the case for the healthy volunteers as well as for Implant C. The MCR and corresponding LCR measurements are identical for Implant A and Implant B.

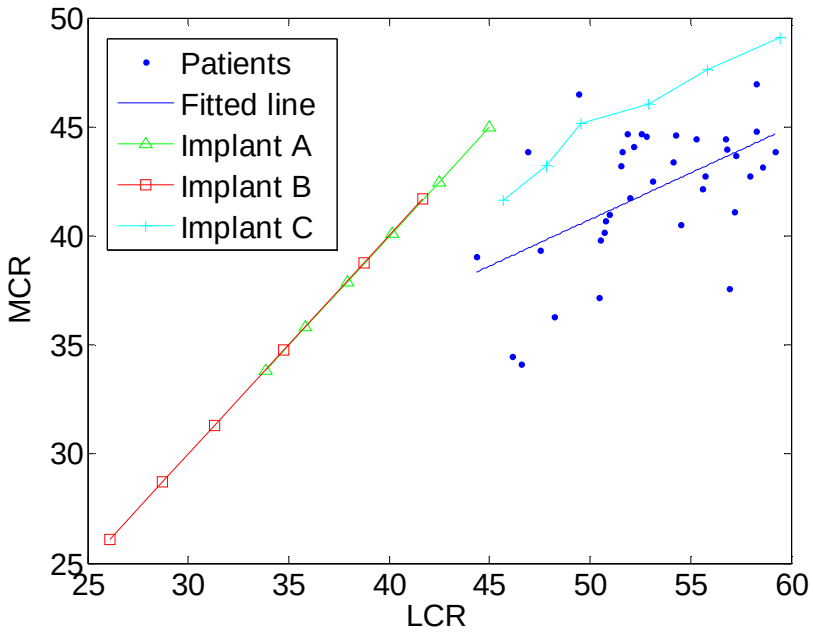

Figure 3-8: MCR vs LCR for different implants

3.5 Discussion

The aim of any total knee replacement is to restore the individual patient's articulating surfaces to the original levels. But, because each individual's knee geometry is different, a different knee replacement design could be the optimal design for restoring a particular patient's normal articulating geometry. A method for selecting the optimal prosthesis design for a specific patient from a variety of different types and sizes can therefore be helpful in selecting the best prosthesis. This might result in more normal knee kinematics. By giving different weights to certain aspects of the prosthesis, a system was suggested whereby the surgeon might be able to preoperatively select the best type and size of prosthesis for a specific patient. All the surgeons who responded to the survey listed AP_{BOX}, ML and AP as the most important aspects in that particular order. The model is sensitive to the weights given to the parameters and it is important to select the weights accordingly.

Average cartilage thickness was determined for healthy knees and added to the CT models in the healthy knees database used in the algorithm. These values are similar to those obtained by Koszyca et al. (1996), who found a mean value of cartilage thickness at the medial femoral condyle of 2.23 mm, and Stockwell (1971), who found the mean femoral cartilage thickness to be 2.26 mm.

The weights attributed to the different morphological measurements were derived from a questionnaire sent out to orthopaedic surgeons. The result was as expected, with the ML and AP measurements rated as the most important when performing knee replacement surgery. Wang et al. (1992) suggested that the width of the femoral condyle might be taken as the leading index in determining the size of the knee.

Current templating techniques only consider the ML and AP measurements for selecting the appropriate size prosthesis from a specific implant type. However, to restore normal kinematics it is argued that the other measurements should also be considered, as they have an influence on the eventual postoperative knee kinematics.

Komistek et al. (2008) investigated knee kinematics and found that, in the flexion/extension range up to 90º, the leading factor for more normal kinematic patterns seems to be the implant design. The prostheses used in their study had asymmetrical condylar radii, with the lateral condyle radius being larger than the medial condyle radius. This asymmetrical design showed more normal kinematics than prostheses with a symmetrical design, especially when considering posterior femoral rollback of the lateral condyle, as well as axial rotation. Implant C in this study also had an asymmetrical condylar design, with the lateral condyle radius being larger than the medial condyle radius.

Implant C was found to be the best fit in 59% of the cases according to the GoF method. This can be attributed to the asymmetrical design, which is more anatomically correct than the symmetrical design of the two other implants used. This phenomenon is evident in Figure 3-8. The MCR vs. LCR slope of Implant C is similar to that measured in the healthy volunteers, whereas the other two implants have different slopes. Implant C also had slightly larger measurements for PMR and PLR for the respective sizes, which were in accordance with the data shown in Table 3-3. Another important factor was that Implant C had more sizes available in a smaller range compared with the other two prostheses. This contributed to Implant C being the best fit in the majority of the cases for the specific population.

It was also established that Implant B tended to have a larger ML measurement in relation to its $AP_{BOX,}$ compared to the same sizes for Implants A and C. Implant B thus has a wider design compared to the other two implant designs. This resulted in the ML measurement being too large in Implant B for sizes having a good fit with respect to the other measurements for most of the cases. Implant B was,

however, the suggested implant type in one case, showing that a different design might be the ideal implant for a specific patient or a different population group.

A survey by Sharkey et al. (1999) showed that 52.7% of orthopaedic surgeons use two or more types of knee implant brands. Howcroft et al. (2006) found marked variations in the accuracy of templating with the accuracy varying between 38% and 75% for three different prosthesis types. A reason for this variation can be the varying degree of magnification needed for the different prostheses (115% for the one and 110% for the other). Heal et al. (2002) found the preoperative radiograph template of a specific prosthesis to be accurate in only 57% of the cases. A possible reason for the inaccuracy of the templates, according to Heal et al., is that the magnification of the knee on the radiograph is also not always accurate. There can be significant differences in magnification on radiographs as a consequence of the varying distances of the X-ray tube to the patient.

Incavo et al. (2004) compared two different methods for selecting femoral size, “size-matched resection” and “flexion-spaced balancing”. In 56% of the cases, the different methods suggested different sized components. The method proposed in this study only focussed on the selection of the optimal prosthesis type and size and did not take the rotational alignment of the components into account. Han et al. (2006) compared the accuracy of rotational alignment of the femoral component in TKR using a non-image-based navigation system and a conventional technique. They found that the navigation system showed higher accuracy by reducing outliers (abnormally shaped bones).

The validation of the SOM technique indicated that considerable inaccuracies still exist. A 4.8% error results in a 1.9 mm error for a 40 mm MCR measurement. The differences in measurements between different sized prostheses are about 2 mm for the MCR. An error in the range of 4.8% can thus be regarded as satisfactory when assuming that a prosthesis one size out is acceptable, as was believed by Fawzy et al. (2008). Even though the mean errors were slightly too large, the alarming aspect was the large deviations present. It is expected that these values will decrease as the number of healthy knees in the database available for training the SOM increases. This will ensure that the effect of outliers in the database can be minimised. However, these outliers can still serve a useful purpose, as they can give an indication of the original dimensions of abnormal knees, where it becomes more difficult to select the appropriate prosthesis. The ideal scenario would be one where the optimal prosthesis type and size can be selected for any individual patient.

The need for gender-specific knee prostheses has been argued due to certain anatomical differences in the knees of the female population (Conley et al., 2007). However, other studies have found the anatomical differences between male and female knees to be negligible or nonexistent and that there is high variability regardless of sex (Merchant et al., 2008), (Fehring et al., 2009). An advantage of the SOM algorithm is that similar knee shapes and trends are clustered together in the mapping process. Therefore, gender and race differences can be distinguished within a larger database, which could further improve the accuracy of the technique. Such a database would have to include knee parameters of different genders and races. A limitation of this study was the lack of gender variation in the database, which can be argued to have exerted an influence on the results. Further studies should include more healthy female knee measurements in the database.

The accuracy of the measurements performed in the Mimics environment plays a role in the sensitivity of the SOM algorithm. Inter-observer accuracy found measurements involving precise landmarks to be more repeatable compared to measurements that depended on the opinion of the person performing the analysis. Most of the measurements involved well defined landmarks and the use of a template further improved the accuracy. Intra-observer accuracy was good and was better than the accuracies found with the SOM technique.

Computer-assisted methods for decision making in orthopaedics have been investigated for numerous applications (Van der Linden-Van der Zwaag et al., 2008), (Zannger & Detsky, 2008). The outcome of this study suggests that this method can greatly aid a surgeon in selecting the optimal prosthesis type and size for a specific patient. The process presented here can be expanded by including even more types of prostheses, as each type has a different design. This will further improve the chances of a surgeon selecting the optimal prosthesis type and size for a specific patient.

It could be argued, however, that a large variety of types and sizes of prostheses would be needed to always have the best possible fit, which might not always be practical. A solution to this logistical problem could be to produce individualised prostheses using rapid manufacturing techniques. When individualised prostheses are considered, it can become possible to reconstruct the complex articular geometry of the individual patient’s knee. It is therefore necessary to investigate the complex profiles of the femoral condyles and find a mathematical model to accurately reconstruct the articular profiles.

4. MATHEMATICAL RECONSTRUCTION OF HUMAN FEMORAL CONDYLES

4.1 Introduction

There is a direct correlation between ligament function and the articulating surface of the normal knee. If the ligament function is disturbed as a result of injury, the biomechanics of the knee joint will be altered, possibly leading to joint surface damage (Daniel et al., 1994), (Jomha et al., 1999). Alternatively, if the knee surface is deformed through degenerative disease or a traumatic fracture, the ligament function will be disturbed as well (Brage et al., 1994), (Wada et al., 1996), (Fishkin et al., 2002). A similar problem is encountered in knee replacement procedures if the new joint surface is not placed at the exact same position as that of the original undamaged knee and the geometry is different to the original joint surface (Singerman et al., 1996), (Emodi et al., 1999), (Matsuda et al., 1999), (Siebel & Kafer, 2004).

There currently is a tendency to perform joint replacement surgery at a younger age than a few years ago because of the improvements made in the techniques (Hernigou et al., 2004), (Morgan et al., 2006), (Murphy et al., 2007). This could possibly compromise the longevity of the replaced joint, as younger patients are more active and will place a higher demand on the resurfaced knee joint. In order to accommodate this younger patient population, the knee joint surface needs to be restored to as near to “normal” as possible, with the least amount of bone resection. This will allow the prosthesis to be placed on stronger sub-cortical bone and will preserve maximum bone amount for possible future revision procedures.

Restoring the joint surface and ligament tension to as near as possible to normal with minimal bone resection should therefore lead to more natural biomechanics and an increase in the longevity of the artificial knee.

Biščević et al. (2005) suggested that the articulating geometry of the femoral condyles in sagittal view from extension to 90º flexion can be seen as an involute. That is, radii of the posterior part of the condyle are smaller than the radii of the anterior part. Other studies defined the condyle geometries as one or two circular arcs or cylinders (Elias et al., 1990), (Hollister et al., 1993), (Nuño & Ahmed, 2003), (Freeman & Pinskernova, 2005), while further researchers have used more complex mathematical equations to define the femoral geometries (Wismans et al., 1980), (Ateshian, 1993), (Boyd et al., 1999), (Hirokawa et al., 2004), (Kosel et al., 2010).

Biščević et al. (2005) argued that the curving of the femoral condyles is important for knee mechanics and therefore they attempted to define the curvature. They divided the femoral condyles into quarters (four quadrants) when viewed sagittally. They then defined the posterior distal part, the part that articulates with the tibia from extension to 90º flexion, as a quarter of an ellipsoidal curve. The anterior distal part and the posterior proximal part of the femoral condyles are reported as quarters of circles. Biščević et al. (2005) calculated the radii of 20 volunteers to compare the shapes and sizes using side view knee X-rays. On average, the radii of the medial condylar curve decreased from 45 mm at 0º flexion to 17 mm at 90º flexion. On the lateral side, the radii decreased from 31 mm to 18 mm over the same range. There was great variation between the subjects.

Nuño and Ahmed (2003) suggested a similar method for describing the geometry of the knee and also included the radial profiles of the knee. Their technique is based on surface coordinate measurements of human femurs with a range finder using a laser beam. Using the principle of triangulation, the device scanned and digitised the femoral articulating surface in three dimensions with a density of 1 point/mm^2. The sagittal profiles were reconstructed by means of two circular arcs while the radial profiles were represented by single circular arcs. Nuño and Ahmed (2003) further indicated that the medial and lateral condyles were significantly asymmetrical in geometry.

Hirokawa et al. (2004) created a parametric polynomial function that was applied to unstructured data sets obtained by scanning joint surfaces. The polynomial model was applied to unstructured data sets of an artificial joint and produced a smooth and accurate model. Wismans et al. (1980) used fourth-order polynomials to represent the medial and lateral femoral condyles mathematically, while Herzog et al. (1993) used polynomials to represent the lines of action of the muscles and ligaments in the knee joint. Ateshian (1993) used B-splines to create geometric models of diarthrodial joint articular surfaces. The method was successfully tested on human femurs and the results showed that the method is precise, highly flexible, and can be applied to a large variety of different articular surfaces.

Kosel et al. (2010) investigated the radius and centre of curvature of 16 cadaveric distal femurs. B-splines were fitted to describe the articulating surfaces, and the radii of curvature along the articulating surfaces were calculated. The centres of curvature were also defined. It was found that the condyle radii were continuously varying and that there was a difference between the lateral and medial condyle geometry. Figure 4-1 and Figure 4-2 show the articulating curvature of the lateral and medial femoral condyles of a typical cadaveric specimen. The centres of

rotation can also be seen in the figures. The radii are defined over a typical articulating range from 0º flexion (point p_1) to about 150º flexion (point p_{nL}). The region of smallest curvature variation is highlighted in bold.

a)

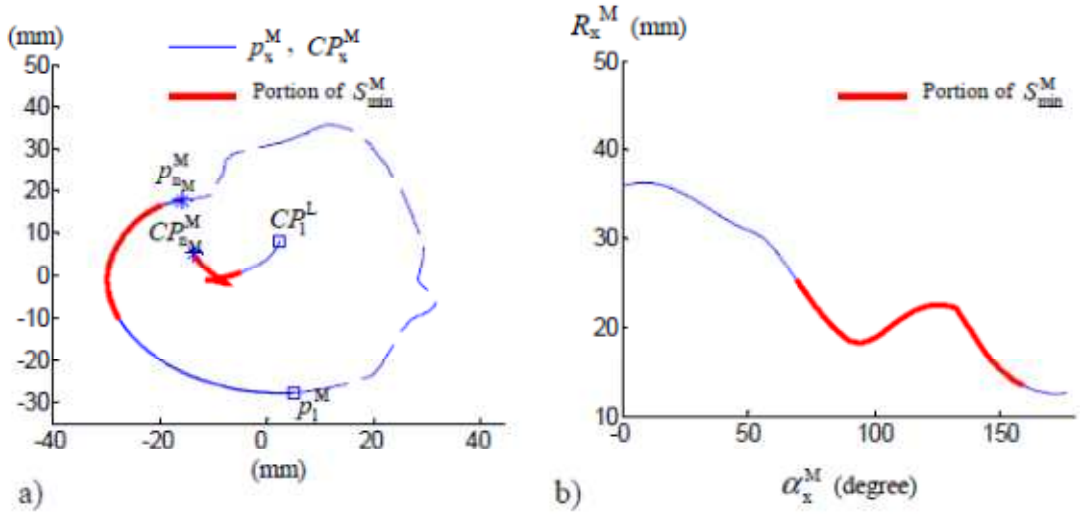

Figure 4-1: a) Articulating curve of a medial condyle and b) local radius values (Kosel et al., 2010)

b)

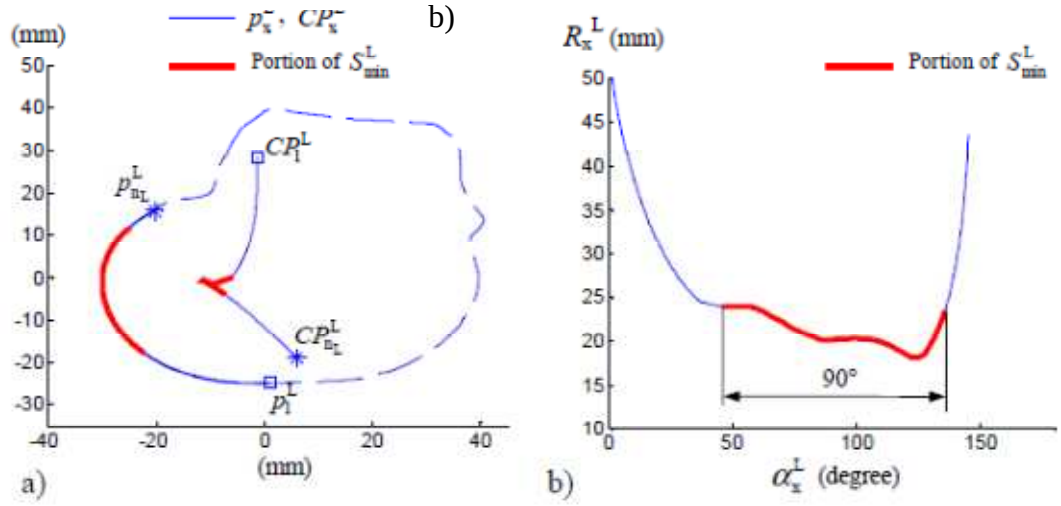

Figure 4-2: a) Articulating curve of a lateral condyle and b) local radius values (Kosel et al., 2010)

Note:	
p_x	The investigated section
CP_x	Track of the centre points from □ to *
S_{min}	Region of smallest curvature variation
R_x	Radius of condyle surface curvature
α_x	Angular position

It can be seen in Figure 4-1 and Figure 4-2 that the condyle radii are continuously varying and that there is a difference between the lateral and medial condyle geometry. The lateral condyle radius becomes almost flat at 0º flexion as well as at full flexion. The medial condyle radius seems to decrease gradually through the active flexion range. This, however, can differ between individual knees.

Matsuda et al. (2003) developed a new condylar geometry model of a knee replacement based on moving with low effort. The knee displacement is determined as a function of muscle force and soft tissue restraints and, by minimising these factors, a femoral condyle shape is produced. The produced femoral geometries are shown in Figure 4-3, together with the geometries of three prostheses available in the market.

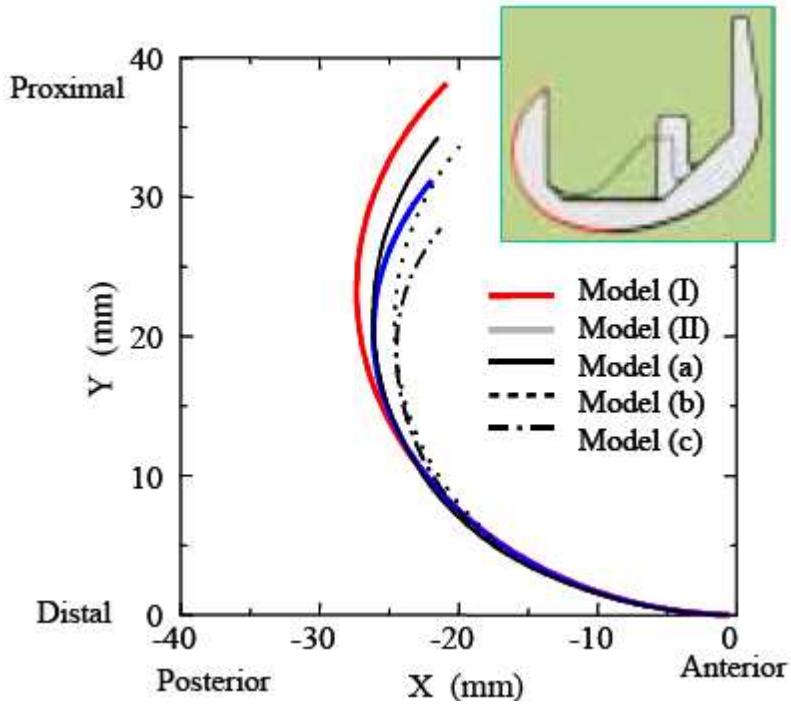

Figure 4-3: Geometries of femoral condyles in the sagittal plane (Matsuda et al., 2003)

Model (I) is the proposed design of Matsuda et al. determined under weight-bearing conditions, while Model (II) is the proposed design determined under no-weight bearing conditions. Models (a), (b) and (c) are commercial designs available on the market. The proposed models have continuous radii variations, similar to the natural knee geometry, while the existent models have only two or three radii (Figure 4-4).

All knee morphometry reports agree on the large variation between individual knees. Some studies show distinct anatomical differences between genders (Conley et al., 2007), (Chaichankul et al., 2009), while others have found the anatomical differences between male and female knees to be negligible or nonexistent with high variability regardless of sex (Merchant et al., 2008), (Fehring et al., 2009).

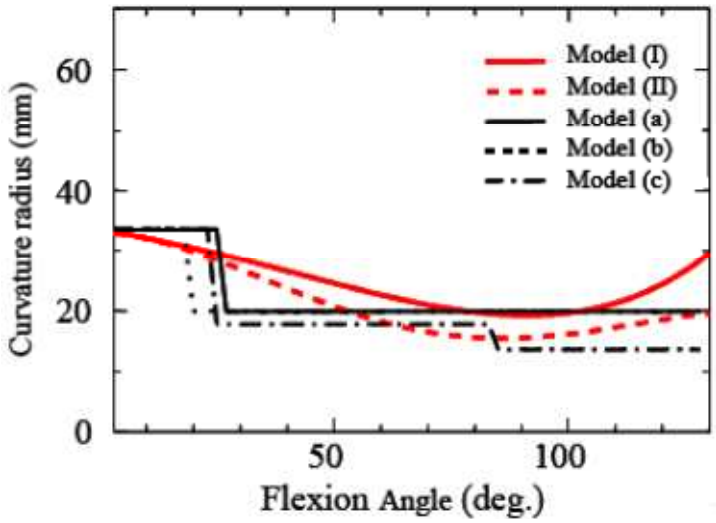

Figure 4-4: Femoral surface curvature radii of different designs (Matsuda et al., 2003)

The aim of this chapter was to find the best mathematical technique to describe the complex articular profile geometries of the femoral condyles. This was done by comparing different models in terms of the accuracy with which the original knee joint geometry can be constructed. These models are used in a system where the measurements in a degenerative knee joint are compared to a database that contains measurements of normal knees in order to design a patient-specific joint surface with maximum bone coverage and the least possible bone resection.

4.2 Methods

4.2.1 Specimens

Natural knee geometry was investigated by using cadaveric specimens as well as MRI data from volunteers with healthy knees. 3D computer models of 18 embalmed cadaveric distal femurs (mean age of 51.7 years) were obtained using a 3D laser scanner. The scanner combined 12 high-quality images for each cadaver, with a scan accuracy of 0.13 mm. A further 42 3D models of healthy knees were obtained through segmentation of MRI data (mean age of 32.9 years). The MRI scans had a resolution of 512 x 512 pixels, with a pixel size of 0.412 mm using a 0º gantry tilt. The segmentation of the MRI data was accomplished using the *thresholding* function in Mimics. All distal femurs investigated were normal, with no visible signs of arthritis or any other disease.

4.2.2 Intersection planes

Sagittal and transverse intersection planes (in which the geometries are defined) were created for both condyles of the distal femurs using 3-matic v. 5.01 (Materialise, Leuven, Belgium). Clearly visible and easily defined landmarks were used in order to ensure that the placement of the planes was repeatable for subsequent interspecimen comparison. A femur coordinate system as defined by Grood and Suntay (1983) was used. The transverse planes were positioned at the most posterior points of each condyle, perpendicular to the femoral mechanical axis, while the sagittal planes were positioned at the most prominent central part of each condyle, perpendicular to an approximated surgical epicondylar axis (Figure 4-5).

Because of the difficulty in accurately placing the surgical epicondylar axis, it was approximated by the external rotation of the posterior epicondylar axis by 3º (Chapter 3). This approximation is justified as the error made when the plane is viewed 3º off axis is small relative to the accuracy of placing the points. The posterior epicondylar axis is defined as a line connecting the most posterior points on the condyles. The repeatability of the placement of the planes was found to be accurate to within 0.47 mm (std dev 0.41). Intersection curves were then created where the condyles intersected the planes.

The resulting point clouds were exported to Matlab, where a variety of mathematical models were fitted to the data. All the models were normalised by defining the most posterior point as the origin (0,0) of the 2D coordinate system. Figure 4-6 shows the intersection planes through the lateral condyle of a distal femur with the corresponding sagittal and transverse intersection curves.

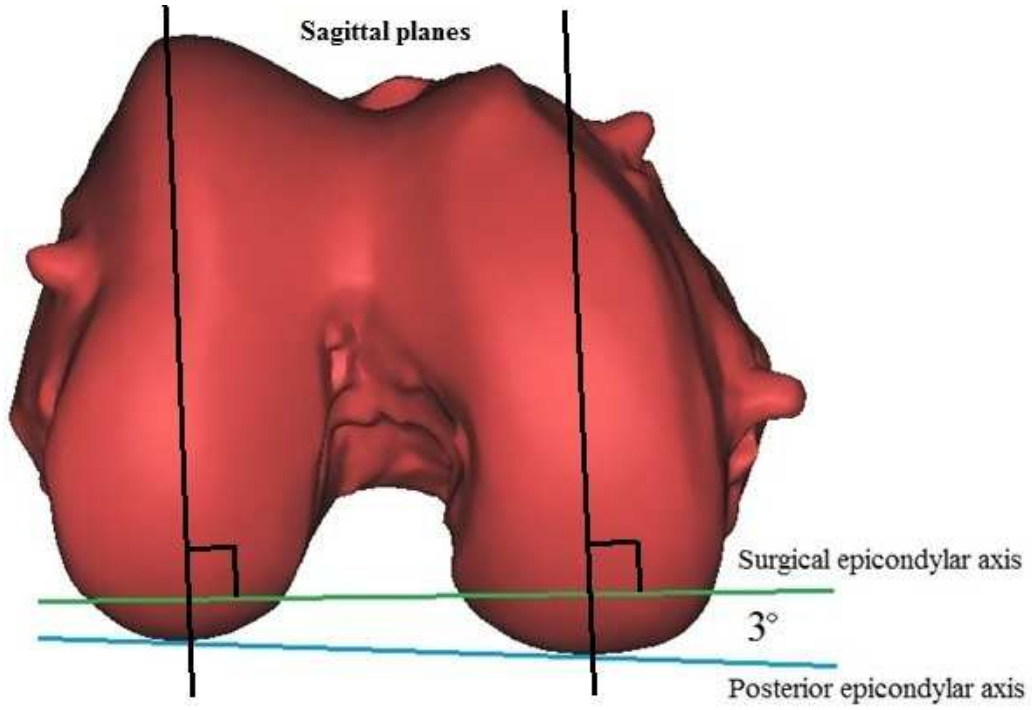

Figure 4-5: Sagittal planes perpendicular to an approximated surgical epicondylar axis

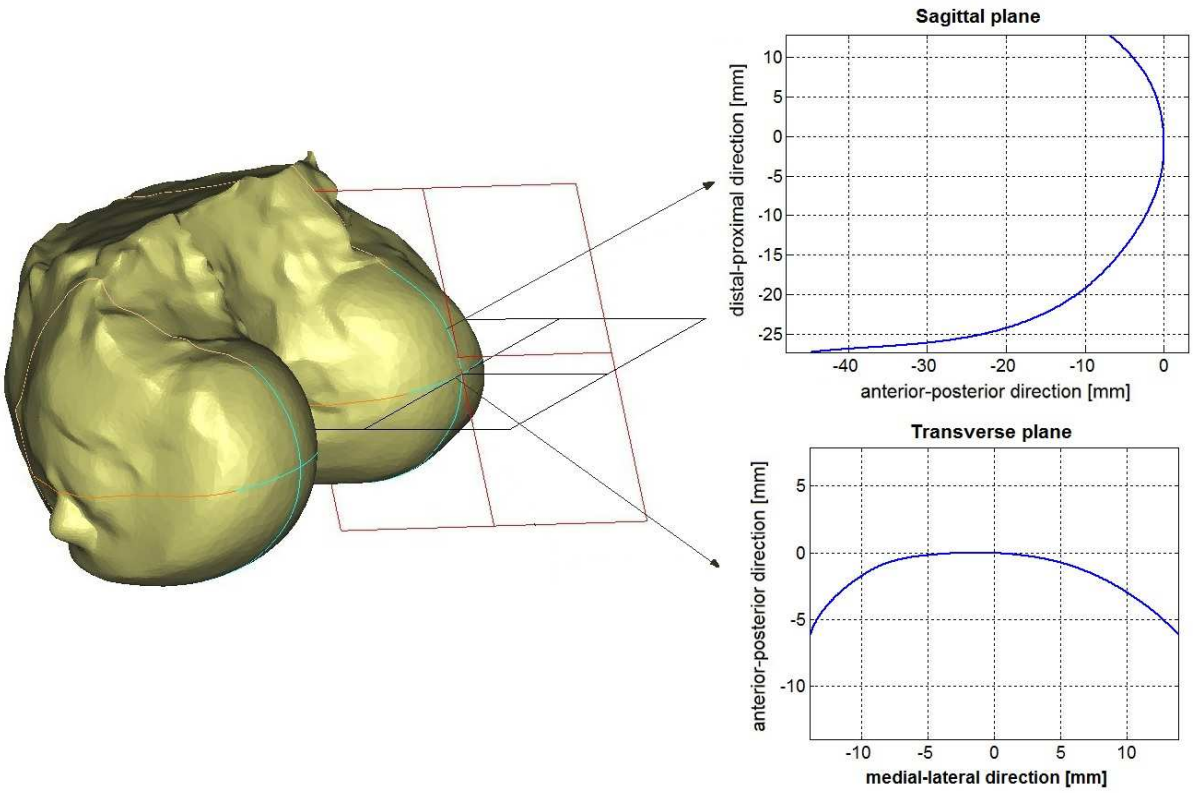

Figure 4-6: Intersection planes through the lateral condyle of a distal femur with the corresponding sagittal and transverse intersection curves

4.2.3 Model fitting

Reconstruction of knee joint geometry can be performed with various different surface fitting techniques, or by using simple equations to describe profile curves, (Wismans et al., 1980), (Elias et al., 1990), (Ateshian, 1993), (Hollister et al., 1993), (Boyd et al., 1999), (Freeman & Pinskernova, 2005), (Kosel et al., 2010). In this study, the sagittal and transverse profiles are described using four common mathematical equations, namely a single radius model, a dual radius model, a polynomial model and a B-spline model.

4.2.3.1 Single radius model

A single radius arc was used to reconstruct both the lateral and medial condyles in both the sagittal and transverse planes, as suggested in previous studies (Kurosawa et al., 1985), (Nuño & Ahmed, 2003). The radius and centre points of the best fitting arcs were determined by minimising the sum of the squared radial deviations (Figure 4-7 and Figure 4-8).

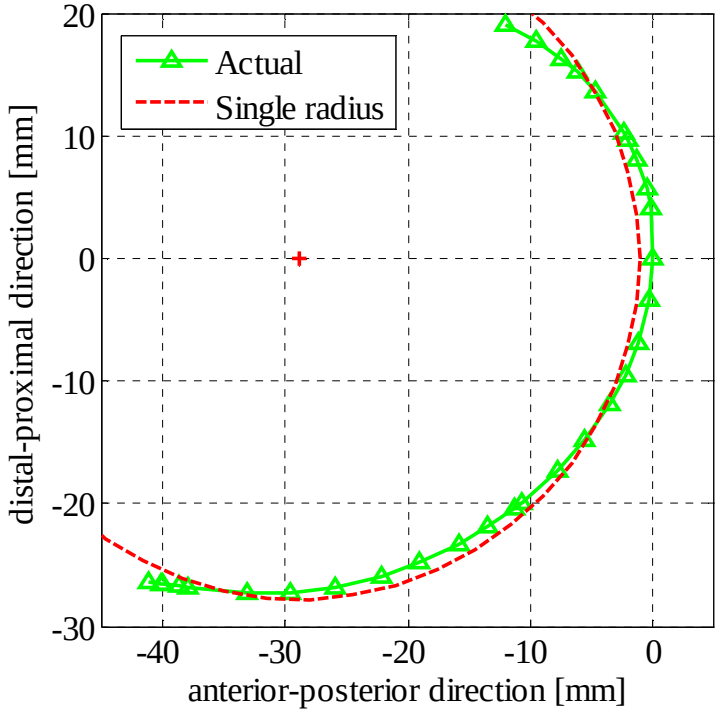

Figure 4-7: Single circle model fitted to a representative medial condyle sagittal profile

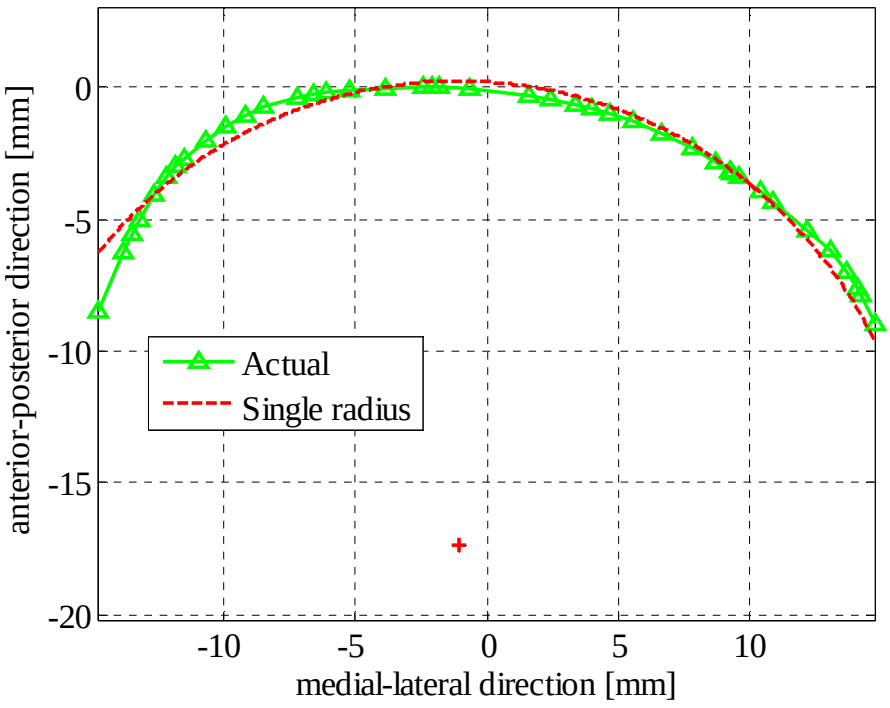

Figure 4-8: Single circle model fitted to a representative lateral condyle transverse profile

4.2.3.2 Dual radius model

A dual radius model was used for the sagittal curves (medial and lateral) similar to what was done in previous studies (Elias et al., 1990), (Nuño & Ahmed, 2003), (Freeman & Pinskernova, 2005). The most posterior point on the condyle was used to divide the curve data into two sections: a distal portion below the point and a proximal portion above the point. A single radius arc was then fitted to each of the two portions, while the radii and centre points of the circles were determined (Figure 4-9).

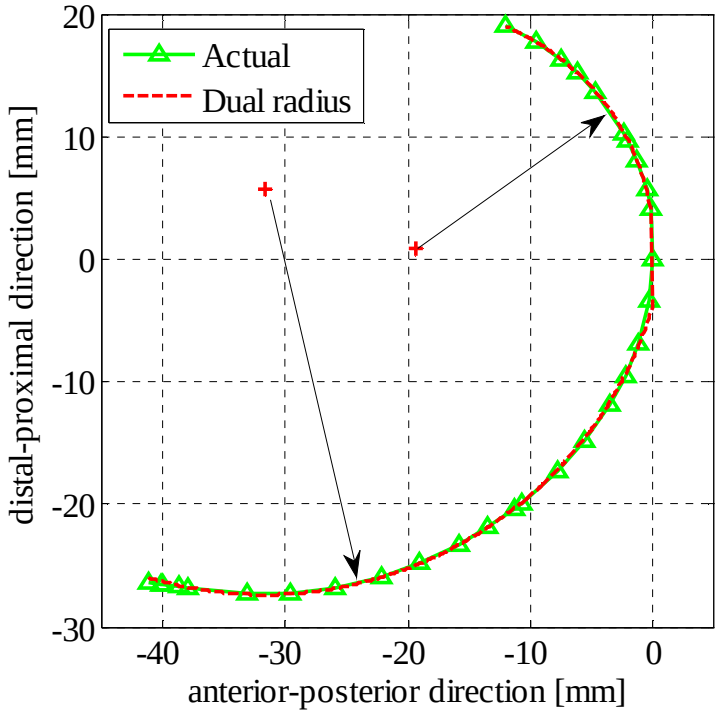

Figure 4-9: Dual radius model fitted to a representative medial condyle sagittal profile

4.2.3.3 Polynomial model

Polynomials were used to reconstruct the femoral condyles in both the sagittal and transverse planes (Hirokawa et al., 2004), (Wismans et al., 1980). Polynomials are mathematical equations of the form

$$f = a_0 x^n + a_1 x^{n-1} + \cdots + a_{n-1} x + a_n \quad (5)$$

where f is the function, a_i are the coefficients and n_i are the exponents.

The Matlab *polyfit* function was used to fit a polynomial to the data. The *polyfit* function finds the coefficients of a polynomial *f(x)* of degree *n* that fits the data *f(x(i))* to *y(i)* in a least squares sense. The result, *f*, is a vector of length *n+1* containing the polynomial coefficients in descending powers.

The degree of the polynomials used was determined by examining the behaviour of different degree polynomials with the knee data. Two polynomials were used to represent the condyles in the sagittal plane, dividing the condyle into distal and proximal portions. A second-order polynomial was used for the proximal portion and a fourth-order polynomial for the distal portion. The most posterior points on the condyles defined the points of separation. A single fourth-order polynomial was used for the condyles in the transverse plane. Choosing the degrees of the polynomials as such produced smooth functions with good accuracy (Figure 4-10 and Figure 4-11). Using polynomials of higher degrees caused ripples, whereas polynomials of lower degrees could not reconstruct the data satisfactorily.

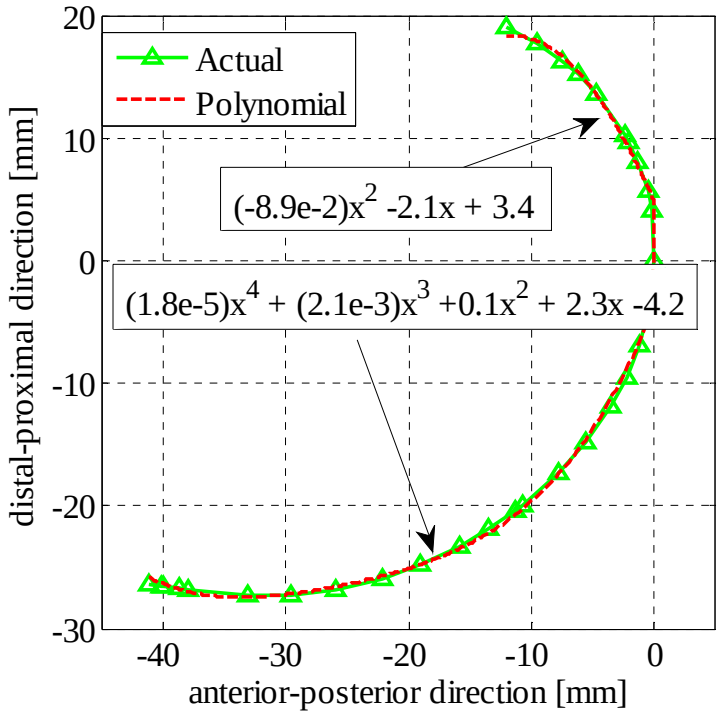

Figure 4-10: Polynomial model fitted to a representative medial condyle sagittal profile

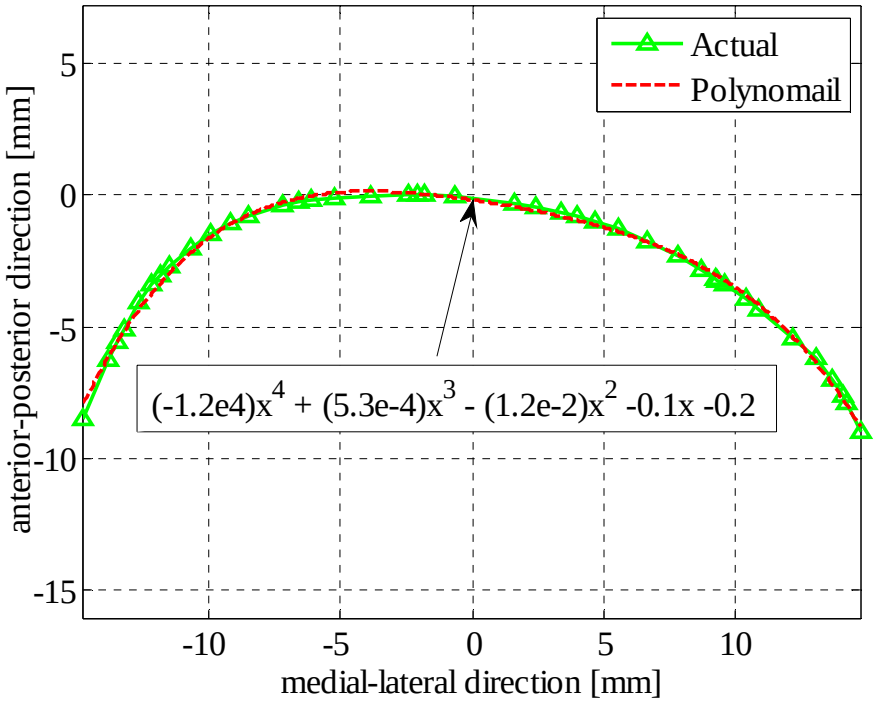

Figure 4-11: Polynomial model fitted to a representative lateral condyle transverse profile

4.2.3.4 B-spline model

Non-uniform rational B-splines (NURBS) were also used due to their flexibility to design a large variety of shapes (Ateshian, 1993), (Piegl & Tiller, 1997), (Kosel et al., 2010). A NURBS curve is defined by its order, a set of weighted control points and a knot vector. Quadratic curves or third-order NURBS curves were used to reconstruct the femoral condyles for both planes and condyles. The B-spline curve, *C(u)*, is defined as follows:

$$C(u) = \frac{\sum_{i=0}^{n} w_i P_i N_{i,p}(u)}{\sum_{i=0}^{n} w_i N_{i,p}(u)} \tag{6}$$

where w_i are the weights, P_i are the control points, and $N_{i,k}$ is the normalised B-spline basis function of degree p.

A global approximation method was used to fit the NURBS curves to the knee data as described by Piegl and Tiller (1997). To avoid a nonlinear problem, the weights, w_i, were set to one. For the given data Q_k, $k = 0,\ldots,n$, we can approximate the points with a pth-degree NURBS curve. A parameter value, $\bar{u}_k$, was assigned to each Q_k, an appropriate knot vector was computed $U = \{u_0,\ldots,u_m\}$, and then a $(n + 1)$ x $(n + 1)$ system of linear equations could be set up:

$$Q_k = C(\bar{u}_k) = \sum_{i=0}^{n} N_{i,p}(\bar{u}_k)P_i \tag{7}$$

with the control points, P_i, the unknowns. Let r be the number of coordinates in Q_k, then the parameters $\bar{u}_k$ can be chosen using the widely used chord length method. Let d be the total chord length

$$d = \sum_{k=1}^{n} |Q_k - Q_{k-1}| \tag{8}$$

Then

$$\begin{gathered} \bar{u}_0 = 0, \qquad \bar{u}_n = 1 \\ \bar{u}_k = u_{k-1} + \frac{|Q_k - Q_{k-1}|}{d}, \qquad k = 1, \ldots, n-1 \end{gathered} \tag{9}$$

The placement of the knots should then reflect the distribution of $\bar{u}_k$. If s is a positive real number, denote $i = \text{int}(s)$ as the largest integer such that $i \leq s$. We need $n + p + 2$ knots. There are $n - p$ internal knots, and $n - p + 1$ internal knot spans, thus let

$$s = \frac{m+1}{n-p+1} \tag{10}$$

Then the internal knots are defined by

$$\begin{gathered} i = int(js) \qquad \alpha = js - i \\ u_{p+j} = (1-\alpha)\bar{u}_{i-1} + \alpha\bar{u}_i \qquad j = 1, \ldots, n-p \end{gathered} \tag{11}$$

and

$$u_0 = \cdots = u_p = 0, \qquad and \qquad u_{m-p} = \cdots = u_m = 1$$

This ensures that $Q_0 = C(0)$ and $Q_m = C(1)$.

Now let

$$R_k = Q_k - N_{0,p}(\bar{u}_k)Q_0 - N_{n,p}(\bar{u}_k)Q_m, \quad k = 1, \ldots, m-1 \tag{12}$$

Applying the standard technique of linear least squares fitting and simplifying yields the system of $n - 1$ equations in $n - 1$ unknowns,

$$(N^T N)P = R \tag{13}$$

where N is the $(m - 1)$ x $(n - 1)$ matrix of scalars or basis function

$$N = \begin{bmatrix} N_{1,p}(\bar{u}_1) & \cdots & N_{n-1,p}(\bar{u}_1) \\ \vdots & \ddots & \vdots \\ N_{1,p}(\bar{u}_{m-1}) & \cdots & N_{n-1,p}(\bar{u}_{m-1}) \end{bmatrix} \tag{14}$$

and R is the vector of $n - 1$ points

$$R = \begin{bmatrix} N_{1,p}(\bar{u}_1)R_1 + & \cdots & +N_{1,p}(\bar{u}_{m-1})R_{m-1} \\ & \vdots & \\ N_{n-1,p}(\bar{u}_1)R_1 & \cdots & N_{n-1,p}(\bar{u}_{m-1})R_{m-1} \end{bmatrix} \tag{15}$$

The basis function $N_{i,k}$ is computed as

$$N_{i,p} = f_{i,p}N_{i,p-1} + g_{i+1,p}N_{i+1,-1} \tag{16}$$

with

$$f_{i,p}(u) = \frac{u - u_i}{u_{i+p} - u_i} \tag{17}$$

and

$$g_{i,p}(u) = \frac{u_{i+n} - u}{u_{i+n} - u_i} \tag{18}$$

The control points P, can then be computed.

$$P = \begin{bmatrix} P_1 \\ \vdots \\ P_{n-1} \end{bmatrix} \tag{19}$$

The curve is then defined in terms of the knot vector *u* and control points *P*. Using ten control points the knot vector contained fourteen knots. Applying more control points had no considerable effect on the accuracy, but increased the computational time considerably (Figure 4-12 and Figure 4-13).

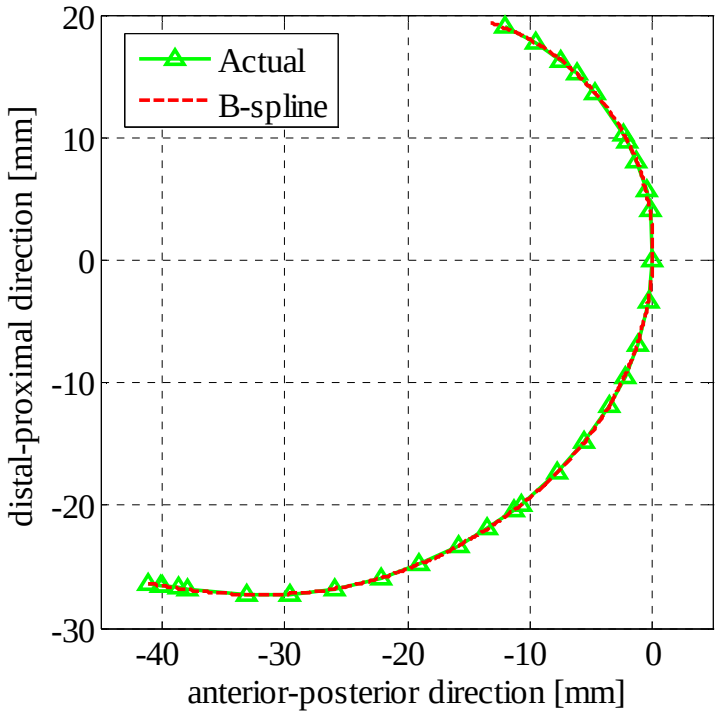

Figure 4-12: B-spline model fitted to a representative medial condyle sagittal profile

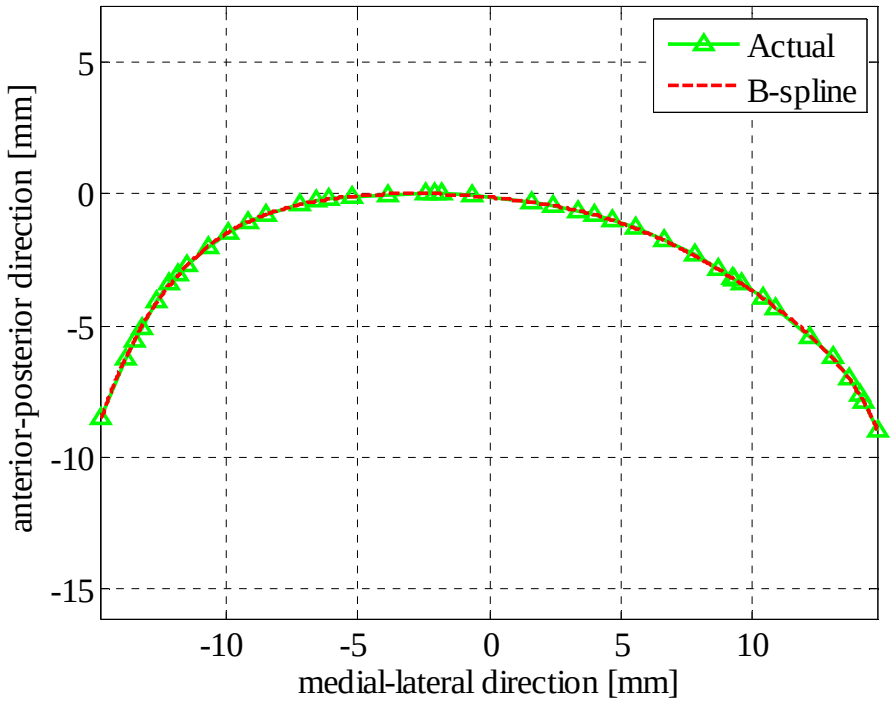

Figure 4-13: B-spline model fitted to a representative lateral condyle transverse profile

4.2.4 Fit accuracy

The different models described above were fitted to each of the 60 specimen data. The distance between each point in the original data and the fitted curve was calculated. This was used to determine the maximum error as well as a root mean square error (rms). The rms error is a good measure of the precision with which a fitted model represents the actual data and is given by

$$rmse(\hat{\theta}) = \sqrt{\frac{\sum_{i=1}^{n}(\hat{\theta}_i - \theta_i)^2}{n}} \tag{20}$$

where $\hat{\theta}_i - \theta_i$ is the distance between *i*th points of the fitted model and actual data, and *n* is the number of data points.

4.2.5 Predicting original joint profiles

It can be advantageous to develop a method for predicting or estimating an individual patient's original condyle geometries. This method can form the basis for developing custom knee prostheses. The approach used is similar to the one

used in Chapter 3 for the estimation of the original articulating measurements. In this case, the parameters of each fitted model are used in the SOM.

The calculated parameters of each model for each of the femoral specimens were stored in a database. These parameters are the parameters necessary to describe the models and are the centre points and radii for the single and dual radius models, the polynomial coefficients for the polynomial model, and the control points and knot vectors for the B-spline model. For each of the femoral specimens, certain other reference measurements were also performed and stored in the database, together with the corresponding model parameters. These reference measurements are not greatly affected by degenerative diseases such as osteoarthritis, and include the medial-lateral length (ML), the anterior-posterior length of both condyles (APL and APM), the distance between the most anterior points on the condyles (DAP), and the distance between the most posterior points on the condyles (DPP) (Erasmus & Dillon, 2008). These measurements were performed using a template in Mimics. All the measurements were performed by one person to eliminate inter-observer bias. Measurements were performed on three occasions to determine repeatability, with the second set of measurements being performed two weeks after the first, and the third set being performed two hours after the second. The database was used in an SOM algorithm to predict the healthy knee geometries.

In this case the input space is the database containing the healthy knee geometries in mathematical form. Hidden relationships between the reference measurements and the model parameters are identified by the SOM and then used to predict the articulating geometries for a knee joint with only the reference measurements known. The output will be the model parameters of the different mathematical models, and this output can then be used to reconstruct the knee joint geometry.

The accuracy of the predicted joint curves was calculated using the same technique as described earlier for the fitted models. The maximum error and the rms error were calculated for each of the mathematical models compared to the original joint geometry. Each time a specific femoral specimen was used as the test subject for which the geometry should be predicted, the specimen data were removed from the database in order not to affect the outcome. In other words, the specific knee data comprised the input vector and were removed from the database so that it did not form part of the SOM training phase. When it was presented to the SOM in the mapping phase, the output vector was a single neuron whose weight vector lay closest to the input vector. This output vector contained the parameters of the specific fitted model and could then be used to reconstruct the knee geometry.

The effect of increasing the number of healthy knees in the database was investigated by comparing the accuracy of the predictions when using 15, 30 and 60 knees in the database. The impact on an abnormal knee was also investigated.

4.2.6 Abnormal knee case study

An abnormally shaped knee was used as a case study to see the effect on the accuracy of the predictions as the number of knees in the database was increased. An rms difference between the reference measurements of all knees was calculated. That is to say, for each knee specimen, an rms difference between the knee and all the other knees in the database was calculated in terms of the reference measurements. The same equation as for the rms error was used (Section 4.2.5).

$$rmsd(\hat{\theta}) = \sqrt{\frac{\sum_{i=1}^{n}(\hat{\theta}_i - \theta_i)^2}{n}} \tag{21}$$

In this case, $\hat{\theta}_i - \theta_i$ is the difference between the reference measurements. For each knee, the mean rms difference between the specific knee and the other knees was calculated. This gave an indication of knees that were most unlike the others. The knee with the largest mean rms difference was chosen as the abnormal case study. The predicted knee joint geometry using the B-spline models was determined and compared using a database with sample size $n = 15$, $n = 30$, and $n = 60$ for the abnormal knee.

In order to accurately predict the geometry of an abnormal knee, similar abnormal knees should be present in the healthy knee database. These knee geometries can be seen as outliers in the database and can have negative effects on the SOM network. According to Lavine et al. (2004), an outlier will only affect one map unit and its neighbourhood, but it can have a drastic effect on certain of the principal components. The negative effect of outliers must be minimised, bearing in mind that they can play an important role in certain cases. Predicting the geometry of an abnormal knee joint will necessitate an abnormal knee joint being present in the database. However, the effect of the abnormal knee in the database must be minimised when predicting the geometry of a normal knee. An additional step was added to the SOM algorithm to implement this.

4.2.7 Outlier compensator

Minimising the effect an outlier has on the prediction of normal knee geometries requires reducing the contribution of the outlier to the eventual prediction

outcome. Or conversely, maximising the contribution of the normal knees to the eventual prediction outcome. After training, when presented with an input vector, the SOM network calculated the best matching unit as the outcome. Averaging the contribution of several map units that closely match the input vector can reduce the effect of an outlier. But, as stated, an outlier can play an important role for certain abnormal knee geometries, and in these cases the effect must not be reduced. Only map units within a certain tolerance of the input vector contribute to the calculation of the parameters. This ensures that an outlier will have a large contribution for abnormal knees, but not for normal knees.

After training, when presented with an input vector, an average percentage difference is calculated for each map unit and the input vector using

$$\%D = \frac{\sum_{i=1}^{n} \sqrt{\left[\left(\frac{V_i - W_i}{V_i}\right) \times 100\right]^2}}{n} \tag{22}$$

where V_i is the reference measurements (of length n) of the input vector and W_i is the reference measurements of the map units. *%D* gives an indication of the average percentage difference between the reference measurements of the input vector and each map unit. Letting all map units with a *%D* value lower than a certain tolerance contribute to the outcome will thus ensure a more accurate prediction by minimising the effect of outliers. If none of the map units falls within the tolerance, only the BMU is used to calculate the outcome parameters. Abnormal knees will thus still benefit from the outliers by choosing a small enough tolerance. This will ensure that only the outliers in the database contribute to the prediction for the abnormal knee and the prediction will not be affected by the normal knees in the database. The impact of the outlier compensator is investigated using different tolerances.

The effect of different map sizes (number of units in map) was also investigated. Lee et al. (2005) suggest that using too few output nodes or units can cause the congestion of input vectors at an output node. They suggest using slightly more output units than input vectors to avoid this problem. With 60 input vectors, map sizes of 100, 225 and 400 units were compared.

4.3 Results

4.3.1 Model fitting

The accuracy of the fitted models in the sagittal plane is illustrated in Figure 4-14 and Figure 4-15, using a representative case of a medial and lateral condyle. The B-spline model fitted the original data most accurately and showed a mean maximum error of 0.11 mm (standard deviation 0.04 mm) and 0.13 mm (standard deviation 0.24 mm) for the medial and lateral condyles respectively. The mean values mentioned are the means calculated for all 60 of the cases. The B-spline model further showed mean rms errors of 0.06 mm (standard deviation 0.01 mm) and 0.05 mm (standard deviation 0.01 mm) for the medial and lateral condyles respectively. The single radius models showed the largest mean maximum errors and mean rms error in the sagittal plane. All the mean errors with standard deviation are listed in Table 4-1.

In the sagittal plane, the maximum errors for the B-spline curves tended to occur distally, whereas they occurred posteriorly for the polynomial and dual radius models and for the single radius model on the medial side. For the single radius model on the lateral side, the maximum error tended to occur at the most anterior point. This is where the lateral condyle tends to flatten out.

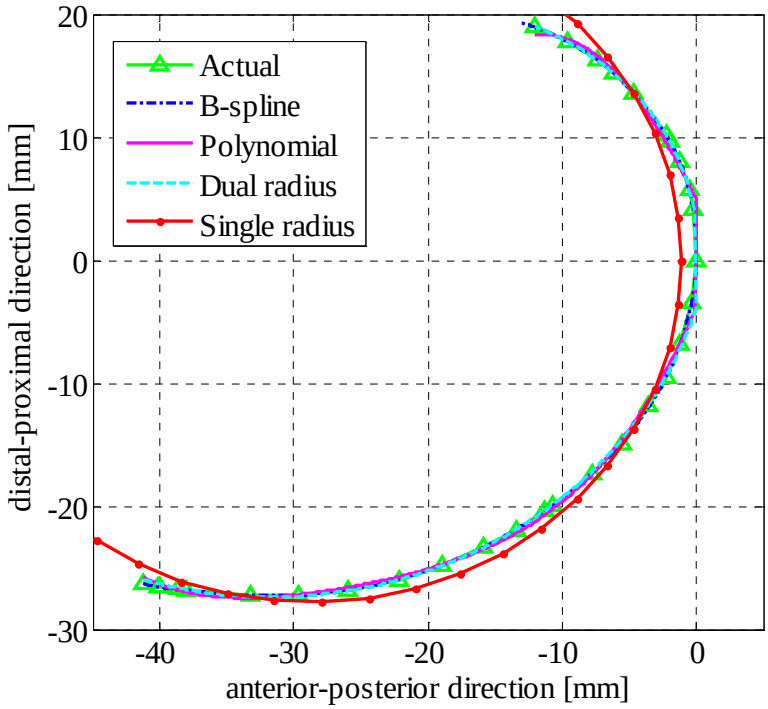

Figure 4-14: Fitted models on the medial condyle in the sagittal plane

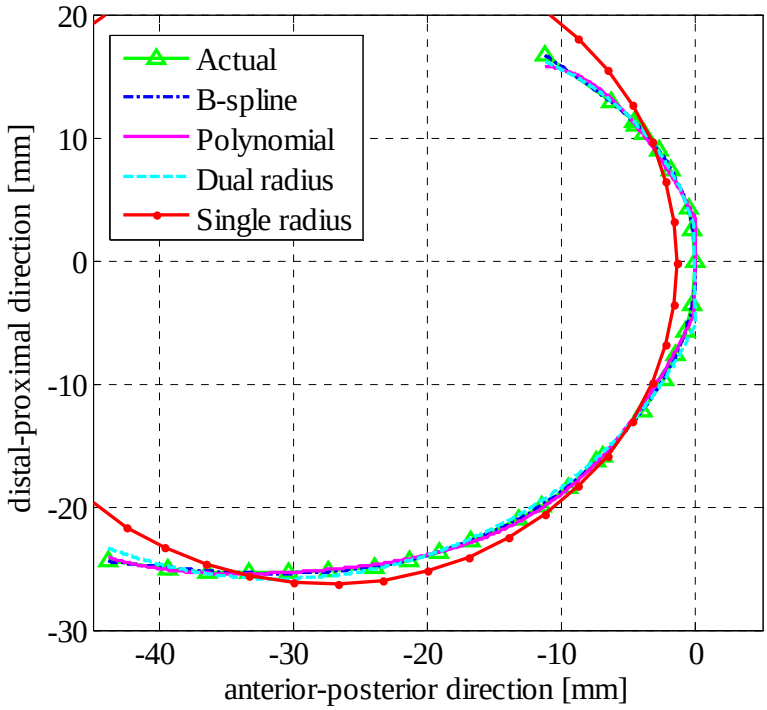

Figure 4-15: Fitted models on the lateral condyle in the sagittal plane

Table 4-1: Mean errors and standard deviation (±) of fitted curve data [mm]

		B-spline		Polynomial		Dual radius		Single radius	
		Max	rms	max	rms	max	rms	max	rms
	SAGITTAL								
Medial	mean	0.11	0.06	0.95	0.28	1.44	0.40	2.09	0.87
	±	0.04	0.01	0.28	0.06	0.42	0.12	0.49	0.21
Lateral	mean	0.13	0.05	0.97	0.27	1.38	0.40	1.55	0.59
	±	0.24	0.01	0.33	0.06	0.50	0.13	0.77	0.31
	TRANSVERSE								
Medial	mean	0.05	0.02	0.28	0.09	n/a	n/a	0.65	0.20
	±	0.07	0.01	0.26	0.06	n/a	n/a	0.44	0.12
Lateral	mean	0.05	0.02	0.42	0.13	n/a	n/a	0.95	0.29
	±	0.02	0.01	0.40	0.10	n/a	n/a	0.67	0.19

The accuracy of the fitted models in the transverse plane is illustrated in Figure 4-16 using a representative case of a lateral condyle. The B-spline model fitted the original data most precisely and showed a mean maximum error of 0.05 mm (standard deviation 0.07 mm) and 0.05 mm (standard deviation 0.02 mm) for the medial and lateral condyles, respectively. The mean rms errors were 0.02 mm (standard deviation 0.01 mm) for both the medial and lateral condyles. For the transverse profiles, the maximum error tended to occur laterally for the lateral condyle and medially for the medial condyle regardless of the model.

Results from the single and dual radius models were used to make certain comparisons between the geometries of the medial and lateral condyles. These were also compared to results in the literature. Student's t-tests were used to perform these comparisons between the medial and lateral condyles, with $p < 0.05$ taken to be statistically significant. The single radius model produced mean radii of 25.1 mm (standard deviation 2.0 mm) and 23.3 mm (standard deviation 2.2 mm) for the medial and lateral condyles ($p < 0.001$) in the sagittal plane. The centre point of the lateral condyle radius was situated a mean distance of 1.6 mm more anterior and 0.9 mm more proximal compared to the medial condyle radius ($p < 0.001$ and $p = 0.01$). The dual radius model produced mean radii of 30.8 mm (standard deviation 2.7 mm) and 26.8 mm (standard deviation 4.1 mm) for the distal portion ($p < 0.001$), and mean radii of 20.0 mm (standard deviation 4.3 mm) and 23.8 mm (standard deviation 6.2 mm) for the posterior portion ($p < 0.001$) of the medial and lateral condyles respectively.

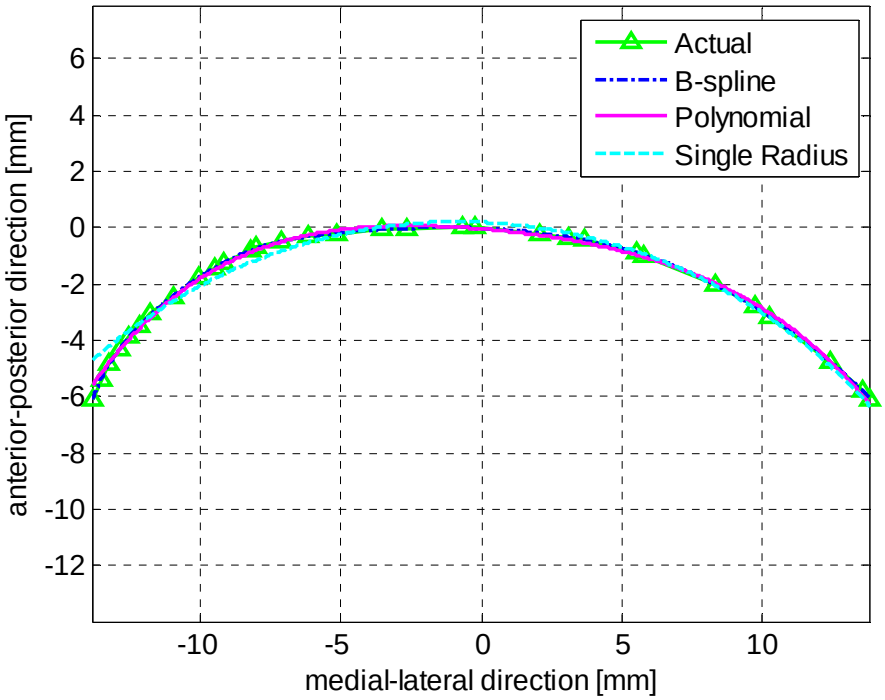

Figure 4-16 Fitted models on the lateral condyle in the transverse plane

In the transverse plane, the medial and lateral condyles had mean radii of 20.0 mm (standard deviation 3.9 mm) and 16.8 mm (standard deviation 2.4 mm) respectively.

4.3.2 SOM-predicted joint profiles

The repeatability of the measurements was satisfactory and did not show any significant difference between the measurements performed two weeks apart and those performed two hours apart, with mean errors between all measurements of 0.87 mm (std dev 0.32 mm) and 0.73 mm (std dev 0.41 mm) respectively ($p = 0.16$).

The accuracies of the knee geometries predicted using the SOM are listed in Table 4-2. Here the sample size in the database was $n = 60$ patients. The accuracies can be compared to those with $n = 15$ (Table 4-3) and $n = 30$ (Table 4-4). The B-spline model ($n = 60$) shows the best results, with mean rms errors in the sagittal plane of 0.71 mm (standard deviation 0.34 mm) and 0.68 mm (standard deviation 0.31 mm) for the medial and lateral condyle respectively. In the transverse plane, the B-spline model shows mean maximum errors of less than 1 mm.

Table 4-2: Mean errors and standard deviation (±) of SOM-predicted curve data [mm] with n = 60

		B-spline		Polynomial		Dual radius		Single radius	
		Max	rms	max	rms	max	rms	max	rms
	SAGITTAL								
Medial	mean	1.38	0.71	2.82	1.19	3.00	1.32	3.49	1.45
	±	0.68	0.34	1.45	0.51	0.94	0.70	1.43	0.49
Lateral	mean	1.34	0.68	2.62	1.01	2.78	1.14	2.95	1.17
	±	0.56	0.31	0.87	0.35	0.82	0.40	1.15	0.43
	TRANSVERSE								
Medial	mean	0.73	0.35	1.19	0.55	n/a	n/a	1.60	0.67
	±	0.40	0.19	0.68	0.28	n/a	n/a	0.94	0.34
Lateral	mean	0.76	0.38	1.07	0.47	n/a	n/a	1.37	0.54
	±	0.41	0.20	0.50	0.20	n/a	n/a	0.57	0.21

Table 4-3: Mean errors and standard deviation (±) of SOM-predicted curve data [mm] with n = 15

		B-spline		Polynomial		Dual radius		Single radius	
		Max	rms	max	rms	Max	rms	max	rms
	SAGITTAL								
Medial	mean	1.63	0.82	3.29	1.26	3.32	1.38	4.22	1.70
	±	0.78	0.37	1.90	0.64	1.24	0.57	2.28	0.77
Lateral	mean	1.63	0.80	3.59	1.33	3.74	1.43	3.74	1.44
	±	0.73	0.38	1.77	0.59	1.35	0.53	1.48	0.53
	TRANSVERSE								
Medial	mean	1.18	0.56	1.93	0.85	n/a	n/a	1.98	0.83
	±	0.61	0.27	1.13	0.46	n/a	n/a	1.09	0.12
Lateral	mean	0.86	0.43	1.21	0.54	n/a	n/a	1.34	0.58
	±	0.43	0.20	0.61	0.27	n/a	n/a	0.69	0.28

Table 4-4: Mean errors and standard deviation (±) of SOM-predicted curve data [mm] with n = 30

		B-spline		Polynomial		Dual radius		Single radius	
		Max	rms	max	rms	max	rms	max	rms
	SAGITTAL								
Medial	mean	1.41	0.74	3.07	1.23	3.25	1.31	3.84	1.46
	±	0.66	0.38	1.36	0.49	0.88	0.53	1.61	0.55
Lateral	mean	1.34	0.74	3.35	1.27	3.05	1.21	3.21	1.26
	±	0.56	0.34	1.52	0.46	1.03	0.46	1.50	0.50
	TRANSVERSE								
Medial	mean	0.81	0.40	1.19	0.57	n/a	n/a	1.41	0.63
	±	0.44	0.22	0.62	0.29	n/a	n/a	0.64	0.26
Lateral	mean	0.84	0.45	1.17	0.53	n/a	n/a	1.40	0.56
	±	0.44	0.24	0.64	0.27	n/a	n/a	0.55	0.22

4.3.3 Abnormal knee case study

The abnormal knee chosen for the case study is a very large knee, and Table 4-5 shows the abnormal knee reference measurements compared to the mean reference measurements of all 60 knees in the database.

Table 4-5: Case study measurements versus mean measurements [mm] with standard deviation (±)

	APL	APM	ML	DAP	DPP
Mean of all knees	68.6	67.0	72.0	35.7	47.6
±	4.6	4.5	6.0	3.7	4.0
Case study	75.52	75.49	91.99	44.76	59.45

Figure 4-17 to Figure 4-20 show the predicted B-splines compared to the actual knee data for the abnormal case, with different database sample sizes of *n = 15*, *n = 30*, and *n = 60*. Table 4-6 shows the mean maximum errors and rms errors calculated for each of the predicted models.

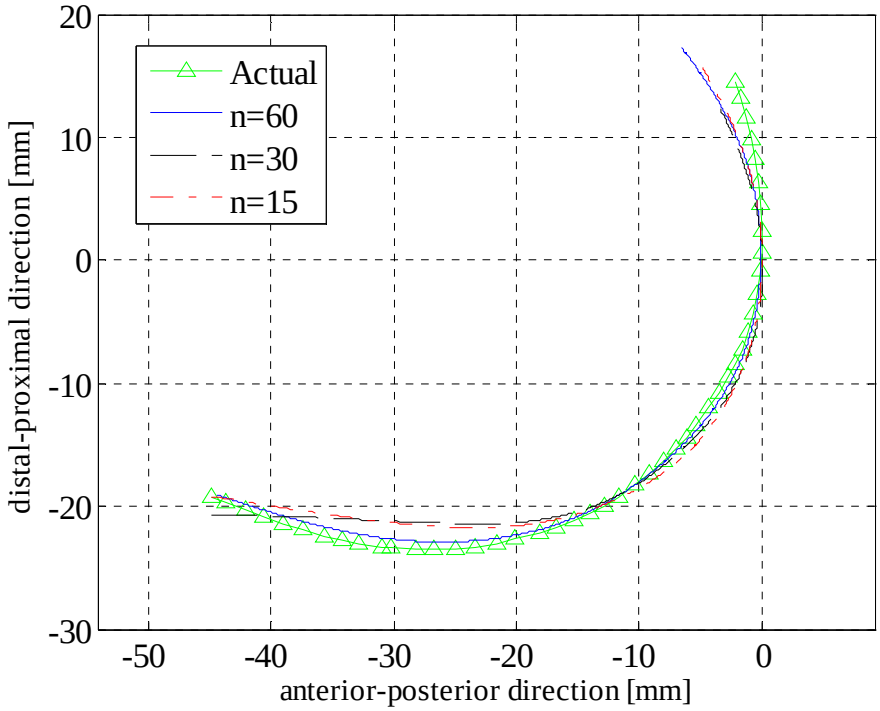

Figure 4-17: Fitted models on the case study knee; lateral condyle in the sagittal plane

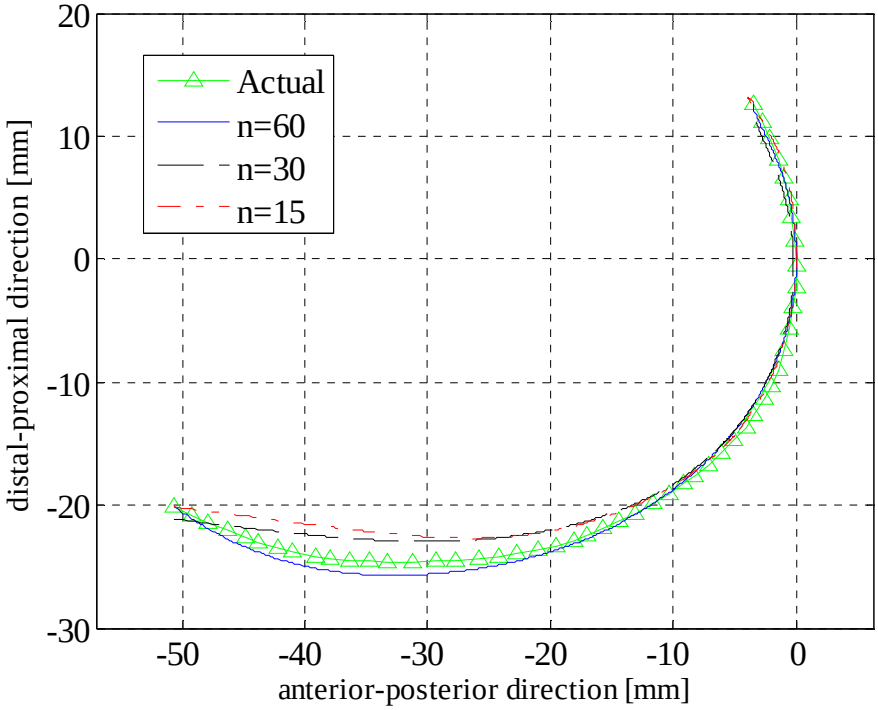

Figure 4-18: Fitted models on the case study knee; medial condyle in the sagittal plane

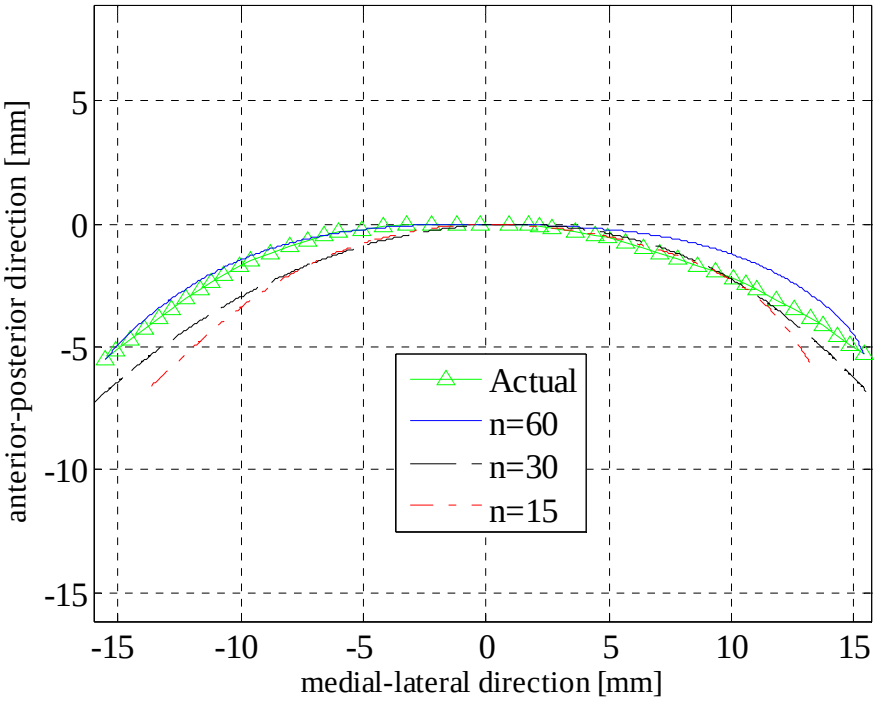

Figure 4-19: Fitted models on the case study knee; lateral condyle in the transverse plane

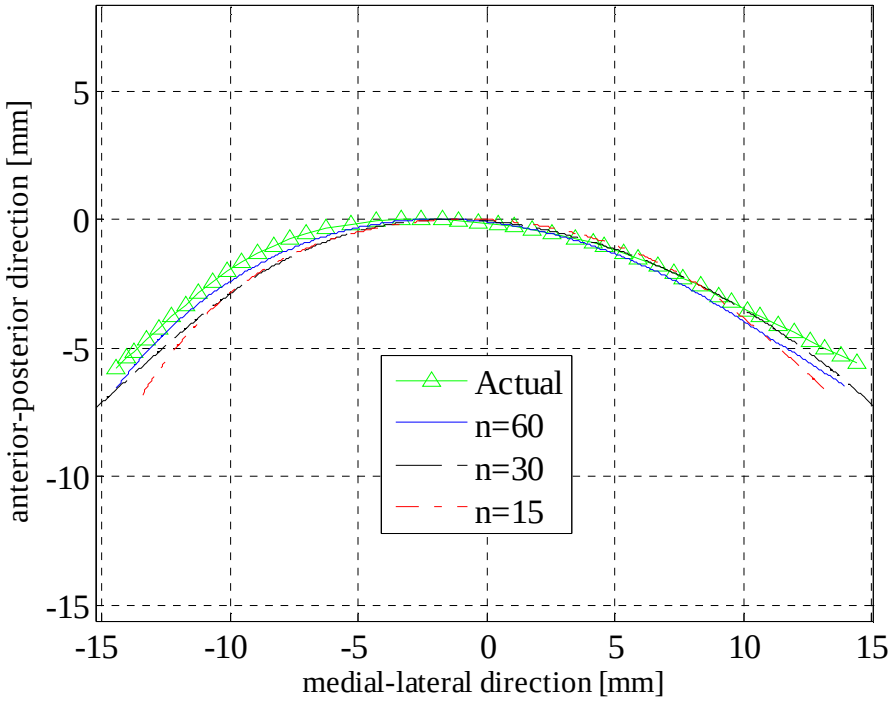

Figure 4-20: Fitted models on the case study knee; medial condyle in the transverse plane

Table 4-6: Case study accuracies

	Sagittal plane				Transverse plane			
	Lateral		Medial		Lateral		Medial	
	max	rms	max	rms	max	rms	max	rms
n = 15	2.03	1.11	2.58	1.25	1.63	0.69	2.18	1.10
n = 30	2.54	1.19	1.80	1.01	0.84	0.46	1.14	0.71
n = 60	2.01	0.61	1.10	0.55	1.02	0.40	0.95	0.47

It can be seen that, as the number of healthy knees in the database increases, the accuracy of the prediction model also increases for the abnormal case study.

4.3.4 Outlier compensator

The impact of the outlier compensator is depicted in Table 4-7, which shows the B-spline accuracies for different tolerance compensator and no compensator.

Table 4-7: Mean errors and standard deviations (±) of SOM-predicted B-spline data with outlier compensator using different tolerances [mm]

		Sagittal plane				Transverse plane			
		Medial		Lateral		Medial		Lateral	
		max	rms	max	rms	max	rms	max	rms
No	mean	1.38	0.71	1.34	0.68	0.73	0.35	0.76	0.38
compensator	±	0.68	0.34	0.56	0.31	0.40	0.19	0.41	0.20
Compensator	mean	1.33	0.69	1.30	0.65	0.73	0.35	0.78	0.39
tol <1%	±	0.65	0.33	0.56	0.28	0.40	0.19	0.41	0.20
Compensator	mean	1.25	0.64	1.21	0.60	0.74	0.36	0.71	0.36
tol <2%	±	0.57	0.30	0.55	0.29	0.41	0.19	0.39	0.19
Compensator	mean	1.26	0.66	1.27	0.63	0.73	0.36	0.70	0.35
tol <3%	±	0.60	0.32	0.65	0.34	0.38	0.18	0.41	0.19

Using the SOM network with $n = 60$ training examples and an outlier compensator with a tolerance of 2%, the impact of using different map sizes is summarised in Table 4-8.

Table 4-8: Mean errors of SOM-predicted B-spline data for different map sizes [mm]

		Sagittal plane				Transverse plane			
		Medial		Lateral		Medial		Lateral	
		max	rms	max	rms	max	rms	max	rms
Map size									
100	mean	1.22	0.65	1.22	0.61	0.74	0.36	0.70	0.35
	±	0.60	0.34	0.62	0.34	0.38	0.17	0.41	0.20
225	mean	1.25	0.64	1.21	0.60	0.74	0.36	0.71	0.36
	±	0.57	0.30	0.55	0.29	0.41	0.19	0.39	0.19
400	mean	1.36	0.70	1.23	0.61	0.77	0.38	0.71	0.36
	±	0.67	0.33	0.68	0.36	0.41	0.19	0.38	0.18

4.4 Discussion

Many studies have proposed different models to describe or reconstruct the geometry of the femoral condyles (Wismans et al., 1980), (Ateshian, 1993), (Boyd et al., 1999), (Nuño & Ahmed, 2003), (Hirokawa et al., 2004), (Biščević et al., 2005). However, these different models have not been compared for their accuracy. The objective here was to describe the complex morphometry of the articulating profiles of the femoral condyles with several different models. These models were then compared with regard to their precision of fit by equating them to the measured original profiles of several femoral joints.

The B-spline models showed the best results with respect to accuracy. This can be attributed to the ability of B-splines to provide the flexibility to design a large variety of shapes. B-splines are invariant under affine as well as perspective transformations. The mean maximum errors in the sagittal plane for the B-splines were 0.11 mm (standard deviation 0.04 mm) and 0.13 mm (standard deviation 0.24 mm) for the medial and lateral condyles respectively.

As expected, the single radius models showed the largest mean maximum errors of 2.0 mm (standard deviation 0.49 mm) and 1.55 mm (standard deviation 0.77 mm) for the medial and lateral condyles respectively in the sagittal view. The single radius model also showed the largest mean rms errors of 0.87 mm (standard deviation 0.21 mm) and 0.59 mm (standard deviation 0.31 mm) for the medial and lateral condyles respectively.

For the radial curves (transverse plane), the B-splines showed mean maximum errors of 0.05 mm (standard deviation 0.07 mm) and 0.05 mm (standard deviation 0.02 mm) for the medial and lateral condyles, respectively. The single radius models showed mean maximum errors of 0.65 mm (standard deviation 0.44 mm) and 0.95 mm (standard deviation 0.67 mm) for the medial and lateral condyles respectively and mean rms values of 0.20 mm (standard deviation 0.12 mm) and 0.29 mm (standard deviation 0.19 mm). The differences were statistically significant ($p < 0.001$) and suggest that in the transverse plane the medial condyle is more circular than the lateral condyle.

The differences in condyle radii obtained in this study are similar to those found in the literature. The radii of the posterior portions of the condyles are reported to be between 18.7 and 22.8 mm for the medial condyle, and 19.6 and 22.5 mm for the lateral condyle (Mensch & Amstutz, 1975), (Kurosawa et al., 1985), (Röstlund et al., 1989), (Elias et al., 1990), (Hollister et al., 1993), (Nuño & Ahmed, 2003). In this study, the mean radii were found to be 20 mm for the medial condyle and 23.8 mm for the lateral condyle. For the distal portions of the condyles, radii of between 32 and 35 mm for the medial condyle and between 32 and 36.9 mm for the lateral condyle were found in the literature (Iwaki et al., 2000), (Nuño & Ahmed, 2001), (Nuño & Ahmed, 2003). The results in the present study were found to be smaller than those in the literature with mean radii of 30.8 to 26.8 mm for the medial and lateral condyles respectively. A reason for this can be the way in which the distal circles were defined. In this study, the distal circles were fitted to data that included points from the most anterior point to the most posterior point. This definition of the distal circle might contain more of the posterior portion than in other studies.

With an accurate and reproducible mathematical technique to describe the knee joint, it becomes possible to design complex, patient-specific knee implants. To accomplish this it is necessary to be able to predict the original articulating surfaces for a specific individual. A method was developed to use a database containing the parameters of the models described in order to predict the articulating surfaces for any individual.

The SOM, in conjunction with B-splines, showed the most potential as a method that can be used to predict the knee joint profiles. A 15 x 15 map size (225 units) yielded the best results. Increasing the number of iterations showed no considerable effect and the default setting was used throughout. It is further shown that the accuracies of the prediction models can be improved by increasing the number of samples in the database of healthy knee geometries. This can ensure that the effect of outliers (abnormally shaped knees) in the database is

minimised. These outliers can nonetheless serve a useful purpose as they can offer an indication of the original dimensions of abnormal knees.

It can be seen in the case study selected that the accuracy of the prediction model improved for the abnormal case as the number of samples in the database increased. With more knees in the database, it is expected that there will be more knees similar to the study case and therefore the prediction will become more accurate. It is especially evident in the transverse planes, where the small sample sizes predicted profiles that were too narrow. It is expected that accuracy can be further improved with even more knees of diverse sizes (including the extremes) in the database. However, these extremes or outliers can have a negative effect on the prediction of normal knee geometries. Thus, the negative effect of outliers must be minimised, bearing in mind that they can play an important role in certain cases. This is accomplished with the outlier compensator.

Averaging the contribution of map units that closely match the input vector and fall within a certain tolerance of the input vector reduces the effect of an outlier. This also ensures that the outlier still makes a large contribution for abnormal knees with a correctly chosen tolerance. Table 4-7 shows that using a tolerance of 2% produces the best results. The average number of units used to calculate the outcome parameters with a 2% tolerance was 12, compared to one and 20 for the 1% and 3% tolerances respectively. The best matching unit for the case study knee had an average percentage difference of 3.3%, and thus only the one unit was used to calculate the outcome parameters and the calculation was thus not affected by the other normal knees.

The SOM has the further advantage of clustering or grouping together similar inputs during the mapping process. This can enable the automatic classification of different knees according to gender and race if there are indeed any morphological differences.

5. CLASSIFICATION OF GENDER AND RACE IN THE DISTAL FEMUR USING SELF-ORGANISING MAPS

5.1 Introduction

The concept of gender-specific and, to some extent, race-specific knee replacement designs has generated much interest and discussion (Ho et al., 2006), (Conley et al., 2007), (Greene, 2007), (Kwak et al., 2007), (Merchant et al., 2008), (Chaichankul et al., 2009), (Cheng et al., 2009), (Dargel et al., 2010), (Yue et al., 2011). Studies advocating the need for gender-specific implants cite certain anatomical differences between the male and female knee. Merchant et al. (2008) examined 19 peer-reviewed articles and concluded that, when normalized for size, the only notable difference between male and female knee anatomy is the reduced medial-lateral to anterior-posterior femoral condylar aspect ratio in female knees. They argue, however, that the difference is so small that it is unlikely to have any clinical effect. They further found that women have equal or better clinical results after total knee replacement (TKR) compared to men.

Similarly, studies advocating the need for race-specific implants cite anatomical differences between different races. Yue et al. (2011) found that Chinese knees are generally smaller than white (European descent) knees and that the femoral aspect-ratio of knees of Chinese females is significantly smaller than that of white females. Kwak et al. (2007) and Chaichankul et al. (2009) found sizing problems when using certain traditional TKR systems in the Korean and Thai populations, respectively. The TKR systems tended to cause mediolateral overhang of the component, i.e. the TKR systems had a larger aspect-ratio. It is argued that this mismatching influences clinical outcome after TKR. Iorio et al. (2007) found that Japanese patients receiving a traditional TKR system had significantly less postoperative range of motion compared to white patients. These findings have led some researches to suggest that certain races should have special designs of TKR systems.

Most researchers have either used intraoperative methods that may not allow for standardised and reproducible measurements (Ho et al., 2006), (Guy et al., 2011), or have performed the measurements on CT data that do not include the articular cartilage (Conley et al., 2007), (Kwak et al., 2007), (Cheng et al., 2009), (Yue et al., 2011). The thickness of the cartilage must be considered in order to measure the true dimensions of the femoral condyles (Seedhom et al., 1972). Furthermore, studies to date have made direct comparisons between the different anatomical dimensions of the knees to formulate their conclusions. In some cases the measurements were normalised for size, with the most common parameter being

medial-lateral to anterior-posterior femoral condylar aspect ratio. In other instances measurements were normalised with femur length (Dargel et al., 2010).

The aim of this chapter is to obtain reliable anatomic knee measurements and investigate the possibility of gender and race differences using an artificial neural network to classify the data. The SOM is used because it is trained using unsupervised learning; the classification of gender and race is not forced (Chapter 3). Rather, it shows whether such classification is present. The SOM will find arbitrary patterns in the data and these can then be analysed to see if there are any gender or race differences.

It was hypothesised that the absolute knee dimensions of white males are larger than those of black males and white females, and would clearly cluster together on the SOM map. It was further hypothesised that the differences would diminish when the data were normalised for differences in size, and that the SOM map would show no clear classification between the data. All data were normalised with AP length, thus in the process producing medial-lateral to anterior-posterior femoral condylar aspect ratio.

5.2 Methods

Sixty distal femurs were investigated (the same knees used in Chapter 4). Knee measurements were obtained by means of two methods, namely MRI and direct laser scanning of cadaver specimens using a 3D laser scanner. The MRI data comprised 20 white males with a mean age of 33.3 years (range 14 to 74 years) and 22 white females with a mean age of 32.5 years (range 14 to 63 years). The direct scanning data comprised 18 black male cadaver specimens with a mean age of 51.7 years (range 30 to 85 years). Data were imported into the Mimics software environment where the measurements were performed.

All measurements were performed by one person to eliminate inter-observer bias. Measurements were performed on three occasions to determine the repeatability, with the second set of measurements being performed two weeks after the first, and the third set being performed two hours after the second (the same database used as in Chapter 4). The measurements included the anterior-posterior length of the medial (APM) and lateral (APL) condyles, the posterior medial-lateral width (ML), the distance between the most posterior prominent points on the condyles (DPP), and the distance between the most anterior prominent points of the trochlear ridges (DAP) (Figure 5-1).

MRI data of several of the cadaver specimens were recorded in order to compare the accuracy of the measurements performed on the direct scanning data with the

measurements performed on the MRI data. Measurements between the two were found to be accurate to within 2% of one another. This 2% can result in errors between measurements of 0.5 mm to 1.8 mm, which is acceptable when taking into account that the MRI slice thickness is 1 mm. Victor et al. (2009) investigated the determination of bony landmarks on a CT scan of the knee and demonstrated intra- and inter-observer variability as high as 1.3 mm and 3.5 mm respectively

In order to determine the condylar curvature in the sagittal plane, the 3D models were imported into the 3-matic software environment, where intersection planes were created. The sagittal intersection planes were positioned at the most prominent central part of each condyle, perpendicular to an approximated transepicondylar axis. The transepicondylar axis was approximated by a 3º external rotation of the posterior condylar axis (Chapter 4). Intersection curves were then created where the condyles intersected the planes.

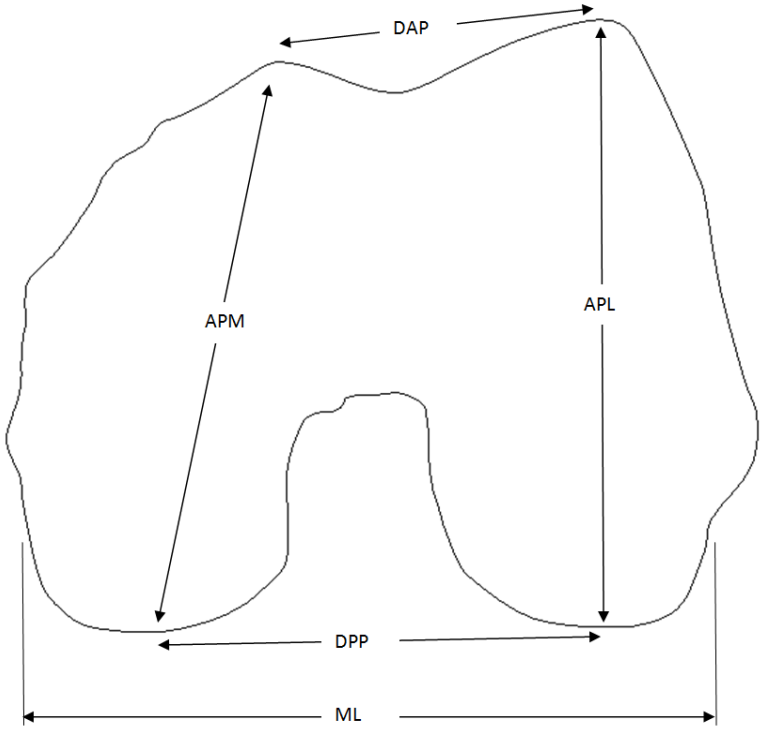

Figure 5-1: Morphological dimensions of the distal femur

Point cloud data of the intersection curves were exported to Matlab, where the radius of the best fitting arc was determined for each condyle by minimising the sum of squared radial deviations. This gave a lateral radius (LR) and medial radius (MR). Each knee specimen is now described by a vector containing the

seven measurements. These vectors were used as the input vectors in the SOM. The result is a network or lattice associating neurons with groups or patterns in the sample input data. Similar data will thus tend to cluster together in certain positions on the lattice or map.

Two maps were created, one using the absolute measurements of all the knees as input vectors, and the other using measurements normalised for size as input vectors. The measurements were normalised by simply dividing all knee data by their respective APL measurement. The APL was used to normalise the data as this then also produced the medial-lateral to anterior-posterior femoral condylar aspect-ratio, a term widely used in the literature to compare different knees (Merchant et al., 2008).

Data were also analysed using a two-tailed Student's t-test, with $p < 0.05$ taken to be statistically significant.

5.3 Results

Figure 5-2 shows the unified distance matrix, also called the u-matrix, created with the SOM using the absolute measurements. The u-matrix visualises distances between neighbouring map units and this helps to see the cluster structure of the map. High values of the u-matrix indicate a cluster border, and uniform areas of low values indicate clusters themselves. Upon examination of Figure 5-2, the labels on the right show the position of the knees on the map, with m = white male, f = white female and b = black male. From the figure it seems that the top part forms a clear cluster, with the last column (right-hand side) also seemingly part of the cluster. When looking at the labels it is seen that this corresponds to the white female measurements at the top and the black male measurements at the right.

Figure 5-3 to Figure 5-9 shows the individual component planes. The ML component and the DPP component have similar shapes to the u-matrix, suggesting that the medial-lateral width in white males tends to be larger than in white females and black males. The other components indicate that larger measurements lie to the bottom of the figures, the portion mostly occupied by white and black males. This suggests that male measurements tend to be larger than female measurements, regardless of race.

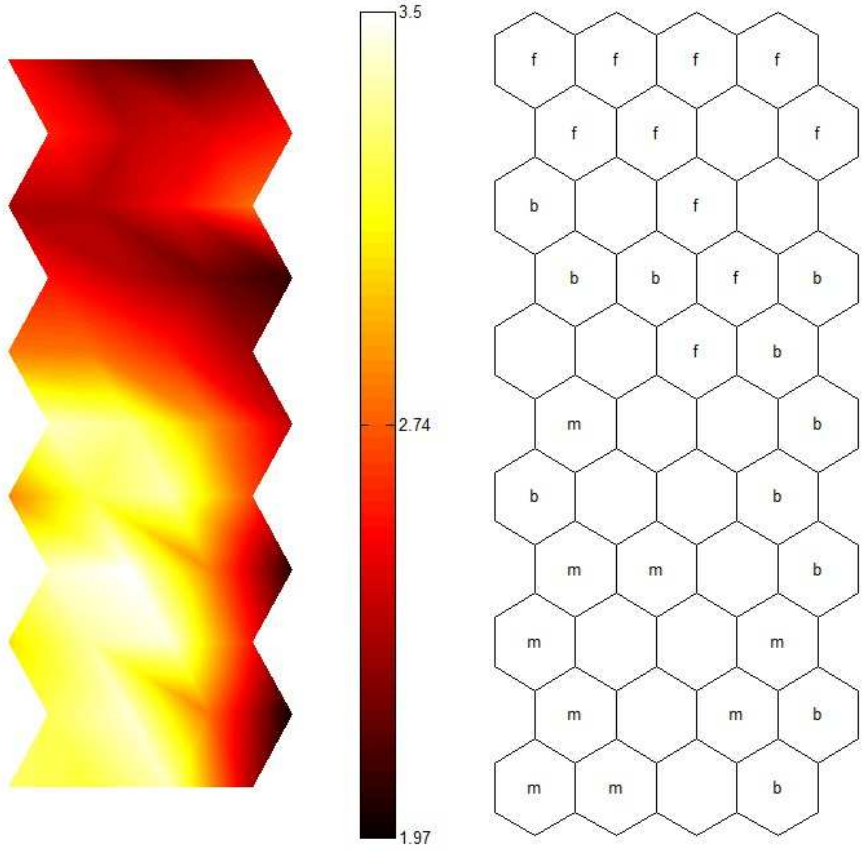

Figure 5-2: U-matrix of the absolute measurements

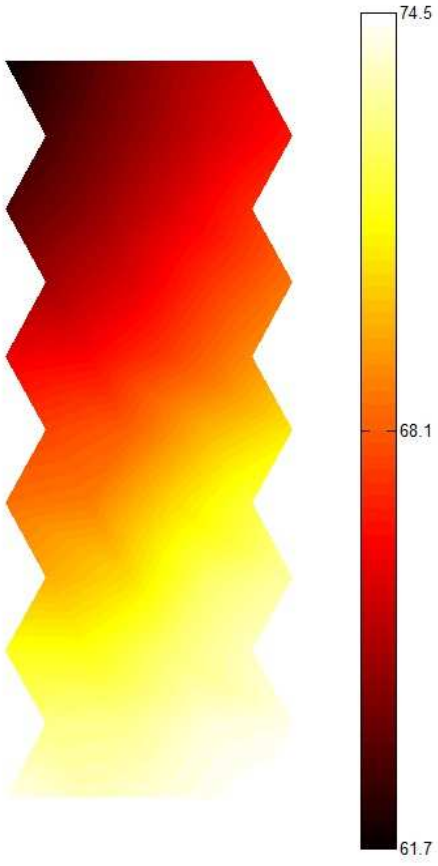

Figure 5-3: APM component plane of the absolute measurements

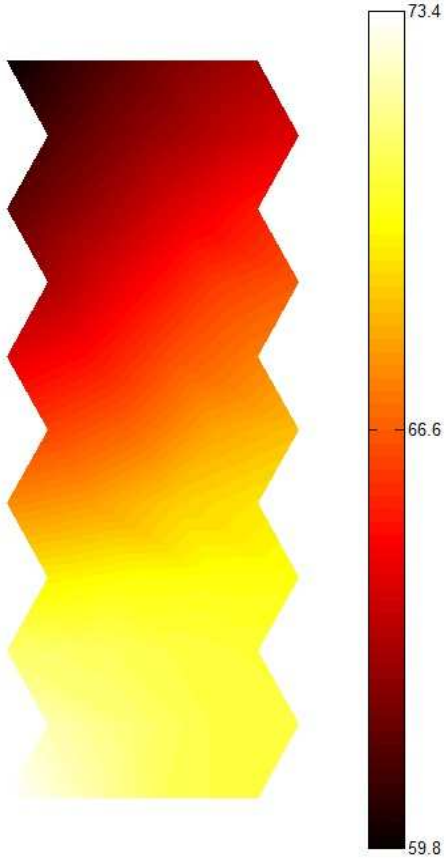

Figure 5-4: APL component plane of the absolute measurements

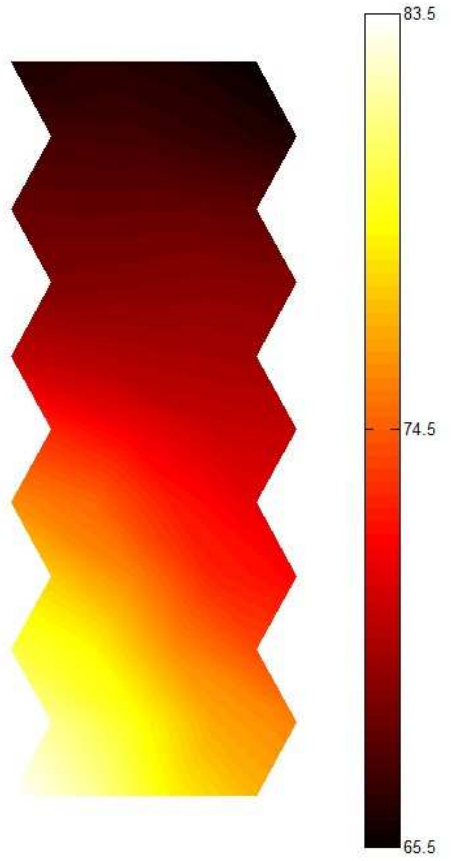

Figure 5-5: ML component plane of the absolute measurements

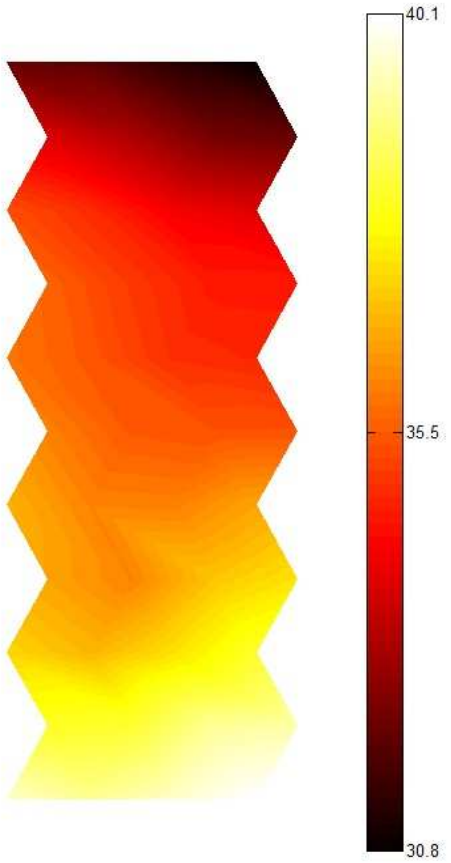

Figure 5-6: DAP component plane of the absolute measurements

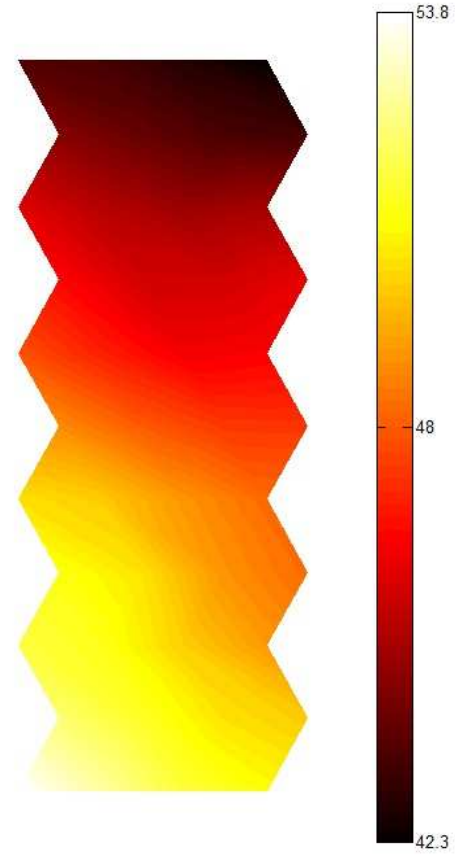

Figure 5-7: DPP component plane of the absolute measurements

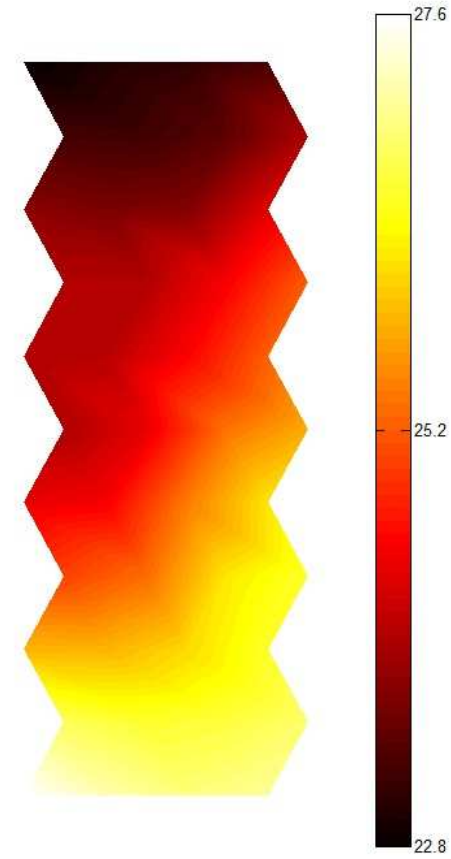

Figure 5-8: MR component plane of absolute measurements

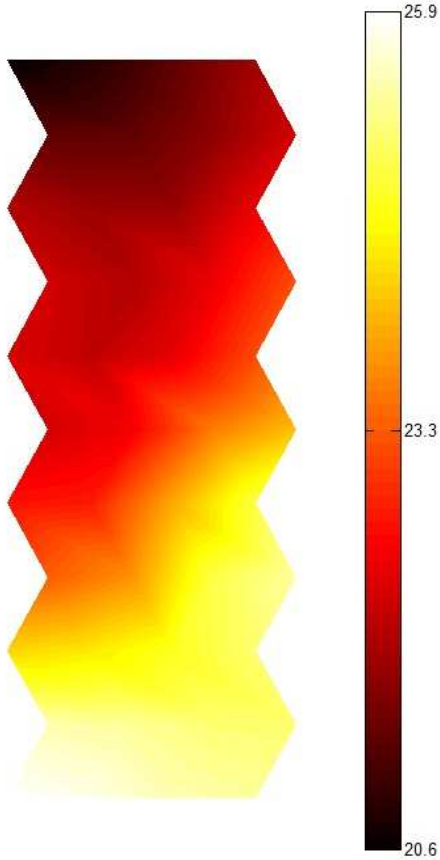

Figure 5-9: LR component plane of the absolute measurements

Figure 5-10 shows the u-matrix when the measurements are normalised. It is more difficult to distinguish a clear cluster in this figure, although the higher values in the top right corner can be seen as a cluster. The labels in this region correspond mostly to the black male measurements. Examination of the individual components showed that only the MR component plane and the LR component plane tended to show a similar shape to the u-matrix, with a cluster in the top right corner (Figure 5-15 and Figure 5-16). Other components showed no clear cluster, as can be seen in Figure 5-11 to Figure 5-14. Changing the number of iterations or the map size had no significant effect on the eventual outcome of the maps.

Student's t-tests confirmed the SOM observations (Table 5-1). A value of $p < 0.05$ was considered as statistically significant (highlighted). The mean ML was significantly larger in white males compared to black males and white females. White males had a mean ML of 77.7 mm (SD 5.7 mm), compared to 71.1 mm (SD 3.3 mm) for black males and 67.7 mm (SD 3.6 mm) for white females. The lateral anterior-posterior width was significantly larger in white males compared to white females, but not compared to black males. White males had a mean lateral anterior-posterior length of 71.5 mm (SD 3.7 mm), compared to the mean lengths of 68.9 mm (SD 4.6 mm) of black males and 66.4 mm (SD 4.2 mm) of white females.

When normalised for size, the SOM indicated that the ratio of the lateral condyle radius to the lateral anterior-posterior length was larger for black males than for white males and females. This was found to be the case, with the ratio for black males 0.36 (SD 0.016) and for white males 0.33 (SD 0.02), with a statistical significance of $p < 0.001$. Table 5-1 further shows that white males tended to have wider knees than white females. White males had significantly larger ratios for all three of the width measurements (ML/APL, DAP/APL, DPP/APL). White males also had a statistically significant ML/APL measurement compared to black males, but not for the other two width measurements.

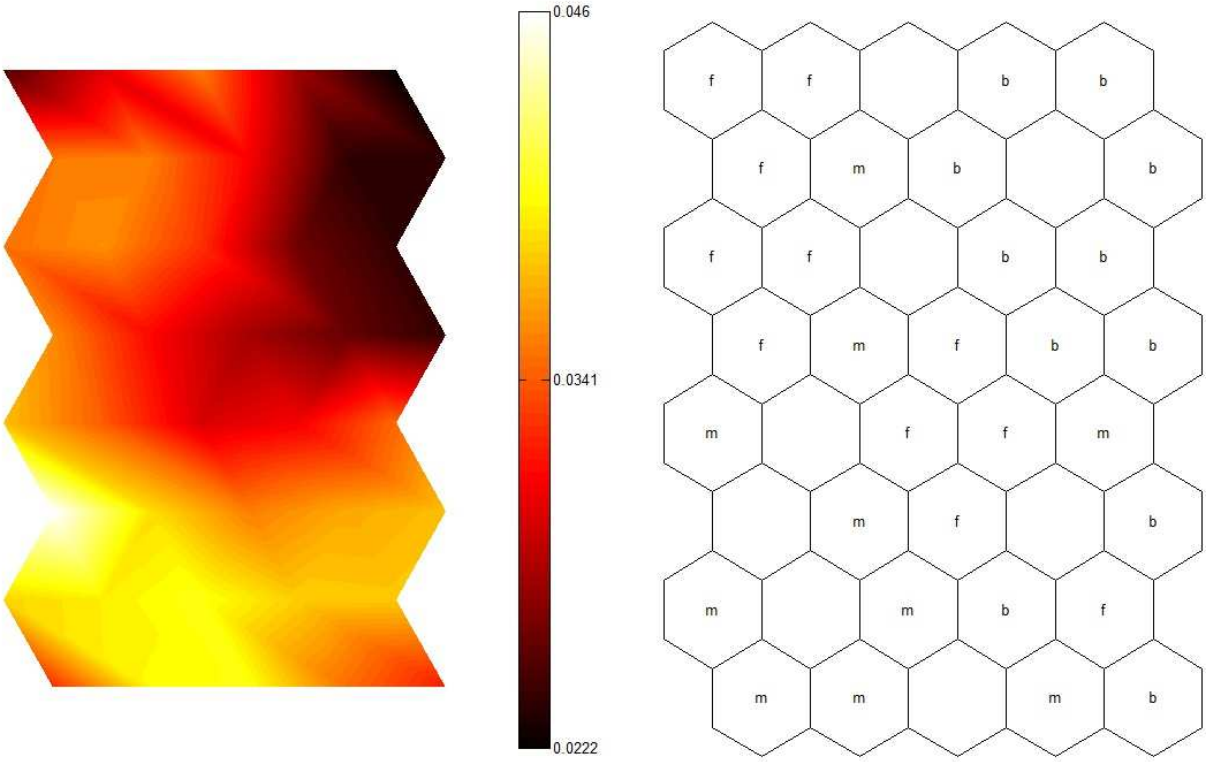

Figure 5-10: U-matrix of normalised data

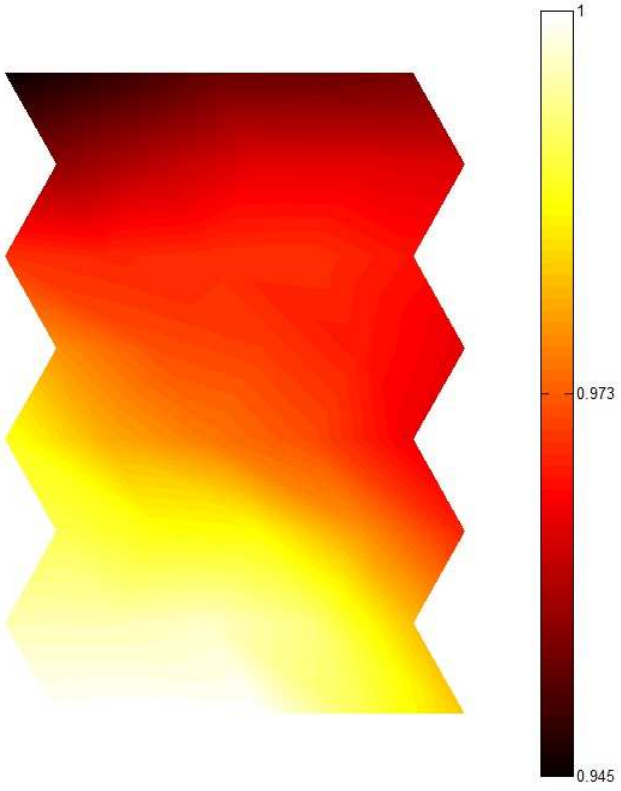

Figure 5-11: APM component plane of the normalised data

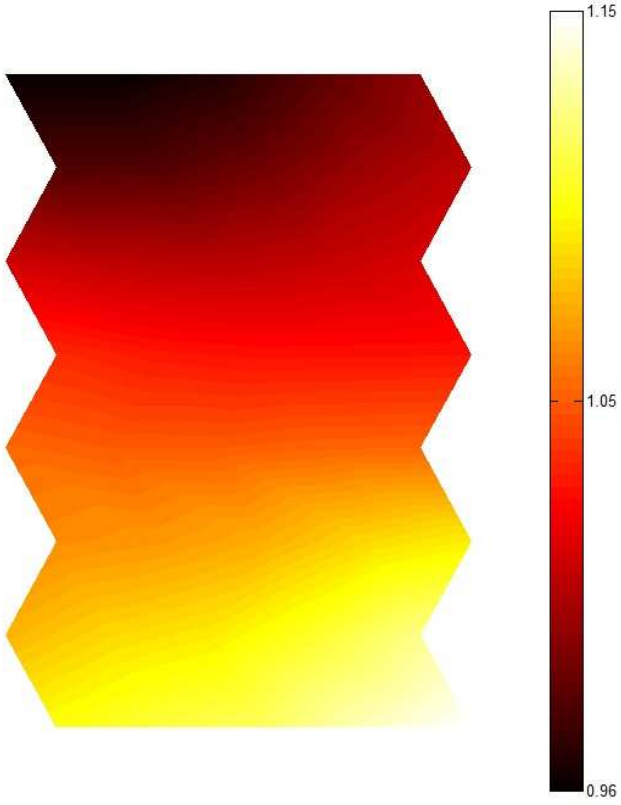

Figure 5-12: ML component plane of the normalised data

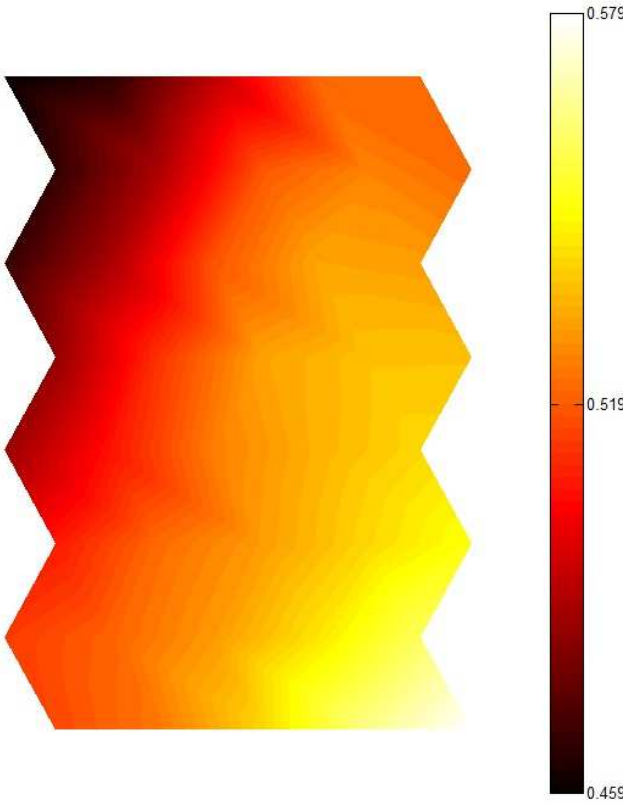

Figure 5-13: DAP component plane of the normalised data

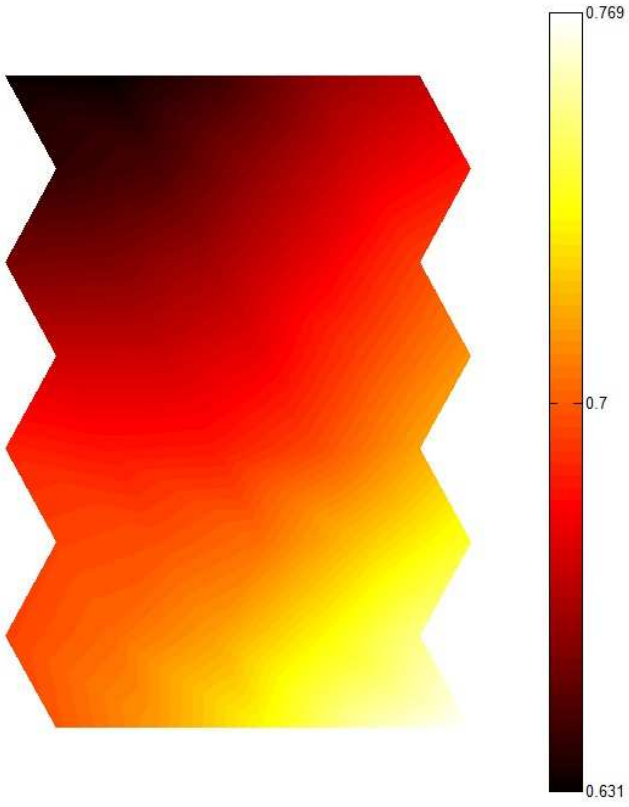

Figure 5-14: DPP component plane of the normalised data

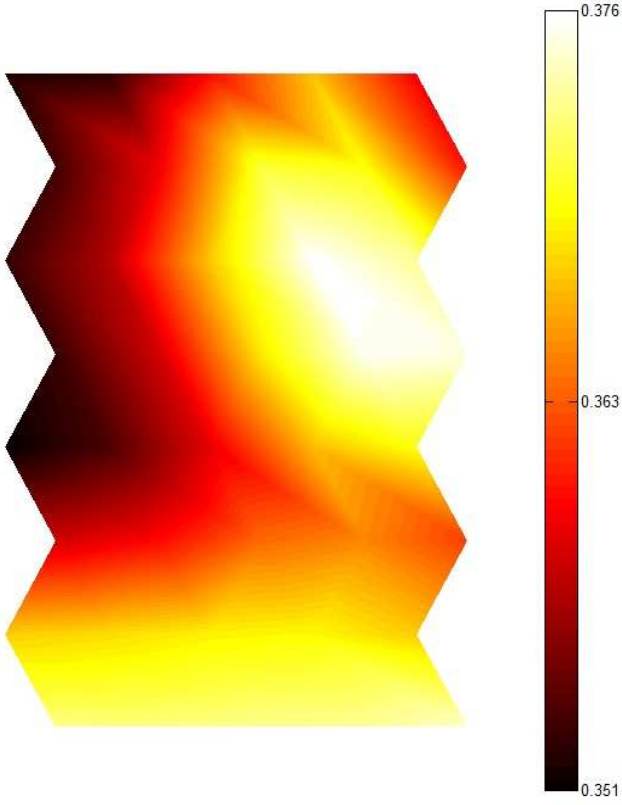

Figure 5-15: MR component plane of the normalised data

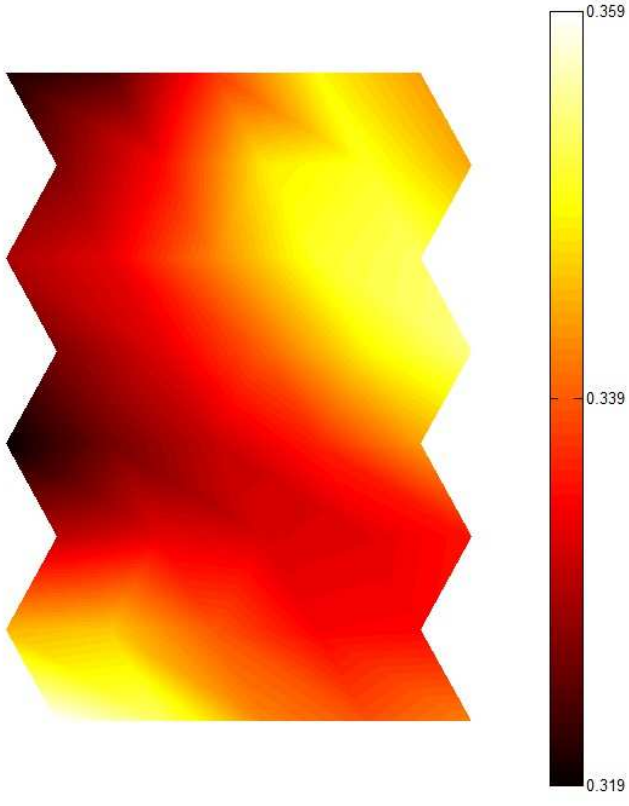

Figure 5-16: LR component plane of the normalised data

Table 5-1: Femoral knee joint dimensions (in mm with standard deviations) of white male, white female and black male specimens, with p < 0.05 taken as statistically significant.

	White males	White females	p	Black males	p
	Mean ± SD	Mean ± SD		Mean ± SD	
Absolute (mm):					
APL	71.5 ± 3.67	66.4 ± 4.17	< 0.001	68.9 ± 4.55	0.174
APM	70.4 ± 3.65	64.0 ± 3.66	< 0.001	66.7 ± 3.73	0.019
ML	77.7 ± 5.70	67.7 ± 3.56	< 0.001	71.1 ± 3.25	< 0.001
DAP	37.8 ± 3.20	32.4 ± 2.62	< 0.001	37.3 ± 2.19	0.645
DPP	50.9 ± 3.36	44.0 ± 2.36	< 0.001	48.5 ± 2.33	0.021
LR	24.1 ± 2.14	21.5 ± 1.12	< 0.001	24.6 ± 1.95	0.244
MR	25.6 ± 1.96	23.5 ± 1.31	0.001	26.3 ± 1.57	0.322
Normalised (ratios):					
APM/APL	98.5 ± 3.10	96.5 ± 2.80	0.060	96.9 ± 2.44	0.154
ML/APL	108.6 ± 619	102.1 ± 5.79	0.003	103.5 ± 5.75	0.025
DAP/APL	52.9 ± 3.75	49.0 ± 4.25	0.009	54.3 ± 3.21	0.271
DPP/APL	71.2 ± 4.02	66.3 ± 3.89	< 0.001	70.7 ± 4.46	0.563
LR/APL	33.7 ± 2.64	32.4 ± 1.52	0.128	35.8 ± 1.58	< 0.001
MR/APL	35.8 ± 1.92	35.5 ± 1.70	0.900	38.2 ± 1.66	< 0.001

5.4 Discussion

There is much debate on the need for gender-specific or race-specific knee replacements. The debate centres on the opinion that there are major anatomical differences between genders and races (Conley et al., 2007), (Merchant et al.,

2008), (Chaichankul et al., 2009), (Cheng et al., 2009). The aim of this chapter was to determine whether anatomical differences between genders and races could be classified using an artificial neural network. This would give an objective opinion on the existence of differences and, if they existed, what they might be. SOMs can be used to cluster large amounts of data, thereby simplifying, streamlining and speeding up the process of data interpretation (Dow et al., 2004). SOMs have been used in numerous applications, including the analysis of NMR spectra (Dow et al., 2004), gene clustering (Chang et al., 2010), gait analysis (Barton et al., 2007), (Scheffer & Cloete, 2011), reflex evaluation (Busch et al., 2009) and many more. In this study they were used to classify knees according to anatomical measurements.

When absolute measurements were used, a cluster was formed in the top part of the u-matrix, corresponding to white females. White males clustered together at the bottom left of the u-matrix, and the black males were present in the middle to top and also to the right of the u-matrix. This suggests, that when considering the absolute measurements, there is a definite difference between gender and race, and that different knees can be classified into their respective groups. White male knees were larger than white female knees across all measurements. This was further confirmed by Student's t-tests. Only the ML and DPP component planes had similar shapes to the u-matrix, in that the bottom left corner showed distinctly different results to the rest. In this case it is suggested that white males have wider knees compared to black males and white females. This was again confirmed by the Student's t-tests, as these dimensions were significantly larger in white males compared to black males, with the ML dimension having $p < 0.001$. All other component planes had a similar shape to that of the APL component, showing larger values at the bottom and also to the right, corresponding to both the white males and black males. This can also be seen in the Student's t-tests, where the white males had significantly larger measurements compared to the white females, but not compared to the black males.

When the measurements were normalised for size it was more difficult to define a clear cluster. The u-matrix did show a distinct area in the top right corner corresponding to most of the black males. Looking at the labels it can be seen that white males and females were not confined to a specific and distinct area. This suggests that, when measurements are normalised for size, there is no definite differences between white male and female knees. The LR and MR component planes showed similar shapes to that of the u-matrix, suggesting that black males have a larger LR and MR to APL ratio compared to the white males and females. This was confirmed by Student's t-tests, which showed that these ratios are the only ones that are significantly larger. All the other component planes showed no

distinct region corresponding to a particular group and suggest that, when normalised for size, there are no gender or racial differences in these measurements. There is, however, still interspecimen variation regardless of gender or race.

The Student's t-test results show that the three width measurement ratios, ML/APL, DAP/APL and DAA/APL, are significantly larger in white males than in white females. The aspect ratio of white male knees is also significantly larger than that of black male knees, suggesting that white males tend to have wider femurs. Conley et al. (2007) and Hitt et al. (2003) also found the female distal femur to be smaller than that of males and to have a smaller aspect ratio. Dargel et al. (2010) also found the ML dimension of the male knee to be significantly larger than that of the female knee, but there was no significant difference in femoral aspect ratio. Guy et al. (2011) found larger aspect ratios in women compared to men, with the mean ratio for women at 1.02 (same as in this study) and for men 0.98. There are thus conflicting opinions in the literature, and it is suggested from the results of this study that there is high variation regardless of gender.

Yue et al. (2011) found a statistically significant difference between the femoral aspect ratio of Chinese females and white females but not between Chinese men and white men. No data were found in the literature comparing anatomical differences between South African white male and black male knees. It is therefore a new concept to suggest that South African black males have a larger condyle radius to anterior-posterior length ratio compared to white males. A limitation of this study is the relatively small sample sizes investigated (60 knees). The sample size was in the same range as that used in similar studies (Ho et al., 2006), (Dargel et al., 2010), (Yue et al., 2011) in which sample sizes of between 60 and 76 were used, but in some other studies the sample sizes were more than 100 (Kwak et al., 2007), (Cheng et al., 2009), (Guy et al., 2011). Nonetheless, even with a small sample size it is apparent that, when normalised for size, there is large variation between individual knees, regardless of gender or race.

Numerous genetic diversity studies have shown that human genetic diversity is more pronounced within a population than between populations (Lewontin, 1972), (Relethford & Harpending, 1994), (Barbujani et al., 1997), and that Africans have the greatest genetic diversity (Bowcock et al., 1994), (Jorde et al., 2000). Patterns of human genetic variation are indirectly influenced by geographic and cultural factors (Xing et al., 2010). However, in recent times the distribution of human populations has tended to be spread out and not confined to certain geographical regions. This is due to the ease with which people now travel and immigrate to new parts of the world, thus being introduced to new populations.

This study, using a neural network to classify data, confirms the findings of Merchant et al. (2008) that the only notable difference between male and female knee anatomy is the reduced medial-lateral to anterior-posterior femoral condylar aspect ratio in female knees. When normalised for size, black males tended to have larger LR and MR to APL ratios compared to white males. However, there still exist large variation between knees regardless of gender and race. It is argued that with this large variation in knee measurements and populations as a whole, it can become advantageous not to focus on gender-specific or race-specific knee replacement designs, but rather patient-specific designs.

6. DEVELOPMENT OF A PATIENT-SPECIFIC KNEE REPLACEMENT

6.1 Introduction

It was shown in the preceding chapters that the knee joint has a very complex geometry. There are important anatomical differences between the medial and lateral condyles, and there is great variation between different individual's knee geometries. However, conventional knee replacement designs are based on simplified geometries and are supplied in sets of standard shapes and sizes predetermined by the manufacturer.

Harrysson et al. (2007) suggest that the custom design of implant components based on patient-specific anatomy can overcome the existing shortcomings of current designs. They propose an approach where the custom design is based on CT data of the patient's joint. The proposed custom design uses a CAD model of the patient's distal femur as the base for the design. The articulating surface is kept intact to avoid altering the gait. However, if the patient's distal femur is heavily deformed due to the arthritis, problems can arise because the original articulating surface is not known. Harrysson et al. (2007) show a more even stress distribution at the bone-implant interface. This reduces uneven bone remodelling that can lead to premature loosening. This more uniform stress distribution is achieved by making patient-specific curved cuts. The uneven stress distribution in conventional designs is caused by the planar cuts made on the distal femur to fit the implant (Figure 3-6). This results in sharp edges and corners, which produce stress peaks. A further advantage is that bone loss is reduced by 40% due to the customisation of the bone-implant interface (Harrysson et al., 2007).

Sathasivam et al. (1999) used CAD-CAM techniques to develop custom total knee replacements in five case studies. It was necessary to develop custom implants due to the small size and abnormal bone shapes found in the patients. The geometry of existing total knee replacements was used as the basis for the custom prostheses with only the size being customised. Special software was written and interfaced with CNC machines to manufacture the implants. Follow-up examinations showed good geometrical fit and satisfactory function. The design showed improved stability and strength and is adaptable to unusual shapes, including extremely small sizes. Lin et al. (2005) suggest a similar approach of changing local data of existing prostheses to meet the different requirements of a particular patient.

He et al. (2006) proposed the use of rapid prototyping (RP) techniques to fabricate titanium-alloy femoral components. A dog's knee joint was scanned using a helical CT machine. The noise and redundant information were removed from the CT images and a 3D model was constructed. Point cloud data representing the knee joint surface were obtained from the 3D model, which was then imported into reverse engineering (RE) software. The negative pattern of the surface was custom designed to include interconnected pores to facilitate blood circulation and promote new bone growth when implanted.

Stereolithography (SLA), an RP technique, was used to fabricate the resin prototype of the hemi-knee joint. The RP prototype was polished to uniform thickness and then cured in an oven, after which a casting shell was fabricated. Molten titanium alloy was then poured into the casting shell. After solidification, the shell was broken off and the titanium-alloy knee joint was taken out. After post-processing, which included trimming, sandblasting, polishing and drilling, the implant was ready for implantation. He et al. (2006) reported satisfactory results after the custom prosthesis was implanted into the dog. Normal functioning of the damaged joint began to restore gradually and the composite prosthesis displayed sufficient mechanical strength. In order to function like a natural joint, a joint substitute needs to have certain characteristics, according to He et al. (2006). These characteristics include:

- Mechanical requirement. The prosthesis should possess the necessary mechanical strength and stiffness.
- Anatomical requirement. The prosthesis should have a customised geometric size.
- Biological requirement. The prosthesis material should be biocompatible.

Liska et al. (2007) used a similar approach to develop a custom TKR to manage a medial femoral condylar non-union in a dog. CT data were used to build a stereolithography model of the femur, which was used to create a custom augment to replace the missing medial femoral condyle. The CAD model of the femoral component is shown in Figure 6-1.

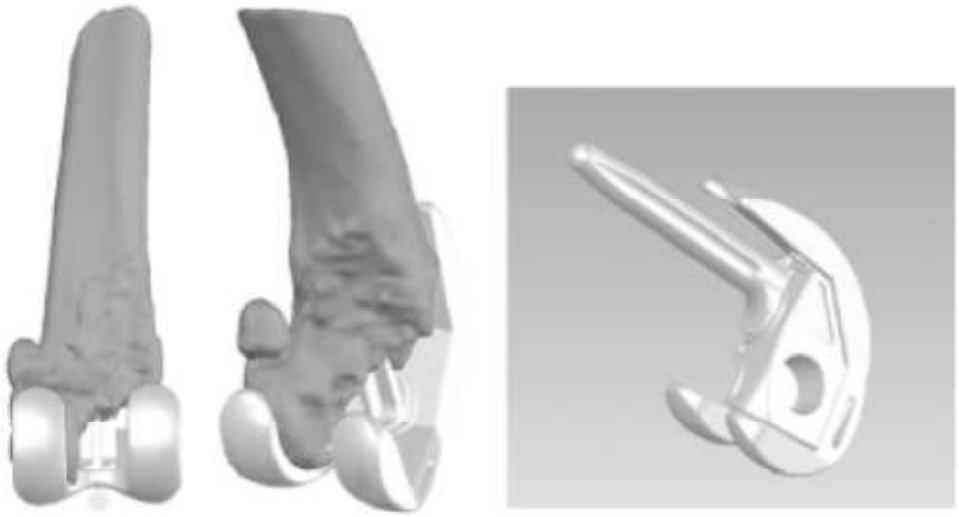

Figure 6-1: CAD model of custom femoral component for a dog (Liska et al., 2007)

It is clear that custom-designed knee prostheses hold various advantages for a patient. Conventional knee prostheses have many shortcomings in their design and alter the gait of a patient once implanted. The advances in rapid prototyping and rapid manufacturing (RM) techniques open the door to the possibility of developing patient-specific prostheses. A custom-designed implant can have the advantage of restoring the particular patient's original articulating surfaces more accurately than conventional knee replacement implants. Furthermore, most conventional UKRs only consider the sagittal and transverse profiles in their designs. However, curvatures of the individual condyles, as viewed in the anterior-posterior (transverse) plane are also present. This curvature is shown in Figure 6-2.

Conventional prosthesis designs typically do not consider this transverse curvature. As can be seen in Figure 6-2, the curvature on the medial side is more pronounced than on the lateral side. This curvature plays an important role in knee kinematics, as the contact areas/points of articulation between the femoral condyles and the tibia surface also follow a curved path. Walker et al. (2006) researched the relative positions of the contacts on the cartilage surfaces of the knee joint and found a similar curvature. Figure 6-3 shows a distal femur with the contact paths for the eight cadaveric specimens examined. The yellow lines show the centres of the contact areas for the tibia while the blue lines represent the centres of the contact areas of the patella (Walker et al., 2006).

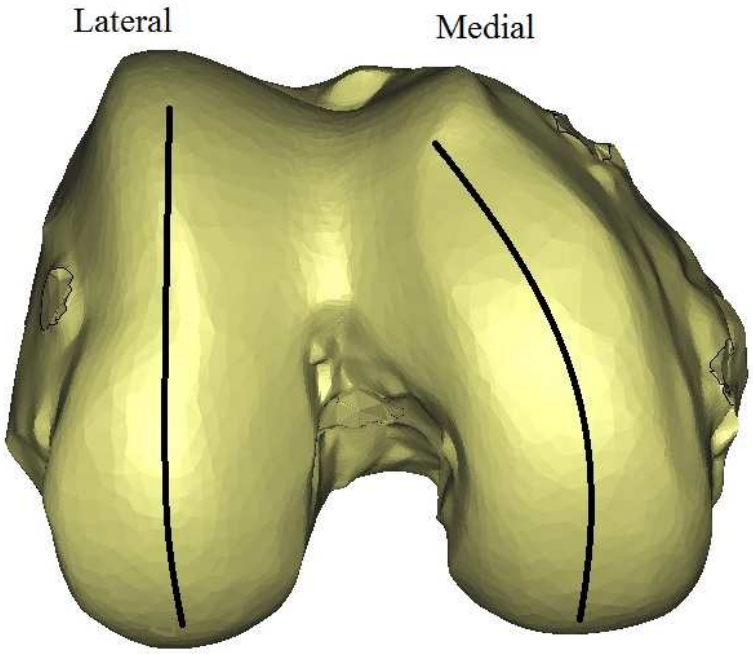

Figure 6-2: Curvature of femoral condyles in coronal view

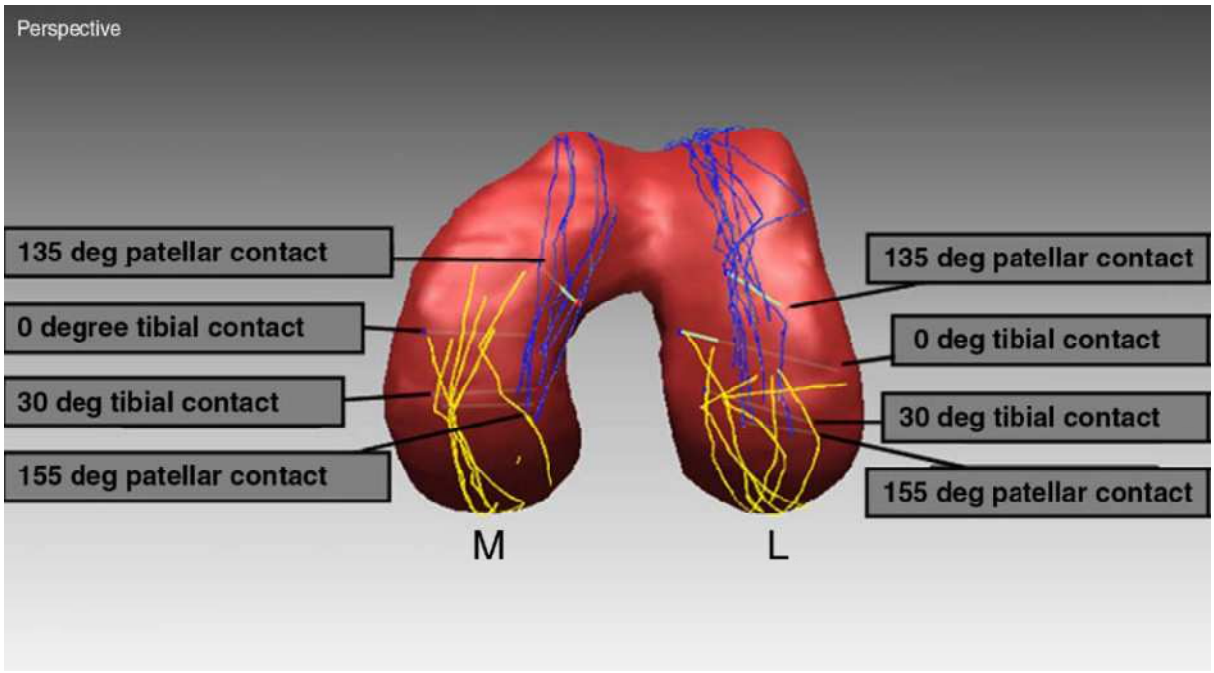

Figure 6-3: Paths of centres of contact areas on distal femur (Walker et al., 2006)

Most conventional prosthesis designs use the same components for both the medial and lateral compartments and do not take this curvature into account. They also dismiss the other anatomical differences between the lateral and medial condyles. Osteoarthritis of the knee commonly starts in the medial compartment and only later progresses to the lateral compartment (White et al., 1991), (Carr et al., 1993), (Gunther et al., 1996). The Oxford UKR and numerous other UKRs were therefore designed for the medial compartment. Patients suffering from osteoarthritis in the lateral compartment only also receive the same implant designed for the medial side. However, the geometry and kinematics of the two compartments differ and the lateral compartment is anatomically and biomechanically unique (Ashraf et al., 2002). Gunther et al. (1996) reported a survival rate of 67% at ten years follow-up using a mobile-bearing UKR for the treatment of lateral OA. Ashraf et al. (2002) reported survival rates of 83% at ten years follow-up and 74.5% at 15 years follow-up. Pandit et al. (2009) reported unacceptably high dislocation rates for mobile-bearing UKRs in the lateral compartment. They demonstrated that the dislocation rates could be decreased to an acceptable level by using a modified surgical technique and a new implant design. Pennington et al. (2006) reported good long-term survivorship with the tibial component positioned in 10º to 15º of internal rotation. This is to compensate for the lateral compartment kinematics. Nägerl et al. (2008) proposed an asymmetrical design for the lateral and medial compartments in a novel TKR. In the sagittal direction, the lateral tibial articulating surface is shaped convexly. This is similar to the shape of the lateral tibial surface in the natural knee and different to the medial surface, which is concave.

When developing patient-specific knee replacements, it becomes possible to overcome these shortcomings of conventional knee replacements.

6.2 Methods

In Chapter 4, a method of estimating an individual's original knee joint profiles was presented. The method is based on an SOM algorithm that uses a database of normal knees as the training data. A compensator was added to the algorithm and was shown to improve the accuracy of the estimations. The algorithm, in conjunction with the B-spline models, showed the best results and can be used as the basis for designing patient-specific unicompartmental knee replacements.

An individual requiring a patient-specific UKR will undergo MRI and CT scans. 3D models are then constructed in Mimics and the reference measurements not affected by arthritis as described in Chapter 4, can then be taken from the models. The reference measurements are the inputs to the SOM estimation algorithm

described in Chapter 4. The outputs of the algorithm are a set of B-spline parameters that can be used to develop the articulating surfaces of the femoral components. Figure 6-4 illustrates the process.

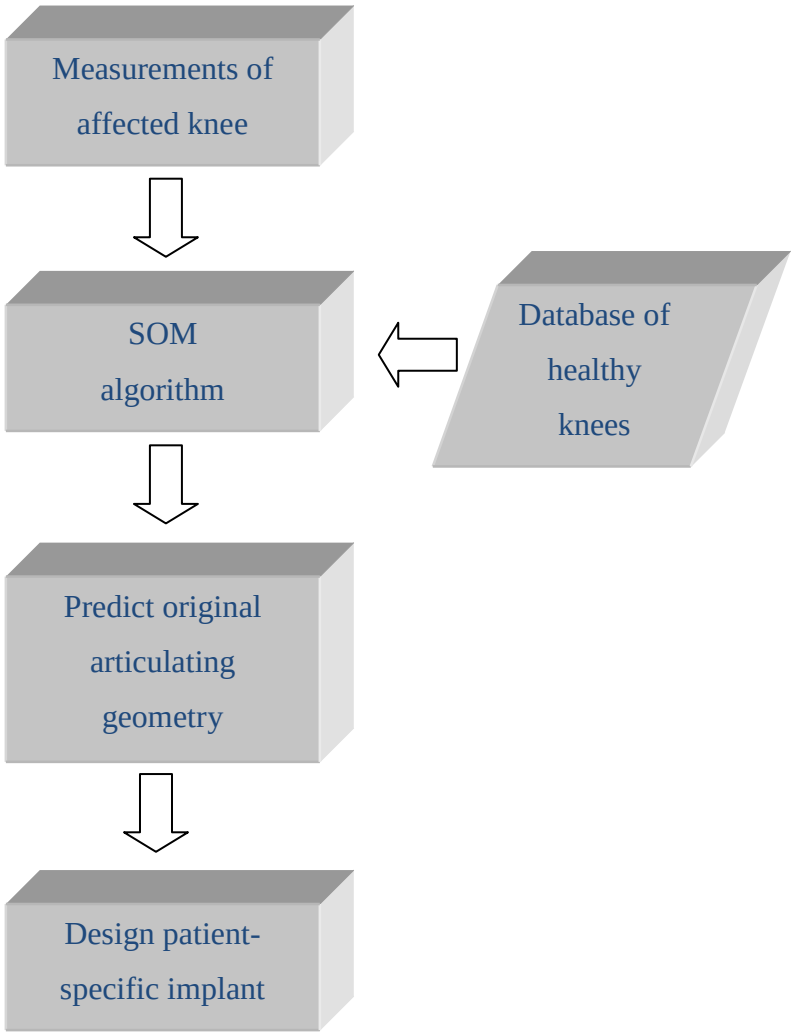

Figure 6-4: Process of designing a patient-specific implant

6.2.1 Femoral component

The output of the SOM estimation algorithm is used to design the articulating surfaces of the prosthesis. The output for a specific individual is a set of B-spline

parameters. These are used to draw the sagittal and transverse profiles for the specific individual. The profiles are then exported to a Microsoft Excel spreadsheet as a set of points. These points are then imported into Autodesk Inventor Professional 2008 (Autodesk Inc, San Rafael, USA) and used to create solid models. However, the B-spline profiles only describe the articulating profiles in two planes, namely the sagittal plane and the transverse plane. The anterior-posterior curvature of the specific individual must also be considered in the design.

This is accomplished when the reference measurements are made in Mimics. Three points are placed on each femoral condyle (Figure 6-5). The first point is placed in the middle of the condyle, at the most posterior part. The second and third points are placed proximally and distally, defining the length of the implant (the length of articulation). The latter point can generally be found on the lateral condyle, where a distinct groove is present, called the sulcus terminalis. On the medial side, this point is taken after the condyle starts to show proximal curvature. The proximal points are chosen at the proximal border of the condyles.

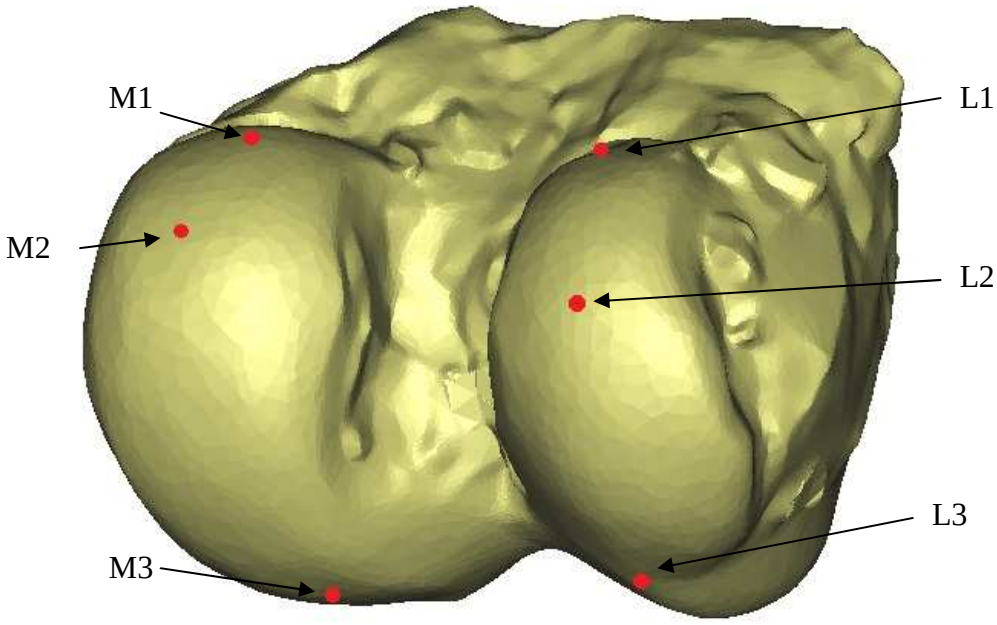

Figure 6-5: Points describing the anterior-posterior curvature

These points are used to create a second-order polynomial (a parabola) to describe the curvature. A parabola is used because of the simplified shape and few points

used. The points describing this curvature are combined with the sagittal profile points to form a 3D set of profile points. These are exported to an Excel spreadsheet together with the 2D points of the transverse profile. The Excel data are imported into Inventor and fitted with splines. Inventor is a CAD package that is used to prepare solid mechanical models. The initial component thickness is defined in the transverse view (Figure 6-6). The sweep function is then used to sweep the transverse profile along the 3D sagittal/coronal path to create the solid component. The component now has its patient-specific articulating surface. The next step is to customise the bone-implant interface.

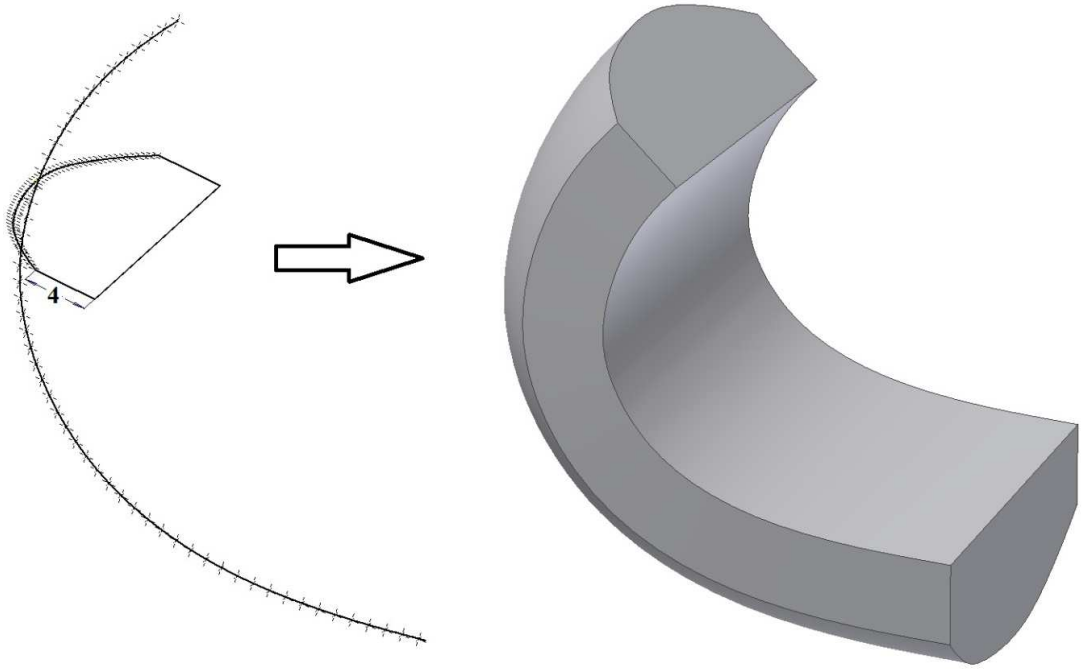

Figure 6-6: Turning splines into a solid component with a thickness of 4 mm using Autodesk Inventor

The bone-implant interface of the femoral component is the surface of the component directly in contact with the patient's femoral condyle. Currently, most designs require the femoral condyles to be reshaped to fit the implant. The resultant bone shape is squared-off to fit the implant, with surfaces as shown in Figure 6-7. These shapes are restricted by the surgical techniques currently available and cause uneven stress distribution with the 'corners' experiencing peak amounts of stress (Harrysson et al., 2007).

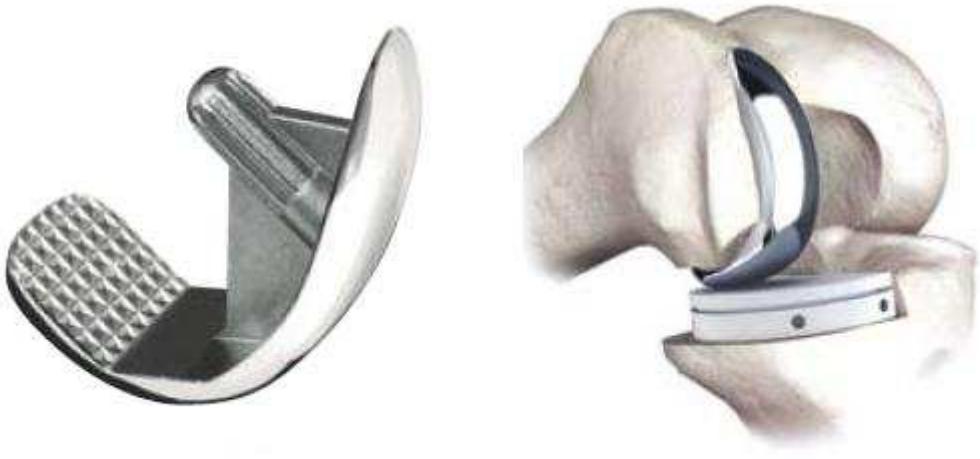

Figure 6-7: Conventional femoral component showing the square bone-implant surfaces (Tornier, 2009)

To avoid this uneven stress distribution, and to minimise bone loss, a patient-specific bone-implant interface is suggested. The Inventor model is imported into 3-matic together with the CT model of the patient's femur. The femoral component is then manually moved to the desired position on the femur (Figure 6-8). A *Boolean subtract* function is used to cut the femur geometry into the component. What is left is a femoral component with the femur surface geometry on the bone-implant interface (Figure 6-9).

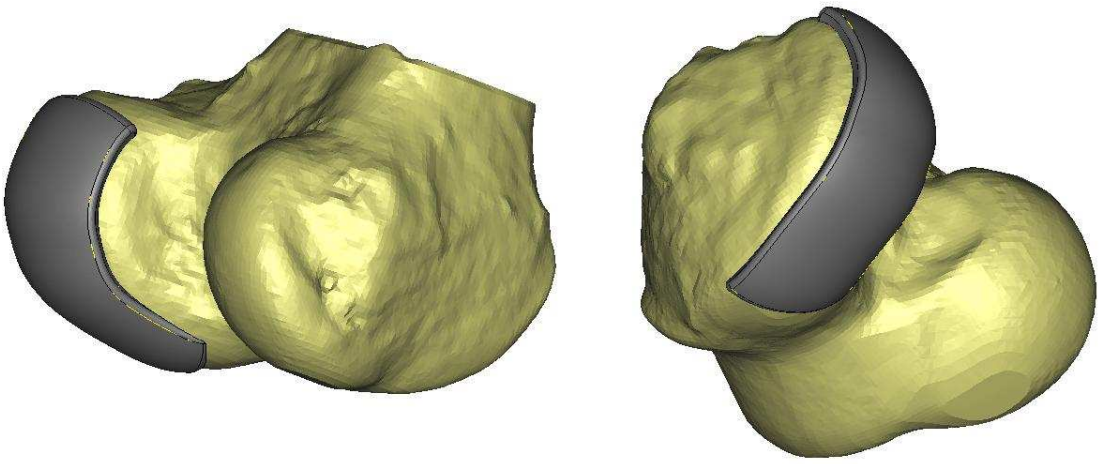

Figure 6-8: Femoral component in desired position

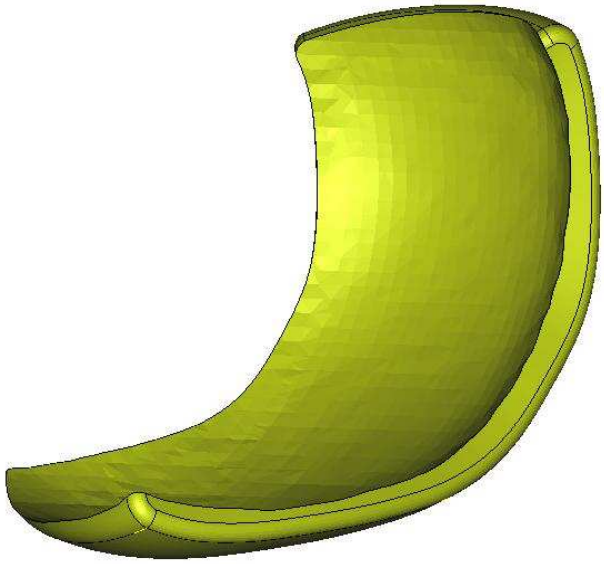

Figure 6-9: Femoral component with patient-specific bone-implant interface surface

In theory, the component should fit perfectly on the patient's femur once all the cartilage is removed. However, some detail is lost in the CT scans and reconstruction in Mimics. The final thickness of the part will be the initial thickness minus the volume cut away. The thickness will thus vary throughout the component. An analysis can be performed in 3-matic to investigate the thickness and to make sure it stays above a certain limit for strength considerations. Steklov et al. (2010) used a femoral component thickness of 3 mm in a novel unicompartmental knee implant, while a minimum femoral component thickness of 2 mm is used in the PB Uni knee system (Sab, 2011). In this study, a minimum thickness of 2 mm was used, which is similar to the average cartilage thickness (Chapter 3).

The next step is to consider the fixation method. The fixation method is the method by which the femoral component is fixed to the femoral condyle. Many different variations exist in the commercially available designs, and there is no clear indication of a superior method. Another consideration is whether to use cemented or cementless fixation. As mentioned, cemented fixation relies on fast-curing bone cement and a solid mechanical bond to hold the prosthesis in place. The cement is usually pressed into the distal femoral surfaces and onto the inner surface of the prosthesis. Cementless fixation relies on bone growing into the special surface topography to hold the prosthesis in place (Chockalingam & Scott,

2000). Cemented fixation shows a slight advantage in terms of component loosening and was the chosen method in the proposed design.

When designing a fixation method like a peg or fin, it is important to consider the surgical technique and instrumentation required to prepare the bone for the peg or fin. Another consideration is the amount of bone to be removed. It is argued that the optimal method of fixation would be one that produces the largest contact area with the lowest volume. This will ensure less bone to be removed and more contact area for the fixation. Following this rationale, the optimal fixation method would be a thin fin. A 10 mm radius semi-circle fin of 3 mm thickness is proposed. It shows a good contact area-to-volume ratio (10% better than a peg of 3 mm radius and 10 mm length).

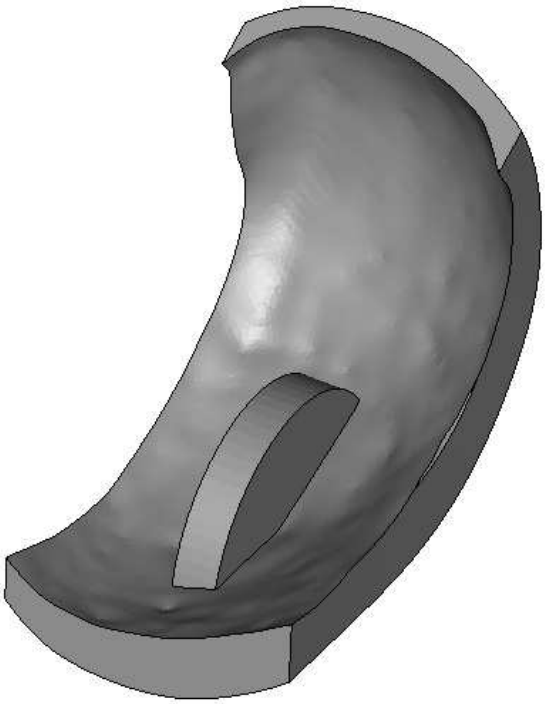

Figure 6-10: Semi-circle fixation peg

6.2.2 Tibial component

There are many different tibial component designs on the market in terms of shape and size. Almost all designs use polyethylene as the articulating surface. Some designs use an all-polyethylene insert (meaning the entire tibial component is polyethylene), while other designs make use of a metal-backed tibial (MBT) baseplate. Figure 6-11 shows these two types.

The metal-backed tibial component was first developed to avoid polyethylene deformation by distributing the stress more evenly through the metal tibial baseplate (Bartel et al., 1982), (Ewald et al., 1984). The MBT component allows for modularity, which can hold numerous advantages. Modularity provides the option to replace only the polyethylene insert if it fails. There is no need to remove the metal baseplate if it shows no signs of wear or fracture. Finite element studies have further shown that metal reinforcement could reduce the bending strains in the stem and also reduce the compressive stresses in the cement and cancellous bone under the baseplate (Taylor et al., 1998), (Udomkiat et al., 2001).

Figure 6-11: a) All polyethylene tibial component, b) metal-backed tibial component (Exactech Inc., 2009), (Weiss Joint University, 2009)

Udomkiat et al. (2001) compared the outcome between all polyethylene and metal-backed tibial components in TKR. At the last follow-up (average three years) they found no statistically significant differences in terms of knee scores, patient self-assessment and radiographic outcomes between the two. Modular MBT components do have micromotion between the polyethylene insert and the metal baseplate, according to Parks et al. (1998). This micromotion causes undersurface backside wear that may contribute to tibial osteolysis (Wasielewski et al., 1997).

Huang et al. (2002) investigated the revisions of TKRs due to the wear of modular tibial polyethylene inserts and found that, in 53.3% of the cases, severe damage to the metal components was noted that required them to be replaced. However, the cases investigated contained both mobile-bearings and fixed-bearings. In only 17.7% of the mobile-bearing cases was there a need to replace the metal components, which means that the metal components were replaced in 83.8% of the fixed cases.

Mobile-bearing UKRs have the further advantage that they allow for unconstrained movement, improving knee kinematics. This is especially important for the lateral compartment of the knee joint, as it has been shown to have greater anterior-posterior displacement than the medial side. Internal and external rotation should also be considered. Mobile UKRs are more suitable for younger, active patients because of this improved knee movement. No statistically significant difference between fixed and mobile-bearings was reported by Confalonieri et al. (2004) in terms of knee score and pain relief. However, Gleeson et al. (2004) reported better results in terms of knee function and pain relief for patients with a fixed-bearing UKR.

Considering all the possibilities, and the advantages and disadvantages of certain designs, it was decided to consider a mobile-bearing tibial component. The tibial baseplate, as well as the polyethylene insert, is customised to ensure optimal fit and greater contact area in order to prevent loosening and wear.

6.2.2.1 Tibial baseplate

If a tibial component is too large it will overhang the bone and impinge on the surrounding soft tissues. A too small tibial component can cause increased contact stresses and poorer load transfer across its surface, and may also result in subsidence if the component is not resting on the cortical bone rim. Proper fit between the tibial component and the resected tibial surface is therefore a critical factor in survivorship of the UKR (Hofmann et al., 1991), (Bloebaum et al., 1994), (Fitzpatrick et al., 2007).

Fitzpatrick et al. (2007) used statistical techniques to create three optimal theoretical unicompartmental tibial designs. These were then compared to current tibial designs. The performance of each implant was measured in terms of the percentage of the tibial component outline that lies on the cortical bone. All three of the theoretically designed implants gave more cortical bone coverage than the two current implants, which had cortical bone coverage of 67% and 57%. Custom patient-specific tibial implants can greatly improve on these values.

When a UKR is done, a transverse cut is made on either the medial or lateral side of the tibia to insert the tibial component. Making this resection parallel to the articulating surface of the tibia enables greater load-carrying capacity compared to a resection perpendicular to the anatomical axis of the tibia (Hofmann et al., 1991).

Using CT data of a patient imported into 3-matic, the resection is simulated. The exact outline of the cortical bone at that section is used as the basis for designing the patient-specific tibial baseplate. This method ensures perfect cortical bone coverage, thus reducing the risk of subsidence (Figure 6-12). A thickness of 2 mm is used to ensure necessary mechanical strength.

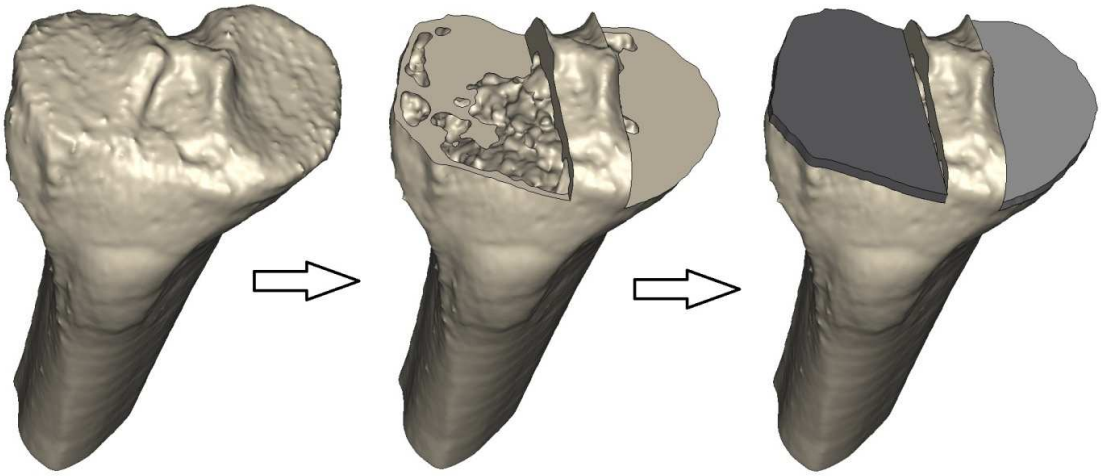

Figure 6-12: Tibial base plate development

Completo et al. (2008) investigated the influence of different tibial stem designs in load sharing and stability at the cement-bone interface in revision TKR. Cemented and press-fit tibial component stem extensions were evaluated with regard to load sharing and stability. The load transferred to the cortical rim bone was higher than the load transferred to cancellous bone and distal bone by the stem. It is therefore very important to have optimal cortical rim coverage when designing a tibial component. The load transferred to cancellous bone was found to be relatively unaffected by the type of stem (cemented or press-fit), with only a 5% difference found. Completo et al. (2008) further found that short cemented stems produce tray stability equivalent to that produced by long press-fit stems. This was in accordance with a parametric study by Jazrawi et al. (2001). A short cemented stem is used in this study.

6.2.2.2 Polyethylene insert

Ultra-high molecular weight polyethylene (UHMWPE) is the norm as the articulating component for the tibial portion of an UKR or TKR because of its strength, low friction coefficient and bio-compatibility.

The polyethylene insert in this study was designed to be congruent with the femoral component at 0º flexion. Because of the design of the femoral component, this will ensure that the mobile polyethylene insert conforms in the medial-lateral direction to the femoral component throughout flexion. This provides a maximum contact area. Bartel et al. (1986) found that, when the articulating surfaces were more conforming in the medial-lateral direction, contact stresses in the tibial components were reduced.

The thickness of the polyethylene insert is a very important factor affecting failure (Friedman et al., 1993). In their study investigating the incidence of revision of the metal component of TKRs, Huang et al. (2002) reported a significant difference in thickness between the group with severe metallic wear and the group that only required the polyethylene insert to be replaced. The mean polyethylene thickness in the group requiring only the polyethylene insert to be replaced was 9.1 mm compared to the mean thickness of 6.5 mm for the group showing severe metallic wear. For mobile-bearings, the thickness can be less and, in this study, the minimum thickness of the conforming bearing was 3 mm.

6.3 Conclusions

This chapter describes the process for developing a patient-specific knee replacement. According to He et al. (2006) a joint substitute should possess the necessary mechanical strength, have a customised geometric size and must be biocompatible. In light of these characteristics the design procedure uses mathematical modelling and an artificial neural network to estimate the original and healthy articulating surfaces of a patient's knee. The models are combined with medical images from the patient to create a knee prosthesis that is patient-specific. The femoral component has a minimum thickness of 2 mm, similar to the average cartilage thickness. The tibial baseplate has a thickness of 2 mm and the polyethylene bearing a minimum thickness of 3 mm. Figure 6-13 shows all the UKR components.

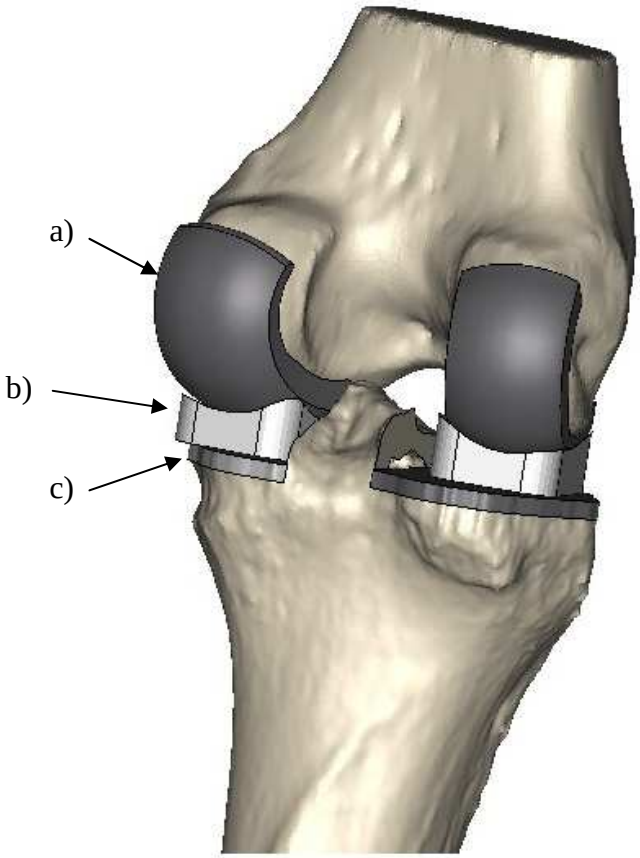

Figure 6-13: Components of the patient-specific UKR

Note:		
	Component	Minimum thickness
a)	Femoral component	2 mm
b)	Polyethylene insert	3 mm
c)	Tibial baseplate	2 mm

7. CONTACT STRESSES IN A PATIENT-SPECIFIC KNEE REPLACEMENT

7.1 Introduction

The main reasons for knee replacement failure are the wear of the polyethylene bearing and aseptic loosening. Other reasons are wear in the opposite compartment, tibial femoral instability, fatigue failure of the tibial tray and infection (Windsor et al., 1989), (Sharkey et al., 2002), (Villa et al., 2004). The early wear of UHMWPE is mainly affected by the conformity of the articulating surfaces, the thickness of the UHMWPE component, the elastic modulus of the component, contact loads and surface kinematics (Petty et al., 1999), (Fregely et al., 2003), (Bei et al., 2004), (McEwen et al., 2005). Retrieval studies have shown that the wear of knee replacements is highly variable due to the diverse kinematics and stress conditions occurring in vivo (Shi, 2007).

A mobile-bearing implant can theoretically increase conformity and improve the stress distribution to the bone-implant interface. It appears that wear can be reduced in mobile-bearing designs compared to fixed-bearing designs because of the increased conformity and contact area. The literature contains several studies comparing mobile-bearing to fixed-bearing UKRs, although the results are inconsistent. Emerson et al. (2002) reported better component survivorship for mobile-bearing UKRs, while Li et al. (2006) found that the use of mobile-bearing UKRs produced better knee kinematics and further reported that the mobile-bearing knees had a lower incidence of radiolucency at the bone implant interface (8% vs. 37%), with no differences regarding pain relief. Gleeson et al. (2004) reported better results in terms of knee function and pain relief for patients with a fixed-bearing UKR. Confalonieri et al. (2004) found no statistically significant difference in outcomes between the two groups.

A very effective way of examining the contact stresses produced in knee replacements is finite element (FE) analysis. Numerous FE analysis studies have been done in accordance with a study on muscle function in locomotion by Morrison (1970). One such study was by Villa et al. (2004), using vertical loads on the knee of 2200 N at 15° flexion, 3200 N at 45° and 2800 N at 60°. They used these loads in a static FE analysis to examine contact stress in a rotating total knee prosthesis. Shi (2007) used these loads in a static FE analysis to investigate varus/valgus malalignment in a total knee replacement. Morra and Greenwald (2003) investigated the effects of walking gait on the polyethylene bearings in four different unicompartmental knee systems, performing static finite element

analysis at 0º, 15º and 20º of flexion. They found that the mobile-bearing designs performed better than the less conforming fixed-bearing designs.

Other studies have examined dynamic FE analysis of knee replacements, such as the effect of thickness, alignment and bearing congruency on the stresses in unicompartmental knee replacements investigated by Simpson et al. (2008). Hopkins et al. (2010) used dynamic FE analysis to investigate the kinematics of the knee joint after implantation with a mobile-bearing unicompartmental knee replacement. Godest et al. (2002), as well as Halloran et al. (2005), used an explicit finite element approach to simulate both the kinematics and the internal stresses of total knee replacements. Godest et al. (2002) argue that the stress distribution within the polyethylene insert of a knee replacement is dependent on the kinematics, which in turn is dependent on the design of the articulating surfaces of the implant.

It is evident that contact pressures and areas are important considerations in knee replacements. Knowledge of the contact pressures and areas is considered a reliable tool for predicting potential UHMWPE wear (Sathasivam et al., 2001). Recent studies have shown that increased contact pressure and low conformity can reduce surface wear in fixed-bearing knee replacements (Galvin et al., 2009), (Fisher et al., 2010). Wear rates with flat UHMWPE inserts are comparable to mobile-bearing knee systems.

The aim of this chapter is to compare the contact stresses in conventional implants to those in a custom implant. The custom replacement is compared with two conventional replacement designs in terms of contact stresses, executed by means of a static FE analysis. The conventional implant designs consist of a fixed-bearing and a fully-congruent mobile-bearing implant. A fully-congruent implant is one in which there is maximum contact area between the femoral component and the tibial component. An example is the Oxford knee system, which uses a single radius design for the femoral components and the same radius for the polyethylene insert. This ensures maximum contact area between the two components throughout flexion. The effect of using different sizes within a type of implant was also investigated.

7.2 Methods

7.2.1 Custom UKR design

Custom femoral and tibial bearing components were developed for seven different cases using the methods discussed in the preceding chapter. Preoperative CT data of individuals requiring knee replacement were used for the designs. For each of

the cases, the femoral component has a customised articulating surface determined with the SOM algorithm. The bone-implant interface was also customised for the specific knee. The mobile polyethylene bearing was designed to be congruent with the femoral component at 0º flexion. The mobile-bearing and femoral component conformed in the medial-lateral direction throughout flexion to provide maximum contact area.

7.2.2 FE models for tibio-femoral contact analysis

Finite element analysis provides the ability to predict the stress distributions within the polyethylene components for unicompartmental knee replacements (Simpson et al., 2008). 3D models of the custom knee replacements (only medial components) as well as two conventional UKRs were developed and imported into MD Patran (MSc Software, USA) as STL files. The custom implants had mobile-bearing designs, as described previously. Custom implant models were created for the seven cases investigated. The conventional UKRs were reverse engineered using the 3D laser scanner, and three different sizes of the fixed-bearing implant and two different sizes of the mobile-bearing implant were investigated. The fixed-bearing design had a partial conforming tibial plateau. All implants were analysed in combination with their accompanying bearing as well as a flat polyethylene bearing. That means that, except for their intended bearing, the three implants were also tested against a flat fixed-bearing design. This was done specifically to examine the effect of a conforming versus a non-conforming tibial insert. All components were modelled as deformable bodies using ten-noded tetrahedral elements (Villa et al., 2004), (Simpson et al., 2008). Figure 7-1 to Figure 7-3 show the finite element models for the three different cases. Table 7-1 shows the details of the meshes.

During the study it was found that decreasing the edge length of the bearings by about 13% (from 0.75 mm to 0.65 mm) resulted in less than 2.5% difference in the calculated contact stresses, and therefore the element sizes were deemed adequate and further mesh refinement was not necessary. Similarly, Halloran et al. (2005) found little difference in contact stresses when decreasing component edge lengths from 1.3 mm to 0.9 mm in a finite element study of TKR mechanics. The convergence tolerance was not altered from the default (MD Nastran 2008).

The femoral components were modelled as linear elastic and isotropic with material properties for cobalt-chromium, $E = 195$ GPa, $\nu = 0.3$ (Simpson et al., 2008). The polyethylene bearings were modeled as a non-linear material with a stress/strain curve as used by Halloran et al. (2005). The stress/strain curve is shown in Figure 7-4. Young's modulus was entered as 1048 MPa (Simpson et al.,

2008). The flat-bearing and conventional fixed-bearing had a minimum thickness of 8 mm, while the custom and mobile-bearings had minimum thickness of 3 mm.

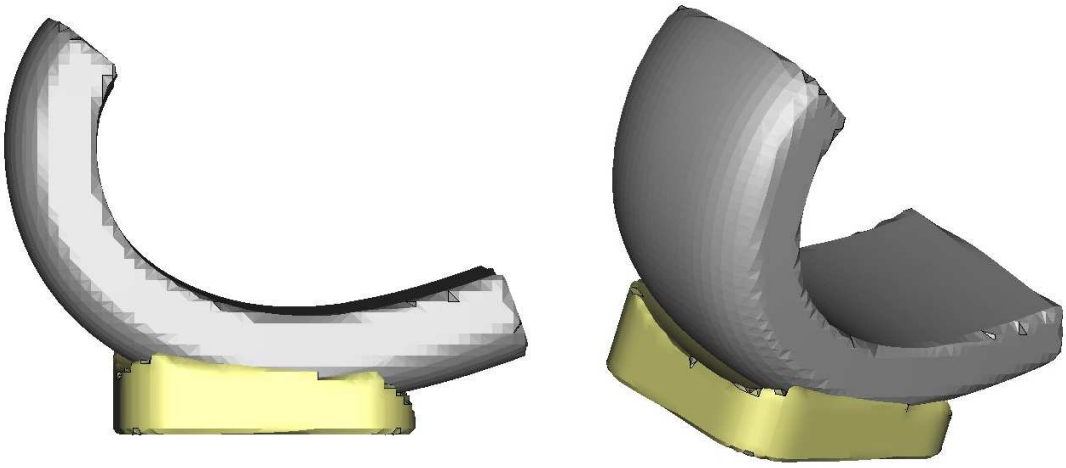

Figure 7-1: Finite element model of one of the custom implants

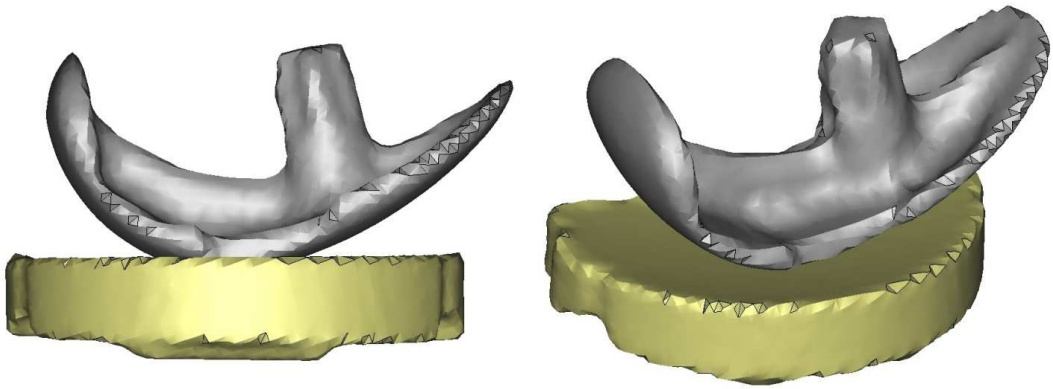

Figure 7-2: Finite element model of one of the fixed-bearing implants

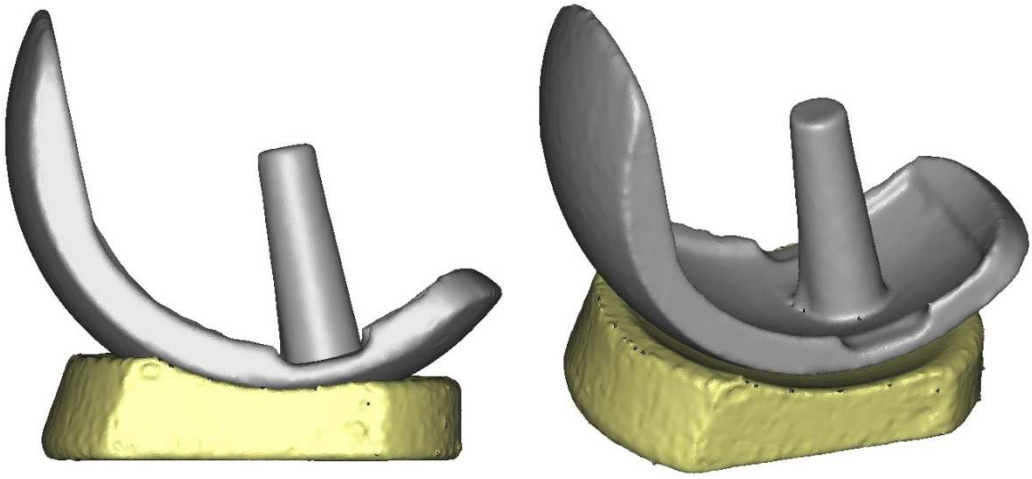

Figure 7-3: Finite element model of one of the mobile-bearing implants

Table 7-1: Details of meshes used in tibio-femoral contact analysis

Component	Description	Ave elements	Ave edge length
Custom implants	Femoral component	67 027	1 mm
	Custom bearing	52 708	0.75 mm
	Flat bearing	90 823	0.75 mm
Conventional implants (fixed-bearing)	Femoral component	73 823	1 mm
	Bearing	139 294	0.75 mm
	Flat bearing	91 307	0.75 mm
Conventional implants (mobile-bearing)	Femoral component	49 780	1 mm
	Bearing	116 465	0.75 mm
	Flat bearing	91 919	0.75 mm

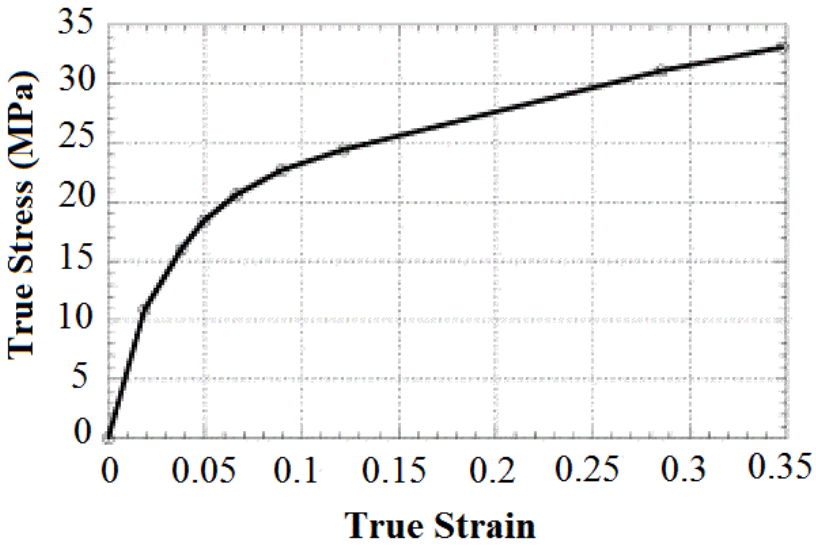

Figure 7-4: True stress/strain curve for UHMWPE (Halloran et al., 2005)

Vertical loads were applied similar to those by Villa et al. (2004) and Shi (2007). The loads were modified for unicompartmental knee replacements by offsetting the load toward the medial condyle with a 60:40 ratio (Morra & Greenwald, 2003), (Halloran et al., 2005). This resulted in vertical loads on the medial condyle of 1 320 N at 15º flexion, 1 920 N at 45º and 1 680 N at 60º, which were

applied to several nodes in the femoral component, with the resultant load as specified (Figure 7-5). The femoral components were further constrained to only move in a vertical direction (i.e. constrained in the other two dimensions) with the inferior surface of the bearings fixed. Static finite element analysis was thus performed for each of the three flexion angles.

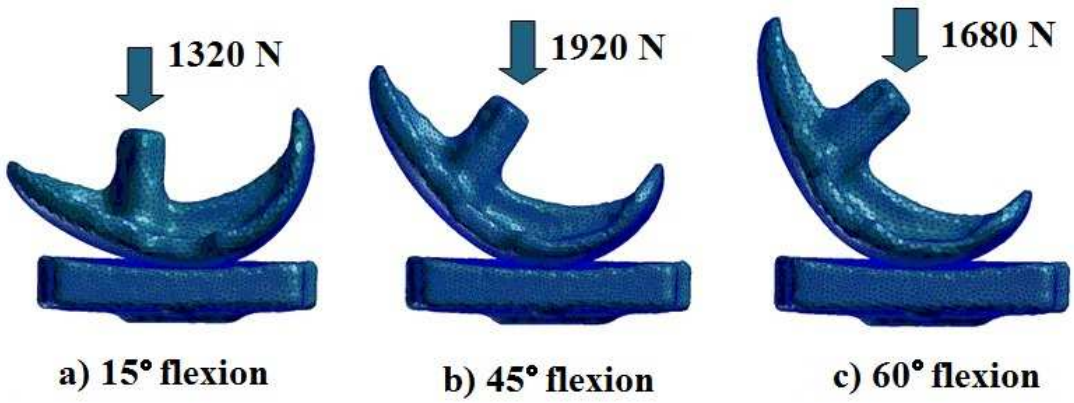

Figure 7-5: Static finite element analysis at the three flexion angles, a) 15º, b) 45º, and c) 60º

7.2.3 FE models for the bone-implant interface contact

Finite element models of each of the seven femurs were also developed. These were used to investigate the contact stresses on the femurs for different femoral component designs with respect to the bone-implant interfaces. The different designs included the custom design (no bone resection needed); conventional implant 1, a flat surfaces design (three flat surfaces); conventional implant 2, a circular design (flat surface posterior and circular distally); and conventional implant 3, a curved design (two flat surfaces posterior and curved distally). Again, only the medial components were analysed. The femoral components were modelled as linear elastic and isotropic with material properties for cobalt-chromium. The femurs were modelled using the bone properties defined by Kulkarni and Sathe (2008): E = 11 737 MPa, ν = 0.22. The static load at 15º flexion for the medial compartment of 1 320 N was applied to several nodes within the femur, with the implants fixed (Table 7-2).

For the conventional implants, the femurs were prepared by making the necessary cuts for the specific implant. The necessary cuts were performed in 3-matic. For

the custom implants, no preparation was necessary as the surface of the implant is designed to correspond to the touching surface of the femur.

All finite element models and analyses were setup and performed in accordance with Viceconti et al. (2005). This entails proper model selection, verification, proper parameter identification and validation of the models.

Table 7-2: Details of meshes used in bone-implant contact analysis

Component	Description	Ave elements	Ave edge length
Custom implant	Uncut femur	181289	2 mm
	Femoral component	35016	1 mm
Conventional implant 1	Resected distal and posterior femur	167079	2 mm
	Femoral component	50112	1 mm
Conventional implant 2	Resected circular femur	175933	2 mm
	Femoral component	37067	1 mm
Conventional implant 3	Resected posterior femur	176983	2 mm
	Femoral component	35365	1 mm

7.2.4 Contact validation

A contact validation model was constructed to be compared with results obtained using Hertz's theory of elastic contact. A similar approach to that of Simpson et al. (2008) was used. A sphere-on-plane model was constructed with a sphere radius of 20 mm in contact with a rectangular object with dimensions of 20 x 20 x 20 mm. This model is analogous to the special case in classical contact mechanics of two cylinders in contact with their axes perpendicular (Simpson et al., 2008). A 100 N load is applied to the top of the sphere in a direction perpendicular to the rectangular object face, such that contact is made between the two. The sphere was modelled as linear elastic with the properties of cobalt-chromium (E = 195 GPa, ν = 0.3). The rectangular object was also modelled as linear elastic with the material properties of polyethylene (E = 1048 MPa, ν = 0.3) (Simpson et al., 2008). The average edge length for the sphere was 1 mm and for the rectangular object it was 0.75 mm. Unfortunately, Hertz's theory is not applicable to non-linear materials. However, linear material contact can be used to validate the models used in the finite element analysis (Simpson et al., 2008).

The contact pressure is calculated from Hertz' theory using the following relationship:

$$p_o = \left(\frac{PE^2}{\pi^3 R^2}\right)^{\frac{1}{3}} \tag{23}$$

where p_o is the maximum contact pressure, $\frac{1}{E} = \frac{1-\nu_1^2}{E_1} + \frac{1-\nu_2^2}{E_2}$ (E_n and ν_n are the respective elastic modulus and Poisson's ratio of the two bodies) and $\frac{1}{R} = \frac{1}{R_1} + \frac{1}{R_2}$ is the relative curvature (R_1 and R_2 are the radii of the two bodies, for the rectangular object R becomes infinity).

7.3 Results

7.3.1 Tibio-femoral contact stresses

Figure 7-6 depicts the mean peak contact stresses on the polyethylene bearings at 15º, 45º and 60º flexion for three cases: a) a custom design; b) a fixed-bearing design; and c) a mobile-bearing design. A single representative figure is shown for each case, but the analysis was performed on all seven custom implants, all three sizes of the fixed-bearing design and both sizes of the mobile-bearing design (see Appendix A for all results). The mean peak contact stresses mentioned for the custom implants are therefore the mean of the peak stresses experienced by each of the seven implants.

Figure 7-7 a) shows the mean peak contact stresses for the three implant designs with conforming bearings. Figure 7-7 b) shows the mean peak contact stresses for each of the designs with a flat bearing (totally non-congruent case). The values shown are the mean of the peak stresses for the different sizes of each knee replacement system.

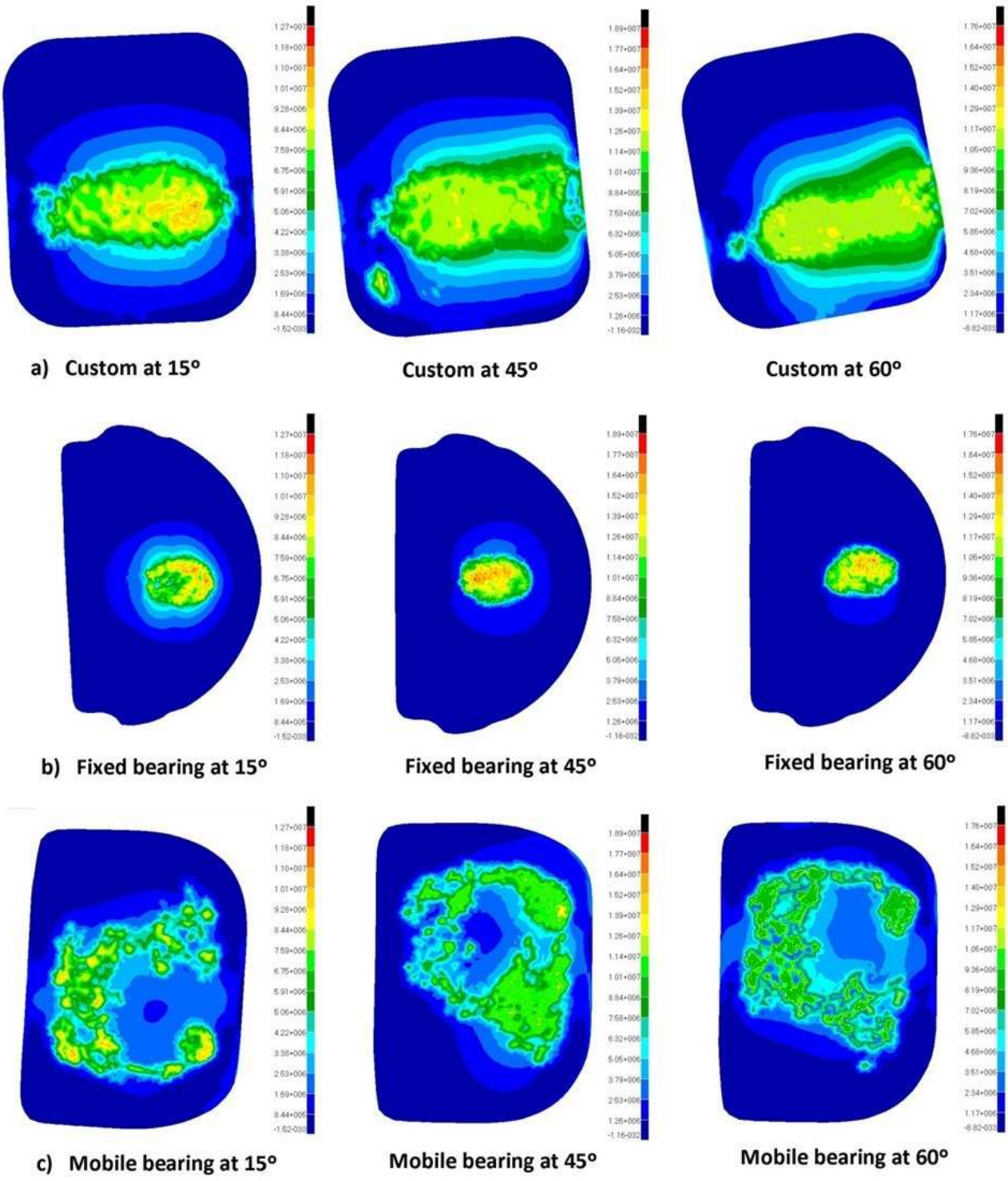

Figure 7-6: Bearing contact stress for the three implant designs: a) custom design, b) fixed-bearing design, and c) mobile-bearing design.

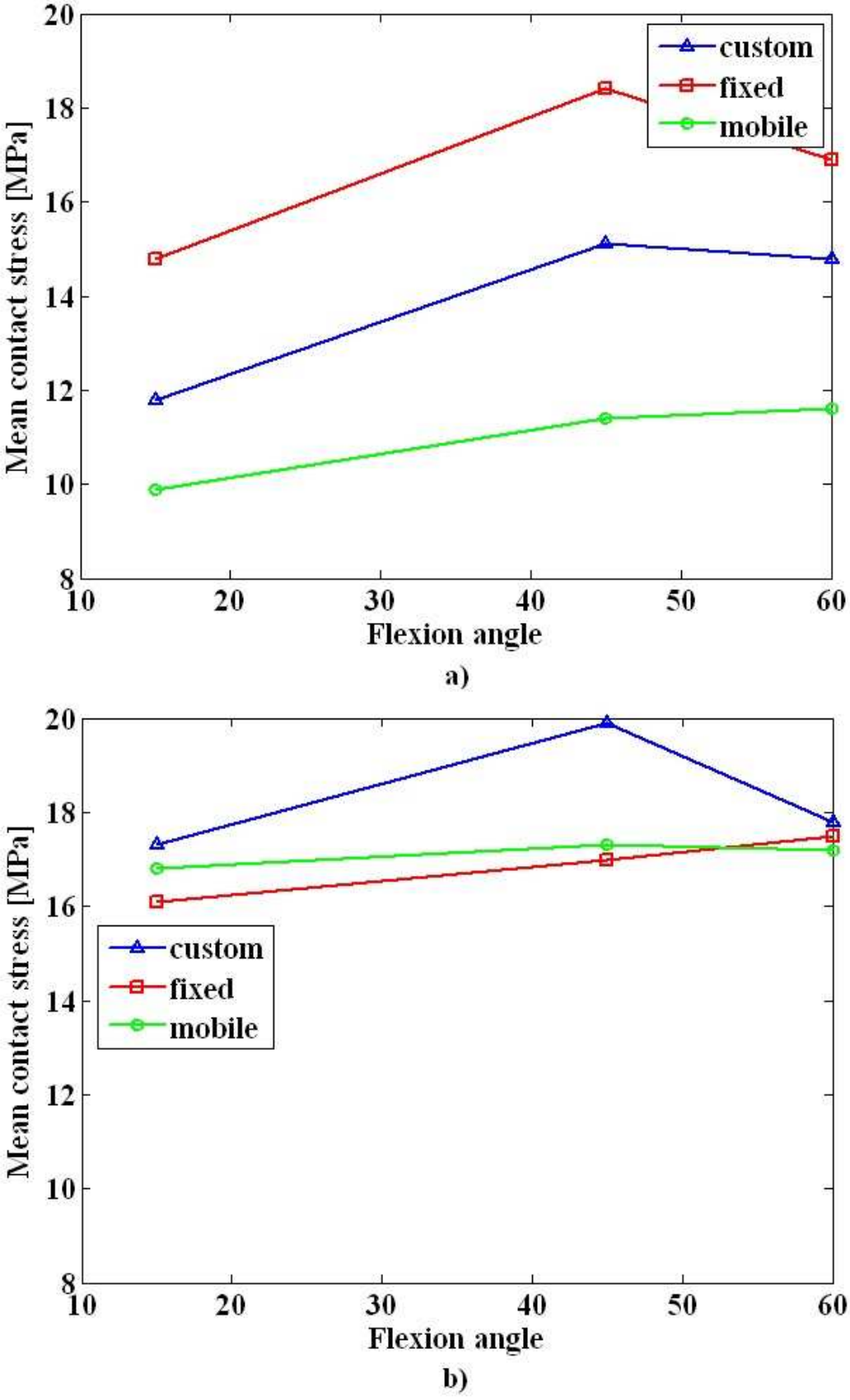

Figure 7-7: Mean peak bearing contact stresses for the three unicompartmental systems, a) femoral components with intended bearings and b) femoral components with the flat fixed-bearings.

The maximum contact stresses for all cases usually occurred at 45º flexion. This was the case for the custom design with a maximum contact stress of 16.6 MPa at 45º flexion for a specific case. The fixed-bearing design showed a maximum stress of 18.9 MPa at 45º flexion for the largest size component. The mobile-bearing design showed a maximum contact stress of 13 MPa at 60º flexion. A maximum contact stress of 21.1 MPa was experienced by a custom component for the analysis with a flat bearing.

For the fixed-bearing design, the stress at 15º flexion decreased from 16.6 MPa to 15.1 MPa to 12.7 MPa as the size of the implant increased. This was not the case at 45º flexion or 60º flexion where the stress was similar for all the sizes. These were around 18 MPa at 45º flexion and 17 MPa for 60º flexion. Similar results were shown for the mobile-bearing.

7.3.2 Bone-implant interface contact

Figure 7-8 shows the contact stress distribution on a chosen femur for the different cases. In the case of the custom implant, as in Figure 7-8 a), the stress distribution is uniform. In the other cases there are stress concentrations at the sharp edges where the square bone cuts were made, clearly visible in Figure 7-8 b), c) and d). Table 7-3 shows the average maximum contact stresses for the four designs.

Table 7-3: Maximum contact stress on femurs

	Mean peak stress
Custom implant	30.07 MPa
Conventional implant 1	34.53 MPa
Conventional implant 2	47.23 MPa
Conventional implant 3	44.43 MPa

7.3.3 Contact validation

The maximum contact pressure predicted by the FE model for the sphere-on-plane validation case was 41.7 MPa. Hertz's theory predicted a maximum contact pressure of 39.9 MPa, which is a 5% difference and hence deemed acceptable.

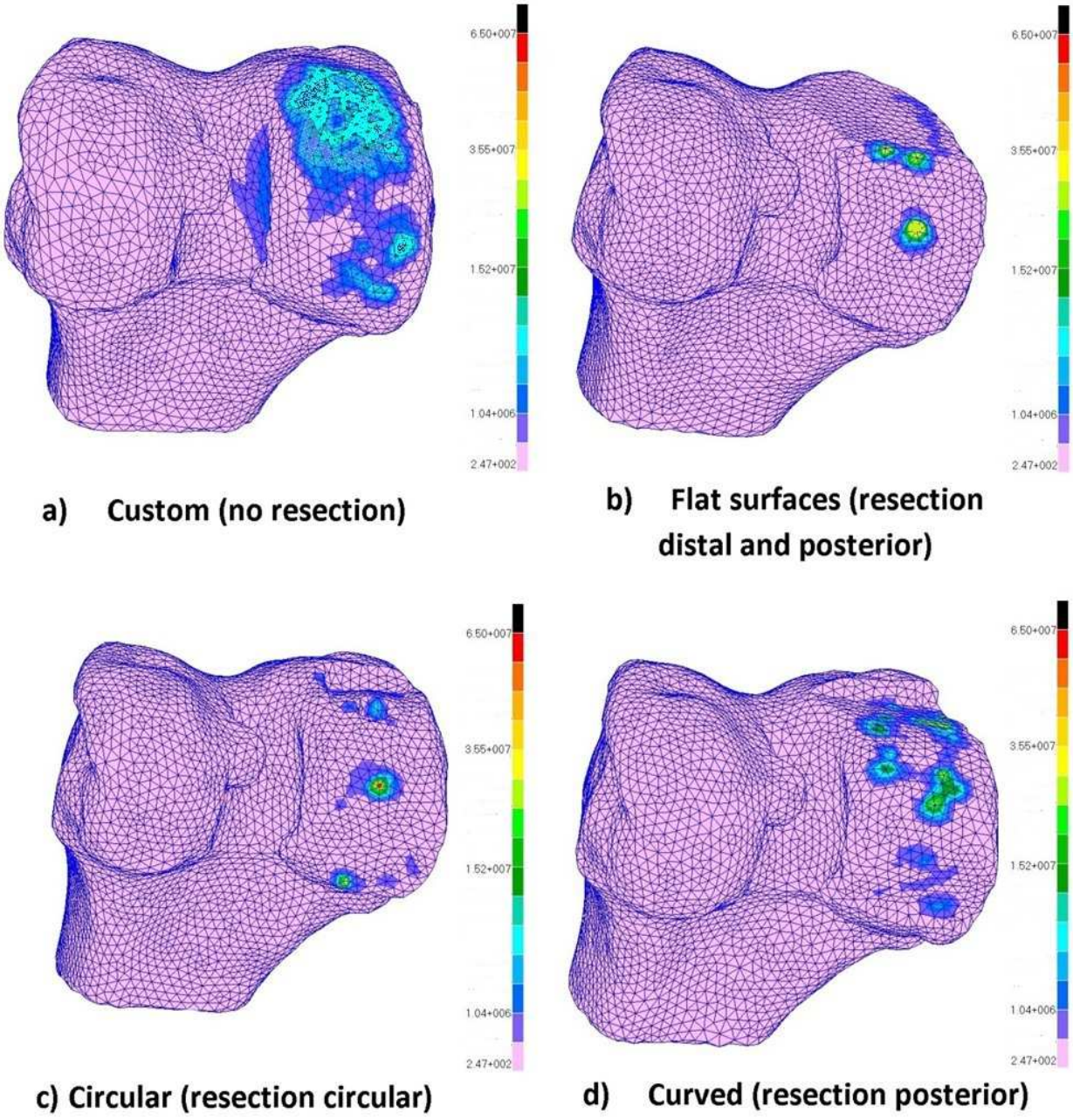

Figure 7-8: Bone-implant stress distribution for the four different unicompartmental knee systems (a-d).

7.4 Discussion

Implant alignment and the shape of the articulating surface of the polyethylene bearing greatly influence the local magnitude and the eccentricity of the tibial bone-implant interface pressure and largely affects the pressure distribution and amount of relative micro motion at the tibial component (Shi, 2007). Implant malalignment usually results in loosening of the component (Vince, 2003). Cheng (2003) found that mobile-bearing designs can reduce maximum contact pressures more significantly than their fixed-bearing counterparts when malalignment conditions occur. Bartel et al. (1986) found that higher contact pressures on the tibial bearing component were associated with more severe damage to the TKR tibial components. Harryson et al. (2007) argued that the sharp edges present in conventional femoral components cause stress concentrations that can lead to bone remodelling and finally to premature aseptic loosening. The contact distributions at the polyethylene bearing as well as at the bone-implant interface are therefore very important considerations. Hence, a great deal of research has recently focused on determining the magnitude and distribution of contact stresses in knee replacements.

The aim of this part of the study was to examine the contact stresses present when using custom, patient-specific unicompartmental knee replacements. A method for designing a custom implant using neural networks was described in the preceding chapters. Custom implants were designed for seven individuals and compared to conventional implants with regard to contact stresses. This was accomplished through the use of finite element models. The models were validated by the classical Hertz contact calculation, and good validation results comparable to those of other studies were demonstrated (Simpson et al., 2008).

Furthermore, the custom implant showed lower maximum contact stress compared to the conventional fixed-bearing implant. However, the fully-congruent mobile-bearing design yielded the best results, due to the large contact area that is maintained throughout flexion. The custom design bearings conformed to the femoral components in the medial-lateral direction throughout flexion, which contributes to the good contact stresses found for the custom design. Bartel et al. (1986) had similar findings and concluded that contact stresses in the tibial components were reduced when the articulating surfaces were more conforming in the medial-lateral direction. They further found that contact stresses were less sensitive to changes in geometry in the anterior-posterior direction.

When considering the results of the different designs with the flat bearing, it is noted that the contact stresses were all similar, except for the custom bearing at 45º flexion, which could be due to the smaller sagittal radius present at that stage for the custom bearing. The custom bearing has a more anatomical design compared to the conventional implants, and therefore has a continuous varying radius. The sagittal radius of the custom design at 45º flexion is considerably smaller than at 15º flexion, in contrast to the fully-congruent design, which is a single radius design, and the fixed-bearing design with a dual radius design. The trends in Figure 7-7 are the same for all implants, with the peak contact stress increasing with increasing force (15º to 45º flexion) and decreasing active radius. As the force decreases again at 60º flexion, so too does the contact stress.

Examining the contact stress between the different sizes of the fixed-bearing design, it is noted that the stress at 15º flexion is smallest for the largest size components. The stress at 45º flexion and 60º flexion is similar for all sizes, again due to the sagittal radius differences. At 15º flexion the active sagittal radius increases from 80 mm to 110 mm from the smallest to the largest femoral component. At 45º flexion and 60º flexion, the active sagittal radius is the same for all three sizes at 38 mm.

Simpson et al. (2008) found improved tibio-femoral contact stress results for a fully-congruent unicompartmental knee replacement, using a dynamic FE model and finding a mean peak contact stress of 2.7 MPa for the fully-congruent case. For a non-congruent, metal-backed UKR they found a mean peak contact stress of 48.6 MPa. A possible reason for the lower contact stresses on the fully-congruent UKR in their case could be that they used ideal computer models with a perfect fit. In this study, the models were reverse engineered using a laser scanner and therefore could contain imperfections, as in practice. Morra and Greenwald (2003) found contact stresses of between 2 MPa and 14 MPa for a fully-congruent design at flexion angles below 20º. Knee joint kinematics are greatly influenced by the geometry of the implant (Walker & Sathasivam, 2000), however, and as a result a simplified design can severely affect normal kinematics.

Galvin et al. (2009) found reduced wear rates for flat UHMWPE inserts compared to curved inserts for fixed-bearing knee replacements under different kinematic conditions. The wear rates with the flat insert were found to be comparable to mobile-bearing knee replacements. This can be due to the lower cross shear present in mobile and low-conforming knee replacement designs. Flat-bearing designs can therefore show lower wear rates even though they have higher contact stresses and smaller contact areas compared to conforming fixed-bearing knee replacement designs.

Villa et al. (2004) achieved similar results to those of this study for their static FE analyses on a rotating platform total knee replacement. They demonstrated maximum contact stresses of 14.5 MPa, 27.7 MPa and 24.6 MPa for flexion angles of 15º, 45º and 60º. The static FE analyses used by Villa et al. (2004) and other studies were modified for the UKR case in this study, as no standard for static UKR FE analysis could be found in the literature. It is hoped that, in the future, other static FE analysis studies focusing on UKRs can make use of the loads and flexion angles presented in this study.

It was also demonstrated that a custom bone-implant interface for the femoral component can achieve more uniform stress distribution at the condyle surface. This will reduce the occurrence of bone remodelling in the region of implantation, reducing the likelihood of aseptic loosening. Stress concentrations produced by the sharp edges of conventional knee replacements can lead to remodelling problems, further complicating revision surgery due to bone loss. The results show that a circular or curved surface also produces more uniform stress distribution and is similar to that of the custom design. Stress concentrations still occur at the sharp edges produced by the posterior resection, as was also found to be the case by Harrysson et al. (2007). It has to be considered here that the femur is often cemented to the bone, which can lead to re-distribution of contact stresses at this interface.

This study has revealed that a patient-specific unicompartmental knee replacement can have adequate contact stress characteristics in both the tibia-femoral and bone-implant compartments. Mean peak contact stresses lower than those of fixed-bearing designs on the polyethylene insert were shown for the custom design. Future work can include the experimental validation of this finding with the use of the Tekscan measurement system (Tekscan Inc., South Boston, USA). More uniform stress distribution, where the femoral component is in contact with the femur, was also exhibited for the custom design. Custom unicompartmental knee replacements have the potential of providing good contact stress distribution, preserving bone stock and could be more anatomically accurate.

The advantages of a custom knee replacement in terms of contact stresses at the tibio-femoral joint and the bone-implant interface are apparent. However, it is necessary to investigate the kinematics of a custom knee replacement. It is believed that a custom, more anatomically accurate implant can produce more normal knee kinematics. This is investigated in the next chapter.

8. IN VITRO MEASUREMENT OF TIBIOFEMORAL KINEMATICS AFTER PATIENT-SPECIFIC KNEE REPLACEMENT

8.1 Introduction

Knee kinematics are complex and has been studied extensively to gain a better understanding of the biomechanics (Biščević et al., 2005), (Varadarajan et al., 2009), (Victor et al., 2009), (Victor et al., 2010). Numerous in vivo methods have been used to investigate knee kinematics, including studies with magnetic resonance imaging (Hill et al., 2000), (Nakagaw et al., 2000), (Johal et al., 2005), fluoroscopy combined with computed tomography (Komistek et al., 2003), (Lu et al., 2008) and Roentgen stereophotogrammetry (Kärrholm et al., 2000), (Uvehammer et al., 2000a), (Uvehammer et al., 2000b). However, Victor et al. (2010) argue that in vivo research is limited due to unknown loading conditions and variations in the performed activities between different studies.

In vitro studies overcome these limitations by applying known loads to the knee joint, which is mounted in a specialised rig or frame. The two most commonly used in vitro systems are the Oxford knee rig (OKR) and the robotic knee testing system (RKTS) (Li et al., 1999), (D'Lima et al., 2000), (Coughlin et al., 2003), (Li et al., 2004), (Most et al., 2004), (Patil et al., 2005), (Lo et al., 2008), (Varadarajan et al., 2009), (Victor et al., 2009), (Victor et al., 2010). Both systems try to replicate the physiological scenario by providing six -degrees- of -freedom at the knee joint, allowing quadriceps loading, and providing a load at the ankle. In other studies, either the tibia or the femur is fixed, and flexion/extension is achieved by loading the quadriceps (Rovick et al., 1991), (Krevolin, 2003), (Bull et al., 2008), (Merican & Amis, 2009); while other studies follow a completely unloaded method where flexion/extension is achieved manually (Iwaki et al., 2000). However, according to Victor et al. (2010), different in vitro methods reveal different kinematic patterns.

The kinematic patterns of the normal knee describe the motion of the femur relative to the tibia with increasing flexion. Normal knee kinematics are believed to include some posterior translation of the femur, which is more pronounced on the lateral side, leading to relative internal tibial rotation. The majority of this rotation occurs at the beginning of the flexion cycle, between full extension and 15º flexion, indicating a screw-home mechanism (Hallen & Lindahl, 1966), (Coughlin et al., 2003), (Varadarajan et al., 2009). Numerous studies have shown that the screw-home characteristic does not necessarily occur after total knee replacement, and that normal kinematics are lost (Uvehammer et al., 2000a),

(Uvehammer et al., 2000b), (Coughlin et al., 2003), (Most et al., 2003), (Patil et al., 2005), (Bull et al., 2008), (Varadarajan et al., 2009). The main reason for the change in kinematics after TKR is attributed to the change in articular geometry (Coughlin et al., 2003), (Patil et al., 2005), (Bull et al., 2008), (Varadarajan et al., 2009).

It is suggested that unicompartmental knee replacement offers the potential to restore normal knee kinematics better than TKR because of retaining the cruciate ligaments, and because of better preservation of the overall geometry (Robinson et al., 2002), (Patil et al., 2005). Most in vivo kinematic studies after UKR only consider the patellar tendon angle and conclude that normal kinematics are restored (Robinson et al., 2002), (Price et al., 2004), (Pandit et al., 2008). Akizuki et al. (2009) investigated in vivo tibiofemoral kinematics of patients implanted with a UKR and found greater posterior translation than that reported for the normal knee. Patil et al. (2005) found similar tibiofemoral kinematics with a UKR compared to normal kinematics in an in vitro study using the OKR.

In this study, individual normal knee kinematics are compared to the kinematics after implantation with a patient-specific UKR and a conventional fixed-bearing UKR. Furthermore, the effect of ankle load is investigated by using two different test setups; one based on the OKR, and one where the femur is fixed and the tibia hangs freely, and flexion/extension is achieved by loading the quadriceps.

8.2 Materials and methods

Three cadaver knee joints were tested in two different rigs, comparing normal tibiofemoral kinematics to kinematics after implantation with a patient-specific UKR. Two of the knees were further implanted with a conventional fixed-bearing prosthesis for comparison. Two knees received medial replacements while one knee received a lateral replacement. One of the medially replaced knees was only tested on the unloaded ankle test rig.

8.2.1 Specimens and preparation

Three embalmed, whole human cadaver knee specimens were used in this study. Ethical approval was obtained from the Faculty of Health Sciences, Stellenbosch University, South Africa. All knees were found to be free from macroscopic anatomic defects after inspection by an experienced orthopaedic surgeon. Each knee was sectioned just below the femoral head, with the ankle and foot kept intact. The knees were dissected leaving the knee capsule, ligaments and quadriceps tendon intact. The ankles were also dissected of skin, subcutaneous tissue and muscle, with movement only constrained by the ligaments. Threaded

intermedullary rods were cemented into the femoral shafts for fixation to the testing rigs. Electromagnetic receiver sensors (Fastrak, Polhemus, Vermont, USA) were rigidly fixed to the femoral and tibial shafts. An electromagnetic transmitter sensor was rigidly fixed to the stationary testing rig frame. An additional stylus was used to digitise bony landmarks to create embedded coordinate systems in both the femur and tibia. The femoral X-axis was defined as the line passing through the centres of the medial and lateral condyles (the transepicondylar line), positive pointing laterally. The Y-axis was aligned with the shaft of the femur, positive pointing proximally. The Z-axis is the vector cross-product of the mentioned two axes, positive pointing anteriorly. The tibial X-axis is defined as a line connecting the approximate centre of each plateau, positive pointing laterally. The tibial Y-axis is aligned with the tibial shaft, positive pointing proximally. The tibial Z-axis is the vector cross-product of the mentioned two tibial axes, with positive pointing anteriorly. Tibiofemoral relative motion is then calculated as follows: flexion/extension was calculated about the femoral X-axis; tibial internal/external rotation was calculated about the tibial Z-axis; tibial varus/valgus was calculated about a floating axis perpendicular to the femoral X-axis and the tibial Z-axis; femoral rollback was defined as the posterior translation of the centre of the transepicondylar line of the femur relative to the fixed tibial coordinate system.

8.2.2 Kinematics calculation

With the embedded coordinate systems defined, the tibiofemoral displacements were calculated using rotation matrices. This was done because the transmitter reference frame remained stationary during the tests. Rotation matrices for both the femoral and tibial receiver sensors were determined in terms of Euler angles as follows (Xsens, 2006):

$$R_{GS} = \begin{bmatrix} \cos\theta\cos\psi & \sin\varphi\sin\theta\cos\psi - \cos\varphi\sin\psi & \cos\varphi\sin\theta\cos\psi + \sin\varphi\sin\psi \\ \cos\theta\sin\psi & \sin\varphi\sin\theta\sin\psi + \cos\varphi\cos\psi & \cos\varphi\sin\theta\sin\psi - \sin\varphi\cos\psi \\ -\sin\theta & \sin\varphi\cos\theta & \cos\varphi\cos\theta \end{bmatrix} \quad (24)$$

with φ = roll, θ = elevation, and ψ = azimuth.
As defined here, R_{GS} rotates a vector in the sensor coordinate system to the global reference system:

$$x_G = R_{GS}x_S \quad (25)$$

It follows naturally that, R_{SG} rotates a vector in the global reference coordinate system to the sensor coordinate system, and $R_{SG} = R_{GS}^{T}$.
The translation matrix is simply:

$$T_{GS} = \begin{bmatrix} t_x \\ t_y \\ t_z \end{bmatrix} \tag{26}$$

where t_x, t_y, and t_z describe the position of the origin of the sensor coordinate system relative to the origin of the global coordinate system. The translations and Euler angles for both receiver sensors relative to the transmitter sensor were sampled at 40 Hz. The static accuracy of the sensors was 0.8 mm for the receiver position and 0.15º for the receiver orientation when the receiver was located within 760 mm of the transmitter.

Using the relationships described, femur displacements can be transformed to the tibia coordinate system and vice versa. For example, to calculate femoral rollback, the centre point of the transepicondylar line is first transformed to the global reference coordinate system and then to the tibial coordinates system. This gives the translation of the point on the femur in the tibial coordinate system, thus the movement of the femur relative to the tibia.

8.2.3 Loaded ankle apparatus

The first rig is a dynamic knee simulator based on the Oxford knee rig design (Figure 8-1 and Figure 8-2). The femoral intermedullary rod is fixed to the hip joint. The hip joint provided all rotational degrees -of -freedom as well as limited medial-lateral movement. The ankle was kept intact, with the foot strapped to a moveable platform. This ensured normal ankle rotations with rotational freedom in flexion/extension, internal/external rotation and a limited range of varus-valgus motion (Varadarajan et al., 2009). The quadriceps tendon was loaded via a pulley and weight system with a static load of 200 N as done in previous studies (Li et al., 1999), (Bull et al., 2008). Knee flexion/extension was achieved by translating the moveable platform along vertical rails controlled by a linear actuator. To eliminate interference with the electromagnetic sensors, all metallic components of the fixture were made from either aluminium or stainless steel. A detailed design of the testing rig can be found in Appendix B. Table 8-1 lists the main products used for the loaded ankle apparatus.

Table 8-1: Products used for loaded ankle apparatus

Description	Product
Position sensors	Polhemus 3Space Fastrak including ST8 stylus, extra RX2 receiver, and Locator software
Linear actuator	Linak LA36-5A73S0P800A24
Frame	Bosch Rexroth 40 mm strut profiles with connectors.
Rails and bushes	Bosch Rexroth Standard 20 mm closed bushings and standard 1200 mm length, 20 mm shafts.

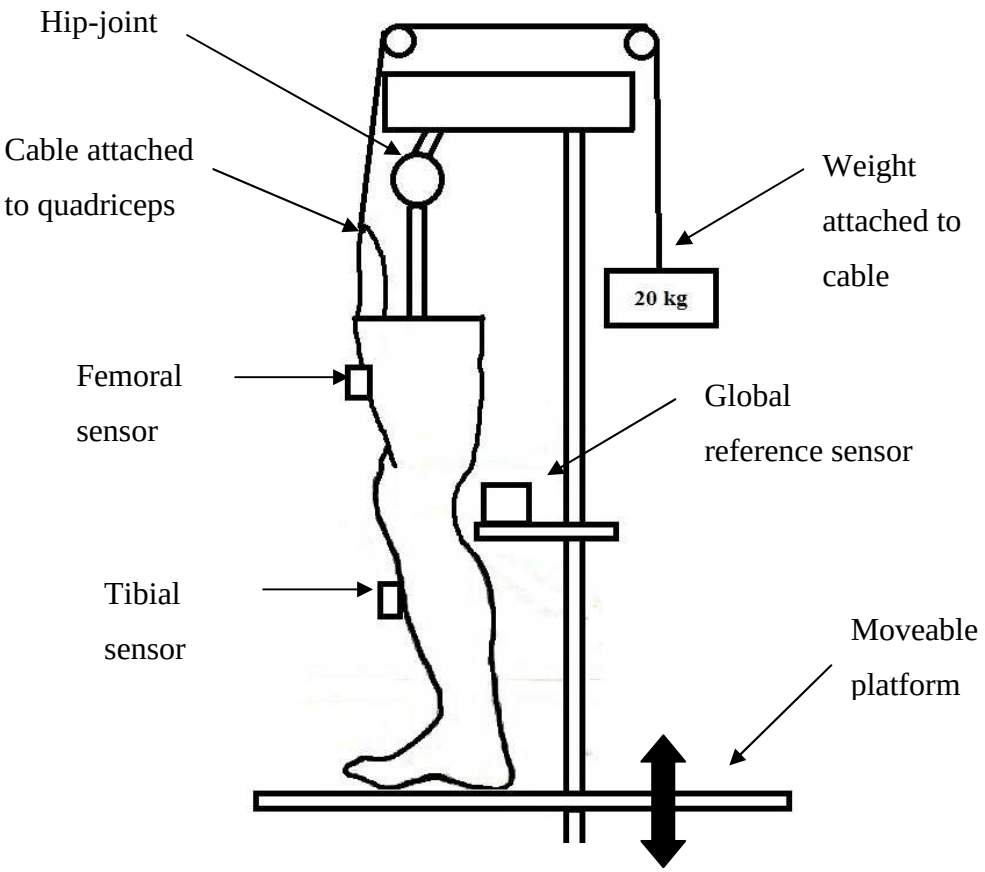

Figure 8-1: Schematic of loaded ankle test

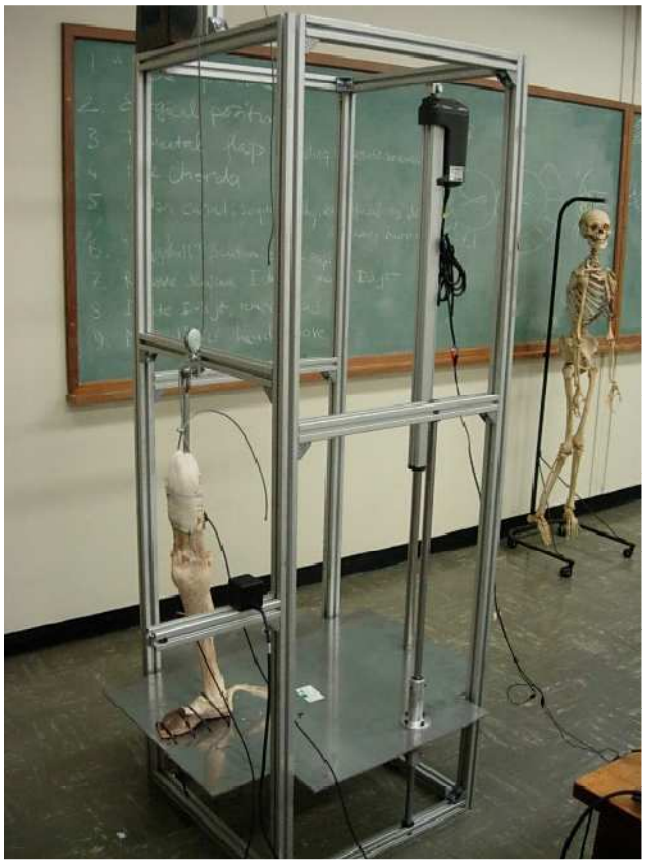

Figure 8-2: Photo of loaded ankle test apparatus

8.2.4 Unloaded ankle apparatus

In the unloaded ankle test rig, the femoral intermedullary rod was fixed horizontally with the tibia hanging freely. Flexion/extension was achieved by controlling a linear actuator attached to one end of a cable, while the other end of the cable was attached to the quadriceps tendon (Figure 8-3 and Figure 8-4), and a 2 kN load cell (HBM, Darmstadt, Germany) was attached between the cable and the actuator, measuring the force transmitted to the quadriceps tendon. The linear displacement of the actuator head in extending the knee was measured with a 200 mm linear variable differential transformer (HBM, Dramstadt, Germany). The rig allows for unconstrained tibial movement relative to the femur with only flexion/extension controlled.

Table 8-2 lists the main products used for the unloaded ankle apparatus.

Table 8-2: Products used for unloaded ankle apparatus

Description	Product
Position sensors	Polhemus 3Space Fastrak including ST8 stylus, extra RX2 receiver, and Locator software
Load cell	HBM 2 kN U2A Range load cell
LVDT	HBM 200 mm WA Range LVDT
Linear actuator	WPR Ball screw gear with 12 V motor
Data acquisition	HBM Spyder 8, 4.8 kHz, with Catman Easy Version 3.1 Software
Frame	Bosch Rexroth 40 mm strut profiles with connectors.

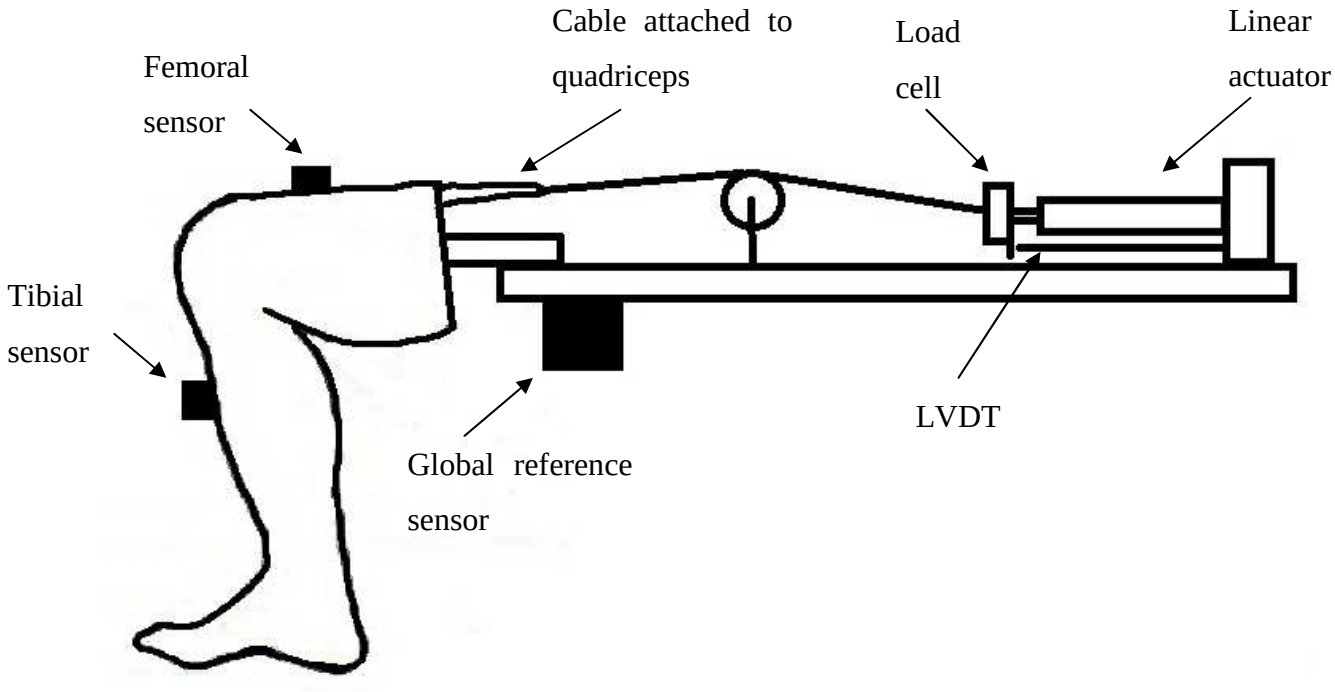

Figure 8-3: Schematic of unloaded ankle test

Figure 8-4: Photo of unloaded ankle apparatus

8.2.5 Knee implants

Normal knee kinematics were compared to kinematics after implantation with two types of unicompartmental knee replacements. The first type is a patient-specific UKR. Prior to testing, CT data of the cadaver knees were obtained in order to develop patient-specific implants. The methods described in Chapter 6 were used to design the implants. STL files of the prostheses were sent to the Centre for Rapid Prototyping and Manufacturing, Central University of Technology, Free State. Here the implants were manufactured using the EOS M270 direct laser sintering platform. The material used for the components was a titanium alloy (Ti-6Al-4).

Instrumentation to aid in the implantation of the prostheses was also developed. These consisted of femoral and tibial components with slots in the correct position in order to make the necessary cuts for the fixation pegs of the implants (Figure 8-5).

The conventional implant used was a non-conforming fixed-bearing UKR. The accompanying instrumentation was used for implantation.

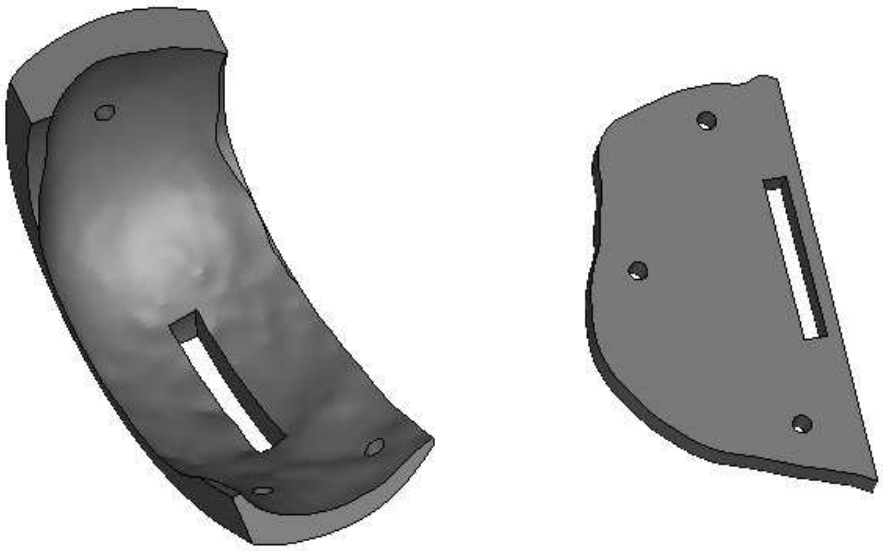

Figure 8-5: Custom instrumentation

8.2.6 Testing protocol

Each specimen was preconditioned by manually flexing the knee at least 10 times between full extension and full flexion. First, knee kinematics were recorded with an intact joint capsule on both the test rigs. Next, the patient-specific knee replacement was implanted and tested on both test rigs and the kinematics were recorded. The femoral component was implanted by removing the cadaver femoral cartilage beneath the implantation region and making the fixation hole with the help of the custom instrumentation. The tibia was prepared as per standard surgical techniques using the fixed-bearing instrumentation. The system uses a tibial cut perpendicular to the tibial shaft axis. The fixation hole was prepared using the custom instrumentation.

The patient-specific components were removed and the cadaver knee was implanted with the fixed-bearing components as per standard surgical techniques with the accompanying instrumentation. The knees were again tested on both test rigs and the kinematics were recorded. Figure 8-6 shows the tibia being prepared for implantation and Figure 8-7 shows an implanted medial patient-specific UKR.

Figure 8-6: Tibia being prepared for implantation

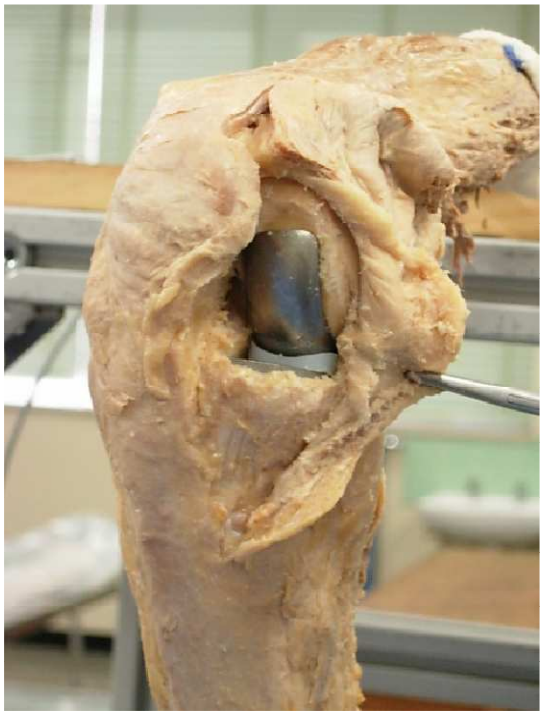

Figure 8-7: Implanted medial patient-specific UKR

8.3 Results

For all three the different knee specimens, and both the test setups, the normal knee displayed femoral rollback and internal tibial rotation. However, the loaded ankle results showed slightly more femoral posterior translation, as well as considerably more internal tibial rotation. Similar kinematic patterns were also present after implantation with both the patient-specific and conventional fixed-bearing UKRs. Some interspecimen variation was also visible. Cadaver 1 and 3 received medial replacements while cadaver 2 received a lateral replacement.

8.3.1 Unloaded ankle apparatus

Figure 8-8 to Figure 8-10 show the tibial rotation and femoral translation of the three knee specimens using the unloaded ankle apparatus. For cadaver 2, only the normal knee and patient-specific UKR kinematics were available (Figure 8-9). Cadaver 1 and 2 showed tibial rotation of more than 20º over a flexion range of 70º. The patient-specific UKR showed very similar patterns to the normal knee. The conventional UKR showed slightly more rotation for cadaver 1, while still following a similar pattern. Cadaver 3 showed tibial rotation of about 10º after 70º flexion. Both the UKRs showed higher rotations over the range of flexion.

For all three normal knees, femoral rollback ranged between 4 mm and 5 mm. The UKRs showed similar but slightly more femoral rollback for cadaver 1. For cadaver 2 the patient-specific translation was very similar to that of the normal knee. For cadaver 3 the conventional UKR followed a similar pattern to that of the normal knee, with slightly more posterior translation. The patient-specific UKR also followed a similar pattern, with even more posterior translation.

Hysteresis effects were negligible and did not impact on the overall kinematic patterns.

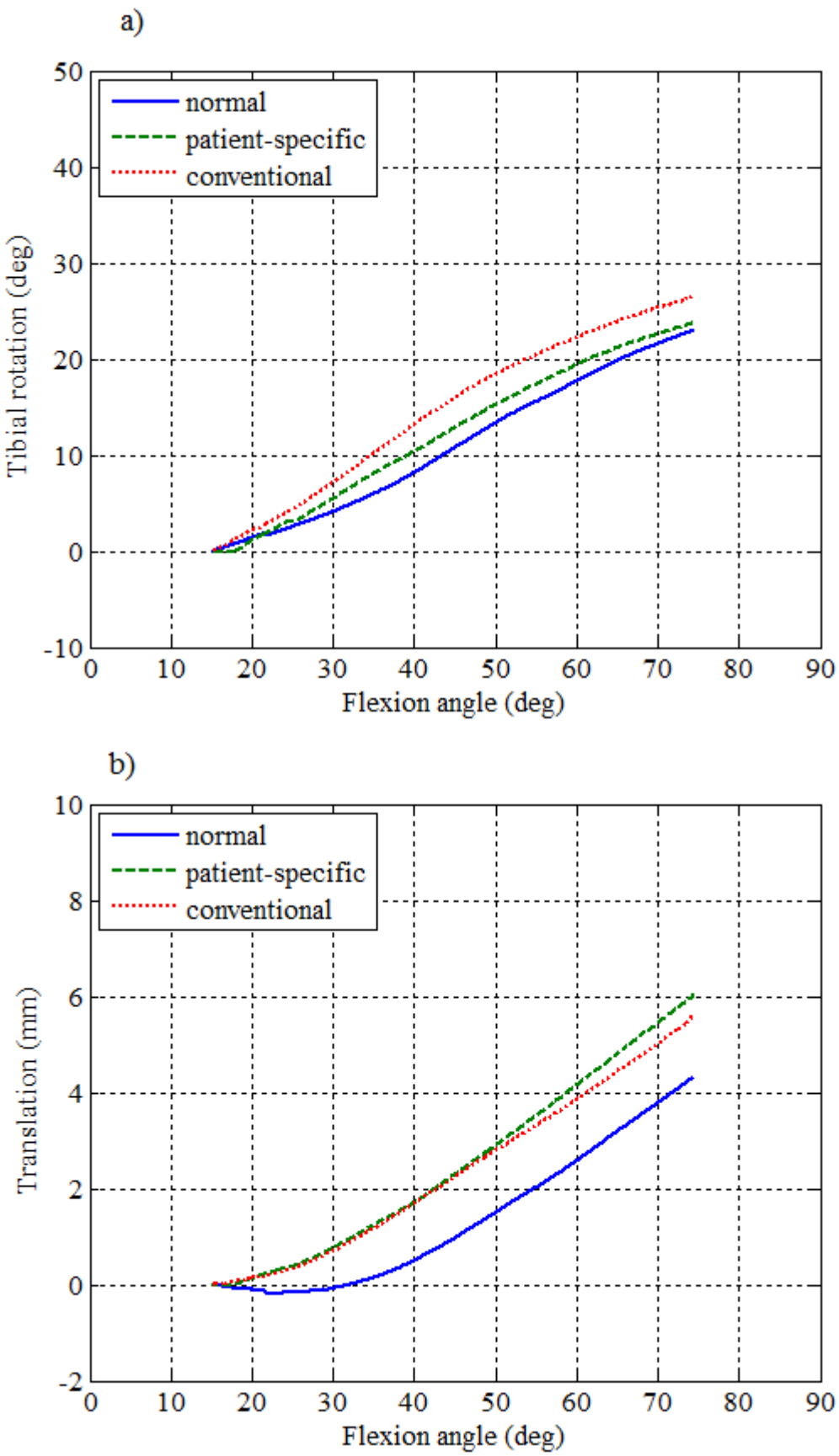

Figure 8-8: Cadaver 1 measurements on unloaded ankle apparatus, a) tibial rotation, b) femoral translation

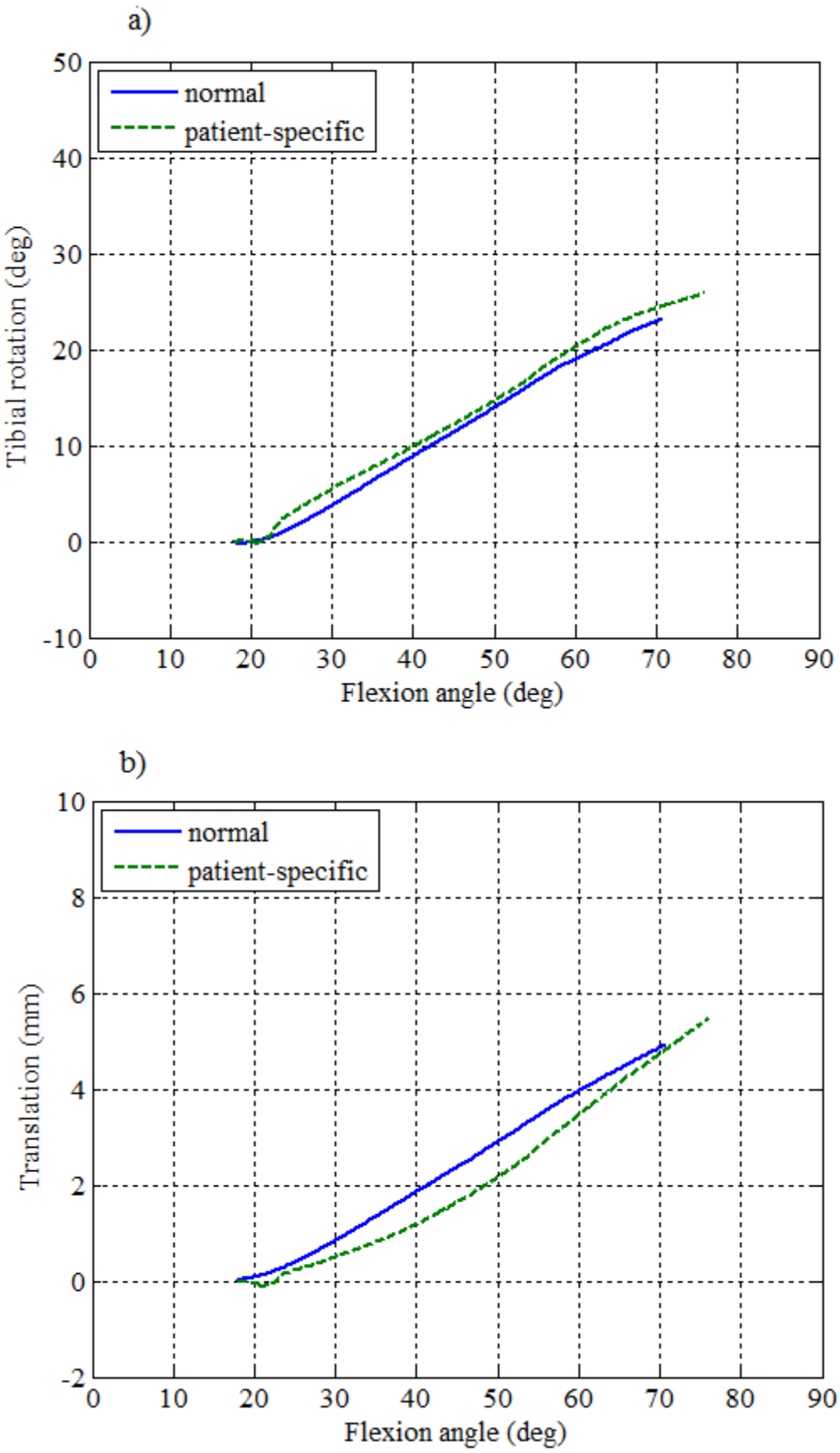

Figure 8-9: Cadaver 2 measurements on unloaded ankle apparatus, a) tibial rotation, b) femoral translation

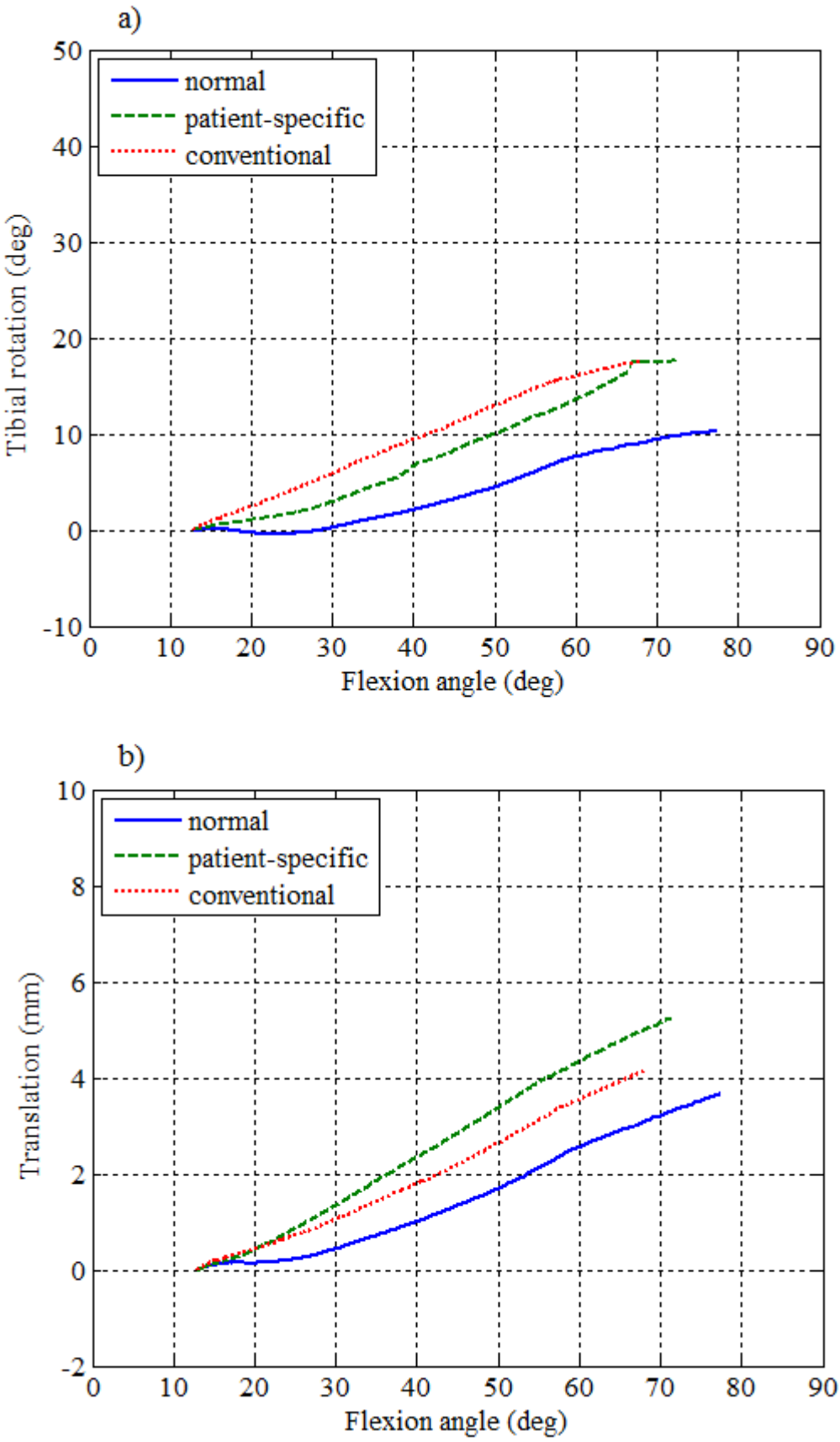

Figure 8-10: Cadaver 3 measurements on unloaded ankle apparatus, a) tibial rotation, b) femoral translation

8.3.2. Loaded ankle apparatus

Only cadavers 2 and 3 were tested on the loaded ankle apparatus and only cadaver 3 was implanted with the conventional UKR (Figure 8-11 and Figure 8-12). The normal knees displayed more internal tibial rotation compared to the unloaded ankle, with cadaver 3 showing four times more rotation. Both knees showed internal tibial rotation of about 40º after 70º flexion. For cadaver 2 the patient-specific UKR showed a similar pattern to that of the normal knee, with slightly less rotation. For cadaver 3 both the UKRs showed a similar pattern to the normal knee up to 60º flexion, after which the normal knee's rotation stopped.

Cadavers 1 and 2 showed femoral rollback of close to 8 mm after a slight anterior translation at the beginning. For cadaver 2 the patient-specific UKR showed a similar pattern to that of the normal knee, with slightly more posterior translation. For cadaver 3, both the UKRs showed considerably less posterior translation. However, the patient-specific UKR showed a similar pattern to that of the normal knee, with a slight anterior translation at first before a steeper posterior translation.

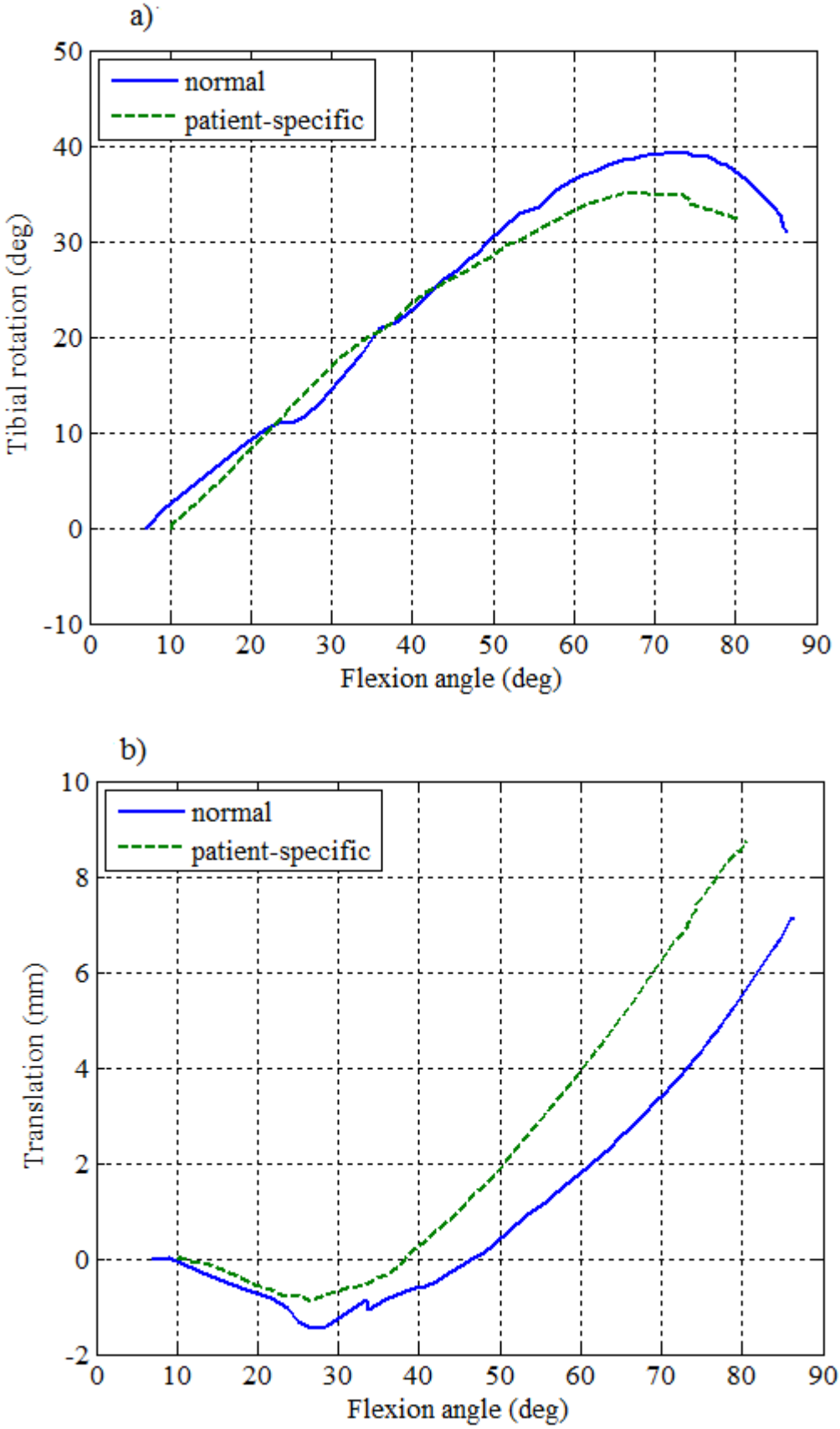

Figure 8-11: Cadaver 2 measurements on loaded ankle apparatus, a) tibial rotation, b) femoral translation

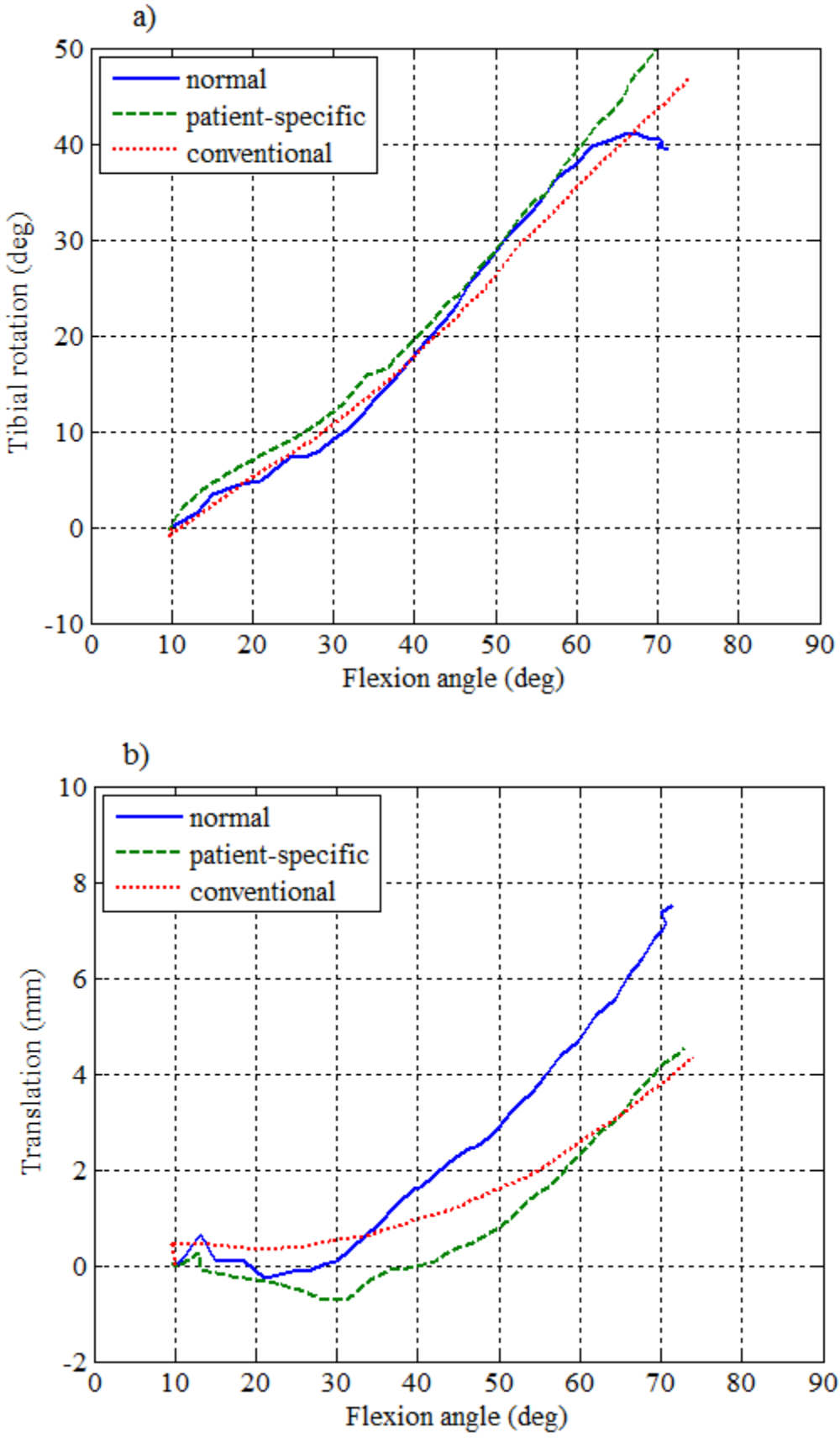

Figure 8-12: Cadaver 3 measurements on loaded ankle apparatus, a) tibial rotation, b) femoral translation

8.4 Discussion

Numerous studies have reported that normal knee kinematics are not achieved after total knee replacement (Coughlin et al., 2003), (Most et al., 2003), (Patil et al., 2005), (Bull et al., 2008), (Varadarajan et al., 2009). Better preservation of the overall knee geometry with unicompartmental knee replacement is believed to restore normal knee kinematics better than TKR (Patil et al., 2005). However, very little research is available comparing normal knee kinematics with knee kinematics after implantation with a UKR. Numerous in vivo studies investigated the patellar tendon angle before and after implantation with a UKR, and found results suggesting that normal knee kinematics are restored (Robinson et al., 2002), (Price et al., 2004), (Pandit et al., 2008). Patil et al. (2005) investigated in vitro knee kinematics before implantation, after implantation with a UKR, and after implantation with a TKR. They found no significant differences in femoral rollback between the cases, but reported that TKR significantly affected tibial rotation. The UKR showed no significant difference in tibial rotation compared to the normal knee.

The aim of this study was to compare normal knee kinematics to knee kinematics after implantation with a patient-specific UKR and a conventional UKR. This was done using two different testing apparatus, one providing a load at the ankle joint and one with an unloaded ankle. The results showed that there were significant differences between the two techniques for the same knees. The loaded ankle tests showed more internal tibial rotations and more femoral rollback for the same knees compared to the unloaded ankle tests. The tibial rotations found with the loaded ankle tests tended to be higher than those reported in the literature (Coughlin et al., 2003), (Patil et al., 2005), (Varadarajan et al., 2009), (Victor et al., 2009), (Victor et al., 2010). A possible reason for this could be the use of embalmed cadaver specimens combined with the ankle joint fixation method used in this study. The ankle joint of the cadaver specimens tended to force the tibia to rotate more internally than is the case with the normal knee. It was decided to keep the ankle joint intact because of the physiological advantages. The normal ankle joint provides rotational freedom in flexion/extension, internal/external rotation and limited varus/valgus rotation (Varadarajan et al., 2009). It was believed that by keeping the ankle joint intact, the ankle movement would be more natural. Using fresh frozen cadaver specimens may still prove this method to be viable. The intermedullary rod of cadaver 2 was fixed to the femur with the D-shackle at an angle, further forcing the knee into internal rotation.

The patient-specific UKR femoral component was easily implanted once the cartilage was removed and had a very good fit. The cutting guides aided in

making the correct cut for the fixation peg. The process was much simpler than with the conventional UKR, which required additional cutting of the femur.

Both the UKRs yielded similar kinematic patterns to the normal knee using both the test apparatuses. Cadaver 2 received a lateral implant and it was seen that the kinematics were similar to that of the normal knee. In the loaded ankle test, the patient-specific UKR followed the same anterior translation before posterior translation as with the normal knee. The patient-specific UKR also showed a slight external rotation after 70º flexion, similar to the normal knee. The geometry and kinematics of the lateral compartment are different to that of the medial compartment, and lower survival rates and other complications have been reported when using conventional UKRs for the treatment of lateral osteoarthritis (Gunther et al., 1996), (Ashraf et al., 2002), (Pandit et al., 2009). Unfortunately, conventional UKR kinematics were not available for cadaver 2. From the results it is evident that kinematics varies from knee to knee and also between different testing methods. There is also high variability between knee kinematics in the literature. Krevolin (2003) studied knee kinematics in the intact cadaver knee versus the cadaver knee implanted with a TKR on an unloaded ankle test rig. Figure 8-13 shows the results for one of the cadaver knees investigated, with other data from the literature also included.

The rotations in this study for the unloaded ankle followed similar trends to that of Rovick (1991) shown in Figure 8-13. Translations were similar to those found by Krevolin (2003) for this specific case. The TKR knee showed distinctly different kinematics compared to the intact knee. It is also important to note the variability between the different studies.

The variability found in knee kinematic studies may be attributed to interspecimen variability (Varadarajan et al., 2009). D'Lima et al. (2000), (2001) obtained different intact knee kinematics in two different studies using identical protocol and OKR setup. Victor et al. (2009) showed that interspecimen variability was greater than interload variability. They further argued that a correct description of normal knee kinematics for clinical applications remained a major challenge. It seems that referring to normal knee kinematics are inherently flawed, since individual knees will behave differently. Rovick et al. (1991) argue that average behaviour is a useful reference, but it does not describe the individual variations. Reference should rather be made to individual normal knee kinematics.

Because each individual's knee geometry and kinematics are specific to him/her, it is suggested that there is significant potential for patient-specific knee replacements.

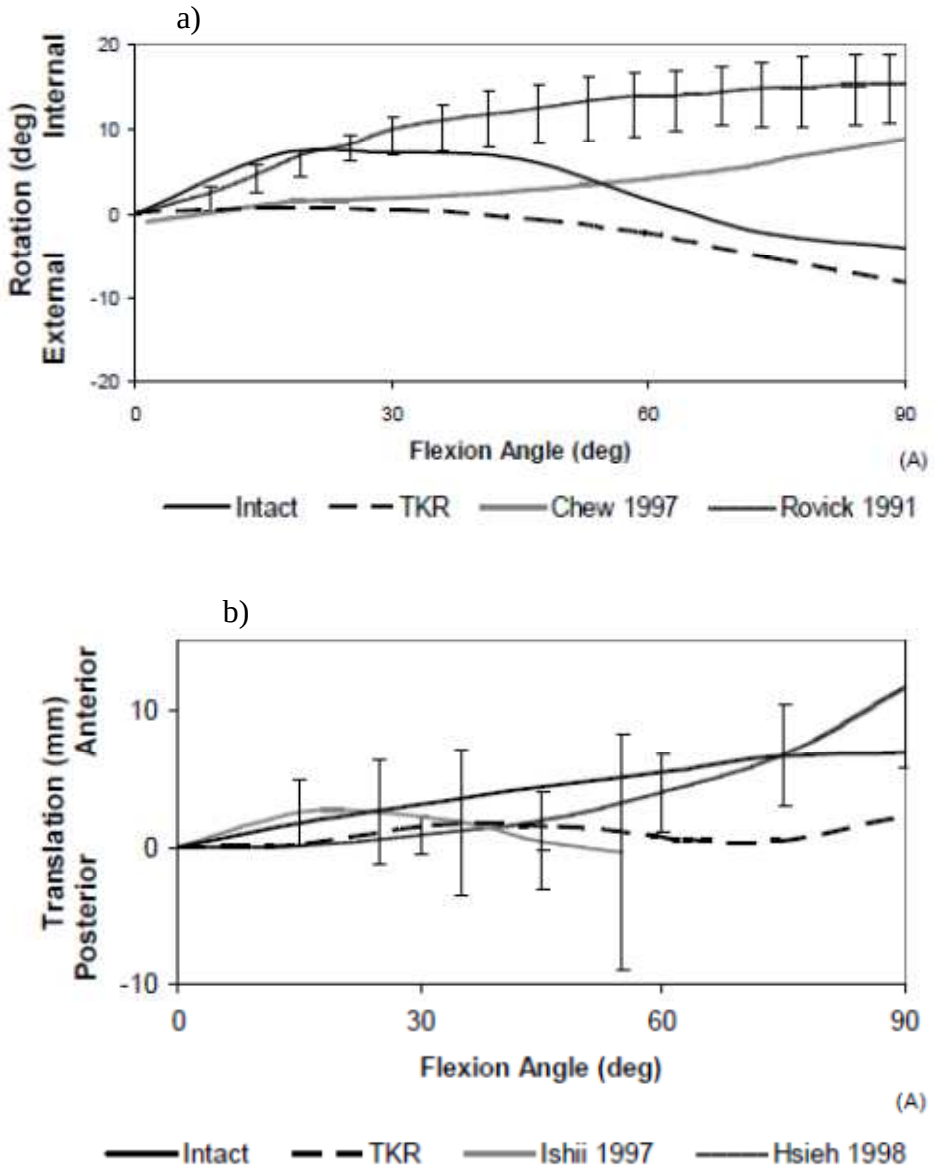

Figure 8-13: Cadaver measurements by Krevolin (2003) and compared to other studies, a) tibial rotation, b) femoral translation

9. CONCLUSION AND RECOMMENDATIONS

9.1 Conclusion

The main aim of knee replacement procedures is to relieve pain and restore normal function to the joint (Krevolin, 2003). An ideal knee replacement prosthesis would have an articulating geometry similar to that of the patient's healthy knee and would be located at the same height as the original joint. This would imply restoring the degenerated articulating regions to the original geometry and level. Commercial prostheses are available in a wide range of types and sizes in order to replicate the human knee anatomy for a host of individuals. However, the large variation in knee anatomy between individuals makes it difficult to always restore a particular patient's articulating surfaces to the original levels. The aim of this research was to find a method to restore an individual's articulating surfaces to normal and thus restore normal function to the knee joint.

A method for selecting the optimal knee prosthesis design for a specific patient from a variety of different types and sizes that are commercially available was investigated. A computer algorithm was used to give an indication of the goodness of fit of a specific prosthesis for a specific individual. This method showed good accuracies comparable to other templating methods in the literature, and has the further advantage of making a choice between different prostheses. A survey by Sharkey et al. (1999) showed that 52.7% of orthopaedic surgeons used two or more types of knee implant brands. However, due to the simplified geometry of commercial prostheses, they are not always able to restore the complex geometry of an individual's articulating surfaces.

Many studies have proposed different models to describe the geometry of the femoral condyles (Wismans et al., 1980), (Ateshian, 1993), (Boyd et al., 1999), (Nuño & Ahmed, 2003), (Hirokawa et al., 2004), (Biščević et al., 2005). However, these different models have not been compared for their accuracy before. In this study, the complex morphometry of the articulating profiles of the femoral condyles was described using several different models. These models were then compared with regard to their precision of fit by equating them to the measured original profiles of several femoral joints.

The B-spline models showed the best results with respect to accuracy. This can be attributed to the ability of B-splines to provide the flexibility to design a large variety of shapes. B-splines are invariant under affine as well as perspective transformations. A method using SOMs was developed to predict the articulating

surfaces for any individual. This method used a database containing the parameters of the different models. The SOM, in conjunction with B-splines, showed the most potential as a method that can be used to predict knee joint profiles.

The SOM has the further advantage of clustering or grouping together similar inputs during the mapping process. In this study, the SOM was used to determine whether anatomical differences between genders and races could be classified. When absolute measurements were used there is a statistically significant difference between gender and race, and different knees can be classified into their respective groups. White male knees were larger than white female knees across all measurements. When the measurements were corrected for size it was more difficult to define a clear cluster and it was suggested that there are no definite differences between white male and female knees, but it was seen that black males have a larger LR and MR to APL ratio compared to the white males and females. However, numerous genetic diversity studies have shown that human genetic diversity is more pronounced within a population than between populations (Lewontin, 1972), (Relethford & Harpending, 1994), (Barbujani et al., 1997). It was argued that with the large variation in populations it can become advantageous to develop patient-specific designs, and not gender- or race- specific prostheses.

The development of a patient-specific unicompartmental knee replacement was presented in Chapter 6. The output of the SOM estimation algorithm was used to design the articulating surfaces of the prosthesis. To avoid the uneven stress distribution caused by the shape of conventional prostheses, a patient-specific bone-implant interface was suggested. In theory, the component should fit perfectly on the patient's femur without the need to remove bone. A custom tibial baseplate was also suggested, providing complete cortical rim coverage for optimal load transfer. The polyethylene insert in this study was designed to be congruent with the femoral component at 0º flexion. Because of the design of the femoral component, this will ensure that the mobile polyethylene insert conforms in the medial-lateral direction with the femoral component throughout flexion. This provides maximum contact area. Bartel et al. (1986) found that, when the articulating surfaces were more conforming in the medial-lateral direction, contact stresses in the tibial components were reduced.

The main reason for knee replacement failure is the wear of the polyethylene bearing and aseptic loosening (Sharkey et al., 2002), (Villa et al., 2004). The early wear of UHMWPE is mainly affected by the conformity of the articulating surfaces, the thickness of the UHMWPE component, the elastic modulus of the

component, contact stresses and surface kinematics (Petty et al., 1999), (Fregely et al., 2003), (Bei et al., 2004), (McEwen et al., 2005). A very effective method of examining the contact stresses produced in knee replacements is finite element (FE) analysis. In this study, the contact stresses in a patient-specific UKR were examined and compared to conventional implants using FE analysis. The custom implant showed lower maximum contact stress compared to the conventional fixed-bearing implant. However, the fully-congruent mobile-bearing design showed the best results, due to the large contact area that is maintained throughout flexion. It was also demonstrated that a custom bone-implant interface for the femoral component can achieve more uniform stress distribution at the condyle surface. This will reduce the occurrence of bone remodelling in the region of implantation, reducing the likelihood of aseptic loosening. Stress concentrations produced by the sharp edges of conventional knee replacements can lead to remodelling problems, further complicating revision surgery due to bone loss.

Numerous studies have reported that normal knee kinematics are not achieved after total knee replacement, (Coughlin et al., 2003), (Most et al., 2003), (Patil et al., 2005), (Bull et al., 2008), (Varadarajan et al., 2009). Better preservation of the overall knee geometry with unicompartmental knee replacement is believed to restore normal knee kinematics better than TKR (Patil et al., 2005). This study compared normal knee kinematics to knee kinematics after implantation with a patient-specific UKR and a conventional UKR. This was done using two different testing apparatus, one providing a load at the ankle joint and one with an unloaded ankle. The results showed that there are significant differences between the two techniques for the same knees. The patient-specific UKR showed similar kinematic patterns to the normal knee. It was especially encouraging to see the normal kinematics being reproduced for the lateral implant. The geometry and kinematics of the lateral compartment are different to that of the medial compartment, and lower survival rates and other complications have been reported when using conventional UKRs for the treatment of lateral osteoarthritis (Gunther et al., 1996), (Ashraf et al., 2002), (Pandit et al., 2009).

In conclusion, this research emphasised the importance of restoring a patient's original articulating surfaces when their knee joints are affected by injury or disease. In some cases this can be achieved with conventional prostheses. A method for selecting the ideal prosthesis implant type and size can aid the surgeon in choosing from a wide variety of implants. However, this option is not always viable. A method for designing a patient-specific UKR was presented and tested with regard to contact stresses and kinematics. It was shown that patient-specific implants can have characteristics comparable to, and in certain cases better, than conventional prostheses. This research made several contributions to the field in

the form of peer-reviewed conference papers, peer-reviewed journal papers and a patent, summarised below:

Peer-reviewed conference papers

- Van den Heever, D., Scheffer, C., Erasmus, P., Dillon, E., Development of a patient-specific femoral component for unicompartmental knee replacement. *30th Annual International Conference of the IEEE Engineering in Medicine and Biology Society (EMBC 2009),* 2-6 September 2009, Minneapolis, USA.
- Van den Heever, D., Scheffer, C., Erasmus, P., Dillon, E., Contact stresses in a patient-specific unicompartmental knee replacement. *32nd Annual International Conference of the IEEE Engineering in Medicine and Biology Society (EMBC 2009),* 31 August – 4 September 2010, Buenos Aires, Argentina.

Journal papers

- Van den Heever, D., Scheffer, C., Erasmus, P., Dillon, E., 2011, Method for selection of femoral components in total knee arthroplasty (TKR). *Australasian Physical & Engineering Science in Medicine*, 34, pp. 23-30.
- Van den Heever, D., Scheffer, C., Erasmus, P., Dillon, E., 2011, Classification of gender and race in the distal femur using self organising maps. *The Knee,* Article in press.
- Van den Heever, D., Scheffer, C., Erasmus, P., Dillon, E., 2011, Mathematical reconstruction of human femoral condyles. *Journal of Biomechanical Engineering,* 133(6), pp. 64504.
- Van den Heever, D., Scheffer, C., Erasmus, P., Dillon, E., 2011, Contact stresses in a patient-specific unicompartmental knee replacement. *Clinical Biomechanics,* 26, pp. 159-166.

Patent

- International application published under the patent cooperation treaty (PCT)., International publication number: WO 2010/140036 A1., Publication date: 9 December 2010., Title: A method of designing a knee prosthesis, Inventors: Van den Heever, D., Scheffer, C., Erasmus, P., Dillon, E

9.2 Recommendations

ISO (the International Organization for Standardization) specifies certain requirements for the design of a new knee replacement (ISO 21534, 2007), (ISO 7207-1, 2007), (ISO 14243-1, 2002), (ISO 14243-2, 2000), (ISO 14243-3, 2004), (ISO 14155-1, 2003), (ISO 14879-1, 2000), (ISO 14630, 2008), (ISO 21536, 2007), (ISO 4287, 1997). One of the requirements specifies relative movement between the articulating components (ISO 14243-3, 2004). The standard requires a wear-testing machine having axial load control, flexion/extension angular motion control, AP displacement control and tibial rotation control. The pattern of the applied force, speed and duration of testing, sample configuration and test environment are specified within the standard. Future work would include testing on such a machine as well as adherence to all other ISO requirements.

Other future work should include the development of a complete patient-specific instrumentation system to aid the surgeon in making the necessary tibial cuts and implantation of the prosthesis.

In this research static FE analysis was performed at three different flexion angles. Future work should also investigate dynamic FE analysis.

Fresh cadavers should be used for the kinematics testing in future work. The embalmed cadavers used in this study were not physiologically correct and influenced normal kinematics.

APPENDIX A: FINITE ELEMENT ANALYSIS RESULTS

Custom prosthesis 1

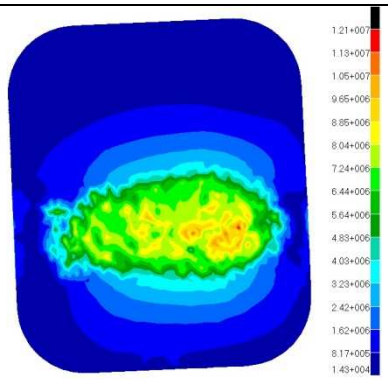

15º custom bearing

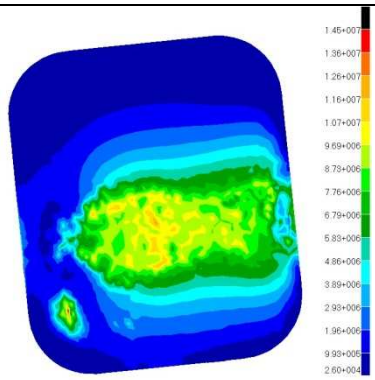

45º custom bearing

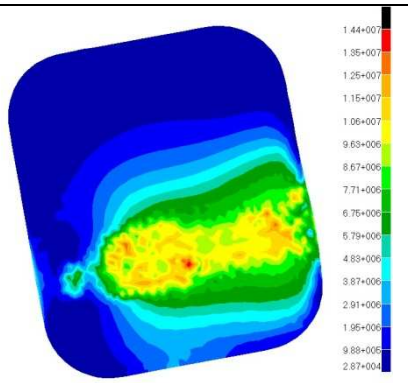

60º custom bearing

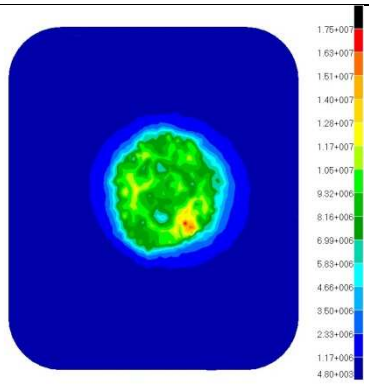

15º flat bearing

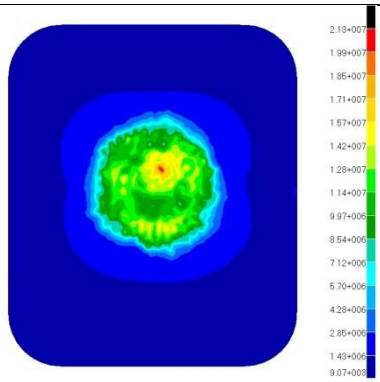

45º flat bearing

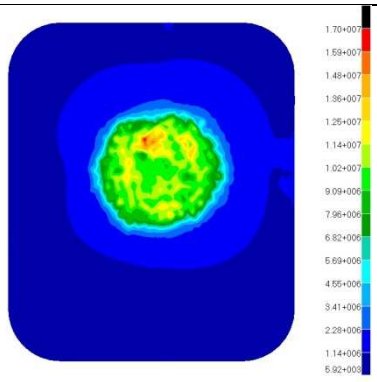

60º flat bearing

Custom prosthesis 2

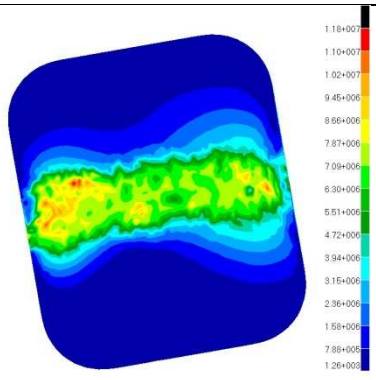

15º custom bearing

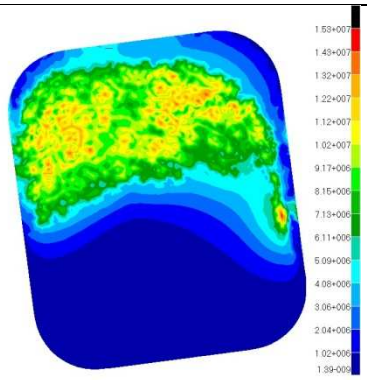

45º custom bearing

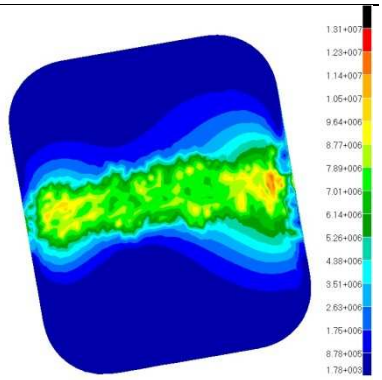

60º custom bearing

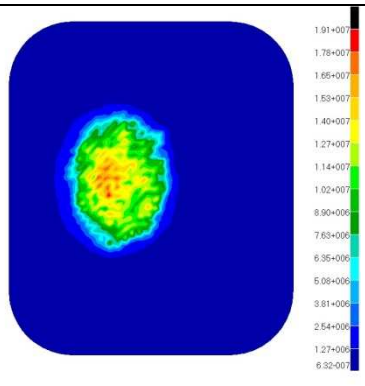

15º flat bearing

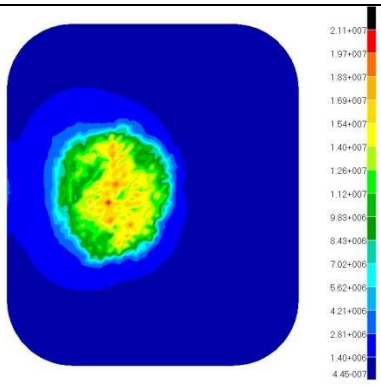

45º flat bearing

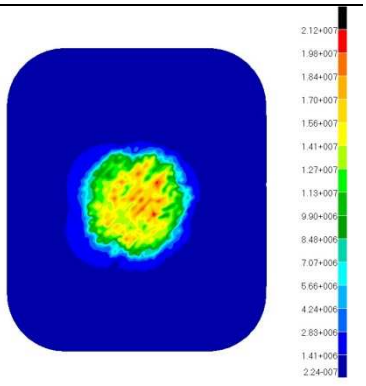

60º flat bearing

Custom prosthesis 3

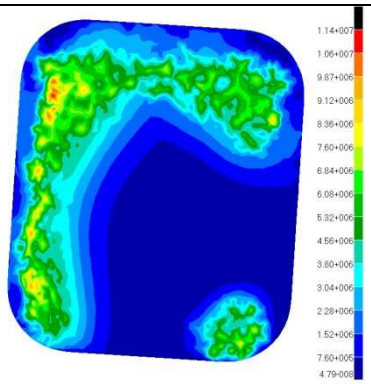

15º custom bearing

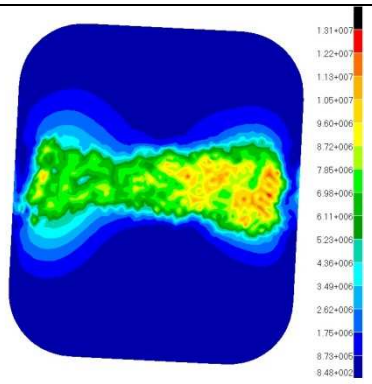

45º custom bearing

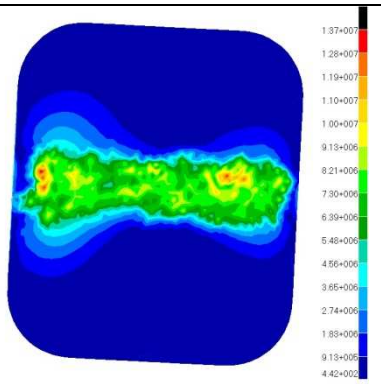

60º custom bearing

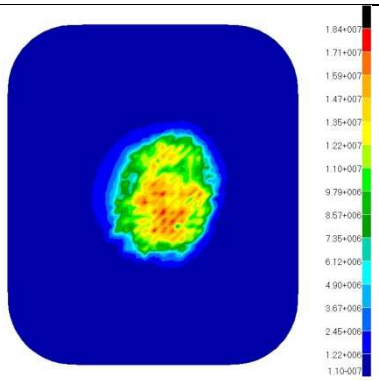

15º flat bearing

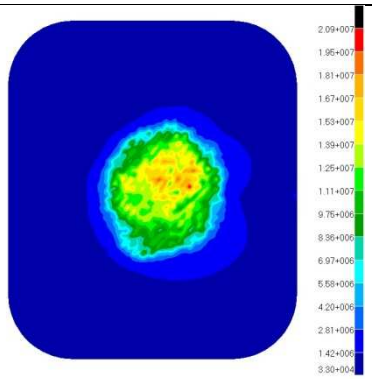

45º flat bearing

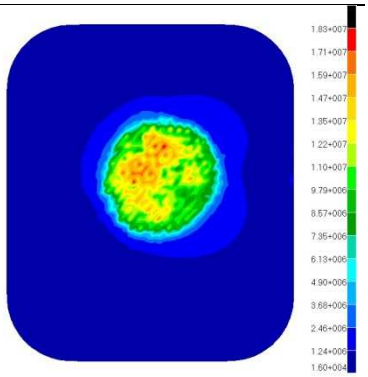

60º flat bearing

Custom prosthesis 4

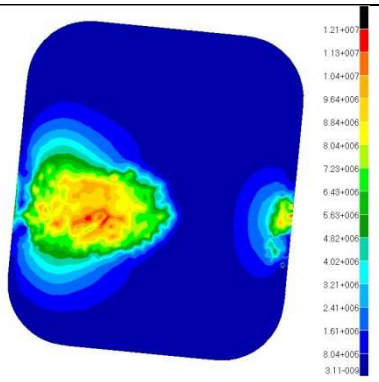

15º custom bearing

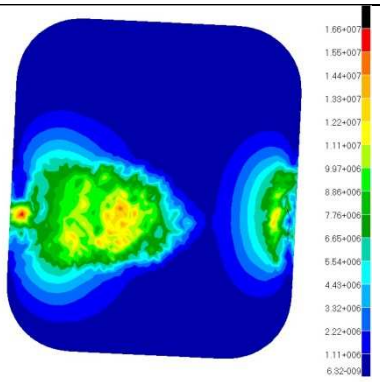

45º custom bearing

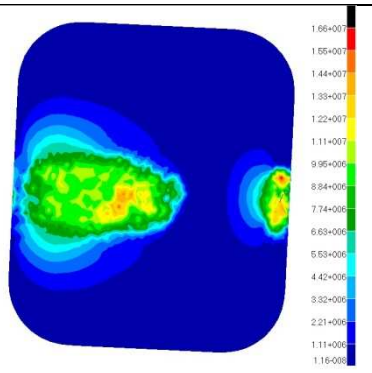

60º custom bearing

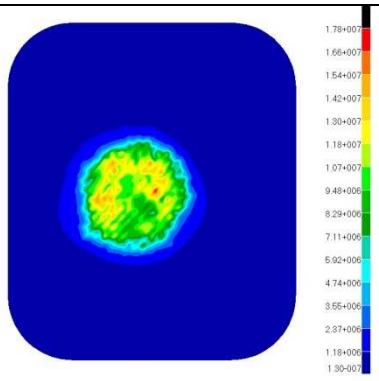

15º flat bearing

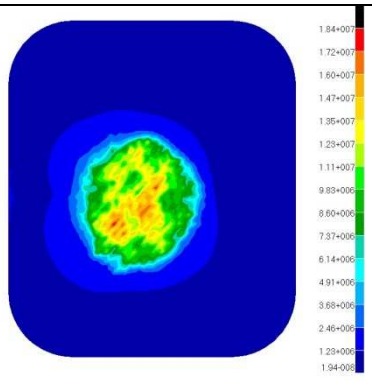

45º flat bearing

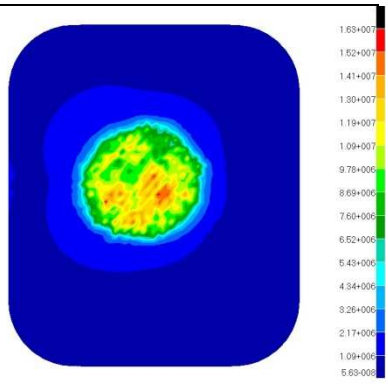

60º flat bearing

Custom prosthesis 5

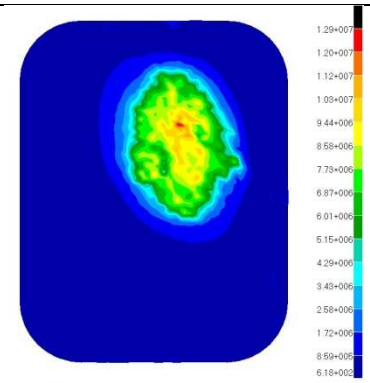

15º custom bearing

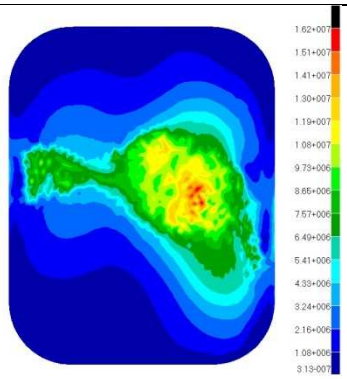

45º custom bearing

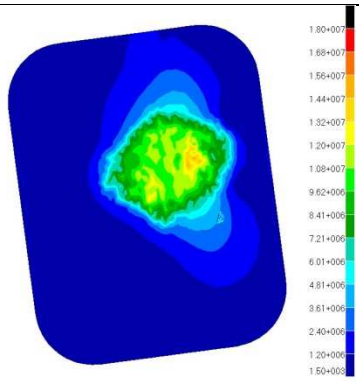

60º custom bearing

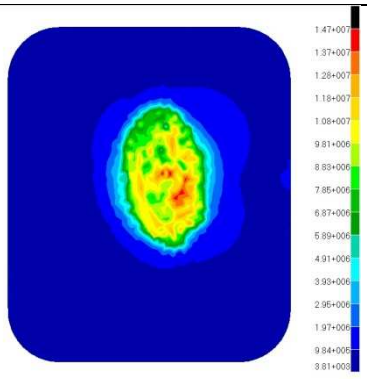

15º flat bearing

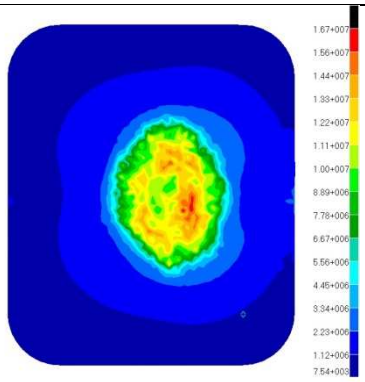

45º flat bearing

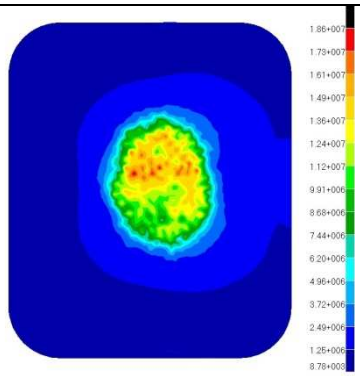

60º flat bearing

Custom prosthesis 6

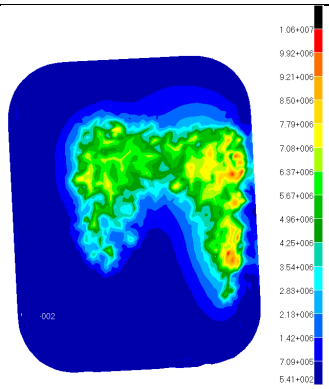

15º custom bearing

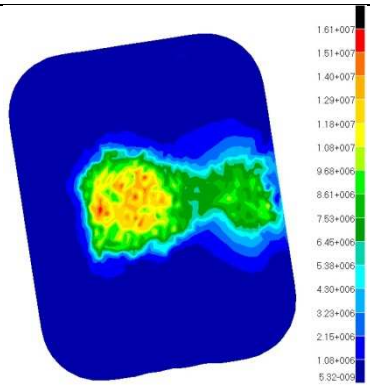

45º custom bearing

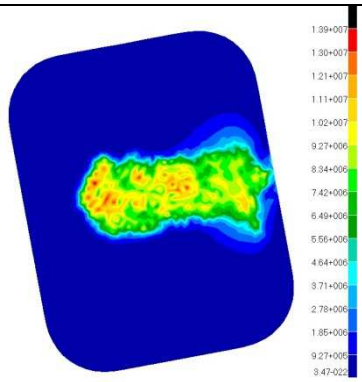

60º custom bearing

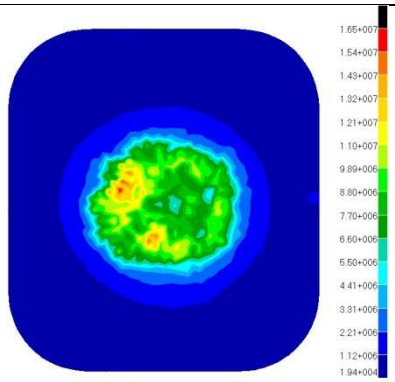

15º flat bearing

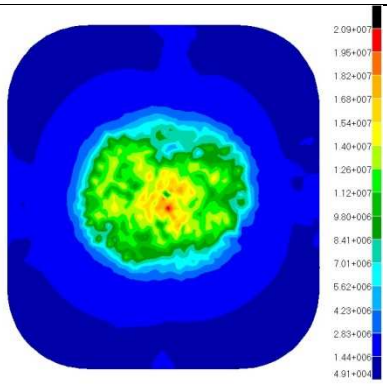

45º flat bearing

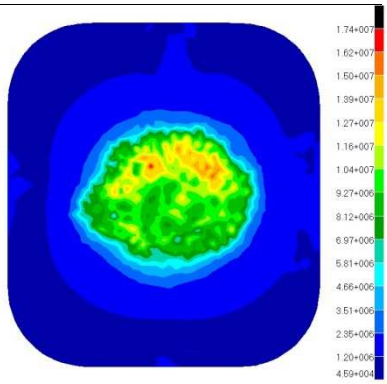

60º flat bearing

Custom prosthesis 7

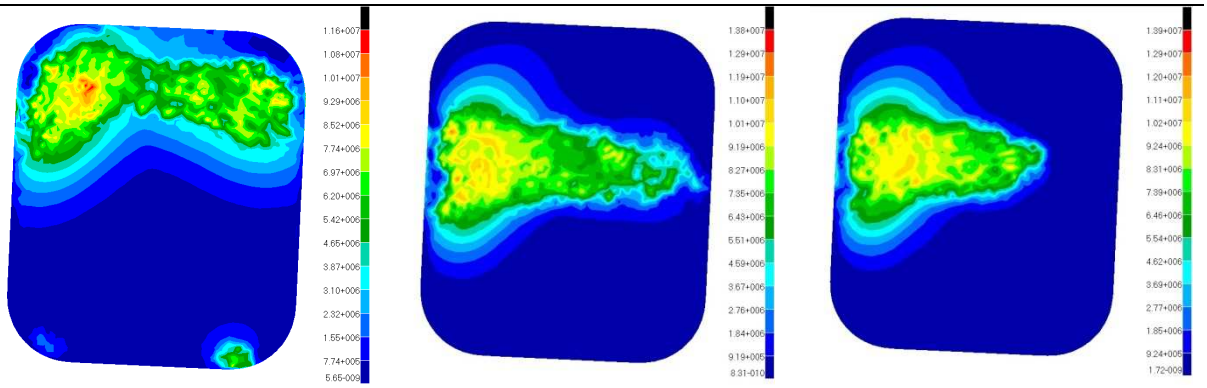

15º custom bearing	45º custom bearing	60º custom bearing

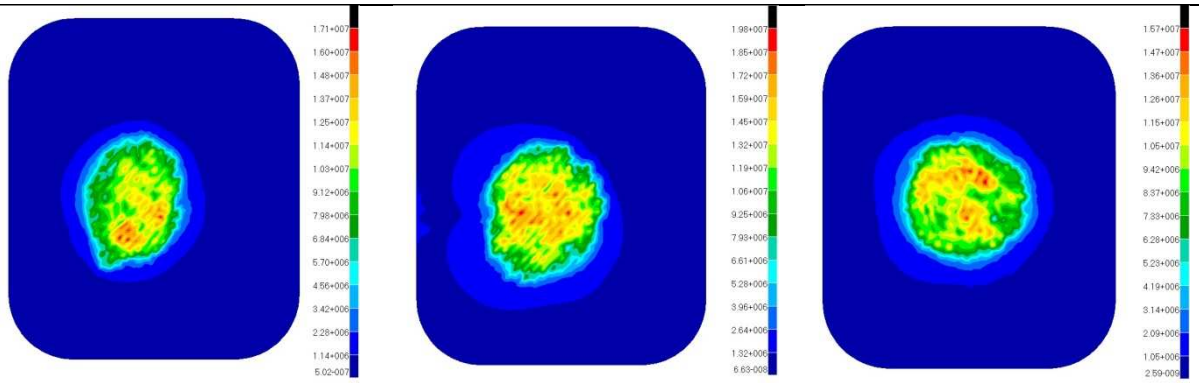

15º flat bearing	45º flat bearing	60º flat bearing

Fixed-bearing prosthesis Small

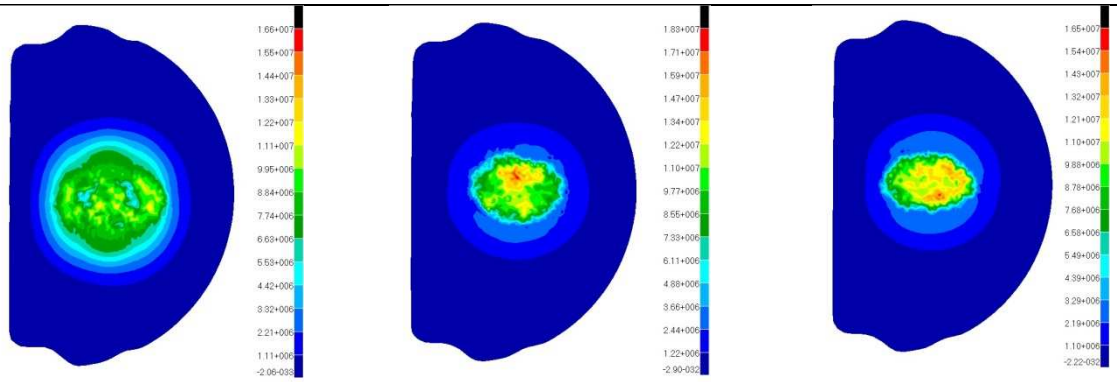

15º partially-congruent	45º partially-congruent	60º partially-congruent

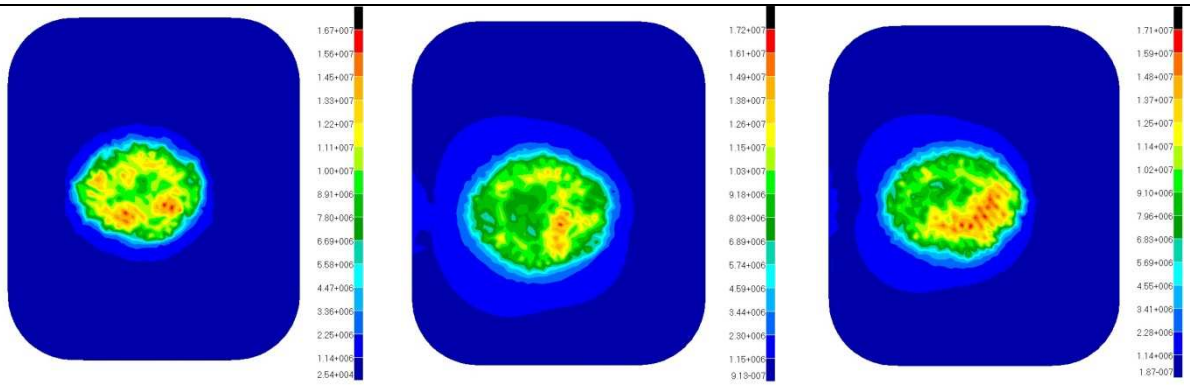

15º flat bearing	45º flat bearing	60º flat bearing

Fixed-bearing prosthesis Medium

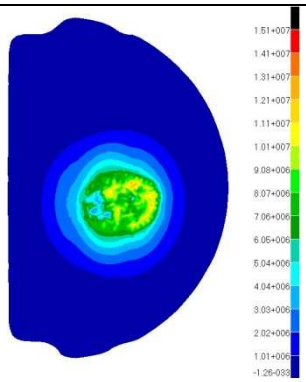

15º partially-congruent

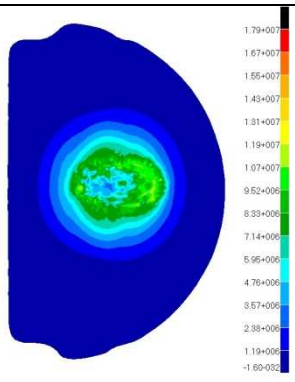

45º partially-congruent

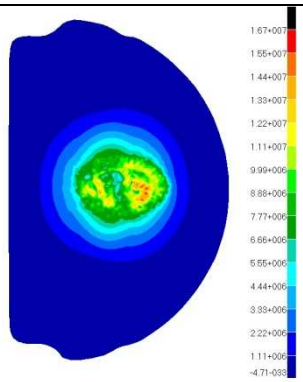

60º partially-congruent

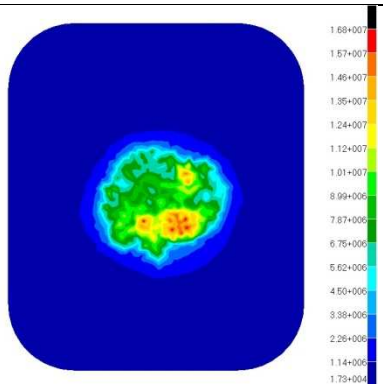

15º flat bearing

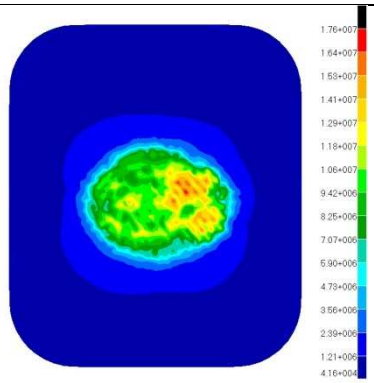

45º flat bearing

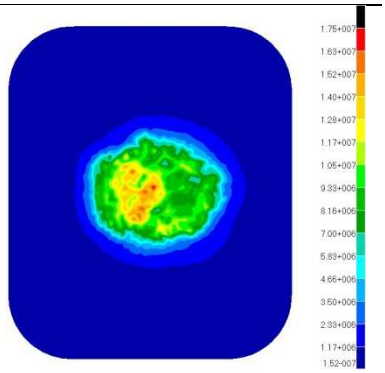

60º flat bearing

Fixed-bearing prosthesis Large

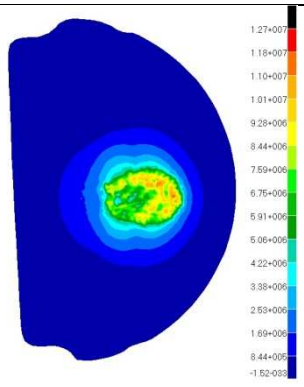

15º partially-congruent

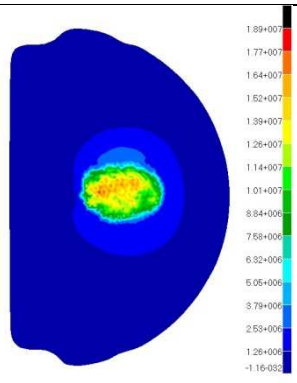

45º partially-congruent

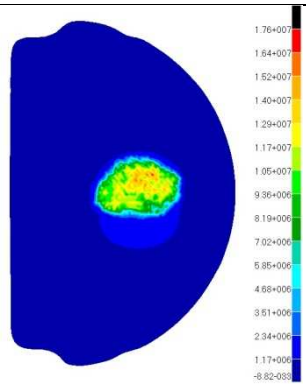

60º partially-congruent

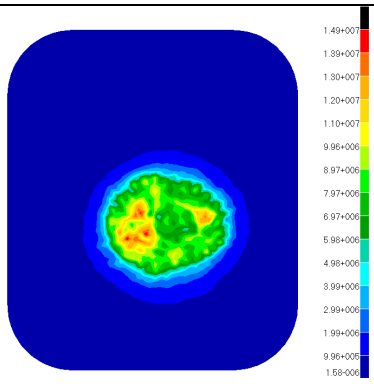

15º flat bearing

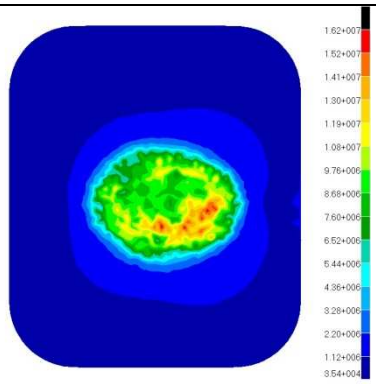

45º flat bearing

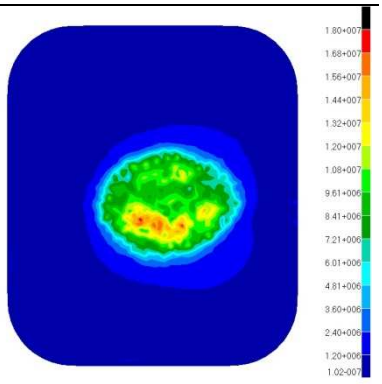

60º flat bearing

Mobile-bearing prosthesis Medium

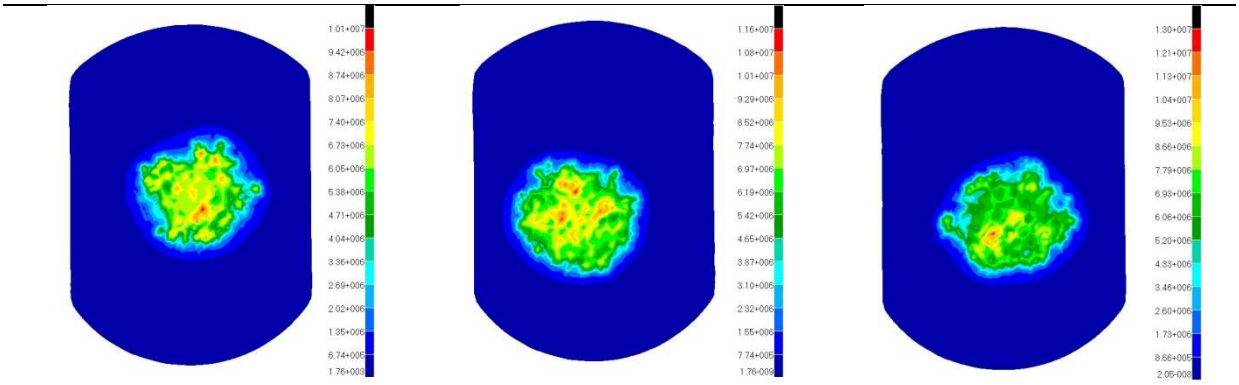

15º fully-congruent bearing | 45º fully-congruent bearing | 60º fully-congruent bearing

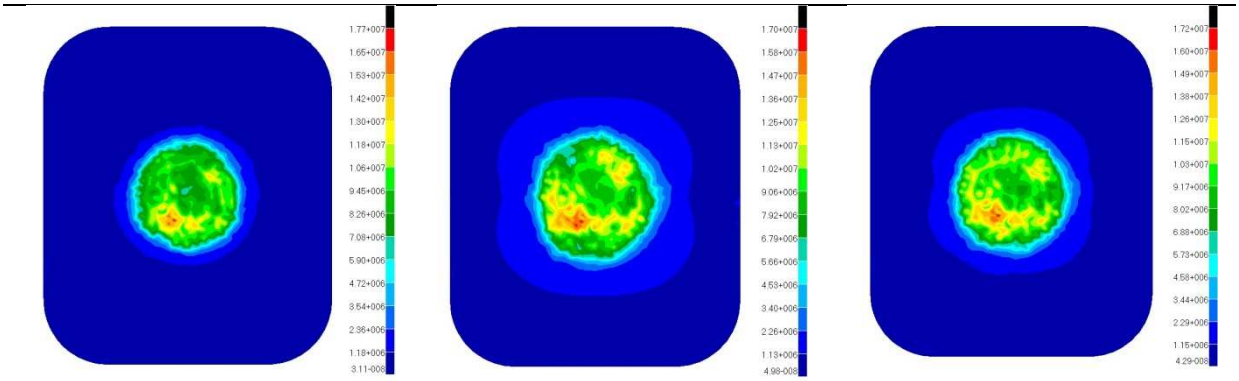

15º flat bearing | 45º flat bearing | 60º flat bearing

Mobile-bearing prosthesis Large

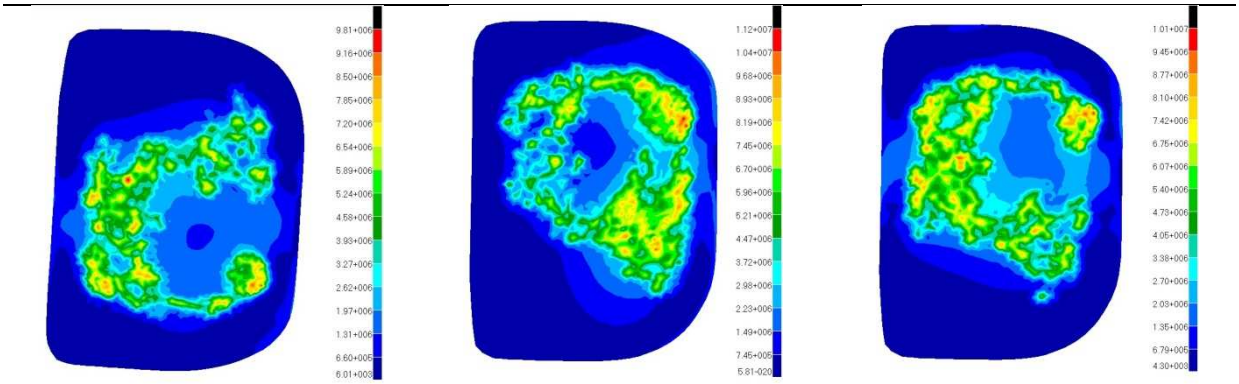

45º fully-congruent bearing | 45º fully-congruent bearing | 60º fully-congruent bearing

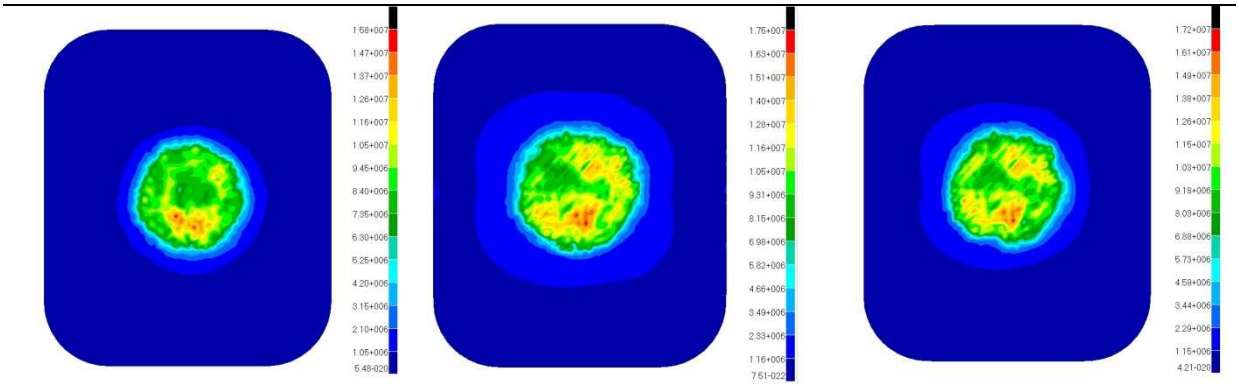

15º flat bearing | 45º flat bearing | 60º flat bearing

APPENDIX B: DETAIL DESIGN OF LOADED ANKLE APPARATUS

A knee testing rig was to be built based on the Oxford knee rig (OKR). The original Oxford knee rig design provides six -degrees -of -freedom at the knee, allows for quadriceps loading, and allows a load to be applied at the ankle joint. However, while the original OKR design provides six -degrees -of -freedom at the knee joint, it is not physiologically correct (Varadarajan et al., 2009). The hip joint constraints allow for two degrees of rotation, while the ankle joint allows for three degrees of rotation. This is different to the normal case, where the hip joint allows for all three rotational degrees of freedom and the normal ankle provides rotational freedom in flexion/extension, internal/external rotation, and a limited range of varus/valgus rotation (Varadarajan et al., 2009).

The criteria for the proposed rig were therefore to also provide quadriceps loading, ankle loading, and six -degrees -of -freedom motion at the knee joint. The constraints at the hip and ankle joints were to be simulated to be more like the normal case.

B.1. Joints

The hip joint must allow for three rotational degrees of freedom. This was accomplished by welding a stainless steel D-shackle to the end of the stainless steel intermedullary rod, which was fixed in the femoral shaft. The D-shackle was then combined with a flex ball joint to provide the three rotational degrees of freedom (Figure B-1). This assembly allows for some medial-lateral movement, which is used to simulate the typical anatomic valgus of the knee.

The ankle joint is slightly more complex in that it provides rotational freedom in flexion/extension and internal/external rotation, but a limited range in varus/valgus. In order to provide the correct constraints, it was decided to keep the ankle intact. The ankle is simply secured to the platform through numerous holes using cable-ties (Figure B-2).

Figure B-1: Hip joint

Figure B-2: Foot fixation

B.2. Loading

A cable and pulley system was used to provide the necessary tension on the quadriceps. One end of the cable was attached to the quadriceps tendon while the

other end was attached to an appropriate weight. The load at the ankle was applied by moving the platform along the vertical rails. The flanges attached to the platform housed two bushes each which slide on the rails with minimum friction. The platform thus provided the flexion/extension rotation. The platform was moved via a linear actuator with a maximum stroke of 800 mm.

B.3. Frame

The test rig is contained in an aluminium frame. The frame has a height of two metres to allow the linear actuator to operate with the maximum stroke of 800 mm. The whole frame was constructed using 40 mm aluminium strut profiles and accompanying connectors. Figure B-3 shows the assembly drawing of the knee rig.

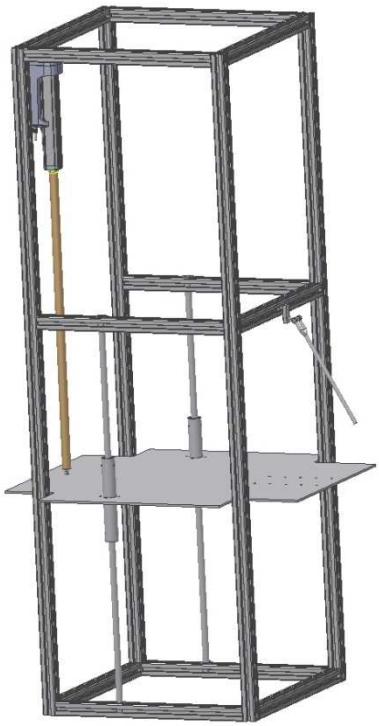

Figure B-3: Assembly of loaded ankle knee rig

REFERENCES

Agaki, M., Yamashita, E., Nakagawa, T. & Nakamura, T., 2001. Relationship between frontal knee alignment and reference axes in the distal femur. *Clinical Orthopaedics and Related Research*, 388, pp.147-56.

Ahmed, A. & Tanzer, M., 1999. in vitro measurement of the tracking pattern of the human patella. *Journal of Biomechanical Engineering*, 121, pp.222-28.

Akizuki, S. et al., 2009. in vivo determination of kinematics for subjects having a zimmer unicompartmental high flex knee system. *The Journal of Arthroplasty*, 24, pp.963-71.

American Academy of Orthopedic Surgeons, 2008. *Your orthopedic connection*. [Online] Available at: http://orthoinfo.aaos.org/topic.cfm?topic=A00221&return_link=0 [Accessed 2008].

Amis, A., Senavongse, W. & Bull, A., 2006. Patellofemoral kinematics during knee flexion-extension: an in vitro study. *Journal of Orthopaedic Research*, 24, pp.2201-11.

Ando, Y., Fukatsu, H., Aoiki, I. & T, Y., 1994. Analysis of knee movement with low-field MRI equipment: a normal volunteer study. *Diagnostic Radiology*, 12, pp.153-60.

Andriacchi, T., 1993. Functional analysis of pre and post-knee surgery: total knee arthroplasty and ACL reconstruction. *Journal of Biomechanical Engineering*, 115, pp.575-81.

Arora, J., Sharma, S. & Blyth, M., 2005. The role of pre-operative templating in primary total knee replacement. *Knee Surgery, Sprots Traumatology, Arthroscopy*, 13, pp.187-89.

Asala, S., Bidmos, M. & Dayal, M., 2004. Discriminant function sexing of fragmentary femur of South African blacks. *Forensic Scientific International*, 145, pp.25-29.

Asano, T., Akagi, M., Tanaka, K. & Nakamura, T., 2001. In vivo three-dimensional knee kinematics using a bi-planar image-matching technique. *Clinical orthopaedics and Related Research*, 388, pp.157-66.

Ashraf, T., Newman, J. & Evans, R., 2002. Lateral unicompartmental knee replacement: Survivorship and clinical experience over 21 years. *Journal of Bone and Joint Surgery*, 84B, pp.1126-30.

Ateshian, G., 1993. A B-spline least-squares surface-fitting method for articular surfaces of diarthtodial joints. *Journal of Biomechanical Engineering*, 115, pp.366-73.

Bae, D., Guhl, J. & Keane, S., 1983. Unicompartmental knee arthroplasty for single compartment disease. Clinical experience with an average four-year follow-up study. *Clinical Orthopaedics and Related Research*, 176, pp.233-38.

Barbujani, G., Magagni, A., Minch, E. & Cavalli-Sforza, L., 1997. An apportionment of human DNA diversity. *The Proceedings of the National Academy of Sciences USA*, 94, pp.4516-19.

Barnes, C. & Scott, R., 1995. Popliteus tendon dysfunction following total knee arthroplasty. *Journal of Arthroplasty*, 10, pp.543-45.

Bartel, D., Bicknell, V. & Wright, T., 1986. The effect of conformity, thickness, and material on stresses in ultra-high molecular weight components for total joint replacement. *Journal of Bone and Joint Surgery*, 68A, p.1041.

Bartel, D., Burstein, A., Sanatavicca, E. & Insall, J., 1982. Performance of tibial component in total knee replacement. *Journal of Bone and Joint Surgery*, 64, pp.1026-33.

Barton, G., Lisboa, P., Lees, A. & Attfield, S., 2007. Gait quality assessment using self-organising artificial neural networks. *Gait & posture*, 25:3, pp.374-79.

Bauer, T. et al., 2010. Influence of posterior condylar offset on knee flexion after cruciate-sacrificing mobile-bearing total knee replacement: A prospective analysis of 410 consecutive cases. *The Knee*, 17(6), pp.375-80.

Bei, Y. et al., 2004. The relationship between contact pressure, insert thickness, and mild wear in total knee replacements. *Computer Modeling in Engineering and Sciences*, 6, pp.145-52.

Bert, J., 1991. Universal intramedullary instrumentation for unicompartmental knee arthroplasty. *Clinical Orthopaedics*, 271, pp.79-87.

Bert, J., 2005. Unicompartmental knee replacement. *Orthopedic Clinics of North America*, 36, pp.512-22.

BioMet, 2011. *Oxford partial knee: Manual of the surgical technique*. [Online] Available at: www.biomet.co.uk [Accessed 2011].

Biščević, M., Hebibović, M. & Smrke, D., 2005. Variations of femoral condyle shape. *Collegium Antropologicum*, 2, pp.409-14.

Blacharski, P., Somerset, J. & Murray, D., 1975. A three-dimensional study of the kinematics of the human knee. *Journal of Biomechanics*, 8, pp.375-84.

Bloebaum, R. et al., 1994. Analysis of the bone surface area in resected tibia. *Clinical Orthopaedics*, 309, pp.2-10.

Bowcock, A. et al., 1994. High resolution of human evolutionary trees with polymorphic microsatellites. *Nature*, 368, pp.455-57.

Boyd, S. et al., 1999. Joint surface modeling with thin-plate splines. *Journal of Biomechanical Engineering*, 121, pp.525-32.

Brage, M., Draganich, L., Pottenger, L. & Curran, J., 1994. Knee laxity in symptomatic osteoarthritis. *Clinical Orthopaedic and Related Research*, 304, pp.184-89.

Brooks, P., 2008. Seven cuts to a perfect knee. *Current Concepts in Joint Replacement Winter Meeting*.

Buechel, F. & Pappas, M., 1989. New Jersey low contact stress knee replacement system. Ten-year ecaluation of meniscal bearings. *Orthopedic clinics of North America*, 20, pp.147-77.

Buechel, F. & Pappas, M., 1990. Long-term survivorship analysis of cruciate-sparing versus cruciate-sacrificing knee prostheses using meniscal bearings. *Clinical Orthopaedics and Related Research*, 260, pp.162-69.

Bull, A., Kessler, O., Alam, M. & Amis, A., 2008. Changes in knee kinematics reflect the articular geometry after arthroplasty. *Clinical Orthopaedics and Related Research*, 466, pp.2491-99.

Busch, A., Scheffer, C. & Basson, A., 2009. Development and testing of a prototype reflex measurement system emplying artificial neural networks. *Computer Methods and Programs in Biomedicine*, 94, pp.15-25.

Callaghan, J., O'Rourke, M. & Saleh, K., 2004. Why knees fail: Lessons learned. *The Journal of Arthroplasty*, 19, pp.31-34.

Cameron, H., Hunter, G., Welsh, R. & Bailey, W., 1981. Unicompartmental knee replacement. *Clinical Orthopaedics and Related Research*, 160, pp.109-13.

Carr, A. et al., 1993. Medial unicompartmental replacement with the Oxford Meniscal Knee. *Clinical Orthopaedics*, 295, p.205.

Cartier, P., Sanouiller, J. & Grelsamer, R., 1996. Unicompartmental knee arthroplasty surgery: 10-year minimum follow-up period. *The Journal of Arthroplasty*, 11(7), pp.782-88.

Chaichankul, C., Tanavalee, A. & Itiravivong, P., 2009. Anthropometric measurments of knee joints in Thai population: Correlation to the sizing of current knee prostheses. *The Knee*, p.Article in Press.

Chang, R., Chu, C., Wu, Y. & Chen, Y., 2010. Gene clustering by using query-based self-organising maps. *Expert Systems with Applications*, 37:9, pp.6689-94.

Cheng, C., Huang, C., Liau, J. & Huang, C., 2003. The influence of surgical malalignment on the contact pressures of fixed and mobile bearing knee prostheses: a biomechanical study. *Clinical Biomechanics*, 18, pp.231-36.

Cheng, F. et al., 2009. Three dimensional morphometry of the knee to design the total knee arthroplasty for Chinese population. *The Knee*, 16, pp.341-47.

Chew, J. et al., 1997. Differences in patellar tracking and knee kinematics among three different total knee designs. *Clinical Orthopaedics and Related Research*, 345, pp.87-98.

Chin, K., Zurakowski, D. & Scott, R., 2002. Intraoperative measurements of male and femal distal femurs during primary total knee arthroplasty. *Journal of Knee Surgery*, 15, pp.213-17.

Chockalingam, S. & Scott, G., 2000. The outcome of cemented vs cementless fixation of a femoral component in total knee replacement (TKR) with the identification of radiological signs for the prediction of failure. *The Knee*, 7, pp.233-38.

Churchill, D., Incavo, S., Johnson, C. & Beynnon, B., 1998. The Transepicondylar axis approximates the optimal flexion axis of the knee. *Clinical Orthopaedics and Related Research*, 356, pp.111-18.

Cloke, D. et al., 2008. 284 press-fit Kinemax total knee arthroplasties followed for 10 years. Poor survival of uncemented prostheses. *Acta Orthopaedica*, 79, pp.28-33.

Coetzer, W., 2004. *Engineering entrepreneurship: steering start-ups to steady-state*. 1st ed. Stellenbosch: W Coetzer.

Completo, A., Simões, J., Fonseca, F. & Oliveira, M., 2008. The influence of different stem designs in load sharing and stability at the cement-bone interface in revision TKA. *The Knee*, 15, pp.227-32.

Conditt, M. et al., 2004. The PCL significantly affects the functional outcome of total knee arthroplasty. *The Journal of Arthroplasty*, 19(7), pp.107-12.

Confalonierir, N., Manzotti, A. & Pullen, C., 2004. Comparison of a mobile with a fixed tibial bearing unicompartmental knee prosthesis: a prospective randomized trial using a dedicated outcome score. *The Knee*, 11, pp.357-62.

Conley, S., Rosenberg, A. & Crowninshield, R., 2007. The female knee: Anatomic variations. *Journal of the American Academy of Orthopaedic Surgeons*, 15, pp.31-36.

Coughlin, K., SJ, I., Churchill, D. & Beynnon, B., 2003. Tibial axis and patellar position relative to the femoral epicondylar axis during squatting. *The Journal of Arthroplasty*, 18, pp.1048-55.

Daněk, J. et al., 2007. Numerical modelling of the weight-bearing total knee joint replacement and usage in practice. *Mathematics and Computers in Simulation*, 76, pp.49-56.

Daniel, D. et al., 1994. Fate of the ACL-injured patient. A prospective outcome study. *American Journal of Sports Medicine*, 22, pp.632-44.

Dargel, J. et al., 2010. Human knee joint anatomy revisited: Morphometry in the light of sex-specific total knee arthroplasty. *The Journal of Arthroplasty*, p.Article in Press.

D'Lima, D. et al., 2001. Quadriceps moment arm and qaudriceps forces after total knee arthroplasty. *Clinical Orthopaedics and Related Research*, 392, pp.213-20.

D'Lima, D., Trice, M., Urquhart, A. & Colwell Jr, C., 2000. Comparison between the kinematics of fixed and rotating bearing knee prostheses. *Clinical Orthopaedics and Related Research*, 380, pp.151-57.

Dow, L., Kalelkar, S. & Dow, E., 2004. Self-organising maps for the analysis of NMR spectra. *Drug Discovery Today*, 2:4, pp.157-63.

Duffy, G., Berry, D. & Rand, J., 1998. Cemented versus cementless fixation in total knee arthroplasty. *Clinical Orthopaedics and related Research*, 356, pp.66-72.

Eisenhuth, S. et al., 2006. Patellofemoral instability after total knee replacement. *Clinical orthopaedics and related research*, 446, pp.149-60.

Elias, S., Freeman, M. & Gokcay, E., 1990. A correlative study of the geometry and anatomy of the distal femur. *Clinical Orthopaedics and Related Research*, 260, pp.98-103.

Emerson, R. et al., 2002. Comparison of a mobile with a fixed bearing unicompartmental knee implant. *Clinical Orthopaedics*, 404, pp.62-70.

Emerton, M. & Burton, D., 2001. The role of unicompartmental knee replacement. *Current Orthopaedics*, 15, pp.406-12.

Emodi, G., Callaghan, J., Pedersen, D. & Brown, T., 1999. Posterior cruciate ligament function following total knee arthroplasty: the effect of joint line elevation. *The Iowa Orthopaedic Journal*, 19, pp.82-92.

Erasmus, P. & Dillon, E., 2008. Interview. Stellenbosch, 2008.

Ewald, F. et al., 1984. Kinematic total knee replacement. *Journal of Bone and Joint Surgery*, 66, pp.1032-40.

Exactech Inc., 2009. [Online] Available at: http://www.exac.com/products/knee/pre-total-joint [Accessed 2009].

Fawzy, E. et al., 2008. Determination of femoral component size in unicompartmental knee replacement. *The Knee*, 15, pp.403-06.

Fehring, T. et al., 2009. Differences between the sexes in the anatomy of the anterior condyle of the knee. *Journal of Bone and Joint Surgery*, 91, pp.2335-41.

Fisher, J. et al., 2010. Polyethylene wear in total knees. *Clinical Orthopaedics and Related Research*, 468, pp.12-18.

Fishkin, Z., Miller, D., Ritter, C. & Ziv, I., 2002. Changes in human knee ligament stiffness secondary to osteoarthritis. *Journal of Orthopaedic Research*, 20, pp.204-07.

Fitzpatrick, C., Fitzpatrick, D., Lee, J. & Auger, D., 2007. Statistical design of unicompartmental tibial implants and comparison with current devices. *The Knee*, 14, pp.138-44.

Flexer, A., 2001. On the use of self-organising maps for clustering and visualization. *Intelligent Data Analysis*, 5(5), pp.373-84.

Font-Rodriguez, D., Scuderi, G. & Insall, J., 1997. Survivorship of cemented total knee arthroplasty. *Clinical Orthopaedics and Related Research*, 345, pp.79-86.

Frankel, V., Burstein, A. & Brooks, D., 1972. Biomechanics of Internal Derangement of the knee: Pathomechanics as determined by analysis of the instant centers of motion. *Journal of Bone and Joint Surgery*, pp.945-77.

Freeman, M., 2001. How the knee moves. *Current Orthopaedics*, 15, pp.444-50.

Freeman, M. & Pinskernova, V., 2005. The movement of the normal tibio-femoral joint. *Journal of Biomechanics*, 38, pp.197-208.

Fregely, B., Bei, Y. & Sylvester, M., 2003. Experimental evaluation of an elastic foundation model to predict contact pressures in knee replacements. *Journal of Biomechanics*, 36, pp.1659-68.

Friedman, R. et al., 1993. Current concepts in orthopaedic biomaterials and implant fixation. *Journal of Bone and Joint Surgery*, 75, pp.1086-109.

Fyhrie, D. & Vashishth, D., 2000. Bone stiffness predicts strength similarly for human vertebral cancellous bone in compression and for cortical bone in tension. *Bone*, 26, pp.169-73.

Galvin, A. et al., 2009. Effect of conformity and contact stress on wear in fixed-bearing total knee prostheses. *Journal of Biomechanics*, 2009, pp.1898-902.

Gao, F., Henricson, A. & Nilsson, K., 2009. Cemented versus uncemented fixation of the femoral component of the NexGen CR total knee replacement in patients younger than 60 years: A prospective randomised controlled RSA study. *The Knee*, 16(3), pp.200-06.

Gioe, T. et al., 2003. Analysis of unicompartmental knee arthroplasty in a community-based implant registry. *Clinical Orthopaedics and Related Research*, 416, pp.111-19.

Gioe, T. et al., 2007. Excellent survival of all-polyethylene tibial components in a community joint registry. *Clinical Orthopaedics and Related Research*, 464, pp.88-92.

Gleeson, R. et al., 2004. Fixed or mobile bearing unicompartmental knee replacement? A comparative study. *The Knee*, 11, pp.379-84.

Godest, A. et al., 2002. Simulation of a knee joint replacement during a gait cycle using explicit finite element analysis. *Journal of Biomechanics*, 35, pp.267-75.

Goodfellow, J. & O'Connor, J., 1978. The mechanics of the knee and prosthesis design. *The journal of bone and joint surgery*, 60, pp.358-69.

Goodfellow, J. & O'Connor, J., 1986. Clinical results of the Oxford knee. Surface arthroplasty of the tibiofemoral joint with a meniscal bearing prosthesis. *Clinical Orthopaedics and Related Research*, 205, pp.21-42.

Greene, K., 2007. Gender-specific design in total knee arthroplasty. *The Journal of Arthroplasty*, 22:7, pp.27-31.

Grelsamer, R., 1995. Unicompartmental osteoarthrosis of the knee. *The Journal of Bone and Joint Surgery*, 77, pp.278-92.

Grood, E. & Suntay, W., 1983. A Joint Coordinate System for the Clinical Description of Three-Dimensional Motions: Application to the knee. *Journal of Biomechanical Engineering*, 105, pp.136-44.

Gunston, F., 1971. Polycentric knee arthroplasty. Prosthetic simulation of normal knee movement. *The Journal of Bone and Joint Surgery*, 53B(2), pp.272-77.

Gunther, T. et al., 1996. Lateral unicompartmental arthroplasty with the Oxford meniscal knee. *The Knee*, 3, pp.33-39.

Guy, S. et al., 2011. Gender differences in distal femoral morphology and the role of gender specific implants in total knee replacement: A prospective clinical study. *The Knee*, p.Article in Press.

Hallen, L. & Lindahl, O., 1966. The "screw-home" movement in the knee joint. *Acta Orthopaedica Scandinavica*, 37, pp.97-106.

Halloran, J., Petrella, A. & Rullkoetter, P., 2005. Explicit finite element modeling of total knee replacement mechanics. *Journal of Biomechanics*, 38, pp.323-31.

Han, H., Seong, S., Lee, S. & Lee, M., 2006. Rotational alignment of femoral components in total knee arthroplasty: nonimage-based navigation system versus conventional technique. *Orthopaedics*, 29, pp.S148-151.

Harrysson, O., Hosni, A. & Nayfeh, J., 2007. Custom-designed orthopedic implants evaluated using finite element analysis of patient-specific computed tomography data: femoral-component case study. *BioMed Central Musculoskeletal Disorders*, 8, p.91.

Hatze, H., 1974. The meaning of the term 'Biomechanics'. *Journal of Biomechanics*, 7, pp.189-90.

Hazelwood, S., Martin, R., Rashid, M. & Rodrigo, J., 2001. A mechanistic model for internal bone remodeling exhibits different dynamic responses in disuse and overload. *Journal of Biomechanics*, 34, pp.299-308.

Heal, J. & Blewitt, N., 2002. Kinemax Total Knee Arthroplasty: Trial by template. *Journal of Arthroplasty*, 17, pp.90-94.

Heegaard, J. et al., 1994. Influence of soft structures on patellar three-dimensional tracking. *Clinical Orthopaedics and Related Research*, 299, pp.235-43.

He, J. et al., 2006. Custom fabrication of a composite hemi-knee joint based on rapid prototypin. *Rapid prototyping journal*, 12, pp.198-205.

Henricson, A., 2008. Total knee arthroplasty: Aspects on improved fixation in the younger patient. *Doctor of Philosophy thesis, Umea University, Sweden*.

Hernigou, P. et al., 2004. Alternative femoral bearing surface options for knee replacement in younger patients. *The Knee*, 11, pp.169-72.

Herzog, W. & Read, L., 1993. Lines of action and moment arms of the major force-carrying structures crossing the human knee joint. *Journal of Anatomy*, 182, pp.213-30.

Hill, P. et al., 2000. Tibiofemoral movement 2: the loaded and unloaded living knee studied by MRI. *The Journal of Bone and Joint Surgery (Br)*, 82B, pp.1196-98.

Hirokawa, S., Ueki, T. & Ohtsuki, A., 2004. A new approach for surface fitting method of articular joint surface. *Journal of Biomechanics*, 37, pp.1551-59.

Hitt, K. et al., 2003. Antropomorpic measurements of the human knee: correlation to the sizing of current knee arthroplasty system. *Journal of Bone and Joint Surgery, American Volume*, 85, pp.115-22.

Ho, W., Cheng, C. & Liau, J., 2006. Morphometrical measurements of resected surface of femurs in Chinese knees: Correlation to the sizing of current femoral implants. *The Knee*, 13, pp.12-14.

Hodge, W. & Chandler, H., 1992. Unicompartmental knee replacement: a comparison of constrained and unconstrained designs. *The Journal of Bone and Joint Surgery American Edition*, 74, pp.877-83.

Hofmann, A., Bachus, K. & Wyatt, R., 1991. Effect of the tibial cut on subsidence following total knee arthroplasty. *Clinical Orthopaedics*, 269, pp.63-69.

Hollister, A. et al., 1993. The axes of rotation of the knee. *Clinical Orthopaedics*, 290, pp.259-68.

Hopkins, A., New, A., Rodriguez-y-Baena, F. & Taylor, M., 2010. Finite element analysis of unicompartmental knee arthroplasty. *Medical Engineering & Physics*, 32, pp.14-21.

Howcroft, D. et al., 2006. The role of preoperative templating in total knee arthroplasty: comparison of three prostheses. *The Knee*, 13, pp.427-29.

Hsieh, Y., Draganich, L., Ho, S. & Reider, B., 1998. The effects of removal and reconstruction of the anterior cruciate ligament on patellofemoral kinematics. *The American Journal of Sports Medicine*, 26(2), pp.201-09.

Huang, C. et al., 2002. The incidence of revision of the metal component of total knee arthroplasties in different tibial-insert designs. *The Knee*, 9, pp.331-34.

Huberti, H. & Hayes, W., 1984. Force ratios in the quadriceps tendon and ligamentum patellae. *Journal of Orthopaedic Research*, 2, pp.49-54.

Hungerford, D. & Barry, M., 1979. Biomechanics of the patellofemoral joint. *Clinical Orthopaedics and Related Research*, 144, pp.9-15.

Illgen, R. et al., 2004. Hybrid total knee arthroplasty: A retrospective analysis of clinical and radiographic outcomes at average 10 years follow-up. *The Journal of Arthroplasty*, 19(7), pp.95-100.

Incavo, J., Coughlin, K. & Beynnon, B., 2004. Femoral component sizing in total knee arthroplasty: Size matched resection versus flexion space balancing. *Journal of Arthroplasty*, 19, pp.493-97.

Insall, J. & Aglietti, P., 1980. A five to seven-year follow-up of unicondylar arthroplasty. *The Journal of Bone and Joint Surgery*, 62(8), pp.1329-37.

Iorio, R. et al., 2007. Primary posterior cruciate-retaining total knee arthroplasty: a comparison of American and Japanese cohorts. *Journal of Surgical Orthopaedic Advances*, 16(4), pp.164-70.

İşcan, M. & Shihai, D., 1995. Sexual dimorphism in the Chinese femur. *Forensic Scientific International*, 74, pp.79-87.

Ishii, Y., Terajima, K., Terashima, S. & Koga, Y., 1997. Three-dimensional kinematics of the human knee with intracortical pin fixation. *Clinical Orthopaedics and Related Research*, 343, pp.144-50.

ISO 14155-1, 2003. *Clinical investigation of medical devices for human subjects – Part 1: General requirements*. First edition ed. Reference number: ISO14155-1:2003(E).

ISO 14243-1, 2002. *Implants for surgery – Wear of total knee-joint prostheses – Part 1: Loading and displacement parameters for wear-testing machines with load control and corresponding environmental conditions for test*. 1st ed. Reference number: 14243-1:2002(E).

ISO 14243-2, 2000. *Implants for surgery – Wear of total knee-joint prostheses – Part 2: Methods of measurement*. First edition ed. Reference number: ISO14243-2:2000(E).

ISO 14243-3, 2004. *Implants for surgery – Wear of total knee-joint prostheses – Part 3: Loading and displacement parameters for wear-testing machines with displacement control and corresponding environmental conditions for test*. First edition ed. Reference number: ISO14243-3:200.

ISO 14630, 2008. *Non-active surgical implants – General requirements*. Third edition ed. Reference number: ISO14630:2008(E).

ISO 14879-1, 2000. *Implants for surgery – Total knee-joint prostheses – Part 1: Determination of endurance properties of knee tibial trays*. First edition ed. Reference number: ISO14879-1:2000(E).

ISO 21534, 2007. *Non-active surgical implants – Joint replacement implants – Particular requirements*. Second edition ed. Reference number: ISO 21534:2007(E).

ISO 21536, 2007. *Non-active surgical implants – Joint replacement implants – Specific requirements for knee-joint replacement implants*. Second edition ed. Reference number: ISO21536:2007(E).

ISO 4287, 1997. *Geometrical Product Specifications (GPS) – Surface texture: Profile method – Terms, definitions and surface texture parameters*. First edition ed. Reference number: ISO4287:1997(E/F).

ISO 7207-1, 2007. *Implants for surgery – Components for partial and total knee joint prostheses – Part 1: Classification, definitions and designation of dimensions*. Third edition ed. Reference number: ISO 7207-1:2007(E).

Iwaki, H., Pinskernova, V. & Freeman, M., 2000. Tibiofemoral movement 1: the shape and relative movements of the femur and tibia in the unloaded cadaver knee. *The Journal of Bone and Joint Surgery (Br)*, 82B, pp.1189-95.

Jazrawi, L., Bai, B. & Kummer, F., 2001. The effect of stem modularity and mode of fixation on tibial component stability in revision total knee arthroplasty. *The Journal of Arthroplasty*, 16, pp.759-67.

Johal, P. et al., 2005. Tibio-femoral movement in the living knee. A study of weight bearing and non-bearing knee kinematics using 'interventional' MRI. *Journal of Biomechanics*, 38, pp.269-76.

Jomha, N., Borton, D., Clingeleffer, A. & Pinczewski, L., 1999. Long-term osteoarthritic changes in anterior cruciate ligament reconstructed knees. *Clinical Orthopaedic*, 358, pp.188-93.

Jorde, L. et al., 2000. The distribution of human genetic diversity: a comparison of mitochondrial, autosomal, and Y-chromosome data. *The American Journal of Human Genetics*, 66, pp.979-88.

Josephine, 2010. *Bone Smart*. [Online] Available at: http://bonesmart.org/public_forum/knee-replacement-surgery-types-and-suggested-videos-t4850.html [Accessed 2011].

Kanisawa, I., Banks, A., Moriya, H. & Tsuchiya, A., 2003. Weight bearing knee kinematics in subjects with two types of anterior cruciate ligament reconstructions. *Knee Surgery Sports Traumatology Arthroscopy*, 11, pp.16-22.

Kärrholm, J., Brandsson, S. & Freeman, M., 2000. Tibiofemoral movement 4: changes of axial rotation caused by forced rotation at the weight-bearing knee studied by RSA. *The Journal of Bone and Joint Surgery (Br)*, 82, pp.1201-03.

Katchburian, M. et al., 2003. Measurement of patellar tracking: assessment and analysis of the literature. *Clinical Orthopaedics and Related Research*, 412, pp.241-59.

Keene, G. & Forster, M., 2005. Modern unicompartmental knee replacement. *Current Orthopaedics*, 19, pp.428-45.

Kiang, M. & Kumar, A., 2001. An evaluation of self-organizing map networks as a robust alternative to factor analysis in data mining applications. *Information Systems Research*, 12(2), pp.177-94.

Kim, Y., Kim, D. & Kim, J., 2007. Simultaneous mobile-and fixed-bearing total knee replacement in the same patients: a prospective comparison of mid-term outcomes using a similar design prosthesis. *Journal of bone and joint surgery*, 89, pp.904-10.

Kim, Y., Kook, H. & Kim, J., 2001. Comparison of fixed-bearing and mobile-bearing total knee arthroplasties. *Clinical Orthopaedics and Related Research*, 392, pp.101-15.

Kitagawa, A. et al., 2009. In vivo comparison of knee kinematics before and after high-flexion posterior cruciate-retaining total knee arthroplasty. *Journal of Arthroplasty*, p.Article in Press.

Knee Joint, 2008. *Knee Joint Anatomy*. [Online] Available at: http://www.arthroscopy.com/sp05001.htm [Accessed 2008].

Kohonen, T., 1998. The self-organizing map. *Neurocomputing*, 21, pp.1-6.

Kohonen, T., 2005. *SOM Toolbox*. [Online] Available at: http://www.cis.hut.fi/somtoolbox/ [Accessed 2008].

Komistek, R., Dennis, D. & Mahfouz, M., 2003. In vivo fluoroscopic analysis of the normal human knee. *Clinical Orthopaedics and Related Research*, 410, pp.69-81.

Komistek, R. et al., 2008. In vivo determination of total knee arthroplasty kinematics. *Journal of Arthroplasty*, 23, pp.41-50.

Kopperdahl, D.L. & Keaventy, T.M., 1998. Yield strain behavior of trabecular bone. *Journal of Biomechanics*, 31, pp.601-08.

Kosel, J. et al., 2010. Anatomical study of the radius and center of curvature of the distal femoral condyle. *Journal of Biomechanical Engineering*, p.91002.

Koszyca, B., Fazzalari, N. & Vernon-Roberts, B., 1996. Quantitative analysis of the bone-cartilage interface within the knee. *The Knee*, pp.23-31.

Krevolin, J., 2003. Specimen-specific, three dimensional knee joint mechanics: Normal and reconstructe. *Doctor of Philosophy Thesis, University of Texas*.

Kulkarni, M. & Sathe, S., 2008. Experimental determination of material properties of cortical cadaveric femur bone. *Trends in Biomaterials and Artificial Organs*, 22, pp.9-15.

Kurosawa, H. et al., 1985. Geometry and motion of the knee for implant and orthotic design. *Journal of Biomechanics*, 18, pp.487-99.

Kwak, D. et al., 2007. Morphometry of the proximal tibia to design the tibial component of total knee replacement for the Korean population. *The Knee*, 14, pp.295-300.

Lachiewics, P., 2001. Cemented versus cementless total knee replacement: is there a place for cementless fixation in 2001? *Current Opinion in Orthopaedics*, 12, pp.33-36.

Lädermann, A. et al., 2008. Fixed-bearing versus mobile-bearing total knee replacement: A prospective randomized, clinical radiological study with mid-term results at 7 years. *The Knee*, 15, pp.206-10.

Laskin, R., 1978. Unicompartmental tibiofemoral resurfacing arthroplasty. *Journal of Bone and Joint Surgery American Edition*, 60, pp.182-85.

Laskin, R., 2002. Session III: Total knee replacement in young patients. *Clinical Orthopaedics and Related Research*, 404, pp.100-01.

Laurencin, C., Zelicof, S., Scott, R. & Ewald, F., 1991. Unicompartmental versus total knee replacement in the same patient. A comparative study. *Clinical Orthopaedics*, 273, pp.151-56.

Lavine, B., Davidson, C. & Westover, D., 2004. Spectral pattern recognition using self-organising maps. *Journal of Chemical Information and Modeling*, 44(3), pp.1056-64.

Lee, K., Booth, D. & Alam, P., 2005. A comparison of supervised and unsupervised neural networks in predicting bankruptcy of Korean firms. *Expert Systems with Applications*, 29(1), pp.1-16.

Levitz, C., Lotke, P. & Karp, J., 1995. Long-term changes in bone mineral density following total knee replacement. *Clinical Orthopaedics*, 321, pp.68-72.

Lewis, J., Askew, M. & Jaycox, D., 1982. A comparative evaluation of tibial component designs of total knee prostheses. *Journal of Bone and Joint Surgery*, 64A, p.129.

Lewold, L., 1998. Revision of unicompartmental knee arthroplasty. *Acta Orthopaedica Scandinavica*, 69, pp.469-74.

Lewontin, R., 1972. The apportionment of human diversity. *Evolutionary Biology*, 6, pp.391-98.

Linde, F., Hvid, I. & Madsen, F., 1992. The effect of specimen geometry on the mechanical behavior of trabecular bone specimens. *Journal of biomechanics*, 25, pp.359-68.

Li, M. & Nilsson, K., 2001. No relationship between postoperative changes in bone density at the proximal tibia and the migration of the tibial component 2 years after total knee arthroplasty. *Journal of Arthroplasty*, 16, pp.893-900.

Lin, Y., Wang, C. & Dai, K., 2005. Reverse engineering in CAD model reconstruction of customized artificial joint. *Medical Engineering and Physics*, 27, pp.189-93.

Li, G. et al., 1999. The importance of quadriceps and hamstring muscle loading on knee kinematics and in-situ forces in the ACL. *Journal of Biomechanics*, 32, pp.395-400.

Liska, W. et al., 2007. Custom total knee replacement in a dog with femoral condylar bone loss. *Veterinary Surgery*, 36, pp.293-301.

Li, M. et al., 2006. Mobile vs. fixed unicondylar knee replacement: A randomized study on short term clinical outcomes and knee kinematics. *The Knee*, 13, pp.365-70.

Li, G. et al., 2004. kinematics of the knee at high flexion angles: an in vitro investigation. *Journal of Orthopaedic Research*, 22, pp.90-95.

Lo, J. et al., 2008. Forces in anterior cruciate ligament during simulated weight-bearing flexion with anterior and internal rotational tibial load. *Journal of Biomechanics*, 41, pp.1855-61.

Lu, T. et al., 2008. In vivo three-dimensional kinematics of the normal knee during active extension under unloaded and loaded conditions using single-plane fluoroscopy. *Medical Engineering & Physics*, 30, pp.1004-12.

Maestro, A. et al., 2000. Preoperative calculation of the femoral transepicondylar axis. *The American Journal of Knee Surgery*, 13, pp.181-87.

Ma, H., Lu, Y., Ho, F. & Huang, C., 2005. Long-term results of total condylar knee arthroplasty. *Journal of Arthroplasty*, 20, pp.580-84.

Mangiameli, P., Chen, S. & West, D., 1996. A comparison of SOM neural networks and hierarchical clustering methods. *European Journal of Operational Research*, 93, pp.402-17.

Marmor, L., 1977. Results of single compartment arthroplasty with acrylic cement fixation. A minimum follow-up of two years. *Clinical Orthopaedics and Related Research*, 122, pp.181-88.

Martelli, S. & Pinskernova, V., 2002. The shapes of the tibial femoral articular surfaces in relation to tibiofemoral movement. *Journal of Bone and Joint Surgery*, 84B, pp.607-13.

Matsuda, M. et al., 2003. Design of the femoral condylar geometry of the artificial knee joint. In *Summer Bioengineering Conference*. Florida, 2003.

Matsuda, S. et al., 2004. Anatomical analysis of the femoral condyle in normal and osteoarthritic knees. *Journal of Orthopaedic Research*, 22, pp.104-09.

Matsuda, S. et al., 1999. Knee stability in posterior cruciate ligament retaining total knee arthroplasty. *Clinical Orthopaedics and Related Research*, 366, pp.169-73.

Matsuda, S. et al., 1998. Contact stress analysis in meniscal bearing total knee arthroplasty. *Journal of Arthroplasty*, 13(6), pp.699-706.

Matthews, J., 2004. *Self-Organising Nets*. [Online] Available at: http://www.generation5.org/content/1999/selforganize.asp [Accessed 2011].

McEwen, H. et al., 2005. The influence of design, materials and kinematics on the in vitro wear of total knee replacements. *Journal of Biomechanics*, 38, pp.357-65.

McPherson, A. et al., 2005. Imaging knee position using MRI, RSA/CT and 3D digitization. *Journal of Biomechanics*, 38, pp.263-68.

Medline Plus, 2008. *Knee replacement*. [Online] Available at: http://www.nlm.nih.gov/medlineplus/kneereplacement.html [Accessed 2008].

Meek, R., Masri, B. & Duncan, C., 2004. Minimally invasive unicompartmental knee replacement: rationale and correct indications. *Orthopedic Clinics of North America*, 35, pp.191-200.

Mensch, J. & Amstutz, H., 1975. Knee morphology as a guide to knee replacement. *Clinical Orthopaedics and Related Research*, 112, pp.231-41.

Merchant, A. et al., 2008. The female knee: Anatomic variations and the female-specific total knee design. *Clinical Orthopaedics and Related Research*, 466, pp.3059-65.

Merican, A. & Amis, A., 2009. Iliotibial band tension affects patellofemoral and tibiofemoral kinematics. *Journal of Biomechanics*, 42, pp.1539-46.

Morgan, M., Brooks, S. & Nelson, R., 2006. Total knee arthroplasty in young active patients using a highly congruent fully mobile prosthesis. *The Journal of Arthroplasty*, 22, pp.525-30.

Morgan, E. & Keaveny, T., 2001. Dependence of yield strain of human trabecular bone on anatomic site. *Journal of Biomechanics*, 34, pp.569-77.

Morra, E. & Greenwald, A., 2003. Effects of walking gait on ultra-high molecular weight polyethylene damage in unicompartmental knee systems. A finite element study. *Journal of Bone and Joint Surgery*, 85, pp.111-14.

Morrison, J., 1970. The mechanics of muscle function in locomotion. *Journal of Biomechanics*, 3, pp.431-51.

Most, E., Axe, J., Rubash, H. & Li, G., 2004. Sensitivity of the knee joint kinematics calculation to selection of flexion axes. *Journal of Biomechanics*, 37, pp.1743-48.

Most, E. et al., 2003. The kinematics of fixed- and mobile-bearing total knee arthroplasty. *Clinical Orthopaedics and Related Research*, 416, pp.197-207.

Murphy, T. et al., 2007. Review of Unicompartmental Knee Arthroplasty in younger patients. *Seminars in Arthroplasty*, 18, pp.162-67.

Näger, H. et al., 2008. A novel total knee replacement by rolling articulating surfaces. In vivo functional measurements and tests. *Acta of Bioengineering and Biomechanics*, 10, pp.55-60.

Nakagaw, S. et al., 2000. Tibiofemoral movement 3: full flexion in the living knee studied by MRI. *The Journal of Bone and Joint Surgery*, 82B, pp.1199-200.

Newman, J., Ackroyd, C. & Shah, N., 1998. Unicompartmental or total knee replacement? Five year results of a prospective, randomized trial of 102 osteoarthritic knees with unicompartmental arthritis. *Journal of Bone and Joint Surgery*, 80B, pp.862-65.

Newman, J. & Weale, A., 1994. Unicompartmental replacement and high tibial osteotomy for osteoarthrosis of the knee. A comparative study with 12 to 17 year follow up period. *Clinical Orthopaedics*, 302, pp.134-37.

Niitsu, M., Akisada, M., Anno, I. & Miyakawa, S., 1990. Moving knee joint: technique for kinematic MR imaging. *Radiology*, 174, pp.569-70.

Nissel, R. & Ericson, M., 1992. Patellar forces during isokinetic knee extension. *Clinical Biomechanics*, 7, pp.104-08.

Nuño, N. & Ahmed, A., 2001. Sagittal profile of the femoral condyles and its application to femorotibial contact analysis. *Journal of Biomechanical Engineering*, 123, pp.18-26.

Nuño, N. & Ahmed, A., 2003. Three-dimensional morphometry of the femoral condyles. *Clinical Biomechanics*, 18, pp.924-32.

Nyman, J. et al., 2004. Long stemmed total knee arthroplasty with interlocking screws: a computational bone adaptation. *Journal of Orthopaedic research*, 22, pp.51-57.

O'Connor, J. & Goodfellow, J., 1996. Theory and practice of meniscal knee replacement: design against wear. *Proceedings of the Institution of Mechanical Engineering*, 210, pp.217-22.

Pagnano, M., Levy, B. & Berry, D., 1999. Cemented all polyethylene tibial components in patients age 75 years and older. *Clinical Orthopaedics and Related Research*, 367, pp.73-80.

Pandit, H. et al., 2009. Mobile bearing dislocation in lateral unicompartmental knee replacement. *The Knee*, p.Article in Press.

Pandit, H. et al., 2008. Combined anterior cruciate reconstruction and Oxford unicompartmental knee arthroplasty: In vivo kinematics. *The Knee*, 15, pp.101-06.

Parks, N., Engh, G., Topoleski, L. & Emperado, J., 1998. Modular tibial insert micromotion. A concern with contemporary knee implants. *Clinical Orthopaedics and Related Research*, 356, pp.10-15.

Patil, S., Colwell, C., Ezzet, K. & D'Lima, D., 2005. Can normal knee kinematics be restored with unicompartmental knee replacement? *Journal of Bone and Joint Surgery*, 87, pp.332-38.

Pennington, D., Swienckowski, J., Lutes, W. & Drake, G., 2006. Lateral unicompartmental knee arthroplasty: Survivorship and technical considerations at an average follow-up of 12.4 years. *The Journal of Arthroplasty*, 21, pp.13-17.

Petty, W. et al., 1999. Total knee contact pressures: the effect of congruity and alignment. *Medscape General Medicine*, 1, p.1.

Piegl, L. & Tiller, W., 1997. *The NURBS book*. 2nd ed. Berlin: Springer.

Pinczewski, L., 2003. Advancements in unicompartmental knee replacement. *Business briefing: Global surgery*, pp.37-42.

Poilvache, P., Insall, J., Scuderi, G. & Font-Rodriguez, D., 1996. Rorational landmarks and sizing of the distal femur in total knee arthroplasty. *Clinical Orthopaedics and Related Research*, pp.35-46.

Price, A. et al., 2004. Sagittal plane kinematics of a mobile-bearing unicompartmental knee arthroplasty at 10 years: a comparative in vivo fluoroscopic analysis. *The Journal of Arthroplasty*, 19, pp.590-97.

Purkait, R. & Chandra, H., 2004. A study of sexual variation in Indian femur. *Forensic Science International*, 146, pp.25-33.

Reilly, D. & Burstein, A., 1975. The elastic and ultimate properties of compact bone tissue. *Journal of Biomechanics*, 8, pp.393-405.

Reilly, D. & Martens, M., 1972. Experimental analysis of the quadriceps muscle force and patello-femoral joint reaction force for various activities. *Acta Orthopaedica Scandinavica*, 43, pp.126-37.

Relethford, J. & Harpending, H., 1994. Craniometric variation, genetic theory, and modern human origins. *American Journal of Physical Anthropology*, 95, pp.249-70.

Repicci, J., 2003. Total knee or uni? Benifits and limitations of the unicondylar knee prosthesis. *Orthopedics*, 26(3), pp.274-77.

Robinson, B. et al., 2002. A kinematic study of lateral unicompartmental arthroplasty. *The Knee*, 9, pp.237-40.

Röstlund, T., Carlsson, L., Albrektsson, B. & Albrektsson, T., 1989. Morphometrical studies of human femoral condyles. *Journal of Biomedical Engineering*, 11, pp.442-48.

Rougraff, B., Heck, D. & Gibson, A., 1991. A comparison of tricompartmental and unicompartmental replacement for the treatment of gonarthrosis. *Clinical Orthopedics and Related Research*, 273, pp.157-64.

Rovick, J., Reuben, J., Schrager, R. & Walker, P., 1991. Relation between knee motion and ligament length patterns. *Clinical Biomechanics*, 6, pp.213-20.

Sab, J., 2011. *ic - implant cat*. [Online] Available at: http://www.implantcast.info/ [Accessed 2011].

Sathasivam, S., Walker, P., Campbell, P. & Rayner, K., 2001. The effect of contact area on wear in relation to fixed bearing and mobiler bearing knee replacements. *Journal of biomedical materials Research*, 58, pp.282-90.

Sathasivam, S. et al., 1999. Custom constrained condylar total knees using CAD-CAM. *The Knee*, 6, pp.49-53.

Saxler, G., Temmen, D. & Bontemps, G., 2004. Medium-term results of the AMC-unicompartmental knee arthroplasy. *The Knee*, 11, pp.349-55.

Scheffer, C. & Cloete, T., 2011. Inertial motion capture in conjunction with an artificial neural network can fifferentiate the gait patterns of hemiparetic stroke patients compared to able-bodied counterparts. *Computer Methods in Biomechanics and Biomedical Engineering*, p.Article in Press.

Schrøder, H. et al., 2001. Cementless porous-coated total knee arthroplasty. 10-year results in a consecutive series. *Journal of Arthroplasty*, 16(5), pp.559-67.

Seedhom, B., Longton, E., Wright, V. & Dowson, D., 1972. Dimensions of the knee: Radiographic and autopsy study of sizes required for a knee prosthesis. *Annals of the Rheumatic Diseases*, 31, pp.54-58.

Shapeero, L. et al., 1988. Functionaldynamics of the knee joint by ultrafast cine-CT. *Investigative Radiology*, 23, pp.118-23.

Sharkey, P., Hozack, W. & Rothman, R., 2002. Why are knee replacements failing today. In *The American Academy of Orthopaedic Surgeons 69th Annual meeting*. Dallas, Texas, 2002.

Sharkey, P. et al., 1999. Factors influencing choice of implants in total hip arthroplasty and total knee arthroplasty: Perspective of surgeons and patients. *The Journal of Arthroplasty*, 14(3), pp.281-87.

Sharma, P. et al., 2007. In vivo contact pressures in total knee arthroplasty. *Journal of Arthroplasty*, 22(3), pp.404-16.

Sherwood, J. et al., 2002. A three-dimensional osteochondral composite scaffold for articular cartilage repair. *Biomaterials*, 23, pp.4739-51.

Shi, J., 2007. Finite element analysis of total knee replacement considering gait cycle load and malalignment. *Doctor of Philosophy Thesis, University of Wolverhampton*.

Shiavi, R. et al., 1987. Helical motion analysis of the knee-II. Kinematics of uninjured and injured knees during walking and pivoting. *Journal of Biomechanics*, 20, pp.653-65.

Shih, Y., Bull, A., McGregor, A. & Amis, A., 2004. Active patellar tracking measurement - a novel device using ultrasound. *The American Journal of Sports Medicine*, 32, pp.1209-17.

Siebel, T. & Kafer, W., 2004. Modification of the posterior cruciate ligament tension following total knee arthroplasty: comparison of the Genesis CR and LCS meniscal bearing prostheses. *The Knee*, 11, pp.203-08.

Simpson, D. et al., 2008. The effect of bearing congruency, thickness and alignment on the stresses in unicompartmental knee replacements. *Clinical Biomechanics*, 23, pp.1148-57.

Singerman, R., Dean, J., Pagan, H. & Goldberg, V., 1996.. Decreased posterior tibial slope increases strain in the posterior cruciate ligament following total knee arthroplasty. *The Journal of Arthroplasty*, 11, pp.99-103.

Soininvaara, T. et al., 2002. Effect of alendronate on periprosthetic bone loss after total knee arthroplasty: A one-year, randomized, controlled trial of 19 patients. *Calcified Tissue International*, 71, pp.472-77.

Soudan, K., Van Audekercke, R. & Martens, M., 1979. Methods, difficulties and inaccuracies in the study of human joint kinematics and pathokinematics by the instant axis concept. Example: The knee joint. *Journal of Biomechanics*, 12, pp.27-33.

Spence, A., 1990. *Basic Human Anatomy*. 3rd ed. Benjamin/Cummings.

Steklov, N., Slamin, J., Srivastav, S. & D'Lima, D., 2010. Unicompartmental knee resurfacing: Enlarged tibio-femoral contact area and reduced contact stress using novel patient-derived geometries. *The Open Biomedical Engineering Journal*, 4, pp.85-92.

Steyn, M. & İşcan, M., 1997. Sex determination from the femur and tibia in South African whites. *Forensic Scientific International*, 90, pp.111-19.

Stockwell, R., 1971. The interrelationship of cell density and cartilage thickness in mammalian articular cartilage. *Journal of Arthroplasty*, 24, pp.411-21.

Stukenborg-Colsman, C., Ostermaier, S., Hurschler, C. & Wirth, C., 2002. Tibiofemoral contact stress after total knee arthroplasty. *Acta Orthopaedica Scandinavica*, 73(6), pp.638-46.

Sugita, T. et al., 2000. Assessment of articular cartilage of the lateral tibial plateau in varus osteoarthritis of the knee. *The Knee*, 7, pp.217-20.

Svärd, U. & Price, A., 2001. Oxford medial unicompartmental knee arthroplasty. A survival analysis of an independent series. *The Journal of Bone and Joint Surgery British Edition*, 83(2), pp.191-94.

Taylor, M., Tanner, K. & Freeman, M., 1998. Finite element analysis of the implanted proximal tibia: a relationship between the initial cancellous bone stresses and implant migration. *Journal of Biomechanics*, 31, pp.303-10.

Terrier, A., 1999. Adaptation of bone to mechanical stress: theoretical model, experimental identification and orthopedic application. *Doctor of Philosophy Thesis, Swiss Federal Institute of Technology*.

Tornier, 2009. *HLS uni evolution brochure*. [Online] Available at: http://www.tornier.com/index.php?option=com_content&task=view&id=492 [Accessed 2009].

Total joints, 2011. *Total joints*. [Online] Available at: http://www.totaljoints.info/TOTAL_KNEE_MAIN.htm [Accessed 2011].

Tsakonas, A. & Polyzoides, A., 1997. Reduction of polyethylene in a congruent meniscal knee prosthesis. Experimantal and clinical studies. *Acta Orthopaedica Scandanavia*, 68, pp.127-31.

Udomkiat, P., Dorr, L. & Long, W., 2001. Matched-pair analysis of all-polyethylene versus metal-backed tibial components. *The journal of Arthroplasty*, 16, pp.689- 696.

Uvehammer, J., Kärrholm, J. & Brandsson, S., 2000a. in vivo kinematics of total knee arthroplasty: concave versus posterior-stabilised tibial joint surface. *The Journal of Bone and Joint Surgery (Br)*, 82, pp.499-505.

Uvehammer, J. et al., 2000b. In vivo kinematics of total knee arthroplasty: flat compared with concave tibial joint surface. *Journal of Orthopaedic Research*, 18, pp.856-64.

Van der Linden-Van der Zwaag, H., Wolterbeek, R. & Nelissen, R., 2008. Computer assisted orthopedic surgery: its influence on prosthesis size in total knee replacement. *The Knee*, 15, pp.281-85.

Van Schalkwyk, E., 2010. Determining femoral component goodness-of-fit using computer segmentation and numerical simulation. *MScEng Thesis, Mechanical and Mechatronic Engineering, University of Stellenbosch*.

Varadarajan, K., Harry, R., Johnson, T. & Li, G., 2009. Can in vitro systems capture the characteristic differences between the flexion-extension kinematics of the healthy and TKA knee? *Medical Engineering & Physics*, 31, pp.899-906.

Vardi, G. & Strover, A., 2004. Early complications of unicompartmental knee replacement: The Droitwich experience. *The Knee*, 11, pp.389-94.

Viceconti, M., Olsen, S. & Burton, K., 2005. Extracting clinically relevant data from finite element simulations. *Clinical Biomechanics*, 20, pp.451-54.

Victor, J. et al., 2010. The influence of muscle load on tibiofemoral knee kinematics. *Journal of Orthopaedic Research*, 28, pp.419-28.

Victor, J. et al., 2009. How precise can bony landmarks be determined on a CT scan of the knee? *The Knee*, 16, pp.358-65.

Victor, J. et al., 2009. An experimental model for kinematic analysis of the knee. *The Journal of Bone and Joint Surgery*, 91, pp.150-63.

Villa, T. et al., 2003. Computer assisted design and evaluation of a knee prosthesis. *Bioengineering Conference, Florida*.

Villa, T. et al., 2004. Contact stresses and fatigue life in a knee prosthesis: comparison between in vitro measurements and computational simulations. *Journal of Biomechanics*, 18, pp.45-53.

Vince, K., 2003. Why knees fail. *The Journal of Arthroplasty*, 18, pp.39-44.

Wada, M., Imura, S., Baba, H. & Shimada, S., 1996. Knee laxity in patients with osteoarthritis and rheumatoid arthritis. *British Jornal of Rheumatology*, 35, pp.560-63.

Walker, P. & Garg, A., 1991. Range of motion in total knee arthroplasty. *Clinical Orthopaedics and Related Research*, 262, pp.227-35.

Walker, P. & Sathasivam, S., 2000. Design forms of total knee replacement. *Proceedings of the Institution of Mechanical Engineers, Part H: Journal of Engineering in Medicine*, 214, pp.101-19.

Walker, P., Shoji, H. & Erkman, M., 1972. The rotation axis of the knee and its significance to prosthesis design. *Clinical Orthopaedics and related research*, 89, pp.160-70.

Walker, P., Yildirim, G., Sussman-Fort, J. & Klein, G., 2006. Relative positions of the contacts on the cartilage surfaces of the knee joint. *The Knee*, 13, pp.382-88.

Wang, S., Feng, C. & Lu, H., 1992. A study of Chinese knee joint geometry for prosthesis design. *Chinese medical Journal*, 105, pp.227-33.

Wasielewski, R. et al., 1997. Tibial insert undersurface as a contributing source of polyethylene wear debris. *Clinical Orthopaedics*, 345, pp.53-59.

Weiss Joint University, 2009. *Unicompartmental (partial) knee replacement surgery*. [Online] Available at: http://www.weisshospital.com/joint-university/knee/unicompartmental.html [Accessed 2009].

White, S., Ludkowski, P. & Goodfellow, J., 1991. Anteromedial osteoarthritis of the knee. *Journal of Bone and Joint Surgery*, 73B, p.582.

Williams, A. & Logan, M., 2004. Understanding Tibio-femoral motion. *The Knee*, 11, pp.81-88.

Windsor, R., Scuderi, G., Moran, M. & Insall, J., 1989. Mechanisms of failure of the femoral and tibial components in total knee arthorplasty. *Clinical Orthopaedics and Related Research*, 248, pp.15-19.

Wismans, J., Veldpaus, F. & Janssen, J., 1980. A three-dimensional mathematical model of the knee-joint. *Journal of Biomechanics*, 13, pp.677-86.

Wolff, J., 1986. *Tha law of bone remodelling*. Berlin: Springer.

Worland, R. et al., 2002. Ten to fourteen year survival and functional analysis of the AGC total knee replacement system. *The Knee*, 9(2), pp.133-37.

Xing, J. et al., 2010. Towards a more uniform sampling of human genetic diversity: a survey of worldwide populations by high-density genotyping. *Genomics*, 96, pp.199-210.

Xsens, 2006. *MTi and MTx user manual and technical Documantation*. Revision G ed. Enshede, The Netherlands: Xsens Technologies B.V.

Yue, B. et al., 2011. Differences of knee anthropometry between Chinese and white men and women. *The Journal of Arthroplasty*, 26:1, pp.124-30.

Zannger, P. & Detsky, A., 2008. Computer-assisted decision analysis in orthopaedics: resurfacing the patella in total knee arthroplasty as an example. *Journal of Arthroplasty*, 15, pp.281-85.